Proteomic and molecular analysis of neural tube defects in the mouse embryo

Sandra Cristina Pena de Castro

Thesis submitted for the degree of Doctor of Philosophy in the University College London

February 2011

Institute of Child Health, 30 Guilford Street, London, WC1N 1EH

I. Declaration of contribution

I, Sandra C. P. de Castro, confirm that the work here presented is my own.

The majority of experiments were performed by me and other contributions are stated in the thesis and declared here. I was assisted by Dr. Peter Gustavsson in sequencing analysis (Chapter 4) and by Dr. Valentina Massa in performing skeleton preparations (Chapter 5). Dr Kit-Yi Leung performed mass spectrometry and analysed the data (Chapter 3). Dr. Ashraf Malhas performed *in vitro* analysis – FLIP and contour ratio analysis (Chapter 4).

Sandra C. P. de Castro

II. Abstract

The aim of this project was to investigate the causes of spinal neural tube defects (NTDs), using the *curly tail* (*ct/ct*) mouse as a model system. The *ct* mutant allele corresponds to a hypomorphic allele of *grainyhead-like-3* (*Grhl3*) gene. A two-dimensional protein gel electrophoresis (2-DE) based approach was used to compare the proteome profile of *ct/ct* embryos with a genetically matched wild-type strain at the stage of spinal neural tube closure. This analysis revealed a series of proteins whose abundance or 2-DE gel migration are abnormal in *ct/ct* embryos. Detailed follow-up analysis was performed on one protein, lamin B1. Differential migration of lamin B1 on *ct/ct* compared with wild-type 2-DE gels was found to result from a sequence change in *Lmnb1*, resulting in the deletion of a glutamic acid (E) in a region of 9 glutamic acids in the wild-type protein. Lamin B1 in *ct/ct* therefore only has 8 glutamic acids in this part of the protein. Further analysis showed that the lamin B1 variants functionally differ. Genetic crosses were performed to generate sub-strains of *ct/ct* mice carrying different combinations of the *Grhl3* mutation and lamin B1 variants. These studies support the hypothesis that *Lmnb1* can modify the risk of NTDs in the *ct/ct* strain. Finally, while *ct/ct* NTDs result from diminished *Grhl3* expression, the effects of *Grhl3* over-expression were also investigated by intercrossing *curly tail Grhl3*-transgenic mice (*ct/ct*^{TgGrhl3}). High levels of *Grhl3* expression were found to cause NTDs at high frequency, indicating that *Grhl3* regulation is an important requirement for neural tube closure. Morphological and gene expression analysis in *Grhl3* over-expressing transgenic embryos suggest that the cellular mechanism underlying NTDs differs from that in the *ct/ct* hypomorphic mutant.

III. Acknowledgments

I would like to thank my supervisor Dr. Nick Greene for his excellent supervision. That is reflected in his professionalism, support, patience, and the ability to decipher my "brain-storming" when discussing results, making suggestions, and picking me up when things went wrong. As well, he helped me to focussed, when it was just too tempting to do "ten" different experiments, when choosing the right one or two would have answered a question. I thank Prof. Andy Copp for his support, for his immense contributions to the field, and for giving me the chance to learn more techniques and develop my skills in science by taking on a project in the Neural Tube Development group. I am glad I made the right choice of project, I have learnt a lot.

I thank all the members of the Neural Development Unit for their professionalism and support over these years, and this includes previous members of the team, Ezat Sajedi, Clare Faux and Daniel Alete, outstanding colleagues, who will never be forgotten. I am grateful for Dr. Peter Gustavsson's contributions towards the project I worked on prior to my PhD and to him, Alexis Robinson, Dawn Savery, Kit-Yi Leung, Massimo Signore, and Valentina Massa for their expertise. As well as, I thank all the other members of the Neural Tube Development group including Ana Rolo, Darren Partridge, Saba Rasa, Sophie Prior, and Sarah Escuin, for their day-to-day support, exchange of ideas and for making the work environment an enjoyable place to be.

I would like to acknowledge University College London - Institute of Child Health for giving the staff the opportunity to develop their skills, therefore widening their carrier opportunities, and importantly, their knowledge.

Above all, I thank my family for their unconditional support, understanding that I am a work addict, and for being happy that I am doing what I chose and always wanted to do, science.

Additional projects not described in thesis

In parallel to the development of my PhD project, I have collaborated in two different projects. First, in a project with Dr. Hannah M. Mitchison's group I performed *in situ* hybridisation on mouse sections to analyse the expression pattern of the *Rsph9* and *DNAH5* genes which were candidates for primary ciliary dyskinesia. This work was published:

Castleman VH, Romio L, Chodhari R, Hirst RA, de Castro SC, Parker KA, Ybot-Gonzalez P, Emes RD, Wilson SW, Wallis C, Johnson CA, Herrera RJ, Rutman A, Dixon M, Shoemark A, Bush A, Hogg C, Gardiner RM, Reish O, Greene ND, O'Callaghan C, Purton S, Chung EM, Mitchison HM (2009). Mutations in Radial Spoke Head Protein Genes *RSPH9* and *RSPH4A* Cause Primary Ciliary Dyskinesia with Central-Microtubular-Pair Abnormalities. *American Journal of Human Genetics*, 84:1-13.

In a second project, I generated mouse embryonic fibroblasts, performed genotyping for the *Grhl3* gene mutation, and quantitative RT-PCR analysis. This contributed to a joint first authorship in:

De Castro SC, Leung KY, Savery D, Burren K, Rozen R, Copp AJ, Greene ND (2010). Neural tube Defects Induced by Folate Deficiency in Mutant *Curly Tail* (*Grhl3*) Embryos are Associated with Alteration in Folate One-Carbon Metabolism but are Unlikely to Result from Diminished Methylation, *Birth Defects Research (Part A)*, 88:612-618 (appended to this thesis).

IV. Abbreviations

aa	Amino acid
ANOVA	Analysis of variance
BAC	Bacterial artificial chromosome
BLAST	Basic local alignment search tool
bp	Base pair
BT	Bent tail
C	Carboxyl
°C	Degrees Celsius
Crh	Chromosome
CT	Curled tail
2-DE	Two-dimensional protein gel electrophoresis
DEPC	Diethyl pyrocarbonate
DLHP	Dorsolateral hinge point
DMEM	Dulbecco's Modified Eagle's medium
dNTP	Deoxynucleoside triphosphate
E	Embryonic day
Ex, Exen	Exencephaly
FLIP	Fluorescence loss in photobleaching
GFP	Green fluorescent protein
Glu, E	Glutamic acid
h	Hour
Hg	Hindgut
IEF	Isoelectric focussing
IPG	Immobilised pH gradient
kDa	Kilo Dalton
LPNP	Large posterior neuropore
µ	Micro
m	Milli
M	Molar
mA	Milli Ampere
Mb	Mega base

MEFs	Mouse embryonic fibroblasts
MHP	Median hinge point
MOPS	3-(N-Morpholino)-propanesulfonic acid
MS	Mass spectrometry
MW	Molecular weight
N	Amino
NF	Neural folds, neuroepithelium
NLS	Nuclear localisation signal
NTDs	Neural tube defects
OD	Optical density
p	p-value (probability)
pI	Isoelectric point
PKC	Protein kinase C
PNP	Posterior neuropore
PTM	Posttranslational modification
qG-PCR	Quantitative genomic polymerase chain reaction
rpm	Rotations/revolutions per minute
RT-qPCR	Reverse transcriptase quantitative polymerase chain reaction
SE	Surface ectoderm
SB	Spina bifida
SDS-PAGE	Sodium dodecyl sulphate-polyacrylamide gel electrophoresis
SEM	Standard error of the mean
SPNP	Small posterior neuropore
ss	Somite stage
ST	Straight tail
UTRs	Untranslated regions (5' UTR and 3'UTR)
V	Volt
vLPNP	Very large posterior neuropore
v/v	Volume per volume
W	Watt
w/v	Weight per volume
YFP	Yellow fluorescent protein

V. Table of Contents

VI. List of Figures

CHAPTER 5

VII. List of Tables

Chapter 1

General Introduction

1.0 Introduction

1.1 Mouse development and neural tube closure

The development of the mouse embryo involves a dynamic series of events during embryonic stages prior to the foetal stage. Later, 14-15 days after implantation, the development of the foetus mostly involves growth of the organs until birth, around 19-20 days after conception. The mammalian neural tube is derived from the embryonic ectoderm. Closure of the neural folds proceeds from embryonic days (E) 8.0 to 10.5 resulting in generation of the closed neural tube, the precursor of the entire central nervous system (Copp et al., 2003).

During early embryogenesis, the three germ layers (mesoderm, endoderm, and ectoderm) are formed during gastrulation stage. A midline region of the ectoderm on the dorsal surface of the embryo is induced to become a layer of neuroectodermal cells, the neural plate (**Figure 1.1**). Subsequently the lateral edges of the neural plate elevate, fold, adhere to each other and fuse in the midline to form a tube that develops into the brain and upper spinal cord (Copp et al., 2003; Greene and Copp, 2009b). This process is known as primary neurulation. In contrast, in the lower spinal cord the neural tube develops by the process of secondary neurulation, which involves elongation and cavitation of a condensed mass of cells derived from the tail bud (Greene and Copp, 2004).

Neural tube closure is initiated separately and sequentially at three discrete initiation sites at (1) the cervical/hindbrain boundary, (2) the midbrain/forebrain boundary, and (3) the rostral limit of the forebrain (**Figure 1.2 A**). Closure spreads bidirectionally from initiation sites 1 and 2 and caudally from Closure 3. Thus, from Closure 1 (upper spinal level) fusion progresses rostrally into the brain and caudally down the spine, gradually closing the open regions, termed neuropores, with closure being completed at locations sited in the forebrain, hindbrain, and upper sacral region. The timing of neural tube closure varies among mouse strains, but cranial closure is generally complete at E9.5 and the last part of the neural tube to close in the spinal region is the posterior neuropore (PNP) at E10.5 (Greene and Copp, 2004).

Conversion of the initially flat neural plate requires a complex sequence of shaping and bending events that ultimately results in apposition of the tips of the neural folds to form a closed neural tube (Greene and Copp, 2004). For example, the narrowing of the neural plate during its formation is predicted to be due to apicobasal elongation of cells. In addition, the embryo elongates within the rostrocaudal axis due to cellular convergent extension movements in combination with growth of the caudal region of the embryo, which continues throughout the period of neural tube closure.

Bending of the lateral edges of the neural plate produces folds that fuse in the midline to form the neural tube, and differs between the cranial and spinal regions. At the cranial level, the elevating neural folds acquire a biconvex appearance in the midbrain where the tips of the folds face away from the midline. Subsequently and abruptly the folds assume a biconcave shape, and the tips approach each other in the midline allowing fusion to occur (Greene and Copp, 2009a). The mechanism underlying this complex bending pattern is not fully understood but there is evidence for the importance of expansion of the cranial mesenchyme, which underlies the neural folds, and components of the actin cytoskeleton. Some of these mechanisms will be discussed further in this chapter. In contrast, at the spinal level there is not a phase of biconvex neural folds, but three modes (closure morphologies) which vary in number and location depending on the embryo stage (Shum and Copp, 1996). An initial closure point (Mode 1) is characterised by the presence of a single bend in the midline above the notochord, the median hinge point (MHP; **Fig. 1.A-B**). The neural folds are straight at the site of Closure 1 and subsequently at the level of the posterior neuropore (PNP) at somite stages 6 to 15. From somite stages 16 to 23, when the PNP is at a more caudal level, the neural folds exhibit additional bending sites (dorsolateral hinge points, DLHP; **Fig. 1.C**), and the neural tube has a diamond shaped lumen (Mode 2). Mode 3 occurs from somite stage 24, the PNP is characterised by the absence of a defined median hinge point but the persistence of DLHP such that the lumen of the closed neural tube is circular.

In summary, the process of neural tube closure involves a series of morphological events resulting in the conversion of the flat neural plate into the neural tube. The processes that are required for closure include convergent extension cell movements, expansion of the cranial mesenchyme, contraction of actin microfilaments, regulated

bending of the neural plate, and adhesion of the tips of the neural folds (Greene and Copp, 2009a). These cellular and molecular mechanisms which were acquired mainly from studies in animal models will be further discussed in **section 1.4.1**, with major focus in the mouse.

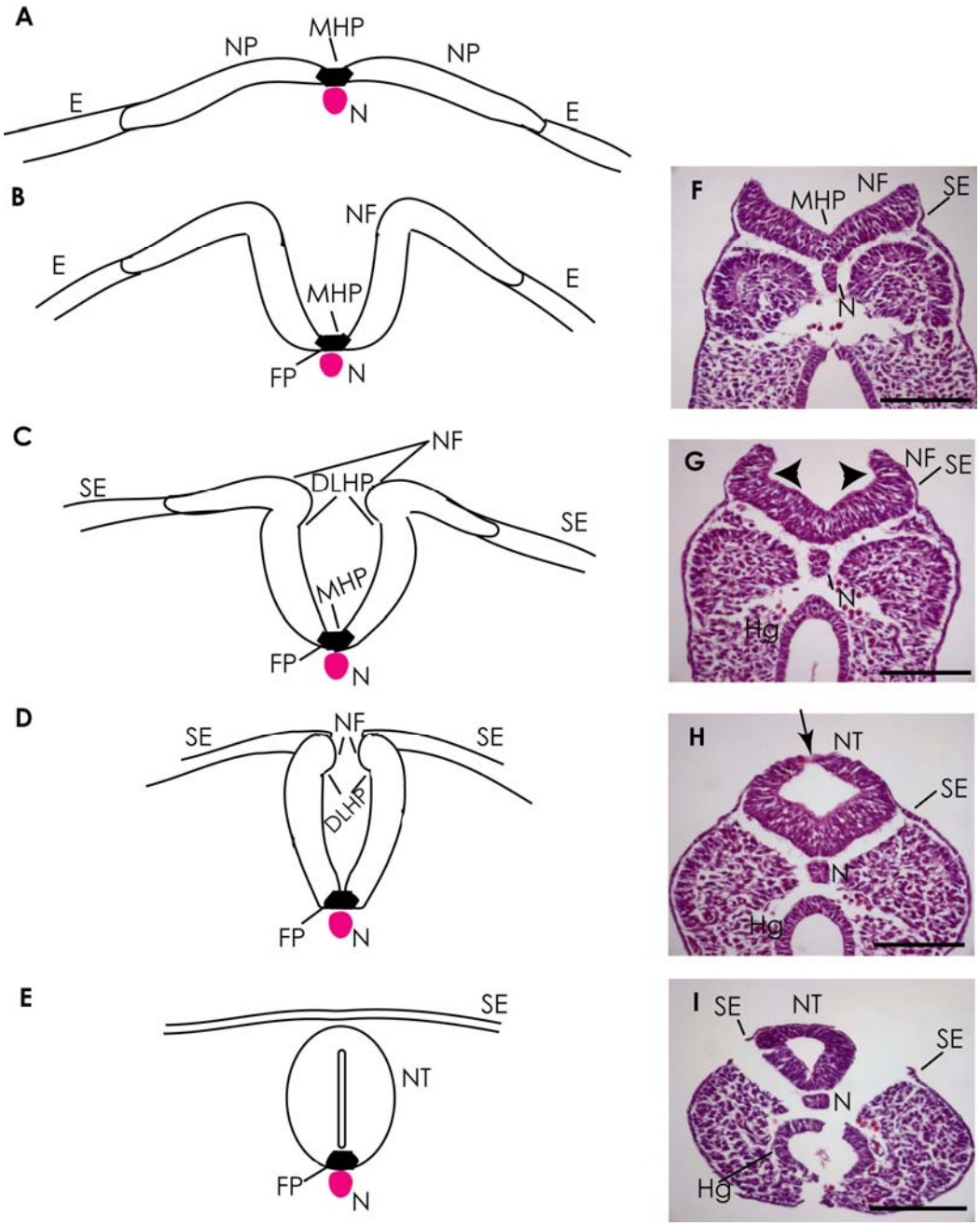

Figure 1.1 Diagrammatic representations and hematoxylin-eosin stained transverse sections showing the main morphogenetic movements during the process of spinal neural tube closure in the mouse. (**A**) The neural plate (NP), which overlies the notochord (N), is a sheet of epithelial cells of ectodermal (E) origin on the dorsal surface of the gastrula-stage embryo. Along the ventral midline of the neuroepithelium, the median hinge point (MHP) forms a bend around which the plate bends. (**B**) Elevation of the neural folds (NF) results in formation of the groove (neural groove). (**C**) In the mid-lower spine, caudal to somite 15, secondary hinge points are formed in the dorsolateral (DLHP) part of the neural folds, facilitating convergence of the tips of the neural folds. (**D-E**) The tips of the neural folds meet and fuse at the dorsal midline and tissue remodelling separates the newly formed neural tube (NT) from the surface ectoderm (SE). (**F-I**) Transverse sections through the PNP region of embryos of increasing somite stages show the events of spinal neural tube closure. These include formation of the MHP and elevation of the NF (**F**), the formation of DLHP (**G**), apposition of the tips of the NF (**H**) and the closed NT (**I**). Other abbreviations: FP, floor plate; Hg, hindgut; N, notochord. Arrowheads in **G** indicate DLHP. Arrow in **F** indicates the point of adhesion at the tips of the neural folds. Scale bars: 0.1 mm.

1.2 Neural tube defects

Abnormalities in the process of neurulation can prevent closure, resulting in neural tube defects (Copp et al., 2003).

1.2.1 Neural tube defects in the mouse

Failure of initiation of Closure 1 (hindbrain-cervical boundary) results in craniorachischisis. In this condition most of the brain (from the midbrain) and the entire spinal cord remains open, while Closures 2 and 3 usually occur normally. Failure of closure in the cranial region results in exencephaly (Closure 2, **Fig. 1.2 C**), with persistent open neural folds, which progresses to anencephaly, characterized by degeneration of the exposed brain tissue and lack of formation of the skull vault. Anencephaly is also observed in individuals with craniorachischisis as observed in **Figure 1.2 B**. Failure of Closure 3 results in a type of exencephaly referred to as a split face phenotype, in which the forebrain remains open. Failure of closure in the lower spine causes spina bifida (**Fig. 1.2 D**). In mice, spina bifida is usually accompanied by tail flexion defects, such as curled tail, as a secondary manifestation (**Fig. 1.2 B-D**). NTDs at different axial levels can occur in isolation or in combination (e.g., spina bifida may occur with exencephaly; **Fig. 1.2 C-D**).

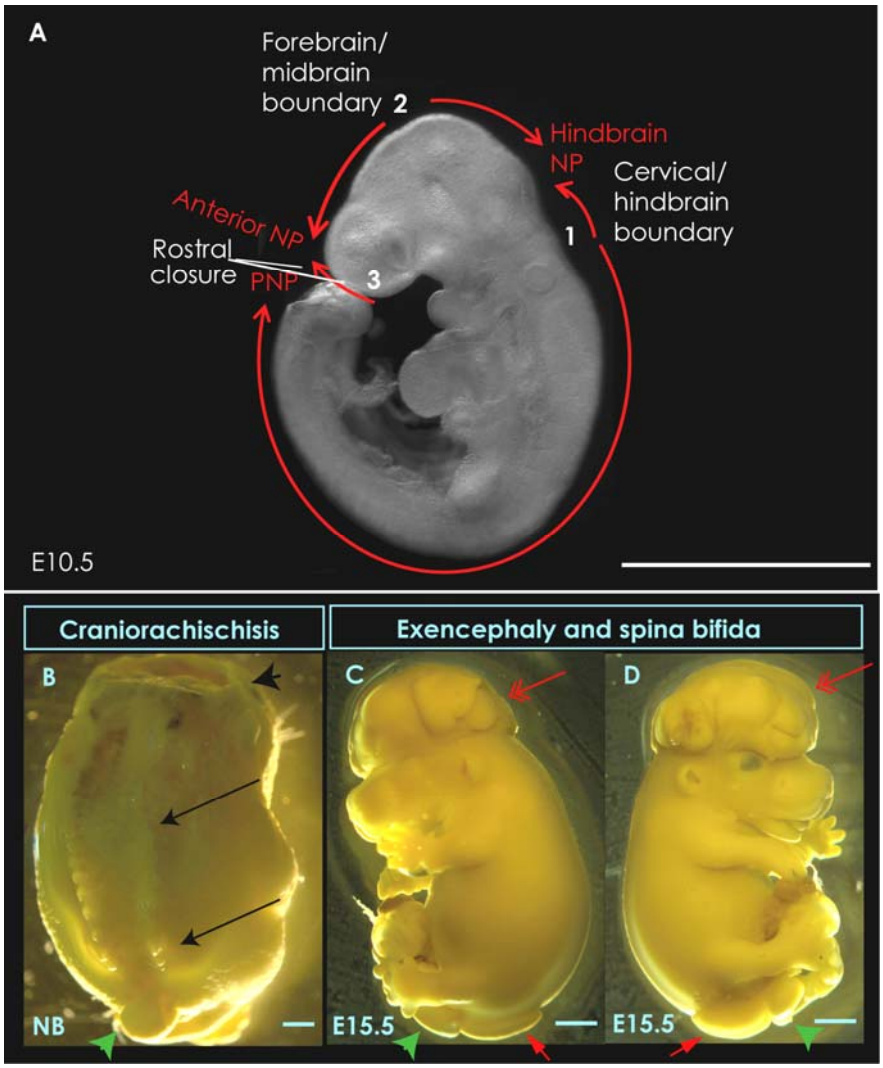

Figure 1.2 Neural tube closure and NTDs. (A) Location of the sites where closure was previously initiated, and the subsequent progression of closure are indicated on an E10.5 embryo, near the final stage of neural tube closure. Closure spreads bidirectionally (red arrows) between the three initiation sites (1, 2 and 3, white) and caudally (red arrows), resulting in shortening of the neuropores (NP), and culminating with the closure of the posterior NP (PNP). Diagram adapted from (Copp et al., 2003). NTDs (**B-D**) arise if closure fails. (**B**) Newborn *Loop-tail* mutant with craniorachischisis in which Closure 1 failed to occur. The whole spine remains open (black arrows), and the brain does not form (black arrowhead). (**C-D**) E15.5 *curly tail* foetus with exencephaly (red double-headed arrow) and spina bifida (red arrow) where Closure 2 and PNP closure failed to occur, respectively. Green arrow indicates curled tail. Scale bars: **A**, 0.5 mm; **B-D**, 1.0 mm.

1.2.2 Neural tube defects in humans

Similar to neural tube closure in the mouse embryo, closure in human embryos is also a discontinuous process characterized by multiple closure sites (Greene and Copp, 2009a). The bending of the neural plate begins at around 17-18 days post-fertilization (dpf). Closure 1 occurs more rostrally than in the mouse, at around 22 dpf, while a corresponding event to closure 2 does not seem to occur, or if it does may be at a more anterior position than in the mouse. Closure 3 seems to occur in the same site as in the mouse (anterior forebrain). Completion of neural tube closure occurs at the level of the posterior neuropore, at 26-28 dpf, followed by secondary neurulation which forms the neural tube in the low sacral and coccygeal regions. Disturbances in the process of primary neural tube closure in the developing embryo, result in open NTDs, as described in the mouse. Both craniorachischisis and anencephaly are lethal malformations. Individuals with spina bifida usually survive birth but are likely to require lifelong medical interventions for severe disabilities including loss of sensation and/or paralysis of the legs, hydrocephalus, spinal curvature, limb deformities and renal tract infections.

In humans, NTDs are common birth defects, occurring in approximately 0.5-2.0 per 1,000 pregnancies (Greene et al., 2009b). These defects have a multifactorial basis with genetic and environmental factors contributing to risk (Copp et al., 1990). Epidemiologic studies have indicated a range of environmental factors which appear to contribute to susceptibility to NTDs in humans, and may summate with predisposing genetic factors. Environmental risk factors include nutritional status (e.g. sub-optimal folate availability or insufficient vitamin B_{12} levels) and teratogenic agents (e.g., excess vitamin A or anti-epileptic drugs such as valproic acid). Other factors include hyperthermia during early pregnancy (Moretti et al., 2005) and maternal hyperglycemia, diabetes or obesity (Detrait et al., 2005; Loeken, 2005; Dheen et al., 2009).

To date, while a few possible ‘risk’ polymorphisms have been described, no genetic defects have been identified as a major cause of human NTDs. This suggests one or more of the following possibilities: that a major NTD has yet to be identified, that some cases involve rare, unique mutations or that cases typically arise from a combination of two or more risk factors (Greene and Copp, 2005; Greene et al., 2009b). In most NTDs a Mendelian pattern of inheritance has not been reported. However, there is an enhanced

recurrence risk among siblings of affected individuals, and a higher frequency in twins than in singletons. These patterns fit a model in which the majority of NTDs are sporadic with multifactorial polygenic or oligogenic inheritance (Detrait et al., 2005; Harris and Juriloff, 2007). One example of a mouse model which seems to fit within the additive, multifactorial genetics of human NTDs is the SELH/Bc strain, in which there appears to be a contribution of several critical genes which have an approximately equal, additive, and interchangeable effect on NTD risk (Juriloff et al., 2001). Another example is the *curly tail* (*ct*) mutant strain, where the presence of the *ct* mutation appears to be essential for NTDs, but with variable penetrance affected by at least three "modifier" loci (Harris and Juriloff, 2007; Neumann et al., 1994).

Identification of the genes that are associated with risk of human NTDs has proven to be a difficult task. In humans, identification of familial cases of NTDs with a significant number of affected members, have proven difficult to ascertain. Other than spina bifida most types of NTDs are lethal (craniorachischisis and anencephaly), such that subsequent generations will not be present. A drawback of direct extrapolation of candidate genes from the mouse is that many of the mouse mutants with NTDs have multiple developmental defects (syndromic), which is not reflected in humans in which most cases are non-syndromic (Harris, 2001). Syndromic cases in humans, which make up less than 10% of all NTDs, are often associated with chromosomal anomalies (Greene et al., 2009b). The search for candidate genes has largely focussed on candidate genes related to: ***i***) folate metabolism, since folic acid supplementation is known to reduce the incidence of NTDs (Wald et al., 1991) and sub-optimal folate status is a risk factor for NTDs (Kirke et al., 1993); ***ii***) mouse models of NTDs of which there are more than 200 (Harris and Juriloff, 2010) positional candidates from linkage analysis (Boyles et al., 2005).

Folate metabolism involves the activation and transfer of one carbon units which are used in a variety of anabolic and catabolic reactions, that are essential for a number of cellular processes including nucleotide synthesis and methylation reactions (Beaudin and Stover, 2007). A number of enzymes catalyse the interlinked network of reactions that make up folate metabolism and polymorphisms in a number of these enzymes have been analysed for possible association with risk of NTDs. The most well studied enzyme is 5,10-methylenetetrahydrofolate reductase (MTHFR) and the C677T

polymorphism in *MTHFR* has been associated with increased risk in some, although not all, populations (Boyles et al., 2005; Greene et al., 2009b). It is hypothesised that some NTDs result from an underlying defect of folate metabolism in the fetus. This idea was supported by biochemical analysis of folate metabolism in primary fibroblastic cell lines derived from fetuses affected with NTDs, which showed abnormalities in folate cycling in a proportion of cases (Dunlevy et al., 2007). These defects were proposed to be genetically determined but did not correlate to genotype for any of the commonly studied polymorphisms in folate-related genes, including 5,10-methylenetetrahydrofolate reductase (MTHFR).

Some genes whose mutation is known to cause NTDs in mice have been screened in human cases. In mice, mutations in the *Pax3* gene result in NTDs in homozygous mutants such as *splotch* (reviewed by Greene et al., 2009). In humans, mutations in *PAX3* are found in Waardenburg syndromes types I and III cases, and spina bifida has occasionally been reported in these syndromes (Carezani-Gavin et al., 1992; Chatkupt and Johnson, 1993). These observations suggest that *PAX3* mutations can cause NTDs in humans (Greene et al., 2009a). However, neither mutation screens (by sequencing) nor association studies have suggested that *PAX3* is a major risk factor for spina bifida (Greene et al., 2009a).

Mutation of *Vangl2*, which encodes a member of planar cell polarity signalling pathway, causes craniorachischisis in *loop-tail* mutant mice (Murdoch et al., 2001). *Vangl1* mutant mice do not develop NTDs, but a possible role in neural tube closure was indicated by the observation of craniorachischisis in *Vangl1/2* compound heterozygous mutants (Torban et al., 2008). Several nucleotide variants and a heterozygous 7 base pair intronic duplication were found in *VANGL1* and *VANGL2* genes in a collection comprising craniorachischisis, spina bifida, and anencephaly, but none were unique to NTDs cases (Doudney et al., 2005). Subsequently, missense variants in *VANGL1* (Kibar et al., 2007; Kibar et al., 2009) and *VANGL2* (Kibar et al., 2010) have been identified in patients with open and closed forms of spina bifida. These studies suggest variants in *VANGL* genes may contribute to some human NTDs.

Genome wide linkage screens may be a powerful method to find risk conferring genes. The drawback of this approach is the lack of families with multiple affected individuals

and access to sufficient numbers of parent-child triads (Boyles et al., 2005). However, one linkage study has revealed two candidate regions for human NTDs, on chromosomes 7 and 10. The region on chromosome 10 included three possible candidates genes, *FGFR2*, *GFRA1* and *PAX2* (Rampersaud et al., 2005). Given the likely heterogeneity of the genetics of NTDs, very large sample sets will be required for a genome wide association study using sporadic NTD cases.

1.3 Prevention of neural tube defects

Studies in the 1980s by Smithells and colleagues suggested that etiology of NTDs in the human population was influenced by maternal diet, social class, maternal age, and smoking (Schorah, 2009). Subsequent studies and small scale non-randomised clinical trials suggested that maternal folate status may influence risk of NTDs. Formal randomised clinical trials showed that maternal folic acid supplementation prior to and during early pregnancy can prevent the first occurrence and recurrence of NTDs (Wald et al., 1991; Czeizel and Dudás, 1992). The recurrence trial analysed the effect of folic acid (4 mg/day) with or without multivitamins, on NTD recurrence in women who have had a previous affected pregnancy. Considering the folic acid groups together, there was an approximately 70% reduction in frequency of NTDs (Wald et al., 1991). In another study the effect of folic acid (0.8 mg per day) on first occurrence was analysed and there was 90% lower frequency of NTDs in the treatment group compared to placebo controls, although this was not statistically significant (Czeizel and Dudás, 1992). These studies raised questions such as what should be the optimal dose of folic acid and whether folic acid should be taken with other vitamins (Czeizel, 2009). Mandatory fortification of food with folic acid was introduced in the USA in 1999, with a subsequent reduction in NTD frequency estimated at around 26% (Mersereau et al., 2004). However, a subset of NTDs, estimated at 30-50% appear to be resistant to prevention by folic acid (Mersereau et al., 2004), and alternative methods of prevention are therefore needed.

1.4 The mouse as a model system for the study of neural tube defects

The normal development of the neural tube is mediated by a number of transcription factors, signalling molecules, and the coordination of several biological processes including cell proliferation, migration and differentiation. This complexity is reflected

in the analysis of the distinct mouse mutants in which NTDs form part of the mutant phenotype. Over 240 mouse genetic mutants exhibit NTDs and may provide useful tools for studying the developmental mechanisms underlying neural tube closure as well as the complex etiology of these diseases in humans (Greene and Copp, 2005; Harris and Juriloff, 2007; Harris and Juriloff, 2010). The occurrence of NTDs in mutants for a range of different genes suggests that neural tube closure depends on a variety of cellular functions and has also shown that the mechanisms acting at differing axial levels may be distinct in some cases, for example in the brain as opposed to spinal cord (Copp et al., 2003).

The main problem in the many of the mouse mutants appears to be failure of elevation of the neural folds, in the cranial region resulting in exencephaly, and/or the posterior neuropore, resulting in spina bifida. Among the total number of mutants, around 70% develop exencephaly alone, 5% exhibit only spina bifida and approximately 20% develop both conditions. In many mouse models, females seem to have a higher rate of exencephaly compared to males, as is observed in human NTDs. The basis to this sex bias is unknown (Harris and Juriloff, 2010; Harris and Juriloff, 2007).

1.4.1 Cellular and genetic requirements for neural tube closure from studies in mice

Mouse models provide useful systems in which to analyse the requirements for neural tube closure (Copp and Greene, 2010). Most of the genes whose mutation causes NTDs are reported to be expressed either in the neuroepithelium or adjacent tissues, suggesting that the causative cellular defect may be intrinsic or extrinsic to the neural folds (Harris and Juriloff, 2007). Mutation of genes of the planar-cell-polarity (PCP) pathway, such as *Vangl2* and *Celsr1* causes failure of Closure 1. This is due to a deficiency of convergent extension cell movements that are necessary for narrowing and lengthening of the neural plate (Ybot-Gonzalez et al., 2007b). Therefore, embryos carrying mutations in planar cell polarity genes exhibit widely spaced neural folds, abnormally short and a wide body axis resulting in association with the severe NTD, craniorachischisis (Copp et al., 2003; Copp and Greene, 2010).

Evaluation of mouse mutants suggest that neural tube closure, particularly in the cranial region, depends on regulation of the balance between cell proliferation, apoptosis and neuronal differentiation within the neural folds (Greene and Copp, 2009a). For example, cranial NTDs occur in association with premature neuronal differentiation in *Hes1* and *Hes1/Hes3* mutant embryos (Ishibashi et al., 1995; Hirata et al., 2001). Excess apoptosis has been proposed to be the cause of cranial NTDs in several mutant strains including the *Cited2* knock-out (Martinez-Barbera et al., 2002). Apoptosis occurs in a characteristic pattern during neural tube closure (Massa et al., 2009) and reduced levels of apoptosis are observed with cranial NTDs, for example in *Apaf-1* or *caspase 3/9* mutant embryos (Massa et al., 2009). However, it appears unlikely that diminished apoptosis is directly causative as direct inhibition of apoptosis shows that it is not required for neural tube closure (Massa et al., 2009). It is thought that NTDs in apoptosis-deficient embryos may result from other cellular defects, such as an associated miss-regulation of proliferation.

Another requirement for normal closure of the cranial neural tube is normal function of the actin cytoskeleton. Disruption of the actin cytoskeleton in embryo culture by reagents such as cytochalasin D causes exencephaly (Ybot-Gonzalez and Copp, 1999), although spinal neurulation is apparently unaffected. Loss of function of cytoskeletal proteins, such as shroom, cytoskeleton associated proteins (e.g. cofilin) or proteins that regulate cytoskeletal function (e.g. MARCKS), can each result in cranial NTDs (Harris and Juriloff, 2007; Copp and Greene, 2010; Massa et al., 2009).

In the spinal region, bending of the neuroepithelium at the median hinge point (MHP) and the dorsolateral hinge points (DLHPs) is regulated by mutually antagonistic signals external to the neural folds. Experimental manipulation of chick and mouse embryos suggest the MHP is induced by signals from the notochord (Greene and Copp, 2004), while formation of DLHPs depends on signals from the surface ectoderm, since unilateral removal of the surface ectoderm results in loss of dorsolateral bending of the subjacent neural fold (Ybot-Gonzalez et al., 2002). However, the neural tube can close in the absence of MHP as shown by the absence of NTDs in mouse embryos in which the floor plate did not form. One example is the sonic hedgehog (Shh) mouse mutant, in which the floor plate of the neural tube does not form owing to loss of Shh signal from the notochord (Copp and Greene, 2010; Echelard et al., 1993).

A cellular mechanism suggested to account for bending of the neuroepithelium at the hinge points is the predominance of cells that are wedge-shaped, with a wider basal (nonluminal) pole (Greene and Copp, 2004). Possible explanations for cell wedging include localised apical constriction of neuroepithelial cells and cell cycle-dependent variations in the apicobasal position of nuclei within the pseudostratified neuroepithelium (Copp et al., 2003, Greene and Copp, 2009a).

Finally, once the tips of the neural folds achieve apposition at the dorsal midline, fusion must occur at the contact points in order to complete neural tube formation. Subsequent to adhesion and fusion, the neural fold apices remodel to create two continuous epithelial layers: the surface ectoderm and the neuroepithelium itself. The mechanism of adhesion and fusion is not well known, however, failure of adhesion would be expected to result in NTDs, and the mouse embryos lacking ephrin-A5 (cell surface Eph ligand) and EphA7 receptor (potential ligand of EphA5) exhibit exencephaly (Greene and Copp, 2004; Holmberg et al., 2000). Recent studies, in which Ephrin A-EphA interactions were disrupted in cultured mouse embryos suggest that these molecules are also required for closure in the spinal region (bdul-Aziz et al., 2009).

1.5 Prevention of NTDs in mouse models

Studies in humans showed that folic acid supplements can prevent NTDs, although the mechanism is not clear. Conversely, sub-optimal maternal folate levels or vitamin B12 or elevated levels of homocysteine are risk factors (Wald et al., 1991; Kirke et al., 1993; Molloy et al., 2009). Some of the mouse models for NTDs have been tested for response to folic acid as well as other agents such as methionine and inositol (examples are listed in **Table 1.1**).

Identification of mouse models of NTDs in which folic acid has a protective effect provides models for investigation of the mechanism by which NTDs are prevented. Treatment of *splotch* (Sp^{2H}) embryos with folic acid *in vivo*, by maternal intraperitoneal injection, (10 mg/kg body weight) or in embryo culture (200 μg/ml) reduces the frequency of NTDs in homozygous mutant embryos by up to 65% (Fleming and Copp, 1998). Folate-deficiency has also been induced in mouse embryos by maintaining females on folate-deficient diets prior to mating. In wild-type mice folate deficiency

causes growth retardation but not NTDs (Burgoon et al., 2002; Burren et al., 2008). However, folate deficiency can increase the frequency of exencephaly in *splotch* (Sp^{2H}) and *curly tail* mutants (Burren et al., 2008; Burren et al., 2010), demonstrating gene-environment interactions between folate status and genetic predisposition to NTDs. In these models the folate content of the embryo appeared to place a strict limit on developmental progression and it was hypothesised that NTDs are caused by inhibition of proliferation in the neural folds.

Mutants that are not responsive to folic acid include *axial defects* (*Axd*) and *curly tail*, in which the incidence of spina bifida is not reduced among embryos which mothers received folinic acid or B_{12} vitamin (Greene and Copp, 2005). Methionine has been tested as for its possible protective effect owing as elevated homocysteine or diminished vitamin B_{12}, both risk factors for NTDs, could indicate reduced conversion of homocysteine to methionine (Beaudin and Stover, 2009). Folic acid (the synthetic form of the vitamin) is converted to the bioactive form, tetrahydrofolate, to enter the folate cycle. Inside the cell, folate molecules function as acceptor and donors of one-carbon units, in pathways required for pyrimidine and purine synthesis and the remethylation of homocysteine to methionine required for the methylation cycle. Moreover, in the mouse folate deficiency causes reduced activity of the methylation cycle (Burren et al., 2008), while direct inhibition of the methylation cycle causes cranial NTDs (Dunlevy et al., 2006b). While methionine has no protective effect in *curly tail* (Van Straaten and Copp, 2001), there was a 40% reduction in frequency of spina bifida in *axial defects* mutants following maternal methionine supplementation (70 mg/kg intraperitoneal injection) at embryonic days 8.0 and 9.0 (Essien, 1992). In other cases, addition of methionine to embryo culture medium actually caused cranial NTDs, including *splotch* heterozygotes (Sp^{2H}) which do not normally develop defects (Fleming and Copp, 1998) and in non-mutant CD1 embryos (Dunlevy et al., 2006a).

Mutant or strain	Type of NTD	Folic/folinic acid response (%)	Methionine response (%)	Inositol response (%)
***Cart1* null**	Exenc	85	-	-
***Cited2* null**	Exenc	80	-	-
***Sp*^{2H}**	SB +/or exenc	40-65	-	-
Axd	SB	None	50	-
***Efna5* null**	Exenc	None	-	-
Ct	SB (occasional exenc)	None	None	70-85
***Grhl3*$^{-/-}$**	SB (occasional exenc	None	-	None

Table 1.1 Prevention of NTDs in mouse models. Examples of mouse mutants in which maternal agents have been tested in the prevention of NTDs. The vitamin response is given as percentage (%) of prevention (Adapted from (Greene and Copp, 2005; Harris and Juriloff, 2007; Harris, 2009). Abbreviations: Exc, exencephaly; SB, spina bifida; -, no information.

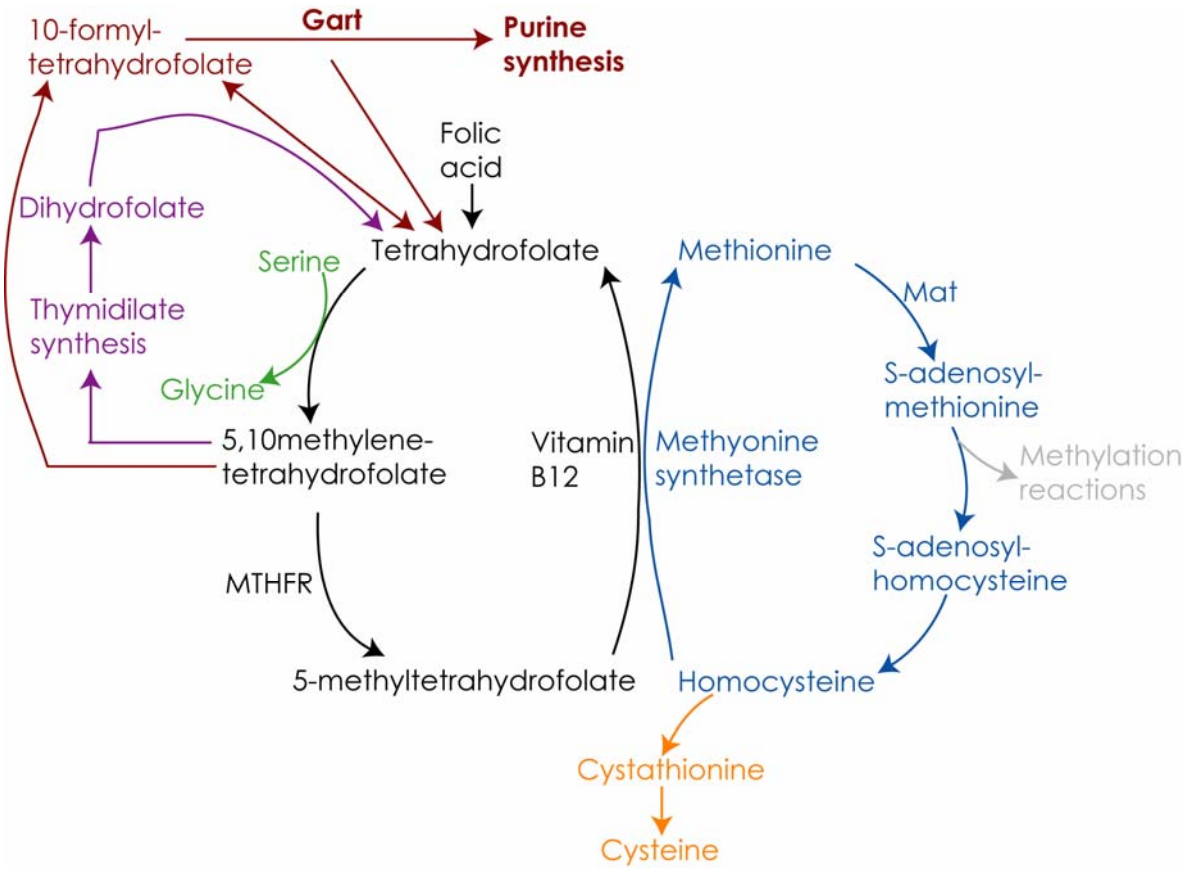

Figure 1.3 Diagram of folate one–carbon metabolism. Folate metabolism (black) is required for *de novo* synthesis of purines (dark-red) and thymidylate (Pyrimidine metabolism, purple) and for the remethylation of homocysteine to methionine (Methylation cycle, blue).

1.6 The *curly tail* mouse model

The *curly tail* (*ct*) mutation arose spontaneously in the GFF inbred strain at the Glaxo Laboratories in 1950, and has been maintained by homozygous matings of an initial cross between an affected *ct/ct* female and CBA/Gr inbred male (Van Straaten and Copp, 2001). The *ct* mutation has incomplete penetrance and variable expressivity such that homozygous *curly tail* embryos (*ct/ct*) develop: normally (40%), whereas 60% develop NTDs comprising exencephaly (3-5%), spina bifida (14-15%) and tail flexion defects (50%; **Fig. 1.4;** (Van Straaten and Copp, 2001).

Initial observations suggested that the defects in these mice were probably caused by a recessive gene, whose effect on neural tube closure is affected by the genetic

background. This was shown in linkage studies to map the *ct* mutation, in which *curly tail* mice were crossed with several inbred strains. On some backgrounds the frequency of NTDs was similar to the original *curly tail* strain (e.g., 18.5% in C57BL/6), while other genetic backgrounds resulted in lower frequency (2.2% in DBA/2; (Neumann et al., 1994). Therefore, penetrance of the *ct* trait is influenced by the genetic background, such that modifier genes act to increase or ameliorate the defects. Modifier genes have been mapped to chromosomes 3, 5 and 17 (Neumann et al., 1994; Letts et al., 1995), but the identity and function of these genes is unknown. These linkage studies also showed that rather than a recessive mutation, *ct* should be considered semi-dominant since abnormal tails were detected in a small proportion of mice heterozygous at the *ct* locus (Neumann et al., 1994; Beier et al., 1995).

The existence of modifier genes provided evidence of multifactorial inheritance in *curly tail* as in humans. A number of other characteristics of the *curly tail* mouse mutant resemble the defects in human cases of spina bifida, and *curly tail* has been considered to be a good model to investigate the human defects. Similarities between *curly tail* and human NTDs include the location of the spina bifida lesion at the lumbosacral level (Manning et al., 2000) the presence of elevated alpha-fetoprotein in the amniotic fluid (Van Straaten and Copp, 2001; Van Straaten and Copp, 2001), and the excess of females compared to males among exencephalic embryos (Embury et al., 1979; Seller, 1987; Brook et al., 1994). In addition, the penetrance of defects can be influenced by environmental factors such as temperature and exogenous agents (see **Section 1.6.1**).

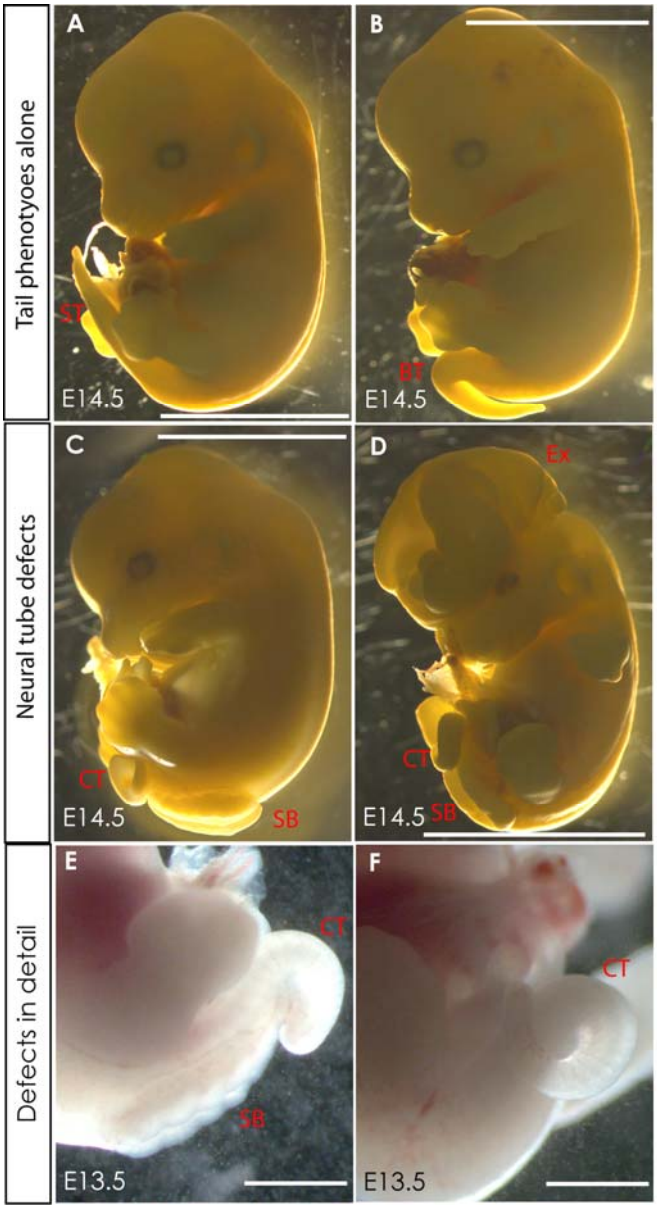

Figure 1.4 Phenotypes observed among homozygous *curly tail* (*ct/ct*) embryos. (**A**) Straight tail (ST), as observed in around 40% of *curly tail* embryos which appear to develop normally. (**B**) Tail flexion defects such as bent tail (BT) occur in 50% of homozygotes. (**C**) Spina bifida (SB) accompanied by tail flexion defect (curled tail, CT) in 14-15% of the embryos. (**D**) Occasionally (~3-5%), embryos develop exencephaly (Ex) which can be in isolation or accompanied by a tail flexion defect and/or SB. (**E-F**) Higher magnifications of the caudal region of embryos with SB and CT (**E**) or CT alone (**F**). Scale bars: 1.0 mm.

The developmental origin of spinal NTDs in *curly tail* embryos is a failure or delay in closure of the posterior neuropore (PNP), progressing to spina bifida and tail flexion defects respectively (Copp, 1985a). Moreover, embryos developing spinal NTDs can be distinguished from their littermates on the basis of the enlarged PNP length at E10.5 (Copp, 1985a). The PNP size can be denoted as category 1/2, small neuropores (SPNP), which correlate with normal development in the majority of embryos; category 3 , moderately enlarged neuropores (MPNP), are observed in embryos that develop normally in 30% of cases, the remainder develop tail defects, and few develop spina bifida; category 4/5 refers to enlarged neuropores (LPNP), which predicts around normal development in 10% of embryos high likelihood of spina bifida and tail defects, or tail defects alone.

Among *curly tail* embryos, those with enlarged PNP (category 4/5; also denominated affected) have an abnormally low proliferation rate in the hindgut endoderm and notochord compared to embryos with small PNPs (category 1/2, closing normally) whereas the neuroepithelium maintains a normal rate of cell division (Copp et al., 1988a; Copp et al., 1988b). This growth imbalance causes pronounced ventral curvature of the caudal region which inhibits closure of the PNP (**Fig. 1.5**; (Brook et al., 1991; Peeters et al., 1996). The increased axial curvature and delayed closure of the PNP in *curly tail* embryos can be recognised from somite stage 25-27, while in those embryos where PNP closure does occur this is complete by the 30-31 somite stage (Copp et al., 1982; Copp, 1985a; Brook et al., 1991; Peeters et al., 1998).

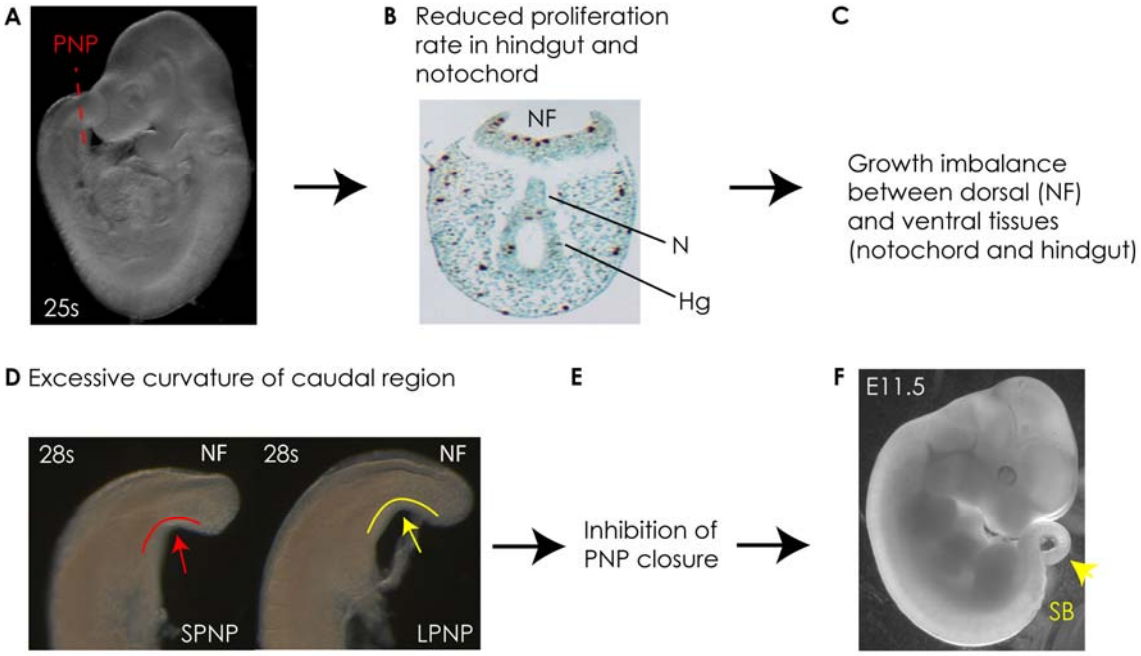

Figure 1.5 Cellular mechanism underlying delay of PNP closure in *curly tail* embryos. (**A**) *Curly tail* embryo at 25 somites stage. (**B**) Section through the posterior neuropore (PNP, dashed line in **A**). In embryos with enlarged PNP there is reduced cell proliferation in the hindgut endoderm (Hg) and in the notochord (N), compared to embryos with small PNP sizes, whereas proliferation in the neuroepithelium (neural folds, NF) does not differ with PNP size. (**C-D**) This cell proliferation defect causes an imbalance between the ventral and the dorsal tissues, resulting in increased ventral curvature (yellow arrow), which mechanically opposes apposition of the NF, inhibiting neural tube closure at the level of the PNP. (**D-F**) In embryos with a small PNP (SPNP) closure occurs normally. Embryos with moderately enlarged PNP (MPNP) are more likely to have a delay in closure, and to develop tail flexion defects. In embryos with large PNP (LPNP) closure is prone to fail resulting in spina bifida (SB) and a curled tail (yellow arrowhead, **F**) as observed at E11.5 (Copp et al., 1988a; Copp, 1985a; Brook et al., 1991; Peeters et al., 1996). Images used in this figure were generated in the course of this project.

Although it has been established that delay of the posterior neuropore closure causes tail flexion defects in *curly tail* embryos, the mechanism by which the tail bends or curls remains unclear. It has been suggested that there is an abnormal transition from primary to secondary neurulation (which starts at around the time of posterior neuropore

closure), subsequent to delayed closure of the PNP (Copp et al., 1982). **Figure 1.6** shows sections at the transition between primary and secondary neurulation.

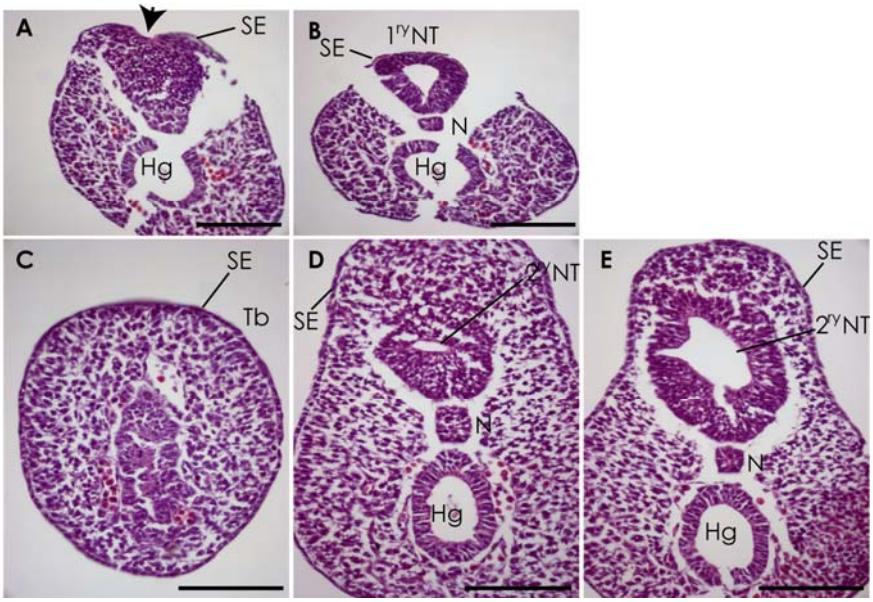

Figure 1.6 Haematoxylin-eosin stained transverse sections of mouse embryos at the level of the tail bud. Sections are arranged caudally to rostrally for two embryos (**A-B** and **C-E**). A condensation of mesodermal cells (arrowhead in **A**) is observed that will canalise to form the secondary neural tube in a section (**A**) caudal to the level of the closed primary neural tube (**B**). (**C-E**) In an embryo with 33 somites in which the posterior neuropore failed to close, a condensation of cells is visible in the tail bud (Tb, **C**). At more rostral levels (**D-E**) a central lumen forms in this condensation which will form the secondary neural tube (2^{ry} NT in D), with a circular lumen as observed in (**E**). Abbreviations: Hg, hindgut; N, notochord; NF, neural folds; SE, surface ectoderm. Scale bars: 0.1 mm. Images used in this figure were generated in the course of this project.

1.6.1 Environmental factors and NTDs in *curly tail*

Several environmental factors have been found to affect the penetrance of spinal NTDs in *curly tail* embryos. These include teratogens such as anti-mitotics, hyperthermia, and levels of nutrients such as inositol and folate (Cockroft et al., 1992; Van Straaten and Copp, 2001; Burren et al., 2010). The interaction of the *ct* mutation with environmental

factors has been useful both in understanding the underlying developmental defects and in identification of possible preventive agents. For example, growth retardation of embryos by exposure to hyperthermia, corrected the growth imbalance between dorsal and ventral tissues and normalised PNP closure (Peeters et al., 1996), supporting the idea that the proliferation imbalance plays a causative role in NTDs.

Retinoic acid (an active metabolite of vitamin A, and a known teratogen) has been shown to play a role in neural tube closure (Seller et al., 1979). Normal expression of retinoic acid receptor-β (RAR-β) is normally expressed in the hindgut, but was found to be down-regulated in affected *curly tail* embryos, while RAR-γ was down-regulated in the PNP and tail bud (Chen et al., 1995). Supporting a possible role for abnormal RAR function in spinal NTDs, administration of low doses of retinoic acid to pregnant *curly tail* females (E10, before posterior neuropore closure), increased the expression of RAR-β in the hindgut, and reduced the frequency of spina bifida (Chen et al., 1994). Therefore, it has been suggested that RAR-β plays a role in the causation of the hindgut proliferation defect in *curly tail* (Chen et al., 1995).

Several studies have examined the possible effect of folic acid or other one carbon metabolites on the frequency of NTDs in *curly tail*. Folate one-carbon metabolism is summarised in **Figure 1.3 (Section 1.5)**

Folic acid has been found to reduce the frequency of NTDs in some mouse models such as *splotch* (*Sp*^{2H}), while methionine has been found to be protective in others such as the *axial defects* (*Axd*) mutant (Essien, 1992). However, neither folic acid nor methionine have been found to reduce the incidence of NTDs in *curly tail* (Van Straaten and Copp, 2001; Van Straaten et al., 1995). However, dietary folate deficiency has been found increase the frequency of cranial NTDs in both *curly tail* and a genetically matched wild-type strain (Burren et al., 2010). These findings suggest the presence of one or more loci in the *curly tail* genetic background that give susceptibility to folate deficiency-related NTDs, as NTDs are not induced by folate deficiency in wild-type embryos of other strains (Burgoon et al., 2002; Burren et al., 2008). In addition, some evidence suggests the possible presence of disturbed folate one-carbon metabolism in the *curly tail* strains, particularly involving the methylation cycle. Adult *curly tail* mice exhibit higher levels of homocysteine and s-adenosylhomocysteine ratio of s-

adenosylmethionine to s-adenosylhomocysteine (SAM/SAH) in the liver than C57Bl/6 mice, suggesting a possible sub-optimal methylation potential (Tran et al., 2002). This could be relevant to the development of NTDs as inhibition of the methylation cycle has been found to cause cranial NTDs (Dunlevy et al., 2006a). In contrast, folate deficiency was found to result in an increase in the SAM/SAH ratio in *curly tail* embryos unlike other strains where folate deficiency causes diminished SAM/SAH ratio (de Castro et al., 2010). Therefore it appears that reduced methylation is an unlikely cause of cranial NTDs in *curly tail* particularly as there is no apparent increase in the frequency of NTDs in homozygous *ct/ct* embryos that are also null for 5,10-methylenetetrahydrofolate reductase (*Mthfr*) and have very low SAM/SAH ratio (de Castro et al., 2010).

The lack of protective effect of folic acid has led to the use of *curly tail* as a possible model for folic acid-resistant NTDs (Greene and Copp, 2005). In contrast to folic acid and methionine, administration of inositol during mouse pregnancy or in whole embryo culture normalises closure of the PNP and reduces the incidence of spina bifida (**Fig. 1.7**; (Greene and Copp, 1997; Cogram et al., 2002). Inositol is thought to act by increasing flux through the inositol/lipid cycle, which stimulates protein kinase C activity), in the underlying hindgut endoderm and corrects the proliferation defect, which normalises neural tube closure (Greene and Copp, 1997; Cogram et al., 2004). PKC acts to phosphorylate other proteins altering their function in a cell-type specific manner. The PKCβI and PKCγ isoforms were found to be specifically required for the prevention of NTDs (Cogram et al., 2004) but the critical downstream targets of PKC have not yet been identified in treated *ct/ct* embryos.

Interestingly, loss of phosphatidylinositol-4-phosphate 5 kinase (*PIP5Kiγ*; (Wang et al., 2007), or reduced levels of inositol 1,3,4-triphosphate 5/6-kinase (*IPTK1*; (Wilson et al., 2009; Majerus et al., 2010), two enzymes in the inositol pathway result in cranial and spinal NTDs.

The preventive effect of inositol in mice encouraged the view that a clinical trial in humans would be worthwhile to test whether inositol may be a useful adjunct therapy to folic acid, for preventing folate-resistant NTDs cases. Studies in Italy reported the first cases of use of periconceptional inositol in patients with a history of NTDs despite use

of folic acid. No NTDs occurred in 6 pregnancies and while this is not a statistically significant finding no deleterious effects of inositol usage during pregnancy were reported (Cavalli and Copp, 2002; Cavalli et al., 2008). A randomised clinical trial, Prevention of Neural Tube Defects by Inositol (PONTI) study, is now being carried out to test whether a combined treatment with inositol and folate is more effective than folic acid alone for prevention of NTDs in women with a high recurrence risk, having a history of at least one affected pregnancy.

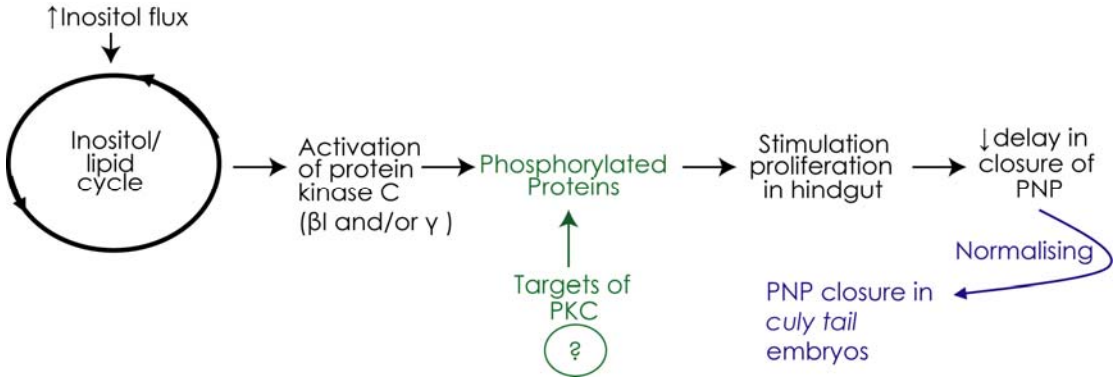

Figure 1.7 Diagrams of the proposed mechanism underlying rescue of NTDs in *curly tail* mice by inositol. Mechanism by which inositol rescues spinal NTDs in *ct/ct* embryos. Exogenous inositol is incorporated into the inositol-lipid cycle, and through downstream signals, PKC isoforms are activated. Subsequent phosphorylation of specific substrates results in the correction of the proliferation defect in the hindgut, and normalises posterior neuropore (PNP) closure. The downstream targets of PKC (?) are not yet known.

1.6.2 *Curly tail* genetics – *ct* is a hypomorphic allele of *Grhl3*

The *ct* genetic defect was mapped to chromosome 4 by linkage studies using microsatellite markers (Neumann et al., 1994; Beier et al., 1995), to a region containing *grainyhead-like-3* (*Grhl3*, also known as *Get-1*), which encodes a transcription factor (Ting et al., 2003a; Kudryavtseva et al., 2003). Gene targeting studies have shown that *Grhl3* is essential for neural tube closure. *Grhl3* knockout mice (*Grhl3*$^{-/-}$) develop NTDs with 100% penetrance and do not survive (Ting et al., 2003a; Yu et al., 2006e). NTDs comprise thoracolumbosacral spina bifida (100% penetrance) and curled tail, and

exencephaly (2-14% depending on the study). Heterozygous (*Grhl3*$^{+/-}$) mice were indistinguishable from their wild-type littermates.

A proliferation assay suggested that there may be reduced proliferation in ventral tissues of *Grhl3*$^{-/-}$ compared with *Grhl3*$^{+/+}$ embryos. No coding mutation in *Grhl3* was identified in *curly tail* leading to the suggestion that *ct* could be a hypomorphic allele of *Grhl3*, with reduced expression (Ting et al., 2003a). Subsequently it was demonstrated that *Grhl3* is indeed expressed in the hindgut endoderm at E10.5, the tissue in which the causative cellular defect is present, and that expression levels are reduce in *ct/ct* compared with matched wild-type embryos at the stage of PNP closure (Gustavsson et al., 2007). This expression deficit was proposed to be due to a putative regulatory mutation 21,350 base pairs upstream of the starting site, characterised by a single nucleotide substitution C/T (C-21350T).

To test the hypothesis that reduced expression of *Grhl3* causes spina bifida in *ct/ct* embryos, a rescue experiment was performed to reinstate *Grhl3* expression in *curly tail* embryos. A bacterial artificial chromosome (BAC) containing the complete *Grhl3* gene and 120 kb of upstream sequence, encompassing the putative *ct* mutation, was used to generate a *curly tail* transgenic line carrying the BAC (summarised in **Fig. 1.8)**. Transgenic, *ct/ct*^{TgGrhl3}, mice were crossed to *ct/ct* mice to generate offspring, among which all embryos that carried the BAC developed normally without spina bifida or tail flexion defects, whereas *ct/ct* littermates showed the usual phenotypes. *Grhl3* transgenic embryos showed up-regulation in the expression of *Grhl3* and the apparent rescue of the spinal defects normally observed in *ct/ct* embryos supported the idea that reduced expression of *Grhl3* is the cause of spina bifida in *ct/ct* embryos (Gustavsson et al., 2007).

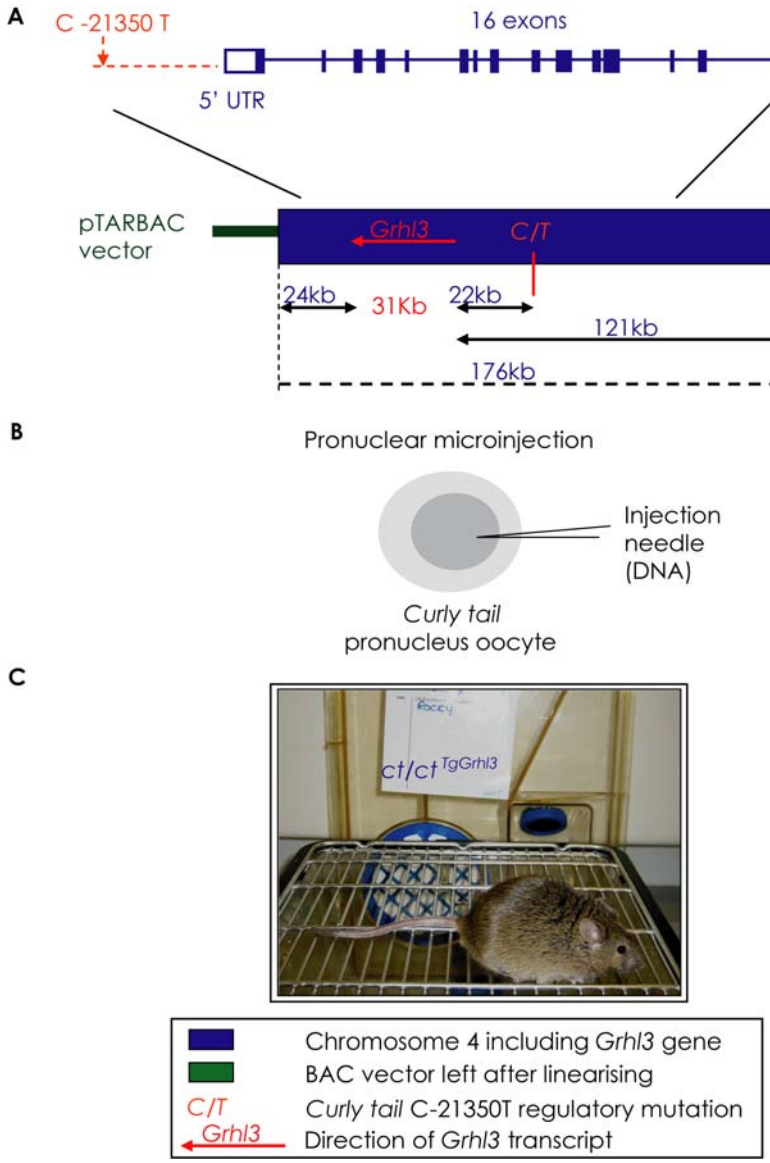

Figure 1.8 Diagram of generation of the *Grhl3*-BAC transgenic mouse. (A) The linearised BAC contained 31.7 kb full-length *Grhl3* gene (2.8 kb transcript length), plus 120 kb upstream of the initiation site (including the region of the single nucleotide substitution) and a short region of pTARBAC vector. **(B)** After linearization and purification of the BAC, the DNA was injected into the pronucleus of fertilised *curly tail* oocytes which were transferred to surrogate CD1 mothers. **(C)** Transgenic litters were generated from a founder transgenic mouse, $ct/ct^{TgGrhl3}$.

1.6.3 Genetic interaction of *curly tail* and *grainyhead like-3* mutant strains with other strains

The effect of combination of *ct* or *Grhl3* null alleles with mutation of other genes has been tested in several studies. Homozygous *splotch* (Sp^{2H}) mutant embryos develop spina bifida in 85-100% of embryos owing to a mutation in *Pax3* (Greene et al., 2009a). Double heterozygous (*ct/+;Sp/+*) exhibited tail flexion defect in 10% of the cases, while mice heterozygous for *curly tail* or *splotch* rarely develop NTDs defects. In addition, backcrossing double heterozygotes to *curly tail* mice generated *ct/ct;Sp/+* which showed almost 100% penetrance of spina bifida and curled tail (Estibeiro et al., 1993). There was no apparent increase in the ventral curvature of the caudal region of *ct/ct* embryos when the *Pax3* mutant allele was present, suggesting that the downstream effects of the *ct* and Sp^{2H} mutations are different but summate to risk of increase spinal NTDs.

Matings between homozygous *curly tail* mice with doubly heterozygous *looptail/ct* mice (*Lp/+*; *ct/+*) allowed generation of embryos with a *Lp/+;ct/ct* genotype that develop spina bifida with high frequency (85%) compared to a low frequency (10%) in *+/+;ct/ct* embryos in this cross (Stiefel and Meuli, 2007); AJ Copp, Personal Communication). Heterozygous (*Lp/+*) mice exhibit tail defects (looped tail) and occasional low sacral spina bifida due to delayed posterior neuropore closure (similar to *curly tail* and *splotch mutants),* but are generally viable (Copp et al., 1994). Thus, the *Lp* allele modifies the risk of spinal NTDs in *curly tail*. *Loop-tail* (*Lp*) mice carry a mutation in *Vangl2*, a gene whose product is necessary for convergent extension of the neural plate during neural tube closure, and *Lp/Lp* homozygous embryos develop craniorachischisis with 100% penetrance (Copp et al., 2003; Greene et al., 1998). However, more recently, another study showed an interaction between *Lp* and *Grhl3* by interbreeding $Vangl2^{+/-}$ (*Lp/+*) mice with $Grhl3^{+/-}$ (Caddy et al., 2010). Both the individual heterozygotes normally complete neural tube closure but 67% of the compound heterozygotes ($Vangl2^{+/-};Grhl3^{+/-}$) exhibited spina bifida resembling that observed in *Grhl3* null embryos By comparison, none of the $Vangl2^{+/+};Grhl3^{+/-}$ embryos exhibited NTDs while 87% of $Vangl2^{+/-};Grhl3^{+/+}$ embryos developed a looped tail alone and 13% exhibited spina bifida, perhaps like *Lp/+* embryos. The authors therefore suggested that *Grhl3* functions like *Vangl2* to regulate the planar cell polarity signalling pathway. However, unlike core members of the planar cell polarity pathway

Grhl3 is not necessary for Closure 1 (Rifat et al., 2010), and is a transcription factor rather than a component of a signalling pathway. Therefore, this connection requires further investigation.

Null embryos for another member of the *Grhl* family, *Grh2*, develop fully penetrant cranial NTDs characterised by 'split-face' malformation (failure of Closure 3), and die at E11.5 with the posterior neuropore still open, indicating that spina bifida would occur if embryos survived (Rifat et al., 2010). A small proportion of $Grhl2^{+/-};Grhl3^{+/-}$ developed mid- and hindbrain exencephaly (failure of Closure 2), similar to cranial NTDs defects in $Grhl3^{-/-}$ mutants. Embryos with a $Grhl2^{+/-};Grhl3^{-/-}$ genotype exhibited thoraco-lumbosacral spina bifida and mid- hindbrain exencephaly with 100% penetrance. Both phenotypes resemble those observed in $Grhl3^{-/-}$ mutants suggesting that *Grhl3* is not necessary for closure of the rostral forebrain. $Grhl2^{-/-};Grhl3^{+/-}$ embryos exhibited split-face and fully penetrant thoraco-lumbosacral spina bifida. Double mutant $Grhl2^{-/-};Grhl3^{-/-}$ embryos had a very severe phenotype in which closure did not progress beyond the site of Closure 1 such that the neural folds remained open throughout the cranial and spinal regions (Rifat et al., 2010).

One of the genes known to interact with *Grhl3* was originally identified on the basis of interaction, in a yeast two hybrid screen, with the LIM-only protein 4, Lmo4 (Kudryavtseva et al., 2003). *Lmo4* expression colocalises with *Grhl3* in the cells of the surface ectoderm, and it is also expressed in dividing neuroepithelial cells within the ventricular zone along the entire rostro-caudal axis of the nervous system (Kudryavtseva et al., 2003). $Lmo4^{-/-}$ null mice, generated by gene targeting, die at birth and show abnormal neural tube closure (Lee et al., 2005). Interestingly, *Lmo4* mutants exhibit exencephaly due to failure of closure of the neural tube at all cranial levels. To generate double knockouts, $Lmo4^{+/-}$ mice were crossed to $Grhl3^{+/-}$ mice, and double knockout embryos exhibited exencephaly in 100% of cases, showing that these two genes not only interact biochemically but also genetically (Yu et al., 2006e).

1.6.4 Functions of *grainyhead-like* transcription factors

Grhl3 belongs to the Grh/CP2 family of proteins (**Fig. 1.9**). Mammalian GRH-like members are involved in transcription regulation, can bind DNA and other proteins, and as well as neural tube closure, have been functionally implicated in biological processes such as epidermis development (Wilanowski et al., 2002; Ting et al., 2005; Kudryavtseva et al., 2003), and wound healing (Ting et al., 2005). *Grhl1, Grhl2* and *Grhl3* have all been found to be expressed in epithelial tissues in developing mouse embryos (Wilanowski et al., 2002; Ting et al., 2003a; Kudryavtseva et al., 2003).

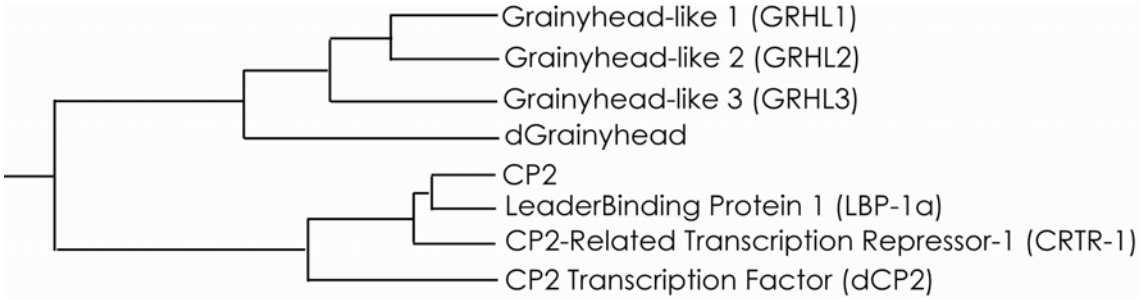

Figure 1.9 Grainyhead-like family members. Sequence alignment of the *Drosophila* (dCP2, dGrainyhead) and mammalian *Grainyhead-like/CP2* genes suggested they share a common ancestor and can be divided into two phylogenetic groups. The mammalian GRHL genes, *GRHL1* (previously known as mammalian *GRH*), *GRHL2* (Brother of Mammalian *GRH*) and *GRHL3* (Sister of Mammalian *GRH*) are homologous to their *Drosophila* counterpart, dGrainyhead. Phylogenetic tree adapted from Wilanowski et al. (2002).

Prior to cloning of the mammalian homologues studies on *grainyhead* (*grh*; also known as Neurogenic element binding transcription factor, NTF-1/Elf-1), had been performed in *Drosophila melanogaster.* Grainyhead was first identified *in vitro* as a protein (GRH) that could bind to and activate transcription from the *Dopa decarboxylase* (*Ddc*) promoter (Bray et al., 1988; Dynlacht et al., 1989). GRH is required for expression of *Ddc* in epidermal cells but it does not influence neuronal expression of *Ddc* (Bray and Kafatos, 1991b). The importance of *grh* during *Drosophila* development is shown by the fact that mutations in this gene result in an embryonic lethal phenotype. Mutant embryos have flimsy cuticles, grainy discontinuous head skeletons, and patchy tracheal tubes (Bray and Kafatos, 1991b).

Grainyhead is a maternal gene, for which the mRNA is synthesized during oogenesis and deposited in the developing oocyte until translated (Huang et al., 1995). Later on, neuroblasts switch on *Grh* expression and maintain it through many subsequent divisions, and this appears to be important for specification of the regionalised patterns of neurogenesis that are characteristic of post-embryonic stages. For example, in the thorax, *Grh* prolongs neural proliferation by maintaining neuroblasts in a mitotically active state. In contrast, in the abdomen, *Grh* terminates neural proliferation by regulating the competence of neuroblasts to undergo apoptosis in response to *Abdominal-A* (*AbdA*, *Hox* gene) expression (Cenci and Gould, 2005). Thus, *Grh* is linked to the *Hox*-mediated axial patterning system in *Drosophila*, and can have pro-proliferative or anti-proliferative functions in different tissues.

The three mammalian *grainyhead-like* genes share a high degree of sequence identity in the DNA-binding, protein dimerization and activation domains (Wilanowski et al., 2002; Ting et al., 2005; Ting et al., 2003b). Protein interaction studies demonstrated that GRHL3 can homodimerize, as well as heterodimerize with GRHL1 and GRHL2, but not with the CP2-like members (Ting et al., 2003b). In addition, the transactivation domain of *Grhl3* located between amino acids 102 and 296 is inhibited when combined with N-terminal or C-terminal sequences. These data suggest that *Grhl3* contains repression domains in the N- and C-termini and this is consistent with strong repression observed in reporter assays using the C-terminus alone. Therefore, it is thought likely that *Grhl3* can act as a transcriptional activator or as a repressor (Kudryavtseva et al., 2003).

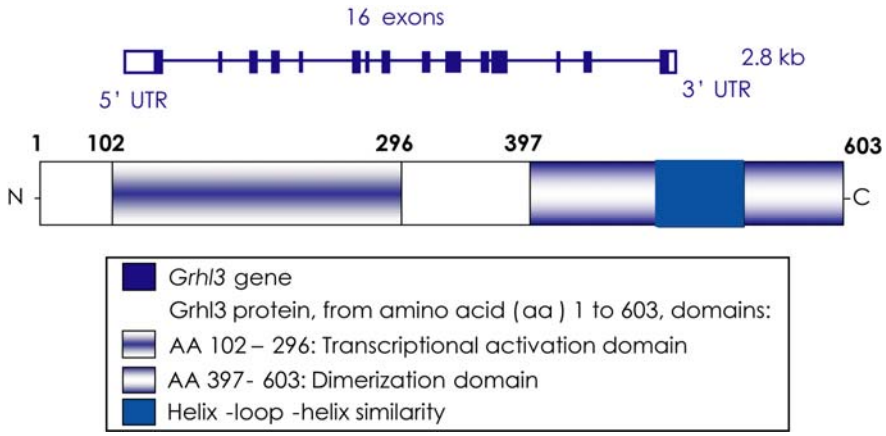

Figure 1.10 Diagram of the mouse *Grhl3* gene and protein. The *Grhl3* gene (Accession No ENSMUST00000105855) spans 31.7 kb and includes 16 exons and 15 introns, encoding a transcript length of 2.8 kb and a protein of 603 amino acids. The protein has two major functional domains, a DNA binding transcriptional activation domain at the N-terminal and a dimerisation domain which mediates protein-protein interactions at the C-terminus. These domains are critical for *Grhl3* function as a transcription factor. There is 90% identity between the predicted human and murine GRHL3 proteins (Ting et al., 2003b).

The three mammalian *Grhl* genes have restricted expression patterns during mouse development (Auden et al., 2006) Similar to *Drosophila* where grainyhead plays an important role in embryonic cuticle formation, *Grhl3* is expressed in surface epidermis as well as epithelial cells of the gastrointestinal, genitourinary and respiratory tracts (Kudryavtseva et al., 2003; Yu et al., 2009). The expression in skin appears essential for formation of the epidermal barrier (Ting et al., 2005; Yu et al., 2006e). It is notable that homologous genes in *Drospohila* and mammals are required for the integrity of the surface structure even though the *Drosophila* cuticle and mammalian skin are structurally quite dissimilar.

During mouse development, E14.5-E15.5, *Grhl1* is predominantly expressed in the epidermis/skin, while *Grhl2* expression is also observed in the skin, and in several internal organs, including lung, oesophagus and kidney (Wilanowski et al., 2002). At early stages of development, *Grhl1*-null mice show a delay in coat growth, and at later stages mice exhibit hair loss as a result of poor anchoring of the hair shaft in the follicle. These mice also develop palmoplantar keratoderma (Wilanowski et al., 2008). While

gene targeting of *Grhl2* in mice results in NTDs (Rifat et al., 2010), a link to human NTDs has not yet been reported. However, mutations in the human *GRHL2* gene are responsible for autosomal dominant type 28 non-syndromic sensorineural deafness (Peters et al., 2002). *GRHL3* has not yet been linked to a human disease. Like *Drosophila grainyhead* (*dgrh*), the human *GRHL* genes produce several distinct isoforms through alternative splicing (Wilanowski et al., 2002; Ting et al., 2005; Ting et al., 2003b) although whether these have any functional role is yet to be determined. However, there is no evidence of alternative splicing of *Grhl3* in the mouse (Gustavsson et al., 2008).

In summary, the Drosophila GRH gene is involved in several important biological processes including regulation of cell cycle, cell growth, and development (Wilanowski et al., 2002). In the mouse *Grhl3* is essential for neural tube closure (Ting et al., 2003a; Gustavsson et al., 2007). Studies in this thesis focus on mouse models in which abnormal expression of *Grhl3* results in development of NTDs. First, a proteomic analysis was performed to identify proteins that are differentially expressed of neurulation-stage *curly tail* and wild-type embryos (**Chapter 3**). One such protein, lamin B1, was investigated in detail and variation in sequence was found to modify the susceptibility to NTDs (**Chapter 4**). Finally, the consequences of over-expression of *Grhl3* were investigated and it was found that both excess and diminished expression of *Grhl3* are sufficient to cause NTDs (**Chapter 5**).

Chapter 2

Materials and Methods

2.1 Embryo collection

2.1.1 Experimental groups

Curly tail (*ct/ct*) stock was previously derived from crosses between an affected *ct/ct* female (GFF inbred strain) and a CBA/Gr male (Van Straaten and Copp, 2001). The colony is kept as a random bred and all individuals are considered to have *ct/ct* genotype. A congenic strain was previously generated by successive backcrosses to *ct/ct* (four generations) following an initial cross between *ct/ct* and mice of the SWR inbred strain, with genotyping of microsatellite markers to maintain SWR sequence at the *ct* locus . These genetically matched wild-type ($+^{ct}/+^{ct}$) mice are thus wild-type at the *ct* locus, while the genetic background is predicted to be 93.75% *curly tail*. These mice are maintained as a homozygous colony. The third strain used in this project is the *Grhl3*-transgenic *curly tail*, *Tg(Grhl3)1Ndeg* (Transgene Accession ID is MGI:3794067, referred to throughout this thesis as $ct/ct^{TgGrhl3}$), in which spinal neural tube closure occurs normally.

Male mice were housed individually once they had reached sexual maturity. Female mice were housed in small cages (capacity for 5 adult mice) and female breeding stocks were housed in larger ones with maximum capacity for ten adult mice. Standard pelleted food and water were freely available. Mouse rooms were maintained at 22˚C, with a relative humidity of 52% and a controlled diurnal cycle of 12 hours light and 12 hours dark.

Mice were used for experimental matings from six weeks of age. Litters were generated by timed matings in which mice were paired overnight and the day of finding a copulation plug was designated embryonic day 0.5 (E0.5). Owing to the fact that this project focuses on neural tube closure and more precisely the closure of the posterior neuropore (PNP), embryos were mostly collected at E10.5. PNP closure occurs in wild-type embryos at around the 30-31 somite stage and embryos were therefore subdivided according to the number of somites: 26-27, 28-29 and 30-31 (**Figure 2.1**).

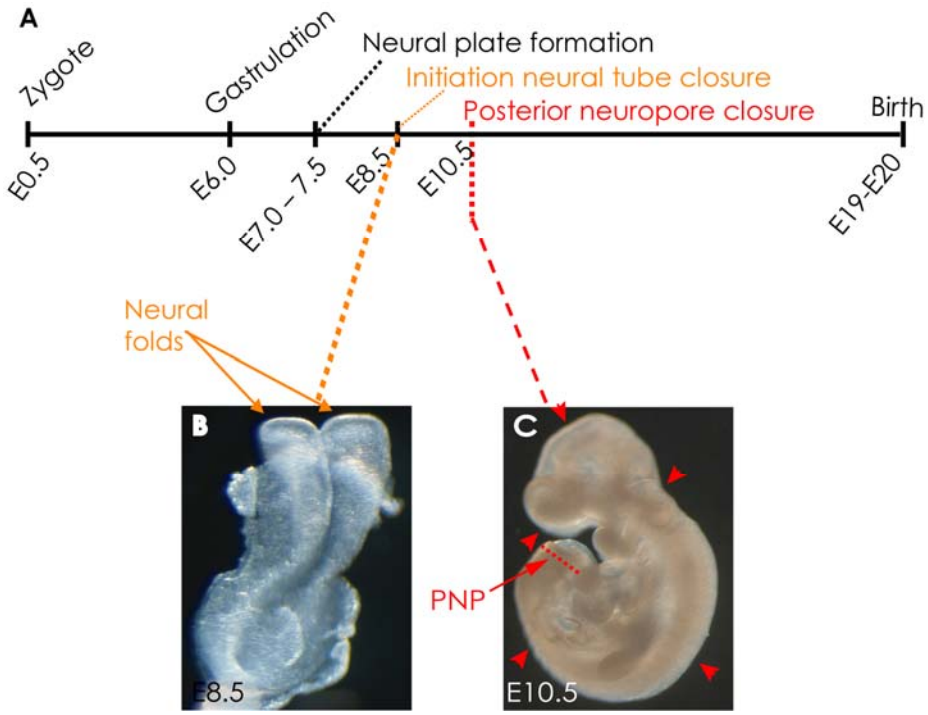

Figure 2.1 Mouse development and stages of posterior neuropore closure. (**A**) Key events during development of the mouse until birth. At embryonic day E8.0, closure of the neural tube initiates as the neural folds begin to elevate (**B**). The posterior neuropore (PNP, highlighted by the red-dotted lines in **C**) is the last region of the neural tube to close. At this same stage (E10.5) all other regions of the neural tube have closed (regions indicated by red arrowheads).

2.1.2 Embryo harvesting and collection

Pregnant females were killed by cervical dislocation. The uterus was removed and transferred to a bijoux containing Dulbeco's Modified Eagles Media (DMEM; Invitrogen) with 10% fetal bovine serum (heat inactivated at 58˚C; Invitrogen). The uterus was then transported to the laboratory for dissection of the embryos under a stereo-microscope (Zeiss SV6 or SV11).

The uterus was dissected in pre-warmed (37˚C) fresh media (**Fig. 2.2 A**). After counting the number of implantations, the decidua was removed from the uterus by tearing the uterine wall and releasing the decidua using forceps. The decidua was opened to allow removal of the conceptus contained within the trophoblast (**Fig. 2.2 B**). The trophoblast

tissue and Reichert's membrane were then removed to expose the embryo within the yolk sac (**Fig. 2.2 C-D**). After removing the yolk sac, the chorion, was also removed to completely expose the embryo (**Fig. 2.2 E**). The number of somites was counted in each embryo and the PNP length was also measured in some embryos using an eyepiece graticule (**Fig. 2.2 F**). The PNP length of *curly tail* embryos was allocated to broad categories; small, intermediate and large (**Table 2.1**).

After dissection, embryos were washed in diethyl pyrocarbonate (DEPC)-treated phosphate buffered saline (PBS; **Appendix A, section A.1-A.2**), or autoclaved PBS depending on the subsequent experiments:

a) For whole mount *in situ* hybridisation whole embryos were fixed in ice-cold 4% paraformaldehyde (PFA; **Appendix A**, **section A.3**) overnight at 4˚C. The following day they were washed twice in ice-cold DEPC-PBS, dehydrated on ice in a methanol (methanol:DEPC H_2O) series, 25%, 50%, 75% and 100%, and stored at -20˚C..
b) For immunohistochemistry whole embryos were fixed in 4% PFA as above. The following day embryos were washed in ice-cold PBS, dehydrated in an ice-cold ethanol series (absolute ethanol:H_2O) - 25%, 50%, and 70% and stored at 4˚C. In a few cases embryos stored in 100% methanol were needed for immunohistochemistry (IHC). In this case, they were washed twice in absolute ethanol, for 30 minutes each, at room-temperature and the appropriate protocol for IHC was then followed.
c) For protein (two-dimensional protein gel electrophoresis or western blot), or mRNA extraction (for quantitative real-time reverse transcription polymerase chain reaction). Whole embryos or the cranial or caudal region (below the level of somite 14-15) were rinsed in PBS to remove excess media and transferred to 1.5 ml clean eppendorfs. Excess PBS was removed and samples were immediately frozen on dry-ice straight before storage at -80˚C.

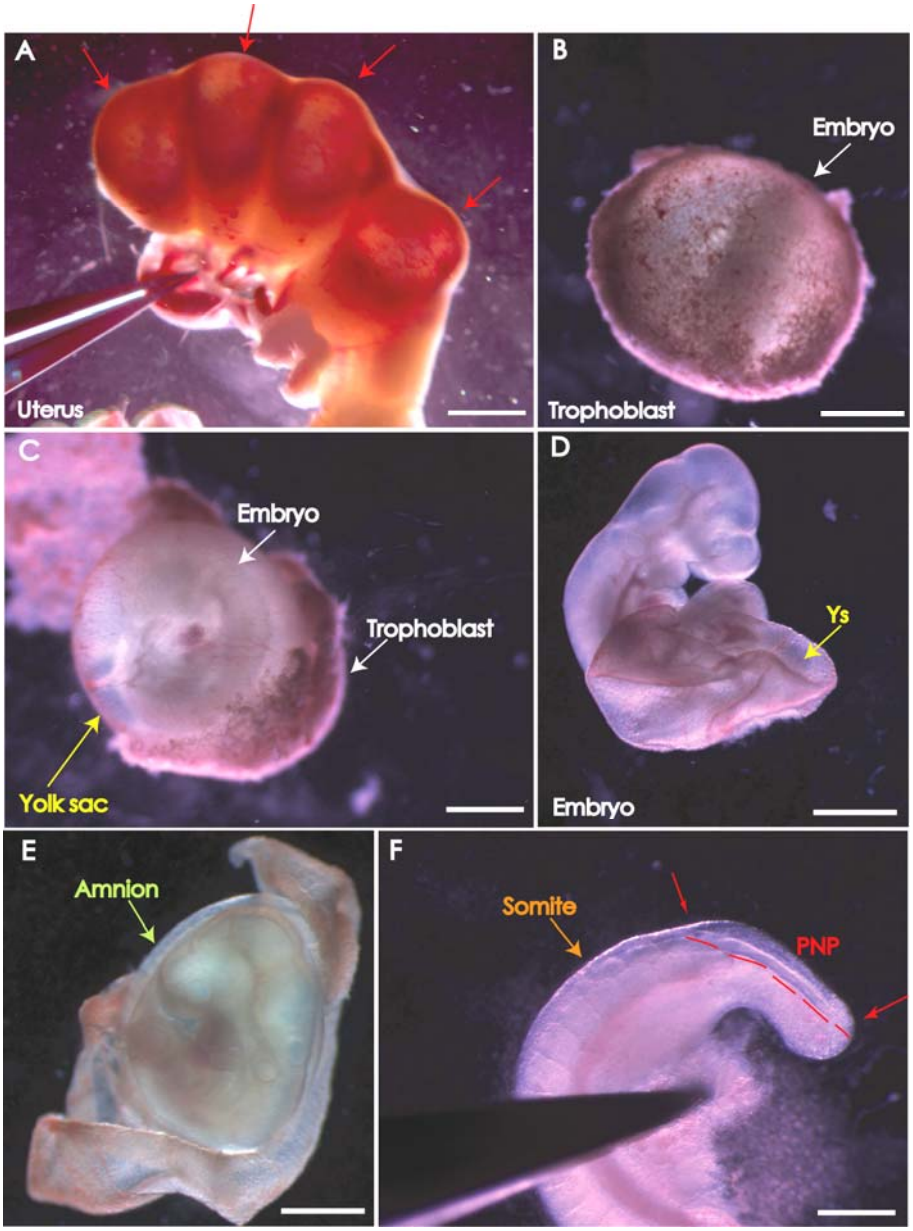

Figure 2.2 Embryo dissection. (**A**) Each individual implantation (red arrows) was removed from the uterus. Decidual tissue was removed to expose the trophoblast (**B**), which was peeled off to expose the embryo within the yolk sac (**C**). (**D-E**) After removal of the yolk sac (ys) the amnion (seen in E) was also removed if this was still intact. (**F**) The number of somites was counted and the length of the PNP was measured (in the image forceps are used to hold the caudal region in place for measurement).

At E11.5 – E18.5 embryos were dissected in ice-cold PBS. Embryos were either fixed in 4% PFA as previously described, or in Bouin's solution (Sigma) at room-temperature

for one or two days depending on the stage. After fixation, embryos were thoroughly washed in cold PBS, and dehydrated in an ethanol series up to 70% ethanol before storage at 4˚C. Bouin's fixative provides better preservation of tissue morphology than PFA and was preferable for histology (e.g., haematoxylin and eosin staining).

The yolk sac (ys) of all transgenic and some *ct/ct* or $+^{ct}/+^{ct}$ (used as controls) embryos were kept for DNA extraction for genotyping. After separation of the yolk sac from the embryo, it was rinsed in PBS and stored in an eppendorf on ice or at -20˚C prior to DNA extraction.

PNP	Category	28-29ss PNP length (mm)	30-31ss PNP length (mm)
Closed	[0]	0	0
SPNP	[1]	0.125-0.25	0.1-0.25
	[2]	0.3-0.45	0.3-0.45
Intermediate	[3]	0.5-0.625	0.5-0.625
LPNP	[4]	0.7-0.8	0.675-0.8
	[5]	0.925-0.95	0.875-1.0

Table 2.1 M**easurement of the posterior neuropore (PNP) length.** PNP length was measured on a stereo microscope (conversion of graticule to unis to mm: graticule units/100 x 2.5) and allocated to PNP categories, classified as small (SPNP), intermediate or large (LPNP).

2.2 Genomic DNA extraction from embryo or adult mouse tissue

Fresh or frozen yolk sacs, ear clippings or tail clippings were digested with proteinase K (10 mg/ml stock; **Appendix A**, **section A.4**). Proteinase K solution (12 µl for E7.5 – E9.5 stage yolk sacs, embryos, or ear clip samples and 24 µl for E10.5 yolk sacs, embryos, limbs of older embryos, or tail clip samples) was added to the sample and the digestion volume made up to a final volume of 500 µl with DNA extraction buffer (**Appendix A**, **section A.5**). Tubes were inverted to mix the contents and incubated overnight at 55˚C. The following day, the samples were vortexed. At this step they can be stored at -20˚C. Genomic DNA was precipitated by addition of 80 µl of 3M sodium

acetate and incubation on ice for 15 minutes. Samples were centrifuged at 4˚C, at 13,000 rpm for 20 minutes to separate tissue debris from the aqueous layer which contains the DNA. The supernatant was transferred to a new tube and 1 ml of ice-cold ethanol was added and vortexed before centrifugation for another 20 minutes, at 13,000 rpm at room-temperature. The supernatant was poured off and the pellet was washed in 70% ethanol, and pelleted by centrifugation for 5 minutes at 13,000 rpm. The liquid was carefully removed by pipetting and the pellet was air-dried. The pellet was then resuspended in 50 µl of autoclaved Milli-Q H_2O. DNA samples were stored at -20˚C until use.

Some samples were genotyped after whole mount *in situ* hybridisation. In these cases DNA was extracted by washing embryos twice for 30 minutes in PBS, with shaking. All other steps were the same as described above, but using half the indicated volumes and the pellets were resuspended in a final volume of 10-20 µl of water (depending on the amount of initial tissue).

2.3 Polymerase chain reaction (PCR)

Most primers for PCR were designed with a length of twenty to thirty bases with melting temperatures ranging from 55˚C to 65˚C, and kept as 100 µM stock solutions at -20˚C (all primers, Sigma, are listed in **Appendix B**). Components of the PCR reaction mixture are listed in **Table 2.2**. The amount of master mix prepared depended on the total number of samples, with enough included for a negative control reaction (water instead of DNA sample as template).

	Volume (µl)	Final concentration
H_2O	38.3	
10x Taq polymerase buffer	5.0	1x
25 mM dNTP	0.4	200 µM
25 mM $MgCl_2$	3.0	1.5 µM
Forward primer (25 µM)	1.0	0.5 µM
Reverse primer (25 µM)	1.0	0.5 µM
Taq polymerase 5 units/µl	0.3	
DNA/cDNA template	1.0	

Table 2.2 PCR reaction mixture. The final volume was 50 µl and the mixture scaled down to 30 µl for some applications and adjusted as required for optimisation of the primers. The PCR reagents (taq polymerase, 10x buffer and magnesium chloride) used were from Bioline (Biotaq) and deoxynucleotides from Promega (dNTPs, **Appendix A, section A.6**).

After combining all reagents, the mix was vortexed and distributed to 0.2 ml or 0.5 ml eppendorf tubes (depending on which Thermocycler was to be used). The template was then added to each tube, with exception of the control-tube (blank) which serves as a standard of the PCR reaction to check for primer dimers or contamination of any of the reagents. The whole procedure was done on ice up to tubes were then transferred to the Thermocycler (PTC-200 Peltier Thermal Cycler, Bio-Rad; Techne TC-512, Thermal Cycler).

The running conditions are listed on **Table 2.3** and the annealing temperatures will varied according to the primers used (**Appendix B**). The PCR cycle includes: denaturation of the DNA sample to separate the strands at high temperatures (≥ 94˚C); an annealing step in which the primers bind to the DNA strands (temperature varied between 50-65˚C, with greater specificity conferred by higher temperature); followed by an extension step in which new DNA strands are generated (65-75˚C). In theory, the

DNA-product doubles in concentration for each cycle (typically 30 cycles used). A final 10 minute extension step was also included.

Following the PCR reaction, products were analysed by agarose gel electrophoresis, with appropriate molecular-weight markers (**Appendix A**, **section A.7**). The gel concentration was varied depending on the product size and/or the similarity in size of products to be separated.

Step	**Temperature (˚C)**	**Duration**
(1) Heating lid/block	96 – 105	4 minutes
(2) Denaturation	96	40 seconds
(3) Annealing	Variable	40 seconds
(4) DNA extension	72	1 minute
(5) Final extension	72	5 minutes

Table 2.3 PCR cycling conditions. Running conditions were varied according to the primer pair used. Steps 2-4 were repeated for 30-35 cycles.

2.4 Genotyping of transgenic embryos (*ct/ct*^{TgGrhl3})

Embryos of the transgenic line were initially genotyped on the basis of the presence of the BAC (**section 2.4.1**). A complementary assay made use of the fact that the BAC carries the wild-type sequence at *Grhl3* position -21350 where the C-21350T mutation is present in homozygous form in *curly tail* genomic DNA (Gustavsson et al., 2007); **Fig. 2.3**). For primer sequences see **Appendix B**, **Table B.2**.

2.4.1 Genotyping *Grhl3* transgenic-BAC *curly tail*

The PCR to genotype for the presence of BAC RP24-327D13, containing the intact *Grhl3* gene, used one primer, pTARBAC1, located in the BAC vector and another, 327D13-R1, located close to the vector but in the genomic sequence 24 kb 3-prime of the *Grhl3* gene (**Fig. 2.3 A**). For this PCR reaction a *curly tail* (no BAC) and a transgenic (BAC) DNA sample were always used as negative and positive controls,

respectively. The PCR reaction mixture and running conditions are summarised in **Table 2.4**. Products were run on 1% agarose gels to verify amplification of a 230 bp band in the presence of the BAC (transgenic embryo) or lack of a band *ct/ct* samples (BAC negative; **Fig. 2.3 B**).

2.4.2 *Curly tail* genotyping assay

To confirm the BAC-PCR genotyping, most *curly tail* samples generated in crosses to the transgenic were also assayed for the C-21350T mutation. This assay consisted of a PCR (**Table 2.4**) reaction using primer pair Grhl3_UF10/UR10 (**Table B.2, Appendix B**) with transgenic and/or wild-type ($+^{ct}/+^{ct}$) DNA samples often used as controls. The resulting PCR product showed a 551 bp band on a 1% agarose gel for all genotypes. Following PCR amplification, the samples were digested with *AciI* restriction enzyme (10,000 U/ml, New England BioLabs) in a reaction containing 10 µl PCR product, 1.5 µl NEB3 10x buffer, 1 µl *AciI*, and 2.5 µl H_2O for a final volume of 15 µl. The products were digested overnight at 37˚C and a 10 µl aliquot was run on a 2% agarose gel. The C/T mutation in *curly tail* results in loss of one *Aci*I restriction site (recognition site CCGC) and therefore results in two bands on the gel (115 bp and 436 bp) whereas three bands are generated for $+^{ct}/+^{ct}$ samples (115 bp, 165 bp and 271 bp). Transgenics ($ct/ct^{TgGrhl3}$) are heterozygous for the mutation, and give rise to four bands (115 bp, 165 bp, 271 bp and 436 bp; **Fig. 2.3 C-D**).

Reagent (final concentration)	Volume (µl)	PCR conditions
H_2O	15.15 or 15.65	5 minutes 96˚C heated lid 30 seconds 96˚C denaturation 30 seconds 54˚C annealing 45 seconds 72˚C extension 35 cycles 5 minutes 72˚C final extension
10x Taq polymerase buffer	3.0	
dNTP (2 mM)	1.5	
$MgCl_2$ (50 mM)	0.7	
Forward primer (10 µM)	1.5	
Reverse primer (10 µM)	1.5	
Betaine	5.0	
DNA template	1.5 or 1.0	
Taq polymerase 5 units/µl	0.3	

Table 2.4 PCR conditions for genotyping *ct/ct^{TgGrhl3}* embryos. Reaction conditions were used for both the BAC-specific and the Grhl3_UF10/UR10 PCR. Only 1.0 µl DNA template was used for the latter reaction and the volume of water was adjusted accordingly. Betaine (Sigma) was used as an enhancing agent for PCR amplification, to improve yield and specificity.

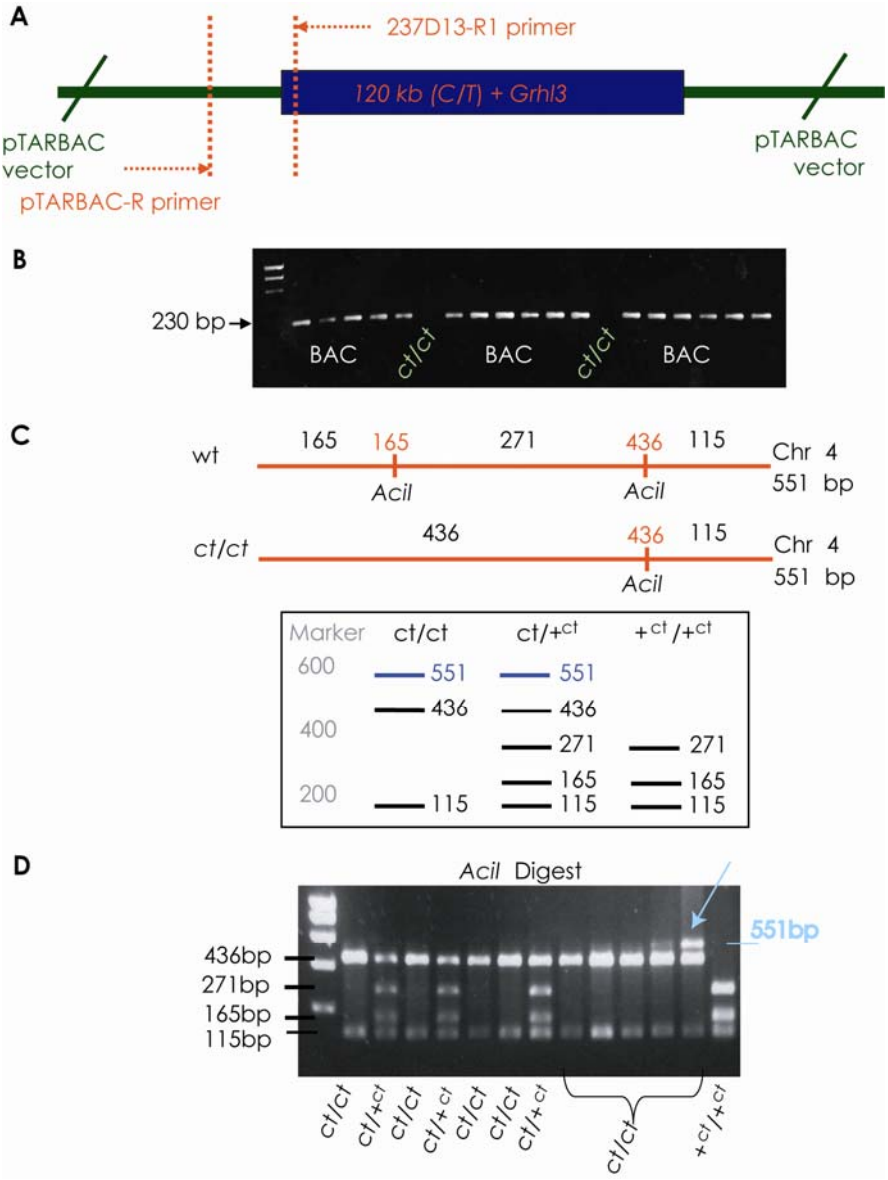

Figure 2.3 Schematic diagrams of the genotyping for the *Grhl3* locus. (**A**) Diagram illustrating the BAC region that is amplified including part of the BAC-vector and part of the insert (region of the chromosome 4 including the whole *Grhl3* gene). (**B**) Gel image showing a 230 bp band for samples which include the BAC (*ct/ct*^{TgGrhl3} transgenic embryos) compared to samples which do not (*ct/ct* embryos). (**C**) Diagram illustrating the 551 bp fragment encompassing the C-21350T single nucleotide change present in *ct/ct*. The fragment includes two *AciI* restriction sites in the $+^{ct}/+^{ct}$ sequence (wt, positions 165 and 436 bp), whereas the presence of a thymidine residue at position 165 results on loss of an *AciI* site in the *ct/ct* sequence. However, partial digestion sometimes occurs, resulting in incomplete digestion of the 551 bp fragment in samples from both strains, as seen on the 2% gel electrophoresis image (**D**, blue arrow).

2.5 Two-dimensional protein gel electrophoresis (2-DE) method

The 2-DE method was first introduced by P. H. O'Farrel and J. Klose (1975). Since then the major technical advance in 2-DE has been the introduction of immobilised pH gradient (strips; (Bjellqvist et al., 1982), created by covalently incorporating a gradient of acidic and basic buffering groups into a polyacrylamide gel at the time it is cast. This technique results in higher resolution, improves reproducibility, increases protein loading capacity and extends the pH ranges used in 2-DE. Whole embryos or samples of isolated cranial or caudal regions were used for 2-DE. Caudal regions were cut at the level of somites 14-15 (**Fig. 2.4 A**), to include the hindgut and posterior neuropore (PNP).

2.5.1 Sample preparation

Protein homogenisation is a crucial step for optimal protein separation. Samples were removed from the -80˚C and kept on dry-ice. Lysis buffer (**Appendix A, section A.8**) was added straight to the frozen tissue and the sample homogenised by sonication (High Intensity Ultrasonic Processor, SONICS VIBRA CELL): at 40% amplitude and 5-10 pulses for 2 seconds each, depending on sample size (**Table 2.5; Fig. 2.4 B**). At this stage is important not to overheat or cause foaming of the sample, which can cause protein degradation. The lysis buffer contains urea to solubilise and unfold proteins exposing the ionisable groups to solution. Detergent (CHAPS) ensures complete sample solubilisation by preventing interactions between hydrophobic protein domains, thus avoiding loss of protein due to aggregation and precipitation. The reducing agent dithiothreitol (DTT) is included, which breaks disulfide bonds and maintain all proteins in their reduced state. Finally, protease and phosphatase inhibitors were included to provide protection against proteolysis and phosphatases.

Duplicate 1-2 µl aliquots of the homogenate were kept in 1.5 ml eppendorfs on ice for analysis of protein content by an adapted Bradford assay (**Appendix A, section A.9**) and returned to dry-ice or storage at -80˚C (if not used on the same day).

Stage	Tissue	Volume of lysis buffer
E10.5	Whole embryo	200 µl (or 300µl depending on embryo size)
	Cranial region	100 µl
	Caudal region	50 µl

Table 2.5 Volumes of lysis buffer used for sonication of different amounts of tissue-sample.

2.5.2 Isoelectric focussing: protein separation by charge using immobilised pH gradient strips

Dependent on the pH of the surrounding environment, proteins carry positive, negative or zero net charge, which is the sum of all the charges of their amino acid side chains, and amino- and carboxyl-termini. In a pH gradient, under an electric field, a protein will move to the position in the gradient where its net charge is zero. This is the principle of the use of pH gradient strips during isoelectric focusing.

This project made use of immobilised pH gradient (IPG) strips of 18 cm (IPG strips: pH4-7, pH3-5.6, pH6-9; GE Healthcare) or 7 cm length (pH 4-7, Bio-Rad; pH 4-7 and pH 6.1-7.1 Invitrogen). The latter were used in the Novex Mini-Cell system cell (Invitrogen). IPG strips are very easy to contaminate or damage, so when handling it was necessary to rinse gloves in 70% IMS and use forceps for manipulation. Narrow range IPG strips were used for better separation of proteins in some experiments.

Prior to use, samples were thawed and centrifuged for 2-5 minutes at 4˚C in a microcentrifuge at 13,000 rpm to remove tissue debris. For whole embryos, 350 µg aliquots of protein sample were initially used. In subsequent experiments the gel loading was reduced to 50 µg, as there was lower protein content in the caudal region and this loading was found to be sufficient to produce clearly stained gels. Samples were then diluted with 175 µl rehydration buffer (**Appendix A, section A.10**) containing 2% volume of IPG buffer (pH range corresponding to IPG strip) or 2% pharmalyte (pH 3-10, Amersham Biosciences), 1x protease inhibitor, and lysis buffer to a 350 µl final

volume. For the 7 cm strips the procedure was the same, 10 μg protein were diluted to a final volume of 125 μl loading sample.

For rehydration, samples were loaded onto a re-swelling tray (levelled on the bench). IPG strips were removed from -20˚C storage just previous to use, plastic backing removed and placed onto tray's slot, gel side down (**Fig. 2.4 C-D**). The strip was moved back- and forwards to ensure the entire length was in contact with the sample and there were no air bubbles. Each strip was covered with approximately 1.5 ml of Immobiline DryStrip cover fluid (GE Healthcare) to avoid drying. The lid was placed on the tray, taped in place, and the tray left overnight at room temperature to allow passive rehydration of the strips. The number on strip, for each sample, was recorded.

Isoelectric focusing (IEF) was carried out the next morning, on a Multiphor (Multiphor II Electrophoresis System with Immobiline DryStrip kit, GE Healthcare), with a cooling water system set to 20º C. A plastic strip holder container was placed onto the Multiphor platform with 10 ml cover fluid underneath to ensure contact between the cooling plate and gel holder. The cathode and anode electrodes were connected at either end. Excess cover fluid was blotted out from rehydrated IPG strips and they were laid gel side up on the strip holder on the Multiphor, with the acidic (+) end towards the anode (+, red). IEF Electrode strips (GE Healthcare) were cut for the anode and cathode, at the required length, depending on how many gels were to be run. The IEF electrode strips were soaked in water (MilliQ) and the excess was blotted off before placing the strips across each end of the IPG gels, overlapping the ends of the gel. The anode and cathode were inserted onto the Multiphor, with the central wire aligned with the IEF electrode strip, and pushed down so the electrode contacts the strip. Gels were then immersed in cover fluid and the lid placed on prior to connection to the power supply. In order to separate proteins by charge, a voltage of 3500 V was applied for a total of approximately 65 kVh. Focussing conditions are summarised in **Tables 2.6 and 2.7**. If second dimension separation was not performed immediately, IEF gels were stored at -80˚C until required.

Step 1 (gradient)	Step 2	Step 3	Step 4	Step 5
1 Vh	6600 Vh	13.4 kVh	1 Vh	100 Vh
200 V	3500 V	3500 V	100 V	100 V
1 mA	1 mA	1 mA	1 mA	1mA
5W	5W	5W	1W	1W

Table 2.6 IEF conditions for 7 cm IPG strips (20 kVh). The first dimension is performed at very high voltages and low current, with active temperature control. After step 4 the run can be stopped. Step 5 was used to maintain a low voltage after the run until the apparatus could be disassembled. Volt-hour (Vh) is the product of the voltage and the hours elapsed at that same voltage.

Step 1 (gradient)	Step 2	Step 3	Step 4	Step 5
1 Vh	7000 Vh	58.0 kVh	6000 Vh	2000 Vh
500 V	3500 V	3500 V	100 V	200 V
1 mA	1 mA	1 mA	1 mA	1mA
5W	5W	5W	1W	1W

Table 2.7 IEF conditions for 18 cm IPG strips (65 kVh).

2.5.3 Second dimension SDS-polyacrylamide gel electrophoresis: protein separation by molecular weight

The second dimension separation (**Fig. 2.4 E-F**) was optimised for two different tank-systems for maximal resolution and reproducibility. Both systems could accommodate 18 cm IPG strips with a well at the side for molecular weight markers), and 1.5 mm thick gels were used in each case. The Hoefer DALT system enabled running of up to 10-gels simultaneously in 23.5 x 19.2 cm cassettes (Anderson ISO DALT Electrophoresis System, HOEFER Scientific Instruments), whereas up to 12 gels could be run in the DALT*twelve* system (GE Healthcare) in 25.5 × 19.6 cm cassettes. The running buffer conditions were adapted according for each tank (**Appendix A, section A.11**). A built-in heat exchanger and buffer circulation pump provided precise temperature control and a uniform thermal environment. The 10 gel tank generated

reliably produced reproducible gels. There was some run to run variation with the 12 gel tank and it was though that this partly resulted from lack of buffer circulation in the upper buffer chamber. However, the 12 gel tank had the advantage of larger gels which allows greater protein separation.

Following IEF on 7cm gels the second dimension separation was performed using pre-cast gels (NuPage 4-12% Bis-Tris gels, 1.5 mm 2D well; Invitrogen) on a Novex Mini Cell tank. The procedure was the same as for the large gels, but the buffer was MOPS based (Invitrogen). The SDS-PAGE gels were prepared in advance (at least two hours polymerisation were needed), usually the previous day and stored at 4˚C (**Appendix A, section A.11**). Prior to loading gels were allowed to reach room temperature. Buffer was added to the gel tank and allowed to circulate with cooling to 10°C for three hours prior to the run.

IEF gels were equilibrated by incubation in plastic tubes (**Fig. 2.4 E; Appendix A, section A.12**) containing 10 ml equilibration buffer with 1% (w/v) dithiotreitol (DTT; GE Healthcare) for 15 minutes, with shaking (70 rpm), at room temperature, followed by incubation for 25 minutes in equilibration buffer containing 2.5% (w/v) iodoacetamide (GE Healthcare). DTT ensure proteins are in a reduced state while iodoacetamide alkylates any free DTT and sulphydryl groups and prevents their reoxidation.

IEF gels were rinsed with running buffer and placed into the gel cassette with the plastic backing of the gel against the glass (**Fig. 2.4 F**). For orientation the acidic end of the IEF gel was always placed on the left-hand side, by the silicone hinge. With a ruler the plastic backing of the IEF gel was pushed down until it reached the surface of the SDS-PAGE gel. Protein molecular weight markers (5 – 8 µl), soaked onto an IEF sample application piece (GE Healthcare), were placed a few cm from the IEF gel. Agarose sealing solution (**Appendix A**, **section A.13**) was used to cover the IEF gel and markers, ensuring that no air bubbles were trapped between the IEF gel and the SDS-PAGE gel.

Once the agarose had set, gel cassettes were loaded in the tank. For the DALT tank the gel cassette was turned 90º (IEF gel stands vertically), dipped in buffer and slid between barrier. Plastic spacers were used if not running 10 gels. The buffer level was adjusted so that the buffer reached the level of the top of the cassette-spacers. For the 12 gel tank the cassettes were slid directly into the tank and plastic spacers were inserted into any unused slots. The lower buffer chamber was topped up with 1 x running buffer and then the upper buffer chamber was fitted and filled with 2.5-3.0 x running buffer. These two buffers do not mix. Electrophoresis conditions are indicated in **Tables 2.8** and **2.9**. An initial low power (1W/gel) step was included to facilitate protein transfer from the IEF gel to the SDS-PAGE gel.

Step 1 (gradient)	**Step 2**	**Step 3**	**Step 4**
10 minutes	1 h 50 min	2 h	25 h
50 V	50 V	125 V	125 V
6 W (1W/gel)	6 W	18 W (3W/gel)	18 W
12 mA (2 mA/gel)	12 mA	180 mA (30 mA/gel)	180 mA

Table 2.8 Electrophoresis conditions for SDS-PAGE using the 10-tank system. Running conditions for 6 gels, at 10˚C.

Step 1	**Step 2**	**Step 3**
0h50 minutes	1h50 minutes	Until front dye falls
20 V constant	50 V constant	125 V

Table 2.9 Electrophoresis conditions for SDS-PAGE using the 12-tank system. Gels were run at 15˚C.

For production of mini 2D gels the procedure was essentially the same as above except only half of the volume of buffer was necessary for equilibration of the IEF gels. At the end of equilibration, strips were washed in MOPS running buffer. The running conditions are summarised in **Table 2.10**.

Step	Time	Limits per gel		
1	20 min	50V	5 mA	1.0 W
2	270 min	100V	20 mA	2.0 W

Table 2.10 Electrophoresis conditions for the SDS-PAGE using 7 cm IEF gels. There was no need to control the temperature because gels were run at low voltage and the run duration was relatively short.

After electrophoresis, the glass plates were disassembled and the gels placed overnight in fixation solution, depending on which downstream stain was going to be used.

2.5.4 2D-gel staining

After electrophoresis gels were fixed overnight, with agitation and stained next day with silver (**Fig. 2.4 H**) or fluorescent dyes (Sypro Ruby or Deep Purple) according to the manufacturers' instructions. All solutions were made with MilliQ water. Glass trays were used for silver staining but metal trays with lids were used for Sypro Ruby or Deep Purple stains.

2.5.4.1 Silver staining

Silver staining involved fixation of gels to remove SDS and other buffer components. This was followed by cross linking of the proteins in the gel matrix with glutaraldehyde, and sensitisation with sodium thiosulfate in the presence of sodium acetate. Gels were washed with water prior to addition of silver stain. Protein spots were then visualised by development with formaldehyde at basic pH and sodium carbonate. This reaction was stopped using EDTA once gel images had developed. PlusOne Silver stain kit (Amersham Biosciences, GE Healthcare) was used according to the manufacturer's instructions with the exception of the volumes for the fixation step (300 ml per gel, instead of the 250 ml on the manual). In addition, when gels were run for the purpose of picking spots for mass spectrometry, glutaraldehyde was omitted from the sensitising step.

2.5.4.2 Sypro Ruby staining

Sypro Ruby (Molecular Probes, Invitrogen) dye is a ready-to-use luminescent stain, which is compatible with mass spectrometry (Berggren et al., 2000). Gels were fixed in fixation solution (7.5% (v/v) acetic acid, 10% (v/v) methanol and water), using 300–500 ml for large gels and 50–100 ml for mini-gels of Sypro Ruby solution, with gentle agitation, overnight. The next day the gels were destained (acetic acid/water) to remove background and washed in water for several times before scanning. Gels stained with this dye had to be carefully handled as they break easily.

2.5.4.3 Deep Purple

Deep Purple (Amersham Biosciences/GE Healthcare) stain contains a naturally occurring fluorophore, epicocconone compound, extracted from a fungal species (*Epicoccum nigrum*), which interacts noncovalently with SDS and proteins. It provides similar sensitivity to Sypro Ruby but has the advantage that it does not contain any heavy metals and is completely reversible. Staining was performed following the manufacturer's instructions. Large gels were fixed overnight in 300 ml (50 ml for NuPage gels) 7.5% acetic acid and 10% ethanol (v/v). Gels were washed in 35 mM sodium hydrogen carbonate (NaHCO) for large gels or 200 mM sodium carbonate (Na_2CO_3) at pH11 for the mini gels, for 30 minutes. Wash solution was poured off and replaced by water before addition of deep purple (1:200), and incubated in the dark for 1 hour (with agitation). Gels were then fixed in 7.5% (v/v) acetic acid, twice, for 15 minutes, and thoroughly washed before imaging.

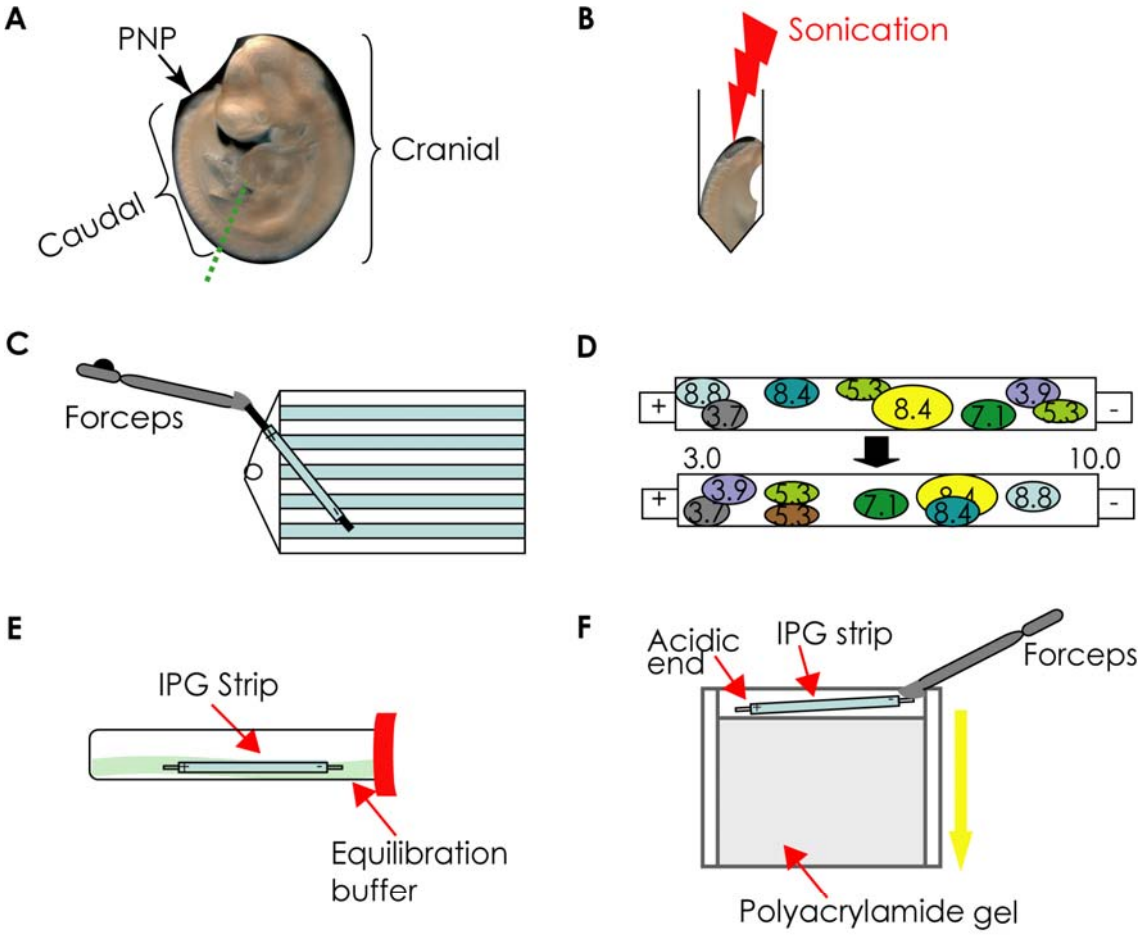
A
PNP
Cranial
Caudal
B
Sonication
C
Forceps
D
8.8
8.4
5.3
8.4
3.9
3.7
7.1
5.3
+
-
3.0
10.0
3.9
5.3
7.1
8.4
8.8
3.7
5.3
8.4
E
IPG Strip
Equilibration
buffer
F
Acidic
end
IPG strip
Forceps
Polyacrylamide gel
G
Acidic side
Basic side
kDa pH
4
7
250
150
100
75
50
37
25
20
15
10
+
-
H
L

Figure 2.4 Diagrammatic representation of 2D protein electrophoresis method. (A) Samples comprised whole E10.5 embryos, or isolated cranial or caudal regions (separated at the level of the green dotted line) encompassing the posterior neuropore, PNP). **(B)** Tissue was homogenised by sonication. **(C)** Samples were loaded onto a rehydration tray for passive rehydration of strips. **(D)** First dimension isoelectric focusing (IEF) was performed on a flat-bed system. Before IEF proteins are randomly distributed across the IPG strip. After IEF proteins had reached their isoelectric point within the pH gradient or migrated to ends of the gels if pI lies outside the pH range of the gel. **(E)** The IPG strip was equilibrated with the SDS buffer system for the second dimension. **(F)** Loading of the IPG strip onto the SDS-PAGE gel for second dimension electrophoresis to separate proteins by molecular weight (yellow arrow indicates direction of electrophoresis). (**G**) After electrophoresis, gels were fixed and stained. Image shows a typical silver stained gel using a pH range of 4.0-7.0 for IEF. Proteins were separated from the higher molecular weight to the lowest as indicated by the protein marker (kDa, kilo Daltons), and each spot corresponds to an individual protein species.

2.5.4.4 Gel imaging

Silver-stained gels were imaged using a GS-800 densitometer (Bio-Rad), and fluorescent-stained gels were imaged using a flat-bed laser based fluorescence imaging system, Typhoon 9400 scanner (Amersham Biosciences). For Sypro Ruby stained gels the scanner protocol involved: excitation with green laser (532 nm); emission at 560 nm with long-pass filter (LP) or 610 band-pass filter (BP). Gels were scanned at 100 microns resolution. For Deep purple stain conditions were: excitation with green laser (532 nm); emission at 560 LP or 610 BP filter and 100 microns resolution. The photomultiplier tube voltage was adjusted for optimal signal intensity of spots.

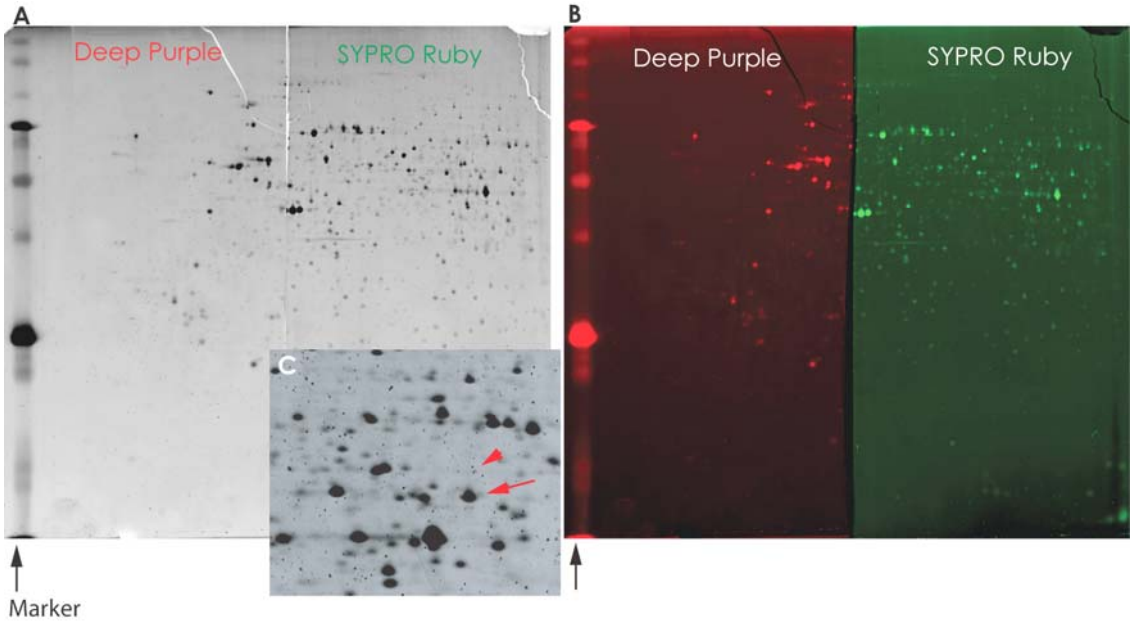

Figure 2.5 Deep Purple and Sypro Ruby stained gels. A 2D-gel was divided in half before staining. (**A**) Image of a gel scanned using the Typhoon scan. The left half was stained with Deep Purple and the right half with Sypro Ruby. (**B**) The same gels were artificially coloured using ImageQuant TL V2005 software (Amersham Biosciences). (**C**) High magnification of a Sypro Ruby stained gel to show the difference between a protein spot (red arrow) and an artefactual speckle (red arrowhead). Black arrows indicate protein marker.

2.5.5 2D-gel analysis

After visualisation of the gel-spots and image acquiring, analysis of the resultant 2D array of spots was performed using Progenesis SameSpots software (Non Linear Dynamics). Analysis included semi-automatic gel alignment, inter-gel calibration and variance stabilisation. Gel images were then separated into experimental groups (usually corresponding to mouse strain), for spot volume quantitation and comparison. Spots found to be differentially abundant were reviewed manually and edited if necessary. Varying spots were ranked according to p-value (ANOVA) and/or fold change.

First the images were loaded into the software and automatically assessed for quality control and a reference gel was chosen for gel image alignment (**Fig. 2.6 A-B**). Ideally, a good reference image showed a clear and representative spot pattern, and a minimum

of distortion. All reference gels used in this study were from the *curly tail* strain unless otherwise stated. Before normalisation, spots were filtered by deleting speckles or spots in damaged areas (**Fig 2.6 C**). Typically of about 5200 spots initially defected, filtering left about 2200 spots to be compared (**Fig. 2.6 C-D**). All spots were reviewed and manually edited if needed. In cases where two spots were close together and detected as a single spot by the software they were manually split and re-analysed.

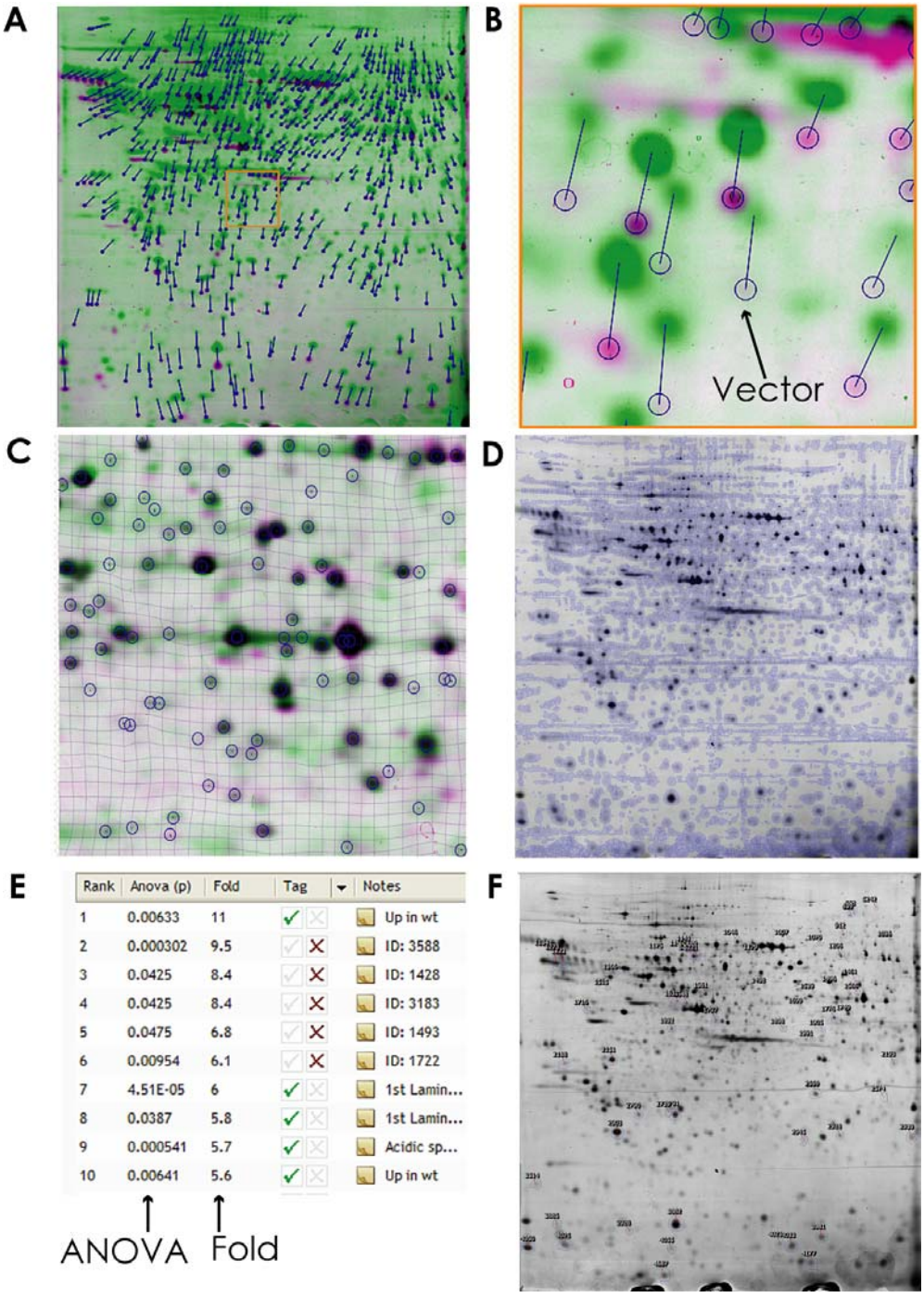
A
B
Vector
C
D
E
F
Rank | Anova (p) | Fold | Tag | Notes
1 | 0.00633 | 11 | Up in wt
2 | 0.000302 | 9.5 | ID: 3588
3 | 0.0425 | 8.4 | ID: 1428
4 | 0.0425 | 8.4 | ID: 3183
5 | 0.0475 | 6.8 | ID: 1493
6 | 0.00954 | 6.1 | ID: 1722
7 | 4.51E-05 | 6 | 1st Lamin...
8 | 0.0387 | 5.8 | 1st Lamin...
9 | 0.000541 | 5.7 | Acidic sp...
10 | 0.00641 | 5.6 | Up in wt
ANOVA
Fold

Figure 2.6 2D gel image analysis with SameSpots software. (**A-B**) After quality checking, images were aligned to a reference gel image. This was done by automatic application of vectors to each detected spot. Full image of a gel with applied vectors, and an enlarged view of one area (orange square). Spots in pink are from the reference image, while spots in green are from the image to be aligned (**B**). (**C**) Region of a gel after alignment. (**D**) 5219 spots were detected before filtering. At this step "false" spots were then deleted. (**E**) Spots were ranked after comparing spots volume between the groups. All spots were reviewed, but only spots that significantly differed ($p<0.05$) were taken into consideration. The fold change was calculated between the highest and the lowest spot volume. (**F**) Gel image with mapped spots of interest.

During the spot review process, some spots that significantly differed between groups were excluded (**Fig. 2.7**). For example, some spots were present or absent in only one or two gels in the replicate group. Some spots were detected as being differently expressed but only as a result of an error during the alignment step with reference gel. False spots, such as streaking or speckles that had not been deleted in the filtering step were also excluded.

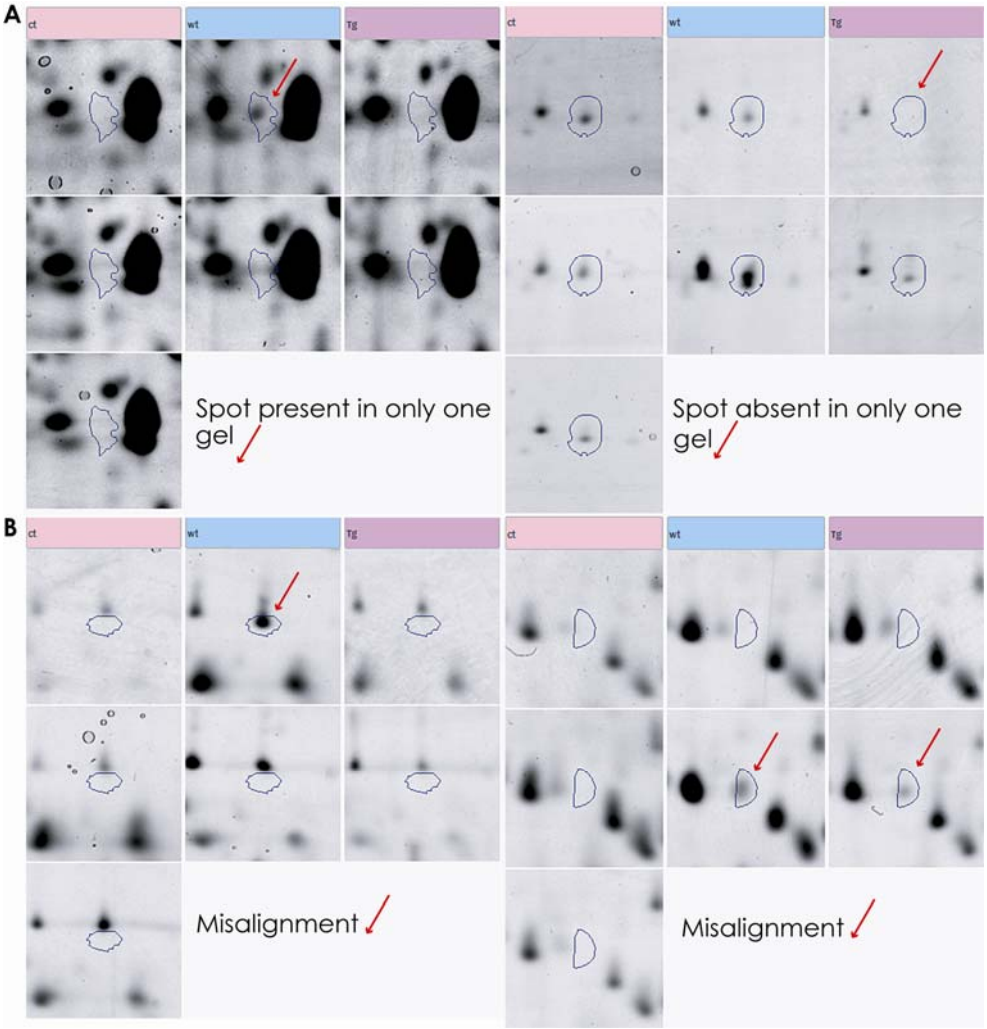

Figure 2.7 Examples of protein spots that were excluded during spot review. (**A**) The spot outlined in blue was present in only one gel image (red arrow) in the replicate group. Conversely, another spot was absent in only one gel (red arrow) in one replicate group. (**B**) Two examples of spots (outlined in blue) detected as being differently expressed but actually were the result of misalignment (red arrow).

2.5.6 Spot picking and in-gel digestion for mass Spectrometry analysis

After analysis and comparison of the 2D gel images, spots of interest were excised from each gel, or pooled in the case of very low spot abundance. Care was taken to not take excess gel from around the spot. Clean gloves were used to avoid contamination of spots with keratin. The cut spot was transferred to a 1.5 ml eppendorf tubes for in-gel digestion of proteins for Liquid Chromatography Tandem Mass Spectrometry (LC-MS/MS) on a QTof (Quadrupole Time-of-Light) micro (Waters Corporation).

2.5.6.1 In-gel digestion

Gel pieces were covered in 50 µl of 100 mM Ammonium bicarbonate (Ambic, Sigma) buffer, for 5 min, to remove stain and SDS. The supernatant was discarded and gel pieces dehydrated by addition of 50 µl acetonitrile (98%; Fisher Scientific), twice. Samples were further dried in a speed vac (4-5 minutes). Gel-spots were rehydrated by addition of 50 µl 10 mM DTT in 100 mM Ambic (made up fresh) and heating at 56^{o}C for 30 minutes. After removal of the DTT solution, acetonitrile was re-added to further dehydrate the gel, excess solution was discarded and the gel piece dried in a speed vac. A 50 µl aliquot of 55 mM iodoacetamide in 100 mM Ambic (10 mg/ml) was added, and incubated at room temperature for 20 minutes (in the dark). Iodoacetamide is added after incubation of the protein with denaturants and reducing agents, in order to covalently modify cysteine residues (to form S-carboxymethyl cysteine), so that disulfide bonds are no longer formed. After discarding the supernatant, the gel was briefly washed with 100 mM Ambic buffer and then washed for a further 15 minutes. Excess liquid was again removed and the gel was dehydrated once again with acetonitrile and dried in a speed vac.

To digest the protein-spots into peptides, 100 µl of 50 mM Ambic was added to 15 µl of trypsin (**Appendix A**, **section A.14**) giving a final concentration of 13 ng/µl. Gel-spots were then rehydrated with 15-30 µl trypsin solution (enough to cover gel pieces) by incubating at 4^{o}C for 30-45 minutes. After this period, excess trypsin was removed and a minimal volume of 50 mM Ambic (10-20 µl) was added to cover the gel pieces and keep them wet during enzyme cleavage. Tubes were incubated at 37^{o}C for 1 hour and then overnight at room temperature.

2.5.6.2 Peptide extraction from the gel pieces (for QTOF analysis)

The supernatant from the overnight in-gel digestion was transferred into a fresh 1.5 ml tube and left aside. To extract additional protein from each gel-spot, approximately 15 µl of 50 mM Ambic was added to the gel piece and incubated for 15 minutes at 37^{o}C. The resulting supernatant was pooled with the initial supernatant (above). The gel pieces were again dehydrated with acetonitrile and incubated for 15 minutes at 37^{o}C until they were small white lumps. The supernatant was transferred and pooled as above. The steps with the 50 mM Ambic followed by acetonitrile were repeated once more and all the supernatants were pooled as above, completely dried in the speed vac and stored at -20 ^{o}C.

The 'in-gel digestion' of all proteins identified in this study was either by Dr Kit-Yi Leung or with her assistance. Dr Leung also performed all the LC-MS/MS.

Peptide sequences obtained by LC-MS/MS were submitted to MASCOT (http://www.matrixscience.com/search_form_select.html) search engine. The proteins were identified by selecting the following items: MS/MS Ion Search; SwissProt database; trypsin digestion; allowance of two missed cleavages; carboxymethyl and oxidation, variable modifications; micromass (.PKL file format). A score of 35 or above was considered sufficient for confident identification of a protein. Lower scores were accepted for proteins with at least one peptide with a score ≥35.

2.5.7 2D-gel analysis of phosphatase digested protein-samples

To test the hypothesis that lamin B1 protein spots were phosphorylated, a method (Yamagata et al., 2002; Raggiaschi et al., 2006) was developed in which *curly tail* and wild-type embryo-samples were treated by phosphatase, to remove phosphate groups from phosphorylated proteins. Whole embryo samples were prepared as described above (**section 2.5.1**) but in a different lysis buffer (**Appendix A**, **section A.8**), using 150-300 µg total protein (embryos pooled if necessary).

2.5.7.1 Dephosphorylation of proteins

From the homogenised sample, 20 µl were mixed with 10 µl of 10% SDS, 945 µl of H_2O, 5 µl of 20 mM manganese chloride, 20 µl of λPPase buffer to a final volume of 1

ml. This solution was then divided into two aliquots (500 µl each) to which 0.25 µl (100 units) of λPPase (Lambda Protein Phosphatase, λPPase; New England BioLabs) were added to one of the aliquots the other was kept as control. Both samples (control and phosphatase treated) were incubated overnight at 30ºC, with rotation. After incubation, samples were purified using the 2-D Clean-Up kit (Amersham Biosciences). Pellets were re-suspended in the same lysis buffer in which they were sonicated (20-25µl) and protein assay was again performed. 2-DE was then carried out using 18 cm IPG strips as described above.

2.5.7.2 Validation of dephosphorylation of proteins

To verify that proteins were digested by the phosphatase, one-dimensional protein gel electrophoresis was performed, the gel blotted onto a membrane and immunostained with an anti-phospho antibody (**Table 2.11**). The antibody should bind to control samples, which contain phosphorylated proteins, but not to phosphatase-treated samples.

2.6 Western blot

2.6.1 One-dimensional protein gel electrophoresis

Protein samples were prepared as described in **section 2.5.1**, but instead of the 2D-lysis buffer, Radio-Immunoprecipitation Assay (RIPA; **Appendix A, section A.15.1**) buffer was used. RIPA buffer is a harsh denaturing buffer due to the presence of SDS and sodium deoxycholate ionic detergents.

Protein samples were stored at -80˚C and thawed on ice. For each lane, samples typically contained 1-5 µg protein (depending on the antibody), with 0.5 µl of β-mercaptoethanol (Sigma) and the volume made up to 25 µl with neat Laemmli sample buffer (Bio-Rad). Samples were spun down in a 4˚C centrifuge and denatured on a 100˚C hot block for 2 minutes, then kept on ice until the gel was loaded.

Pre-cast 1 mm thick Bis-Tris gels (NuPage System, Invitrogen) with 10 wells were used. Uniform 10% gels or 4-12% gradient gels were used depending on the size of the protein to be detected. Gels were washed with Milli-Q water. The comb was removed

and wells washed with 1x MOPS SDS running buffer (from 20x stock; Invitrogen). After placing gel-cassettes in the tank (XCell SureLock), the inner chamber was filled up with running buffer and checked for leakages. The rest of the running buffer was poured into the outer chamber. Samples were then loaded with one well containing 8 µl of protein marker (Precision Plus Protein Standards, Dual Color, Bio-Rad; **Fig. 2.8**). In general the running conditions were 20 minutes at 50 volts to allow samples to slowly enter the gel, followed by 2 or more hours at 100 volts.

2.6.2 Blotting

Protein transfer was optimised for two different systems: semi-dry blot (Bio-Rad, Trans-Blot SD, Semi-Dry Transfer Cell) and wet blot (XCell II Blot Module, Invitrogen). Polyvinylidene fluoride membrane (PVDF, 0.45 µm pore size, Immobilon-P, Millipore) and filter paper (3MM, Chromatography paper, Whatmann) were cut to the same dimensions as the gel. Membranes were first wetted in methanol, then transferred to clean Milli-Q water for 2 minutes and finally equilibrated in transfer buffer for at least 15 minutes. Care was taken to minimise touching the membrane and forceps were used. After electrophoresis was completed (dye front close to the bottom of the gel or fallen), gels were removed from the cassette and the procedure for transfer was:

- Semi-dry: The gel was equilibrated in transfer buffer (**Appendix A**, **section A.15.2**) for at least 15 minutes. Filter paper was soaked in transfer buffer (3 sheets) and assembled on the semi-dry blotter, followed by the equilibrated membrane, the gel and an additional 3 sheets of buffer-soaked filter paper added on top to complete the 'sandwich'. A pipette was rolled over the gel-membrane sandwich to remove any air bubbles (**Fig. 2.8 B**). The lid was connected and conditions were 25V for 25 minutes for one gel; and 25V for 45 minutes for 2 gels.

- Wet: Filter paper soaked in transfer buffer was laid on top of the gel, which was turned over, the cassette discarded, followed by equilibrated membrane. Another buffer-soaked filter paper was placed on the top of the membrane. A pipette was rolled over the gel-membrane sandwich to remove any air bubbles. Blotting pads were soaked in transfer buffer and aligned with the sandwich in the transfer cell (**Fig. 2.8 C**). The cell

was placed in the gel tank, locked in place and transfer buffer was added to cover the blotting pads. The outer buffer chamber was filled with milli-Q water to the same level of the blotting pads (~ 600 ml) to maintain constant temperature. Running conditions were constant 25V for 1 hour.

2.6.3 Immunodetection

After blotting, the transfer system was disassembled and the membrane was quickly washed in 1x tris buffered saline (TBS; **Appendix A, section A.15.3**) to remove excess transfer buffer. Membranes were then incubated in blocking solution (**Appendix A, section A.15.3**), for 1 hour at room-temperature, with shaking (60 rpm). Primary antibody was added to 15 ml blocking solution and incubated with the membrane overnight at 4˚C with shaking. In some cases, membranes were blocked overnight at 4˚C and the primary solution was added next day for 1 hour at room temperature.

Primary antibody solution was poured off and the membranes washed 3 times for 5 minutes with 1x TBST, shaking at room-temperature. TBST was replaced with appropriate secondary antibody in 15 ml blocking solution: with shaking, for 1 hour, at room-temperature. The concentrations of secondary antibody used were dependent on the primary antibody (summarised in **Tables 2.11 and 2.12**). Secondary antibody was then discarded and the membrane washed five times for three minutes with 1x TBST at room temperature. While washing membrane, the chemiluminescent solution (2 ml per membrane; Amersham ECL Plus Western Blotting Detection Reagents, GE Healthcare) was prepared following manufacturer's instructions. ECL provides a non-radioactive method for detection of antigens bound to horseradish peroxidase (HRP)-conjugated antibodies. The membrane was transferred to cling-film covered with ECL solution and left for 5 minutes at room temperature. The membrane was blotted to remove ECL, wrapped up with clean dry cling-film and placed in a cassette with Hi Speed X intensifying screen prior to exposure to X-ray film (Chemiluminescence BioMax Light film, Kodak) between 1 second and 5 minutes. Films were developed in an Autorad Developer.

Optimal conditions for each antibody were determined using two different concentrations of antibody with different protein amounts from two different samples.

Additional membranes were incubated without primary antibody to check for non-specific binding of the secondary antibody.

Protein	Catalogue number	Company	Species	Dilution	Band Size (kDa)
B-Tubulin	sc-9104	Santa Cruz Biotechnology	Rabbit polyclonal	1:1000	55
Lamin B1 (S-20)	sc-30264	Santa Cruz Biotechnology	Goat polyclonal	1:1000	67
Gart (S-20)	sc-83255	Santa Cruz Biotechnology	Rabbit polyclonal	1:1000	110
VCP	#2648	Cell Signalling Technology	Rabbit polyclonal	1:1000	89
Fetuin-A (M-17)	sc-9668	Santa Cruz Biotechnology	Goat polyclonal	1:1000	59
Fetuin-B (C-20)	sc-32535	Santa Cruz Biotechnology	Goat polyclonal	1:5000	60
Mat2a	ab-26174	Abcam	Chicken polyclonal	1:4000	43
Gapdh	#MAB374	Millipore	Mouse	1:100000	38
UBE2N *	GTX13663	Gene Tex, Inc	Rabbit polyclonal	1:1000 – 1:2000	17
Phospho-threonine antibody	9381	Cell Signaling	Rabbit polyclonal	1:1000	Vary

Table 2.11 Primary antibodies used in western blots. * This antibody gave no results or appeared to give non-specific binding. Band size indicates the predicted/expected band size.

Antibody	Catalogue	Company	Species	Dilution	Conjugated
Anti-rabbit immunoglobulins	P0448	DAKO	Goat polyclonal	1:5000-15000	HRP
Anti-goat immunoglobulins	P0160	DAKO	Rabbit polyclonal	1:5000-15000	HRP
Anti-mouse immunoglobulins	P0260	DAKO	Rabbit polyclonal	1:150000	HRP
Anti-chicken IgY	ab-6877	Abcam	Goat polyclonal	1:10000	HRP
Anti-sheep immunoglbulins	61-8620	Invitrogen	Rabbit	1:5000 1:10000	HRP

Table 2.12 Secondary antibodies used in western blots.

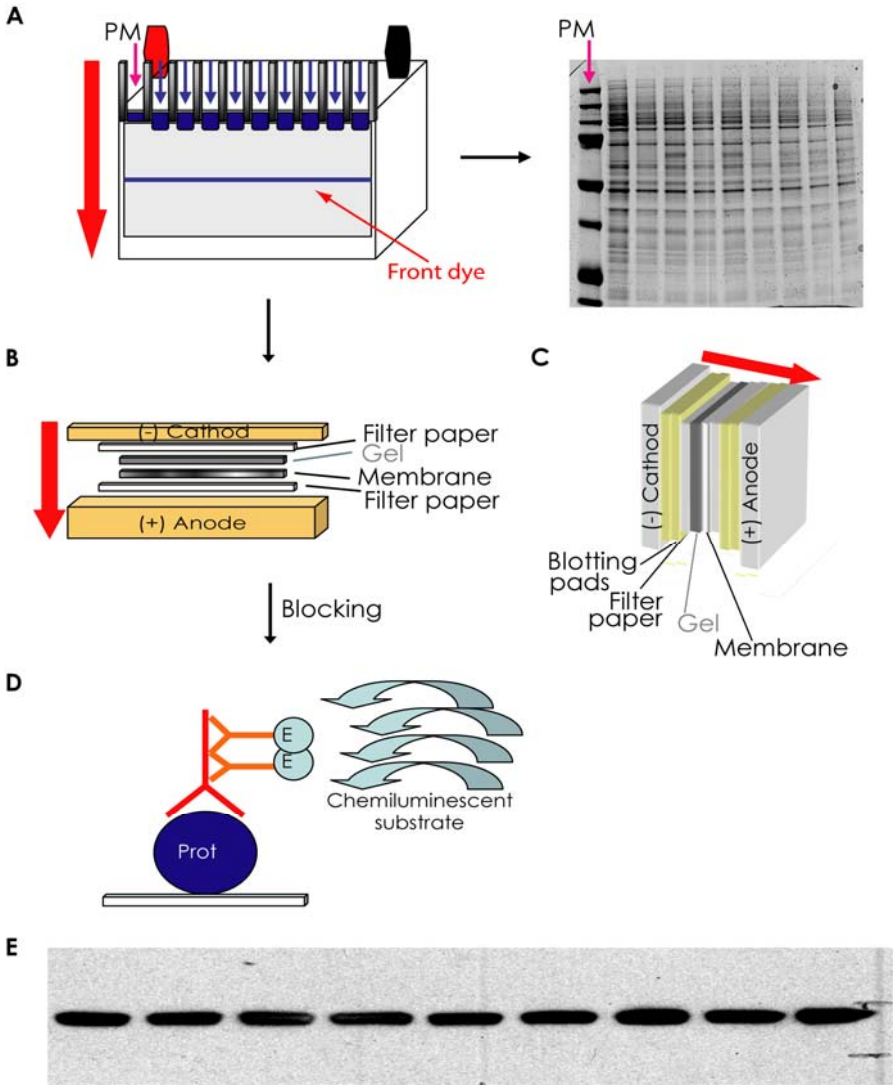

Figure 2.8 Western blot for detection of protein expression. (**A**) Samples were loaded (blue arrows) onto precast gels, and electrophoresed for protein separation. A pre-stained protein marker (PM, red arrow) was used to estimate the size of the protein. Bromophenol blue contained in the sample loading buffer helped to follow progression of the run. Image of a silver-stained gel for total protein visualisation. (**B-C**) Proteins were electro-transferred from the gel to a membrane, using semi-dry (**B**) or wet (**C**) transfer. After transfer, membranes were blocked with a suitable blocking buffer and incubated with primary antibody. (**D**) After washes, membrane was incubated with horseradish peroxidase (HRP) secondary antibody conjugate in blocking solution. The HRP-antibody complex activates chemiluminescent solution for protein detection. (**E**) Image of the protein bands after X-ray exposure and development. Red arrows indicate direction of electrophoresis (**A**) and electrotransfer (**B-C**).

2.6.4 Membrane stripping and re-probing for normalisation of total protein content

To verify equal loading of protein-samples and allow normalisation of protein content against a reference protein, membranes were stripped and re-probed with an antibody against Gapdh or β tubulin (reference proteins assumed not to vary in abundance between genotypes).

After exposure, dried-membranes were wetted in methanol and washed in Milli-Q water (twice, for 6 minutes each). Water replaced with either stripping solution (Restore Western Blot Striping Buffer, PIERCE), at 37˚C for 20 minutes, with shaking every 5 minutes or 0.2 M NaOH, at 37˚C for 10 minutes, with shaking every 2-3 minutes. Membranes were then washed twice for 6 minutes in TBST with shaking at room-temperature. TBST was replaced by blocking solution and the protocol was followed as for immunoblotting (**section 2.6.3**).

2.6.5 Analysis and statistics

All X-ray films were scanned on a GS-800 Densitometer (Bio-Rad). Images were acquired and analysed with Quantity One software (Bio-Rad). The utility of β-tubulin and Gapdh for normalisation were evaluated by first testing whether the band volume increased linearly with total protein abundance. Different concentrations of the same protein sample were western blotted (as **section 2.6.3**) and X-ray films were exposed for 1 second. Band analysis was performed using Quantity One software volume analysis tool which measures the total signal intensity of the pixels inside a defined boundary drawn on the image multiplied by the pixel area (Volume units = intensity units x mm^2). A rectangle of equal size (for each blot) was drawn around each band. An additional rectangle was drawn in a background region of the image and used as the global background volume. The software calculates a single background intensity for the entire image, which is subtracted from all the volumes in the image. To assess linearity of the volume measurements with protein abundance, band volumes were measured for a series of samples and plotted on a bar graph (**Fig. 2.9**).

In order to compare protein levels between samples the adjusted volumes (with background subtracted) of the protein of interest (Protein A) were normalised to the

volumes of the reference protein (β-tubulin or Gapdh), to give the ratio of Protein A/reference. For comparison between strains, one sample (usually a wild-type) was used as the calibrator with a nominal abundance of 1.0. The ratio of normalised volume for a sample/normalised volume for calibrator gave the final volume for each sample. For each western blot, a minimum of three samples per strain were used for comparison. The mean normalised volume for each strain were compared by One Way ANOVA using Sigma Stat software (Jandel Scientific).

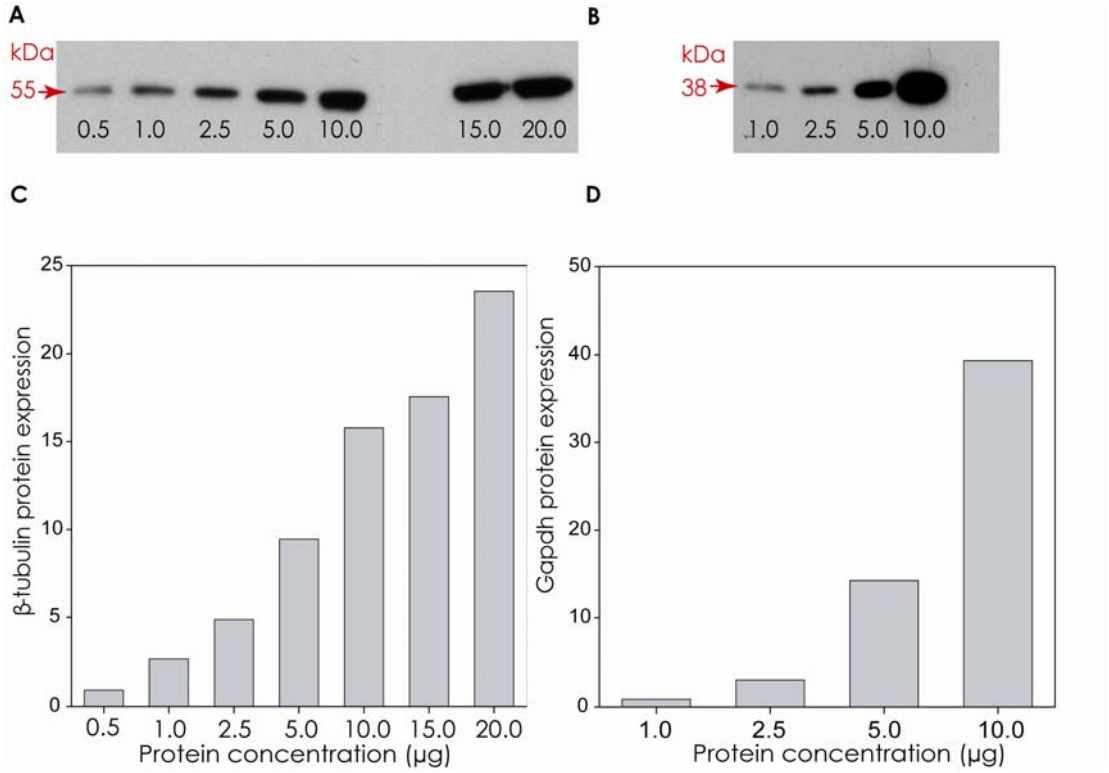

Figure 2.9 Sensitivity and linearity of detection for the antibodies used for protein normalisation. (**A-B**) Scans of Western blots loaded with different concentrations of total embryo protein and blotted with antibodies to β-tubulin (A) and Gapdh (B). (**C-D**) Plot of volumes of each band corresponding to the different concentrations detected by β-tubulin or Gapdh antibodies. The ideal bands for volumetric analysis correspond to 2.5 µg of total protein, which gave sharp, unsaturated bands.

2.7 Quantitative real-time polymerase chain reaction (qPCR)

In this project, fluorescence-based qPCR was used to quantify differences in mRNA expression (reverse transcription; qRT-PCR), and genomic DNA copy number (genomic; qG-PCR).

2.7.1 RNA extraction and first-strand complementary DNA (cDNA) synthesis

Total RNA was isolated from whole, cranial or caudal embryo samples frozen at -80˚C, using TRIzol Reagent (Gibco) Tissue was taken from dry ice and homogenised with 0.5 ml of TRIzol by pipetting and incubated at room-temperature for 5 minutes. A 100 µl aliquot of chloroform (Sigma) was added and tubes were vigorously shaken by hand for 15 seconds and incubated at room-temperature for 3 minutes followed by centrifugation at 12,000x g for 15 minutes at 4˚C for phase separation. The upper aqueous layer, containing the RNA, was transferred to a clean eppendorf tube. To precipitate the RNA, 200 µl of isopropyl alcohol were added and samples were incubated at 4˚C for 10 minutes, followed by centrifugation at high speed at 4˚C. The supernatant was carefully removed, without disturbing the gel-like pellet. The pellet was washed with 75% ethanol (in DEPC-treated water) by vortexing and collected by centrifugation for 5 minutes at 4˚C. Again the supernatant was removed and the pellet air dried for no longer then 10 minutes. The RNA pellet was then re-suspended in 20 µl of DEPC-treated H_2O and 0.7 µl of RNase inhibitor (Bioline) were added. At this stage the RNA was stored -80˚C or on dry ice prior to DNAse treatment.

DNA contamination was removed from RNA samples by DNase treatment, using a DNA-free kit (Ambion). To the 20.7 µl of RNA, 0.5 µl of recombinant DNaseI (rDNAseI, 2 U/µl) and 2.5 µl of 10x DNaseI buffer were added and incubated at 37˚C for 30 minutes. The reaction was stopped by addition of 2.5 µl of DNase inactivation buffer, incubation at room-temperature for 2 minutes with occasional mixing. Samples were centrifuged at 10,000x g for 2 minutes at room-temperature or 4˚C, before transferring the supernatant to a new tube. The concentration of RNA was measured using a NanoDrop (ND-1000 Spectrophotometer) which gives concentration in ng/µl (absorbance 260 nm). Sample purity was assessed by consideration of the ratio of absorbance at 260 nm/280 nm, which is ideally 1.8 for DNA and 2.1 for RNA. A lower value may indicate the presence of contaminants and these samples were discarded.

Typically 300 ng of RNA was used for reverse transcription to generate first strand cDNA, using SuperScript II Reverse Transcriptase (RT) kit (Invitrogen). The reaction mixture contained RNA template, 1 µl dNTP mix (10 mM), 1 µl random hexamers (50 ng/µl) and DEPC H_2O to a final volume of 10 µl per sample. The mixture was denatured by incubation at 65˚C for 5 minutes, and then placed on ice for at least 2 minutes prior to addition of 9.3 µl reaction mix (containing 2.0 µl 10x RT buffer, 4 µl 25 mM $MgCl_2$, 2 µl 0.1 M DTT, 0.5 µl RNase OUT Recombinant (Ribonuclease Inhibitor), and 0.8 µl DEPC-treated H_2O). The samples were gently mixed and briefly centrifuged. After 2 minutes incubation at room-temperature, 0.7 µl of SuperScript II RT was added, gently mixed and incubated at 25˚C for 10 minutes; 42˚C for 50 minutes for cDNA synthesis and then 70˚C for 15 minutes to terminate the reaction. After cooling on ice and brief centrifugation, 1 µl of RNase H was added, gently mixed and incubated at 37˚C for 20 minutes to remove RNA from the sample. First-strand cDNA samples were incubated on ice until use or at -20˚C if not used on the same day.

All cDNA samples were tested to check that the first strand reaction had worked by PCR using 1 µl cDNA as template and a standard PCR reaction using previously tested primers or primers to the housekeeping gene glyceraldehyde-3-phosphate dehydrogenase (*Gapdh*; **Appendix B, Table B.7**). Products were run on 2% agarose gels as most primers for qRT-PCR were designed to give a product of 150–250 bp. Primers for *Gapdh* were previously optimised to allow normalisation of qRT-PCR for a gene of interest to *Gapdh* abundance (Gustavsson et al., 2007).

2.7.2 Reverse transcription qPCR (RT-qPCR)

Quantitative RT-PCR was performed using RealTime PCR Mesa Blue qPCR Master Mix Plus for SYBR assay (EUROGENTEC), which utilises a SYBR green-like dye that fluoresces bound to double stranded DNA. All experiments were performed on a 7500 Fast Real-Time PCR System (Applied Biosystems) which accommodates a 96-well plate format (MicroAmp, Applied Biosystems).

The experimental design included a minimum of three samples per experimental group, each of which was analysed in triplicates. All primers were (SIGMA Aldrich) designed using Primer3 software (http://frodo.wi.mit.edu/primer3/), and analysed by BLAST on

NCBI-BLAST (http://blast.ncbi.nlm.nih.gov/Blast.cgi) to ensure that primers amplify unique products.

A master-mix was prepared on ice for each primer pair, which included: 12.5 µl Mesa Blue mix, 1.5 µl of each primer (10 µM), and 8.5 µl H_2O. A 1 µl aliquot of each cDNA sample was loaded onto a well of a 96-well plate, followed by the 24 µl mix. Three wells were thus used for each primer-pair/sample combination. A negative control (mix with water instead of cDNA) was also included for each primer pair. The plate was sealed (sealing tape; MicroAmp, Applied Biosystems), briefly vortexed and centrifuged, prior to loading of the plate onto the 7500 Fast Real Time-PCR System.

The software was set up as follows: Relative Quantification Plate assay; Standard 7500 running mode; detector - SYBR Green. The protocol involved a two-step standard method involving: pre-run of 50˚C for 2 minutes and 95˚C for 5 minutes followed by 40-46 cycles of denaturation at 95˚C for 15 seconds, annealing/extension at 56-60˚C (depending on primer) for 1 minute.

At the end of the real-time PCR amplification a dissociation curve was generated using a programme in which the temperature is raised by a fraction of a degree and the change in fluorescence is measured. This relies on the fact that there is a rapid decrease in fluorescence when the two strands of cDNA are separated at the melting point. All PCR products for a given primer pair should have the same melting temperature. If not, there is likely to be contamination, mispriming or primer-dimer artifacts. The settings were as for PCR but the running conditions were: 95˚C for 15 seconds (step 1), 58-60˚C for 1 minute (annealing temperature of primer pair), and 95˚C for 15 seconds.

The analysis of both Dissociation and Plate Analysis were performed by using the 7500 Software version 2.1.1 (Applied Biosystems). The analysis consists of:

- Dissociation: All the melting curves were checked. The rate of change of the relative fluorescence units with time on the Y-axis is plotted against the temperature on the X-axis, peaking at the melting temperature (**Fig. 2.11**). A primer-dimer artefact shows as a peak with lower melting temperature, and these wells were removed from the analysis.

- Plate Analysis: A threshold level was set the baseline (background fluorescence signal emitted during the first cycles of the PCR reaction before amplifying the product itself) and within the linear part of the reaction (**Fig. 2.10 A-B**). The reference gene and a calibrator (in general a wild-type sample) were specified. If the Ct (point at which the fluorescence crosses the threshold) for a sample was higher than that of the negative control (later Ct value; **Fig. 2.10 A-B**) the affected wells were excluded from the analysis since this could mean the cDNA quality was bad or degraded. All the Ct values were then checked for consistency within the triplicates for each gene. Finally, the relative quantification (RQ), corresponding to cDNA expression, of all samples (within the experimental groups, e.g., *curly tail versus* wild-type, a minimum of three of each) were analysed using Sigma Stat software (ANOVA or t-test if comparing only two groups) and plotted (mean and standard error) with Sigma Plot software (**Fig. 2.10 C-D**).

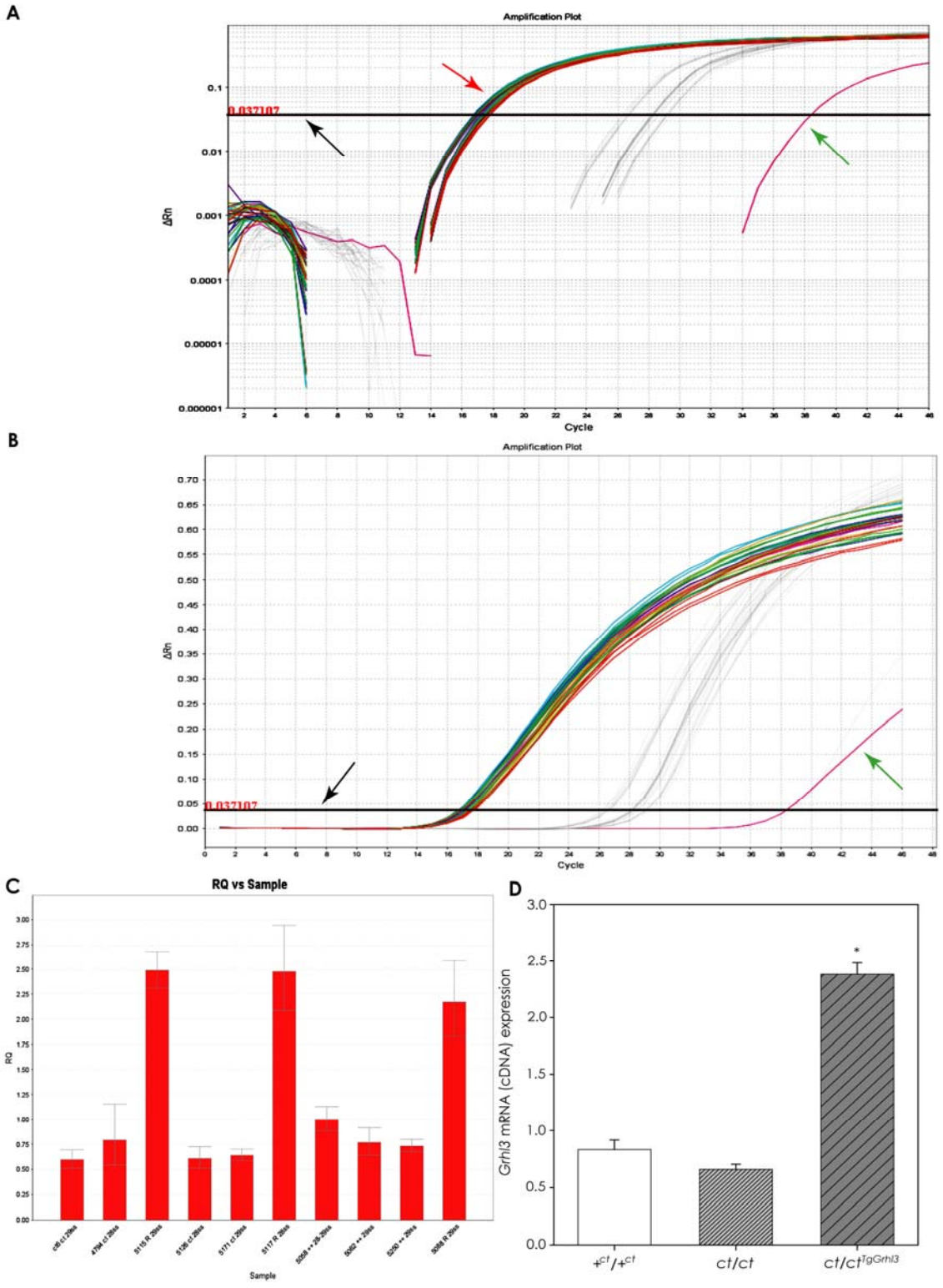
A
Amplification Plot
0.037107
ΔRn
Cycle
B
Amplification Plot
0.037107
ΔRn
Cycle
C
RQ vs Sample
RQ
Sample
D
Grhl3 mRNA (cDNA) expression
*
+ct/+ct
ct/ct
ct/ctTgGrhl3

Figure 2.10 Quantitative real time RT-PCR analysis. (**A-B**) Amplification plot in the 'Log' and 'Linear' views, respectively (software output). These plots show the threshold (black arrow), Ct curves (red arrow), and negative control (green arrow) for the *Gapdh* reference gene. (B) The delta Rn value (Y axis), which is the Rn value of the reaction minus the Rn value of the baseline signal generated by the instrument, is plotted against the cycle number (X axis). Rn is the normalised reporter value = fluorescent signal (SYBR green)/the signal of the passive reference dye for a given reaction. (**C**) Relative gene expression for each sample (*Grhl3* gene, in this example). (**D**) Graphical representation of the expression of a given gene (e.g., *Grhl3*) within the biological groups after statistical analysis (Sigma Stat and Sigma Plot software). * Indicates significant difference to the other groups ($p<0.05$).

2.7.3 Quantitative PCR for genomic DNA quantification

A qG-PCR method was developed to genotype embryos generated from single transgenic intercrosses (*ct/ct*^{TgGrhl3} *versus* *ct/ct*^{TgGrhl3}) litters, in order to distinguish between single and double transgenic embryos on the basis of *Grhl3* genomic copy number. Primers were designed in the intronic region of *Grhl3* and *Grhl2*, the latter to be used as a reference gene whose copy number is identical between samples (**Appendix B, Table B.3**). Each qG-PCR experiment included at least one *ct/ct* sample (normalisation sample, RQ 1.0), two single transgenic samples, for which the genotype was known (BAC positive embryos from crosses between *ct/ct* and *ct/ct*^{TgGrhl3} mice). These samples provided an index level for the copy number of *Grhl3* gene in single transgenics, for comparison with the "unknown" BAC-positive samples which could be either single or double transgenics.

A separate reaction mix was prepared for each sample containing 12.5 µl Mesa Blue (1x), DNA template, and H_2O to a final volume of 22 µl: sufficient volume was prepared for 6 reactions (*Grhl3* and *Grhl2* each in triplicate). Negative controls were prepared separately with no DNA. A separate mix of primers was prepared containing 1.5 µl each of the forward and reverse primers for each reaction), and 3 µl was loaded into each well, followed by 22 µl of reaction mix. The procedure was then the same as for qRT-PCR (as above).

Following analysis (Dissociation and Plate Analysis), the Relative Quantification value of each sample was plotted on a scatter plot using Sigma Plot software. Each plate was treated as a single experiment, i.e. plates were not combined. This analysis allowed the RQ values for individual embryo samples (which is determined by gene copy number) to be compared with the overall distribution of RQ values (Y-axis), which included the known: *ct/ct* and *ct/ct*^{TgGrhl3} samples. Thus, intervals of RQ values were defined which corresponded to the different genotypes: *ct/ct*, *ct/ct*^{TgGrhl3} (single transgenic) and *ct*^{TgGrhl3}*/ct*^{TgGrhl3} (double transgenic).

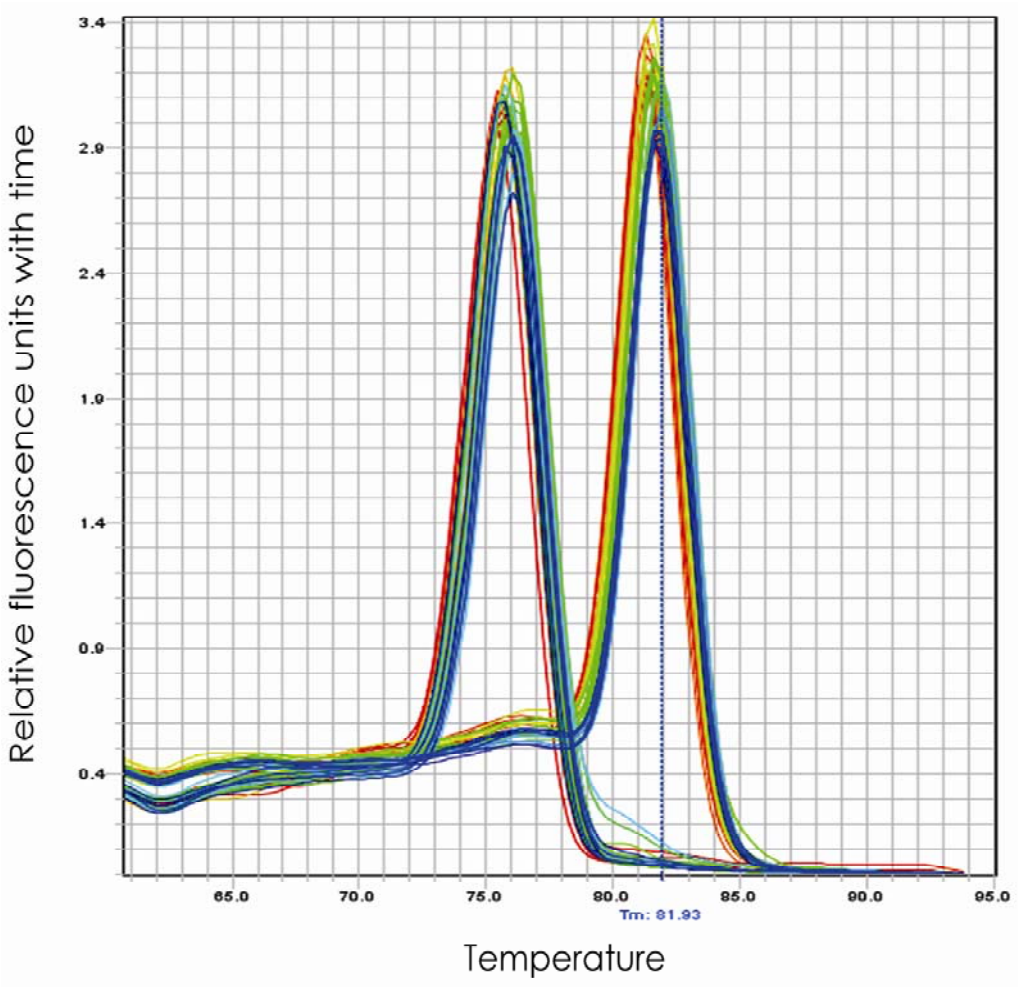

Figure 2.11 Genomic-qPCR analysis. Melting curve slopes for primer pairs used for amplification of *Grhl2* (left) and *Grhl3* (right) genes. Both show specific amplification characterised by sharp, single peaks for each sample, rather than diffuse or multiple peaks which would indicate non-specific amplification.

2.8 Sequencing of DNA and RNA (cDNA)

In order to sequence the coding region of the lamin B1 gene (*Lmnb1*), primers were designed to amplify the genomic DNA and cDNA. Fifteen pairs of primers were designed which flank the coding regions at genomic level (**Appendix B, Table B.5**), and five pairs were designed to amplify overlapping regions to cover the cDNA (**Appendix B, Table B.6**).

2.8.1 Sample preparation and PCR amplification

Genomic DNA was extracted from E10.5 *ct/ct* and $+^{ct}/+^{ct}$ embryonic yolk sac samples (**Section 2.2**). To check the transcript sequence, RNA was extracted from whole E10.5 embryos using TRIZOL, followed by DNase treatment, and first-strand cDNA synthesis (**Section 2.7.1**). Genomic DNA and cDNA samples were used as template for PCR amplification and an aliquot of the products were analysed on an agarose gel electrophoresis. PCR products were then purified using QIAquick PCR Purification Kit (QIAGEN) according to the manufacturer's instructions but eluting the sample in a lower volume (15 µl) of water. Purified PCR samples were re-run on agarose gels to check the product yield.

2.8.2 Sequencing reaction

Sequencing was carried out using ABI Prism BigDye Terminator kit (Version 3.1; Cycle Sequencing kit; Applied Biosystems). Reaction conditions are summarised in **Table 2.13.**

Reagents	Volume (µl)
PCR product	2.0
5x Sequencing Buffer	2.0
Primer	0.5
BigDye Terminator mix	1.5
Milli Q	4.0
Final Volume	10.0

Table 2.13 Sequencing reaction with Big Dye Terminator. Initially, the water, buffer and the BigDye Terminator reagent were mixed together, vortexed, and added to the PCR product. A single primer was added corresponding to one of the primers used in the previous PCR amplification.

Sequencing reactions were amplified on a Thermocycler using the following conditions: 20 seconds at 95˚C denaturation, 15 seconds at 60˚C annealing, 1 minute at 50˚C extension for 24 cycles. Samples were cleaned up by addition of 10 µl water, 2 µl 3 M NaAc and 50 µl absolute ethanol. Samples were vortexed and stored at -20˚C for 30

minutes to precipitate the DNA and then centrifuged at 13,000 rpm for a maximum of 20 minutes. The supernatant was then removed and the pellet was washed with 70% ethanol, followed by 100% ethanol and then air dried and stored at -20˚C until use for sequencing.

The sequencing products were separated and detected on a MegaBACE 1000 (with assistance from Dr Peter Gustavsson). Raw data (Ab1 files) were uploaded and the sequences assembled, aligned and analysed using Sequencher 4.7 software (Gene Codes Corporation).

2.9 Generation of an anti-sense probe for *Lmnb1*

2.9.1 Preparation of PCR product for cloning

In order to examine the expression of *Lmnb1* mRNA and perform whole mount *in situ* hybridisation it was necessary to produce an anti-sense cDNA probe. A 561 bp fragment (**Table B.6, Appendix B**), corresponding to base pairs 726-1286 of the transcript sequence (encoded by part of exon 2, exons 3-5 and part of exon 6) was amplified by PCR from a wild-type cDNA sample using the B1TrsF2/R2 primers. After confirmation of amplification by agarose gel electrophoresis, the PCR product was purified (as **section 2.8.1**) and a 2 µl aliquot was re-run on a 1% agarose gel to determine the concentration to be used for cloning.

2.9.2 Cloning of *Lmnb1* fragment into pGEM-T Easy Vector

The PCR product corresponding to *Lmnb1* cDNA was cloned into the pGEM-T Easy Vector (Promega) which contains *Sp6* and *T7* promoters for RNA polymerase (**Fig. 2.12 A**). For cloning, approximately 50 ng of template were used in a 10 µl ligation reaction containing 5 µl of 2x Rapid ligation buffer, 1 µl pGEM-TEasy (50 ng), 2 µl template (PCR product), 1 µl T4 DNA ligase (3 µg/µl) and 1 µl H_2O. This reaction was incubated at room-temperature for 2 hours and 15 minutes.

A 2 µl sample of ligation product was transformed into 50 µl of DH5α competent cells and incubated on ice for 20 minutes, followed by 50 seconds heat shock at 42˚C, and

cooling on ice for at least 2 minutes. After addition of 950 µl of Luria Broth Base (LB-Broth; Invitrogen), sample was incubated at 37˚C for 1 hour, shaking. At the end of this period, samples were plated onto agar plates (LB-Agar; Invitrogen) containing ampicillin (50 µg/ml, 1:1000 of 50 mg/ml stock; Sigma), and spread with 5-bromo-4-chloro-3-indolyl-β-D-galactopyranoside (X-gal, 100 µl of 20 mg/ml stock; Invitrogen) and isopropyl-thio-2-D-galactopyranoside (IPTG, 100 µl of 100 mM stock; Insight Biotechnology Ltd) for blue/white selection (**Fig. 2.12 B**).

The following day, white colonies were harvested. Half of each colony was streaked onto a LB-agar plate, and the other half mixed into a PCR reaction mix to check for presence of the insert (by PCR using the primers that were used for cloning, see above). For positive colonies a small sample was grown overnight in 10 ml LB-Broth containing 50 µg/ml ampicillin, at 37˚C with shaking. The following day cultures were centrifuged at 6,000x g for 15 minutes at 4˚C to obtain the bacterial pellet. Plasmid DNA was isolated using the QiaPrep Spin MiniPrep kit (Qiagen) according to the manufacturer's instructions. The orientation of the insert was determined by PCR using a 1/50 dilution of plasmid DNA as template and using different combinations of cloning primers together with the T7 and Sp6 vector primers (**Appendix B, Table B.9**). Primer combinations were T7/B1TrsR2, B1TrsF2/T7, Sp6/B1TrsR2, B1TrsF2/Sp6 and B1TrsF2 /B1TrsR2. In addition, orientation of the insert was confirmed by restriction digest of 0.2 µl of plasmid DNA using *EcoRI* (Promega), which excises insert from the vector, *HincII* (Gibco, Invitrogen), which cut the insert at base-pair 436 and the vector at base-pair 88, and *PstI* (Promega), which cut the insert at base-pair 510 and the vector at base pair 92 (**Appendix A, section A.16.1**). These two tests showed that *Lmnb1* insert was orientated in the same direction as the T7 promoter (**Fig. 2.13 C**).

2.9.3 Production of anti-sense *Lmnb1* probe

In order to perform *in vitro* transcription, the circular plasmid was first linearised and linear DNA was purified with phenol-chloroform (**Appendix A, section A.16.1**). After purification, the linearised DNA fragment was resuspended to a concentration 300 ng/µl and used for transcription of digoxigenin-labelled probes (**Appendix A, section A.16.2**). For production anti-sense probe the *Lmnb1* plasmid was linearised with *NcoI* endonuclease (Promega) and transcribed with *Sp6* RNA polymerase (Roche). For the

sense-strand the plasmid was linearised with *SpeI* endonuclease (Invitrogen) and transcribed with *T7* polymerase (Roche).

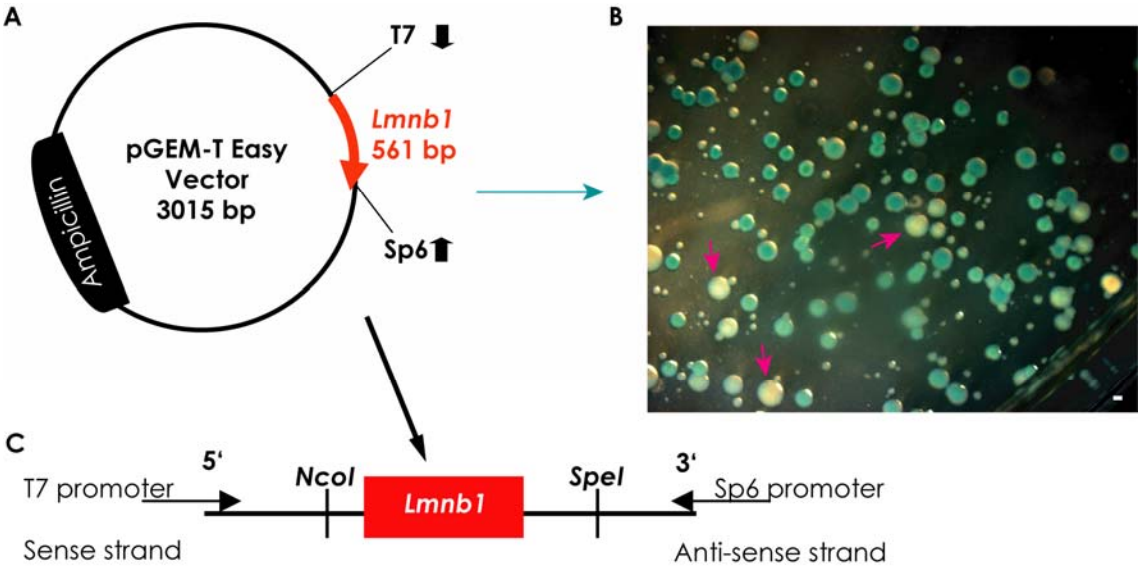

Figure 2.12 Cloning of *Lmnb1* for production of mRNA probe. (**A**) A 561 bp *Lmnb1* fragment was cloned into pGEM-T, which carries an ampicillin resistance cassette and *T7* and *Sp6* promoters. (**B**) Blue-white colony selection (IPTG/X-Gal). IPTG induces expression from the lac promoter and its derivatives. Pink arrows indicate positive clones. (**C**) Direction of the *Lmnb1* insert within the vector. To generate a sense probe, the plasmid was linearised with *SpeI* enzyme and transcribed with *T7 polymerase*, and for the anti-sense probe, plasmid was linearised with *NcoI* and transcribed with *Sp6 polymerase*. Scale bar in **B**: 1 mm.

2.10 Whole mount *in situ* hybridisation (WMISH)

The protocol here described follows that typically used in our laboratory, and is modified from the protocols of R. Conlon (Mt. Sinai, Toronto), P. Ingham (ICRF, London) and D Wilkinson (MIMR, Mill Hill). The probes used in this project are summarised on **Table 2.14**. WMISH was performed on embryos at stages E7.5 to E10.5. For analysis of whole E10.5 embryos a hole was made in the hindbrain using a needle or forceps to avoid trapping of the probe. Large buffer volumes (minimum of 4-5 ml) were used with E10.5 embryos to ensure adequate washing

Gene	Restriction Endonuclease	Polymerase
Lmnb1 - sense	*SpeI*	*T7*
Lmnb1 – anti-sense	*NcoI*	*Sp6*
Grhl3 – anti-sense	*SalI*	*T7*

Table 2.14 Probes used for whole mount ISH.

2.10.1 Day-1: Tissue pre-treatment, pre-hybridisation and hybridisation steps

All solutions used were DEPC-treated unless stated. Washes were carried out in 10 ml round bottom tubes, for 10 minutes at room-temperature with shaking.

Prior to use embryos were stored in 100% methanol at -20˚C.Embryos were rehydrated by a series of washes in cold 75%, 50%, and 25% methanol:PBT, and two subsequent washes in PBT (PBS with 0.1% Tween-20). Embryos were bleached in 6% hydrogen peroxide (10 ml in 50 ml PBT from the 30% stock; Sigma,) for 1 hour and washed three times in PBT. Embryos were then treated with 10 µg/ml proteinase K (10 µl in 10 ml of PBT, from a 10 mg/ml stock solution). Proteinase K permeabilises the tissue by partially digesting cellular proteins and treatment time therefore depended on embryo size: 1 minute for E8.5; 3-5 minutes for E9.5; 8-10 minutes for E10.5 (E7.5 embryos were not treated). The reaction was stopped by adding freshly made 2 mg/ml glycine (Fisher Scientific) in PBT. Next, embryos were washed twice in PBT before refixation in freshly prepared 0.2% glutaraldehyde (0.4 ml in 50 ml of 4% PFA, from 25% stock; Sigma) for 20 minutes, and two washes in PBT.

Embryos were transferred to pre-hybridisation mix (**Appendix A, section A.17.1**), pre-warmed to 70˚C prior to use. When the embryos sank to the bottom of the tube, the mix was replaced by 2-5 ml of fresh pre-hybrdisation mix and incubated at 70˚C for 3-5 hours.

Embryos were transferred to DNase/RNase-free 2 ml tubes with 1 ml pre-hybridisation mix. A 10 µl aliquot of DIG-labelled probe was added, gently mixed and incubated at 70˚C overnight. The single-stranded labelled probe hybridises to the target mRNA.

2.10.2 Day-2: Washes, pre-block and antibody binding

Following hybridization, the embryos were washed at high stringency to remove unbound probe. Probe-mix was replaced by pre-warmed solution 1 (**Appendix A, section A.17.2**), and incubated at 70˚C for 15 minutes. Embryos were subsequently transferred to 10 ml Falcon tubes and washed twice in solution 1 for 30 minutes at 70˚C, followed by two washes for 30 minutes in solution 2 at 65˚C (**Appendix A, section A.17.2**).

Prior to blocking embryos were washed three times for 10 minutes in TBST (**Appendix A**, **section A.17.3**), at room-temperature. Embryos were pre-blocked with 10% sheep serum (Sigma) in TBST for 90 minutes to block non-specific binding sites. At the end of this period the blocking solution was replaced by 2 ml of 1% Sheep serum in TBST containing 1:2,000 alkaline phosphatase-conjugated anti-digoxigenin antibody (AP-anti-DIG; Roche), and incubated overnight at 4˚C, with shaking. The AP-conjugated anti-DIG is an enzyme-conjugated antibody that binds to the DIG-labelled probe thereby allowing detection of the bound probe.

2.10.3 Day-3: Post-antibody washes

To remove unbound antibody embryos were washed three times in TBST for 5 minutes followed by six washes, for one hour at room-temperature and overnight at 4˚C.

2.10.4 Day-4: Development of signal

The TBST was replaced by NTMT (**Appendix A, section A.17.4**), for three washes of 10 minutes each. Embryos were then incubated in a solution of NTMT containing 4.5 µl/ml nitroblue tetrazolium chloride (NBT, Roche) and 3.5 µl/ml 5-bromo-4-chloro-3-indolyl-phosphate (BCIP, Roche) in the dark, at room-temperature, with gentle shaking. NBT/BCIP is a chromogenic substrate for alkaline phosphatase which generates a coloured precipitate.

Embryos were monitored after 20 minutes and then every 1 hour until the colour had developed. When signal had developed, the reaction was stopped by washing twice in PBT for 10 minutes and then overnight. Sense probe was used for *Lmnb1*, and colour reaction was developed for the same period as for the anti-sense probe, but gave no signal. Embryos were stored at 4˚C, in PBT with a small amount of sodium azide

(BDH) to prevent fungal growth and photographed (**Section 2.12**). Some photos were taken with the embryos oriented on agarose plates (made up in 1x PBS).

2.11 Sectioning of embryos after whole mount in situ hybridisation (WMISH)

To visualise the expression pattern in detail for internal tissues embryos were embedded and sectioned. Embryos at E7.5-E8.5 were embedded in wax and sectioned on a microtome. Embryos at E9.5-E10.5 were embedded in agarose or albumin-gelatin and sectioned on a vibrotome.

2.11.1 Microtome sections

After 2-4 hours or overnight fixation in 4% PFA, embryos were thoroughly washed in PBS and then dehydrated through an ethanol series. Each of these steps was for short periods, gradually increasing to 30 minutes in 100% ethanol. Embryos were then washed twice in HistoClear II (National Diagnostics) for 30 minutes each (15 minutes for E8.5 or smaller embryos), with the second wash at 60˚C. Finally embryos were transferred to paraffin wax (Thermo Scientific) at 60˚C and incubated with three changes of wax and then embedded, by allowing wax to cool. Wax blocks were left setting overnight. The next day, wax blocks were removed from the embedding dishes by leaving at -20˚C for at least 15 minutes. Blocks were shaped into cubes and attached to wooden blocks using melting wax.

Sections were cut on a microtome at 10-12 μm thickness and transferred to SuperFrost Plus slides (with a forceps and a paint-brush; VWR) where they were floated on water on a 40˚C heated-plate. When sections had flattened out, with no remaining wrinkles, the water was removed, the slides transferred to metal racks and left overnight to dry, wrapped on tissue, on the 40˚C heated plate.

Wax was removed by two 10 minutes washes in histoclear, and slides were mounted using DPX mountant for microscopy (BDH) and 1 mm cover-slips were applied (Menzel-Glasser, 24x60 mm; Agar Scientific). In some cases sections were counter-stained with eosin (Raymond A Lamb) to enable visualisation of the tissue that does not show gene expression. First, the wax was removed with Histoclear (2x 10 minutes each) and sections were then rehydrated in an ethanol series (75%, 50% and 25% for 1 minute

each) and washed in water for 2 minutes. Slides were then incubated in eosin solution (ready to use) for approximately 3 minutes and washed in water so that intensity of staining could be evaluated under a light microscope. Slides were quickly dehydrated in an ethanol series, washed twice in histoclear for 5 minutes and mounted in DPX mounting media.

2.11.2 Vibrotome sections

Embryos stored in PBT were fixed in 4% PFA for 2-4 hours, washed twice in PBS and then embedded in agarose: 1.5-2 % for E9.5 embryos and 2.5% for E10.5 embryos. Agarose was prepared in PBS, cooled for 15 minutes and then poured over the embryos (in plastic moulds), which were then oriented as the agarose set. Agarose embedded tissue was sectioned within a few hours.

Alternatively embryos were embedded in a gelatine-albumin solution (45 g albumin from chicken egg white, Grade II, Sigma; 0.75 g gelatine from bovine skin made up in PBS, Sigma; 30 g sucrose, Sigma; aliquots kept at -20˚C). After PBS washes, the embryo was transferred to embedding solution, and left overnight at 4˚C. The following day, embryos were embedded in 300 µl of gelatine-albumin to which 30 µl of glutaraldehyde was added and carefully oriented. The moulds were left to set for 30 minutes to 1 hour (longer periods are not recommended since the block and the specimen get over-dried). Blocks were excised from the mould, immersed in PBS and left at 4˚C for at least 1 hour prior to use.

Blocks containing embedded tissue (agarose or albumin) were shaped and attached to the specimen disc of the vibrotome (Leica VT 1000S, Leica Microsystems) with super glue. The vibrotome chamber filled with 1x PBS, and 50 µm sections were cut.

Agarose sections were transferred to PBS-filled wells of a 24 well plate, in sequence, and then mounted on SuperFrost slides with Mowiol mounting media which contains 2.5% 1,4-diazobicyclo-[2.2.2]-octane (DABCO; Sigma), cover-slipped and stored at 4˚C. Albumin sections were directly transferred to slides and mounted in a 50% glycerol (BDH), 50% water solution.

2.12 Microscopy, image capture and analysis

Photography of whole embryos was performed on a Leica MZFLIII microscope (LEICA) using a Leica DC500 camera. Images were captured by IrfanView or IM50 Leica Image Analyser (version 1.20) software. In some cases photography was performed using a Stemi SV11 microscope (Zeiss) with a Leica DFC490 camera, and images imported into Adobe Photoshop (version 6.0) software.

Bright-field images of sections were captured using an Axiophot 2 microscope (Zeiss) with a Leica DC500 camera, with import of images into Adobe Photoshop (Version 6). Fluorescence images of sections were obtained using an Axiophot microscope (Zeiss), with a Leica DC500 camera, and images were imported using Leica FireCam software for Mac.

Images were processed using Photoshop (Version 6.0) for cropping and adjustment of brightness/contrast and figures were prepared using Adobe Illustrator software.

2.13 Preparation of Lamin B1 fusion constructs

In order to perform functional analysis of lamin B1 protein variants, constructs were generated which encoded full-length (FL) and truncated versions fused to fluorescent proteins.

2.13.1 Construct encoding full-length Lamin B1 fused to green fluorescent protein (GFP)

Primers were designed to amplify the full-length *Lmnb1* transcript (ENSMUST00000025486), with restriction sites for *XhoI* and *KpnI* included in the forward and reverse primers respectively (**Appendix B, Table B.8**), to allow cloning into the pEGFP-C1 vector (4.7 kb, Clontech) in frame with an EGFP cassette, which encodes green fluorescent protein (GFP; **Fig. 2.13 A**).

The pEGFP-C1 vector was digested with *XhoI* (Promega) and *KpnI* (Promega) restriction enzymes using Buffer C (Promega) and purified by extraction with phenol/chloroform (**Appendix A, section A.16.1**).

First-strand cDNA synthesis was performed using RNA purified from embryos of the ct^{9E} and *ct* strains and the reverse primer, B1TrsR4, located in the 3'UTR region of *Lmnb1* (**Appendix B, Table B.6**). SuperScript First-Strand Synthesis for RT-PCR kit (Invitrogen) was used for first strand synthesis, according to manufacturer's instructions using the protocol for gene specific-primers. The cDNAs were then amplified by PCR using AccuPrime *Pfx* Super Mix (Invitrogen) which provides high fidelity amplification, using the cloning primers which included *XhoI* and *KpnI* restriction sites. The PCR product was purified (PCR Purification kit, QIAGEN) digested with *XhoI* and *KpnI* (using buffer C, Promega), overnight, at 37°C. Digested PCR products were purified by phenol extraction and ethanol precipitation.

PCR products were ligated into the *pEGFP-C1* vector using in a 7 µl reaction which also contained 1 µl linearised vector DNA, 1 µl *T4* DNA Ligase (Promega), 1 µl T4 Ligase buffer to a final volume of 10 µl. The volumes of PCR product and water were varied to give a molar ratio of vector DNA and insert DNA (PCR product) of 1:2.5 (vector:product). Ligation reactions were incubated over-night or for 48 hours, at 4°C. Ligated products were transformed into OneShot TOP10 Chemically Competent E. coli (Invitrogen) and plated onto agar plates containing Kanamycin (50 µg/ml, 1:1000 of 50 mg/ml stock; Sigma), and incubated overnight at 37°C. The following day, 10 different clones of each strain were selected: half of each colony was used in a PCR reaction with transcript primers to *Lmnb1* (B1TrsF2/R2 and B1TrsF3/R3; **Table B.6, Appendix B**) and half was streaked onto a new media plate to grow overnight. After establishing whether the selected clones had the respective insert, 5 of each of the streaked colonies were grown overnight in 10 ml LB-Broth containing 10 µl of kanamycin (50 µg/ml).

Plasmid DNA was purified from cultures using the QIAprep Spin Miniprep kit (QIAGEN) following the manufacturers' instructions, and plasmid DNA was eluted in 50 µl of water. Plasmids were digested with XhoI and/or *KpnI* in order to confirm overall size of the construct (vector with insert was 6515 bp), and the size of the insert (insert was 1815 bp and the empty vector was 4.7 kb; **Fig. 2.13 B**). Plasmids were then sent for sequencing (DNA Sequencing service at The Wolfson Institute for Biomedical Research, UCL) with primers B1TrsR1, B1TrsF2, B1TrsR2, and B1TrsF4 (**Appendix B**, **Table B.6**). Sequence was analysed using Sequencher software (Gene Codes Corporation).

2.13.2 Cloning of constructs encoding truncated forms of lamin B1 fused to yellow fluorescent protein (YFP)

Primers were designed in the transcript sequence in order to amplify a cDNA encoding the last 40 amino acids of the protein (C40, 123 bp including the stop codon, TGA). For cloning of this construct, Dr Ashraf Malhas kindly sent a plasmid which encoded the C40-human *LMNB1* fused to YFP protein, tagged with a nuclear localisation signal (NLS), sub-cloned into pcDNA 3.1 vector. Plasmid DNA was prepared and the construct sequenced (as above) to check restriction sites. In order to clone the mouse *Lmnb1* C40 sequence, the human *LMNB1* sequence was excised by digestion with *KpnI* and *XbaI* (using buffer C, all reagents from Promega). After electrophoresis of the digest on a 1% agarose gel, the higher weight band (corresponding to the pcDNA 3.1 vector, nuclear localisation signal and yellow fluorescent protein; total size of 6,136 bp) was purified using a QIAquick Gel Extraction kit (Qiagen).

The *Lmnb1* C40 primers (**Table B.8, Appendix B**) were used for PCR amplification of cDNA from ct^{9E} and *ct* strains, and the products were digested with *KpnI* and *XbaI* and purified as in **section 2.13.1**. The purified PCR products were ligated into the linearised vector (as above) and ligated products were transformed into OneShot TOP10 competent cells and plated into agar plates containing ampicillin.

Ten clones of each strain were selected and plasmid DNA was purified by mini-prep (as above) and then digested with *KpnI* and/or *XbaI* to verify the insert and vector sizes (**Fig. 2.13 C-D**). Plasmids for each strain were sent for sequencing with the forward cloning primer (mC40_F2) and the pcDNA3.1 reverse primer (**Table B.9**, **Appendix B**). Sequence-verified clones were grown up in LB broth (with ampicillin) and plasmid DNA was prepared using the Hi Speed Plasmid Maxi kit (Qiagen) which provides sufficient DNA for cell transfections. Constructs were sent to Dr Ashraf Malhas (University of Oxford) for use in FLIP experiments.

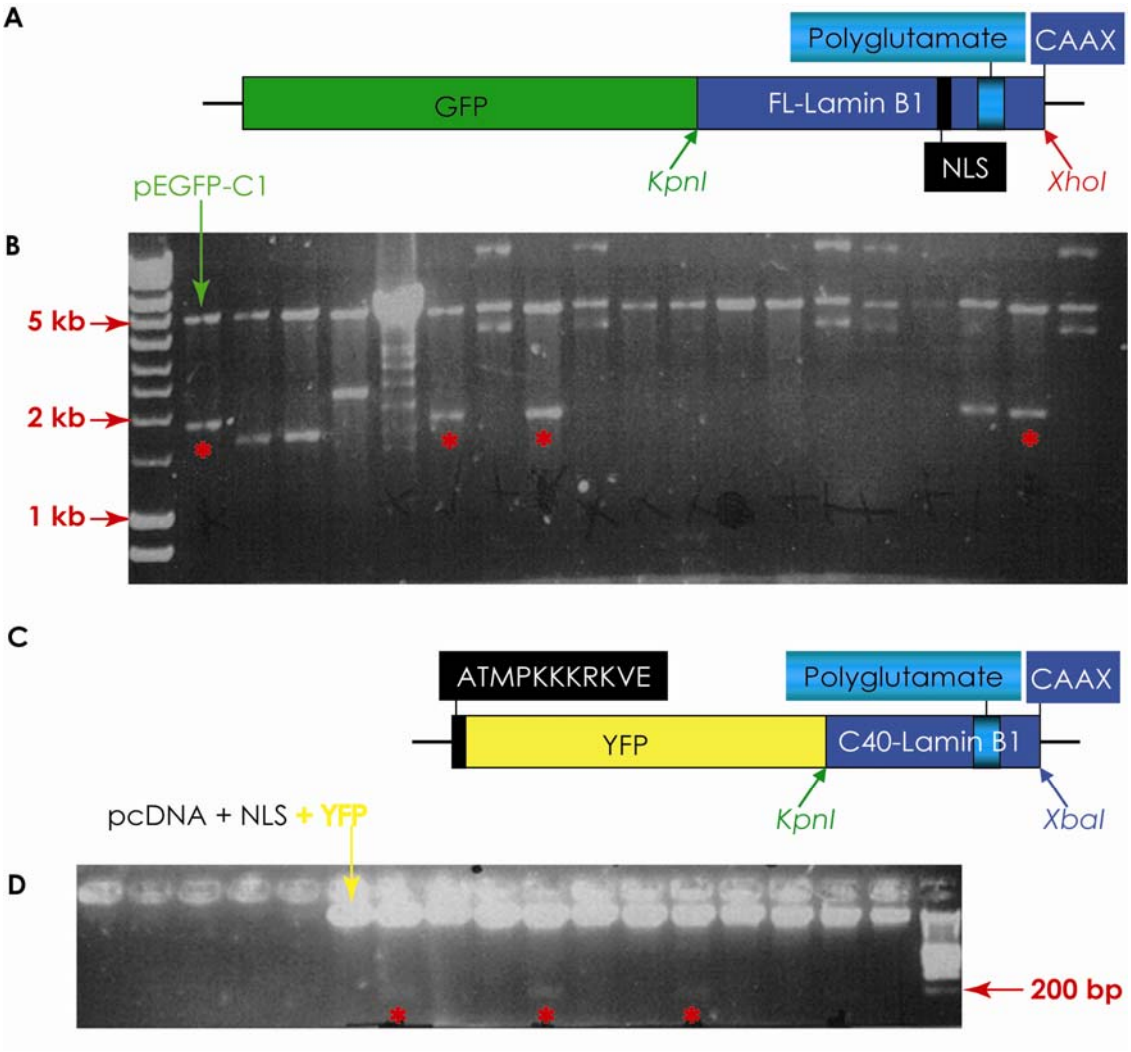

Figure 2.13 Lamin B1 fusion constructs for functional analysis. (**A**) Diagram of the construct encoding full-length Lamin b1 cloned in-frame with GFP coding sequence in the pEGFP-C1 vector which expresses green florescent protein (GFP). (**B**) Agarose gel image of double-digest of plasmids with cloning enzymes to confirm presence of the insert (1.8 kb, red asterisk) prior to sequencing. Green arrow indicates empty vector (4.7 kb). (**C**) Diagram of the construct which includes sequence encoding truncated forms in frame with yellow fluorescent protein (YFP), and sub-cloned into the pcDNA3.1 vector. This construct comprised the last 40 amino acids of the protein including the polyglutamate tract and the C-terminus (CAAX) and a nuclear localisation signal sequence (NLS) for nuclear import. (**D**) Gel image of double-digest of the plasmids to verify presence of the insert (198 bp, red asterisk). Yellow arrow indicates empty vector with NLS and YFP. Gels were loaded with Hypperladder I to give an estimation of the product sizes (indicated by the red arrows).

2.14 BAC localisation in *Grhl3*-transgenic embryos by inverse PCR

This experiment is summarised in **Figure 2.14**. Information about the enzymes used is in **Appendix A, section A.16**. The whole experiment is described in **Chapter 5**.

Genomic DNA was extracted from transgenic embryos using the QIAamp DNA Mini kit (Qiagen) according to the manufacturer's instructions but using half of the volumes since embryo samples were very small. Genomic DNA (1 µg) was digested with *RsaI* (Invitrogen) or *HaeIII* (Fermentas) (**Appendix A, section A.16.1**), overnight at 37°C. Enzymes were inactivated by incubation for 10 minutes at 65°C for *RsaI* and 20 minutes at 80°C for *HaeIII.* For circularisation of DNA fragments a 25 µl aliquot of digested genomic DNA was diluted in a final volume of 500 µl, also containing 50 µl ligase buffer, 10 µl T4 DNA ligase (Promega). Reactions were allowed to proceed for 2 hours at room-temperature. The DNA was then purified by precipitation with 50 µl 3 M sodium acetate and three times the volume with absolute ethanol, followed by centrifugation at 13,000 rpm and the resulting pellet was resuspended in 8 µl of water.

Following purification of the DNA after ligation, the DNA was digested with *BamHI* (Promega) for 2 hours at 37°C, to linearise the circular molecules. The enzyme was inactivated at 65°C for 15 minutes. The linearised product (2 µl) was then amplified by PCR with BAC inverse primers (PCR conditions as described in **section 2.3**, using a 56˚C annealing temperature; primers sequence in **Appendix B**, **Table B.4**). PCR products were run on a 1% agarose gel and all obvious bands were excised from the gel and purified using QIAquick Gel Extraction kit (Qiagen) according to the manufacturer's instructions. DNA was eluted in 15 µl of water, and re-amplified by PCR for subsequent sequencing with each of the inverse primers.

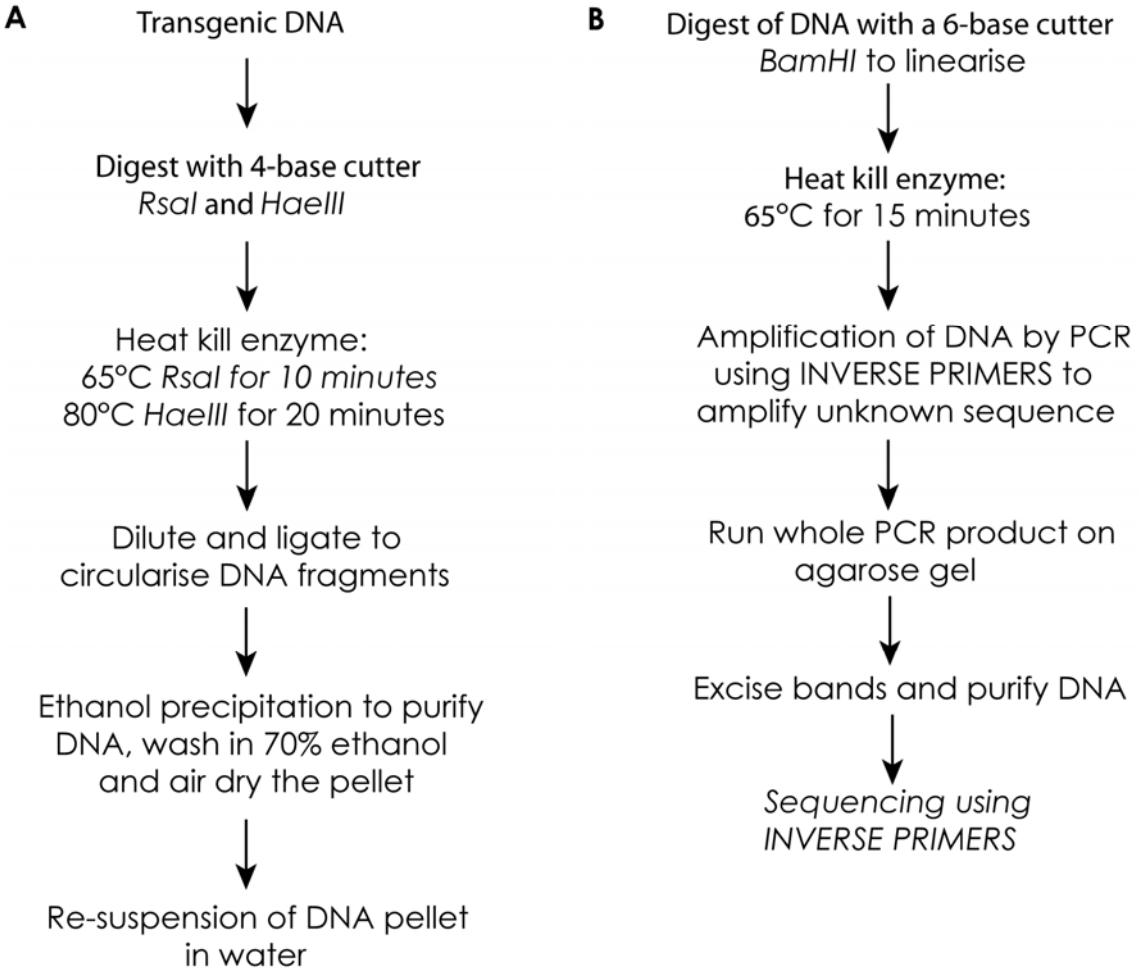

Figure 2.14 Summary of inverse PCR experiment performed for BAC localisation.

2.15 Production of primary mouse embryonic fibroblast cell lines (MEFs)

Mouse fibroblasts (MEFs) were generated for *in vitro* studies from E13.5 fetuses (**Fig. 2.15 A**) of each of the *curly tail* strains (*ct*, $+^{ct}$, ct^{9E}, ct^{8E}, $ct/ct^{TgGrhl3}$), and the *C57BL/6* inbred strain. All materials used were sterilised by autoclaving and spraying with 70% ethanol. Fetuses with NTDs were not used for production of MEFs.

Pregnant females were killed by cervical dislocation, and dipped in 70% ethanol prior to removal of the uterus. The uterus was rinsed in 70% ethanol and transferred to a fresh Petri dish containing 1x Dulbecco's PBS (Gibco), in a laminar flow hood. Embryos were dissected from the uterus, the yolk sacs removed and the embryos transferred to a clean dish. All blood-filled internal organs (e.g., liver) were removed and the embryo

was washed with fresh PBS (removing as much blood as possible). In a new dish, using minimal amount of PBS, embryos were minced as finely as possible using a razor blade. The tissue homogenate was then transferred to a 50 ml falcon tube in a solution of 1x trypsin-EDTA (2 ml/embryo, diluted in PBS from a 10x stock solution, Gibco) and digested at 37°C for 15 minutes. Tubes were occasionally inverted to mix the contents. Care was taken to limit the trypsinisation step to less than 20 minutes.

To the cell suspension were added 3 volumes of MEF medium (**Appendix A**, **section A.18**). Particulates were allowed to settle to the bottom of the tube (approximately 5 minutes) and the supernatant was carefully transferred to a new tube and centrifuged at low speed (5 minutes, 1000 rpm). The supernatant was discarded and the cell pellet was re-suspended in warm MEF medium and plated out at 1 embryo equivalent per 10 cm tissue culture dish (this is "passage No. 0"). The medium was changed on the following day. The fibroblasts are the only cells that attach to the dish and plates were confluent within 2 to a few days (depending on the strain).

For the transgenic line ($ct/ct^{TgGthl3}$) only, embryos were treated individually, in 5 cm Petri dishes for all tissue/cell suspension steps, kept in individual 15 ml falcon tubes and plated individually in 10 cm Petri dishes. This procedure was taken because embryos of the transgenic strain needed to be genotyped for the presence of the BAC.

When the MEFs were confluent (**Fig. 2.15 B**), they were passaged or frozen down. To passage the cells they were first washed in PBS, and trypsinised (1x, 1.5 – 2 ml per 10 cm plate) for 5 minutes at 37°C. The trypsin was inactivated by addition of MEF medium. Cell clumps were then dissociated into single cells by pipetting up and down several times, and the cells were centrifuged at 1000 rpm for 5 minutes. The supernatant discarded and the cell pellet was re-suspended in fresh media (3 or 5 times the previous volume), plated out and cultured until confluent.

To freeze the cells a similar procedure was performed to that described for passaging. However, the cell pellet was re-suspended in cold freezing media (10% DMSO in FBS, Sigma) instead of MEF media, in a volume equivalent to one embryo per vial. Cell suspensions were transferred to cryo-vials (1 ml/vial; Nunc, Thermo Scientific), and

cooled on ice before storing at -80°C. For long-term storage, cells were transferred to liquid nitrogen.

Frozen MEFs were re-plated by quickly thawing them in a 37°C water-bath and transferred to a Falcon tube with 20 ml warm fresh media. Cells were pelleted by centrifugation (5 min at 1000 rpm), to remove the DMSO contained in the freezing medium, and then re-suspended in fresh medium and plated out at the desired ratio.

2.15.1 Generation of chromosome spreads of fibroblast nuclei for Fluorescence *in situ* hybridisation (FISH)

This technique was optimised from the method described by Kulnane et al (2002). C57Bl/6 and *ct/ct*^{TgGrhl3} MEFs were used at different passage numbers. Demecolcine (Sigma) was used to arrest the cells in metaphase. All centrifugation steps were at 1000 rpm for 5 minutes each.

The culture media (MEF media) was removed and replaced with 10 ml of fresh media 2 hours before starting the experiment. Demecolcine (1 μg/ml of the 200 μg/ml stock) was added to each plate and left for a minimum of 1 hour at 37°C. To harvest the cells, plates were washed twice with Dulbecco's PBS and incubated with trypsin (1x, 1.5-2 ml/plate), for 5 minutes to detach the cells from the plate. Fresh warm media was added and cells were suspended by pipetting up and down several times, transferred to a falcon tube and centrifuged.

Each cell pellet was re-suspended drop-by-drop in warm 0.56% KCL (hypotonic solution to eventually cause cell bursting) to a volume of 5 ml and incubated at 37°C for 15 minutes. A 2 ml aliquot of fixative (3:1 methanol/acetic acid) was added, and mixed by inverting the tube before centrifugation. The cell pellet was re-suspended drop-by-drop in fixative up to 5 ml, centrifuged and re-suspended again before being stored at -20°C for at least 1 hour. After this period, cells were again re-suspended in fixative, drop-by-drop and centrifuged three further times. After the last centrifugation, cells were re-suspended in 100 – 200 μl fixative, dropped onto slides (previously kept overnight in 5% acetic acid in ethanol) and dried for 1 hour at 37°C. Slides were

mounted in Vectashield mounting medium with DAPI (Vector Laboratories) and kept at 4°C, protected from light (**Fig. 2.15 C-D**).

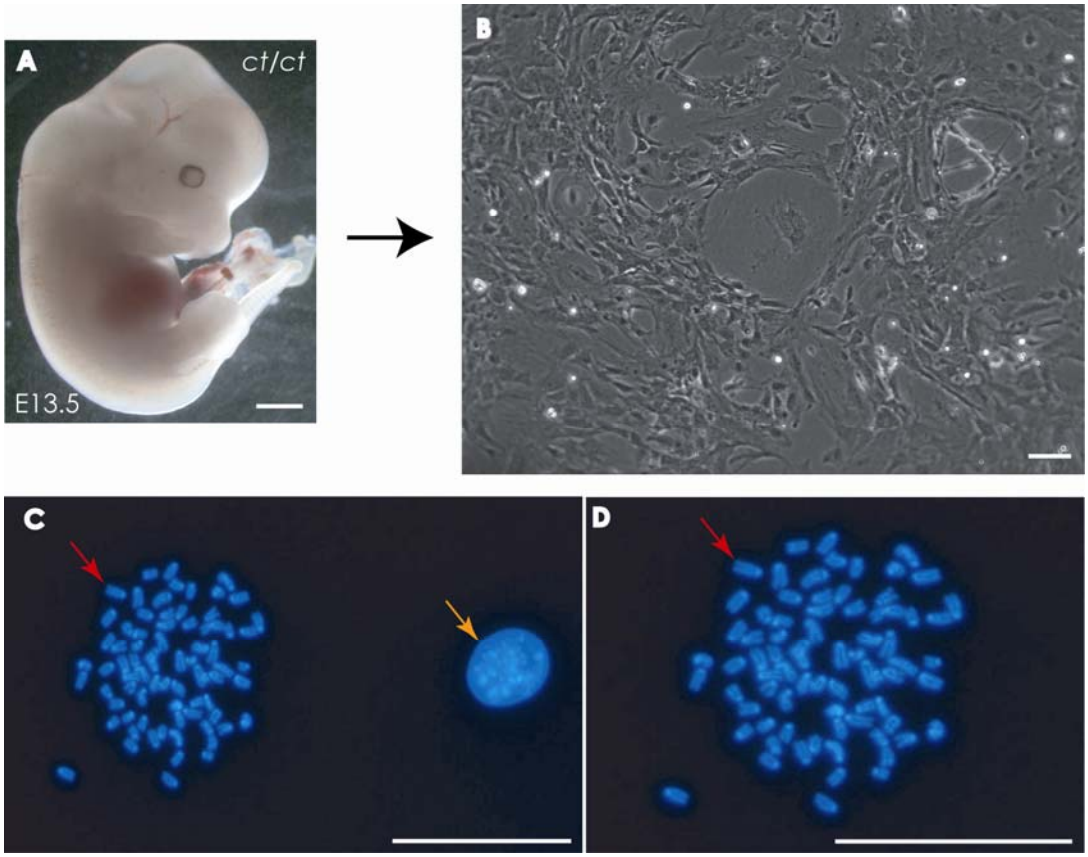

Figure 2.15 Generation of mouse fibroblasts and metaphase spreads of cell nuclei. (**A**) E13.5 fetus for generation of primary cell lines. (**B**) Image of cultured cells. (**C**) Image of chromosomes in metaphase (red arrow, at higher magnification in **D**) and an interphase nuclei (orange arrow). Scale bars: **A**, 1 mm; **B**, 0.5 mm; **C-D**, 0.05 mm. Images were taken on: **A**, Leica MZFLIII microscope; **B**, Time lapse microscope (Zeiss Axiovert 135); **C-D** Axiophot (Zeiss), under UV light for DAPI visualisation.

2.16 Alcian blue staining of cartilage

Fetuses collected at E15.5 were dissected in cold PBS and transferred to cold 100% ethanol to fix the tissue. An incision was made in the abdominal region to allow better entrance of the fixative. After 48 hours the fetuses were washed in clean 100% ethanol for 1 hour with shaking and then incubated in acid staining solution (pH 2.8) composed of 14% Alcian Blue in 70% ethanol (1:10), Glacial Acetic Acid (1:5) and 70% ethanol

(Filtered). Fetuses were left incubating at room temperature until the temporal bone was visible (around five to ten days). Specimens were then incubated in 0.02% KOH to remove part of the epidermal tissue for three to five days until the staining was visible (solution was freshly made and changed twice a day). Stained samples were then "clarified" in a solution made with 1 part Benzyl alcohol, 2 parts Glycerol and 2 parts 70% ethanol. Embryos were finally fixed in 50%:50% 70% ethanol/Glycerol. This experiment was performed with the help of Dr Valentina Massa.

2.17 Statistical analysis

All statistical analysis was performed using SigmaStat software (Jandel Scientific). Embryos were scored for neural tube defects, tail flexion defects or no defects. Two different tests were applied: Chi-square (χ^2) to establish the relationship between two or three of the phenotypic categories according to the observed frequencies; or Z-test, which compares the difference in the proportions of individuals with the characteristic of interest within two groups. For analysis of quantitative data (such as posterior neuropore lengths) experimental groups were compared by t-test or One Way ANOVA.

Appendices

APPENDIX A – Solutions and buffers

A.1 Diethyl pyrocarbonate treated water

DEPC was used to all solutions that needed to be ribonuclease (RNase) free, such as for *in situ* hybridisation, to prevent degradation of the target RNA. One ml DEPC (**Sigma)** was added to 1 L of milli-Q water and vigorously mixed. The following day the water was autoclaved to break down DEPC.

A.2 Phosphate-buffered saline

PBS tablets were dissolved in milli-Q water (100 tablets in 1 litre) to give a 10x stock solution and stirred until the tablets were dissolved. If the PBS was needed for RNAse-free experiments, it was treated with 1 ml of DEPC (see above) and autoclaved the next day.

From the 10x stock, 100 ml were used to make up 1x DEPC-PBS working solution, and diluted in 900 ml of DEPC-H_2O.

Alternatively, 10 PBS-tablets were added to already autoclaved milli-Q water, stirred to make up 1x PBS for other experiments which did not require RNase-free solutions.

A.3 4% paraformaldehyde

40 g of paraformaldehyde (PFA) was dissolved in 800 ml of DEPC-PBS and 1.5 ml of 0.5 M NaOH (made up in DEPC water) was added. The solution was incubated at 55˚C and mixed by inversion once in a while. When in solution, the volume was topped up with extra DEPC-PBS to 1 litre. The solution was cooled on ice, aliquoted and stored in vacuum bags at -20˚C.

A.4 Proteinase K

Proteinase K powder (Roche), stored at 4˚C, was dissolved in DEPC-treated water (250 mg in 250 ml to a final concentration of 10 mg/ml. The flask was inverted several times, and when mixed the solution was aliquoted and stored at -20˚C.

A.5 DNA Extraction Buffer

All solutions listed in **Table A.5.1** were mixed and the volume completed with autoclaved milli-Q water.

Solution	Volume	Final concentration
1 M Tris-HCl (pH 8.5)[a]	12.0 ml	100 mM
0.5 M EDTA (pH 8.0) [b]	1.2 ml	5 mM
5 M NaCl[c]	4.8 ml	200 mM
10% SDS[d]	2.4 ml	0.2%
H_2O	99.6 ml	

Table A.5.1 DNA extraction buffer ingredients for a final volume of 120 ml. Each solution (**a-d**) was prepared individually and kept as stock.

A.6 Deoxynucleotide (dNTP) mix for PCR

A 10 μM working-mix was made by combining equal volumes of the stock solutions of dATP, dTTP, dCTP, dGTP (100 mM each; Promega), and diluted 25 times. Aliquots were stored at -20˚C.

A.7 Agarose gel electrophoresis

In this project different concentrations of agarose gels were needed for different purposes. Routine gels were typically 1% - 2% using UltraPure standard agarose (Invitrogen), 1g/100ml dissolved in 1x Tris-Acetate-EDTA (TAE, 40 mM Tris acetate; 1 mM EDTA). For genotyping purposes higher concentrations of agarose were required such as 3-5%. For example, for 5% gels, 4 g UltraPure Low Melting Point agarose

(LMP; Invitrogen) was mixed with 1 g standard agarose and dissolved in 100 ml TAE. 1-2 µl ethidium bromide (10 mg/ml; Sigma) were added.

Orange G was used as loading buffer: containing 50% glycerol (BDH) and 50% 1x TE buffer (10 mM Tris EDTA pH 8.0) with Orange G (Sigma) to colour.

DNA molecular weight markers depended on the expected size of DNA bands and were Hyperladder I, with bands ranging from 200-10,000 bp (BIOLINE) or Hyperladder V, with bands ranging from 25-500 bp (BIOLINE). The bands on the gel were visualised under ultraviolet trans-illumination (UVITEC) which results in the fluorescence of the Ethidium Bromide dye (Fluka), which binds double stranded DNA by intercalation between the base pairs. The trans-illuminator was fitted with a camera (UVIDOC) for photography (High Density Paper; Mitsubishi Electric).

A.8 Lysis buffer for protein homogenisation

30 g urea was dissolved in 15-20 ml DNase, RNase free water (Sigma), by stirring with periods at 37°C. When the urea was in solution, 2 g amberlite (Amersham PlusOne Amberlite IRN-150) was added, stirred for 10 minutes and filtered through a 0.45 µm circular filter (Whatmann Cellulose Nitrate Membrane Filters). The remaining reagents were added, the volume was completed to 50 ml with water and 1ml aliquots were stored at -80°C.

Reagent		Final concentration
Urea (PlusOne, GE Healthcare)	30.0 g	9.5M
CHAPS (PlusOne, 1g, GE Healthcare)	1.0 g	2%
DTT (Dithiothreitol Cleland's Reagent, USB)	0.5g	1%
Protease inhibitors cocktail tablets, (Complete Mini, Roche)	5 tabs	1x
Phosphatase inhibitor 1 (Sigma)	0.5 ml	1x
Phosphatase inhibitor cocktail 2 (Sigma)	0.5 ml	1x

Table A.8.1 Ingredients of the lysis buffer for protein homogenisation in 2D experiments. Final volume was adjusted to 50 ml. Abbreviation: tabs, tablets.

Prior to use of this buffer, a 2% volume (v/v) of IPG buffer (pH range corresponding to IPG strip) or Pharmalyte (2% volume gives 0.8% final concentration, GE Healthcare) were added.

For phosphatase treatment experiment, the buffer used was the same as in **Table A.8.1** but **no phosphatase inhibitors** were added.

A.9 Protein assay based on Bradford method

Samples (1 or 2 µl in duplicate) were kept on ice and diluted to a 10 µl volume with autoclaved milli-Q H_2O. Standard solutions were made up (**Table A.9.1**). To the 10 µl of protein sample/standard, 25 µl of 0.1 N HCl:H_2O[a] (1:8) was added. Finally, 1 ml of working reagent (diluted 1 + 4 with H_2O; Bio-Rad Protein Assay, Bio-Rad) was added, mixed by inversion and left at room temperature for 10 min. The optic density was measured at 595 (OD_{595}) on a UV-Spectrophotometer (UV Mini 1240, SHIMADZU) and a standard curve plotted to allow protein quantitation in samples.

BSA (µg/ml)	µg in assay	Vol. 1 mg/ml stock (µl)	Vol. lysis buffer (µl)	Vol H_2O (µl)
0	0	0	2	8
1	1	1	2	7
2	2	2	2	6
4	4	4	2	4
6	6	6	2	2
8	8	8	2	0

Table A.9.1 Protein assay. 1 mg/ml BSA (Albumin standard from BCA Protein Assay kit, Pierce) was used as standard protein. Standards and samples were always prepared in duplicates. The lysis buffer was the same as used for protein homogenisation.

A.9.a 0.1 N HCl

For 500 ml, 4.3 ml concentrated HCl (11.6 M, Sigma) were added to 495.7 ml H_2O. From this, 62.5 ml 0.1 N HCl were added to 437.5 ml H_2O to make up HCl:H_2O (1:8).

A.10 Rehydration buffer for IPG strips

For 30 ml final volume, 19.3 g of urea (8 M) were dissolved in 10-15 ml of purified water. 0.5 g amberlite were added, stirred for 10 minutes and filtered (using 0.45 µm circular filter, as above). To the urea mixture, 60 mg DTT (0.2%), 600 mg CHAPS (2%), and a few grains of bromophenol blue (PlusOne GE Healthcare) were added. The volume was then completed with water and 1 ml aliquots were stored at -80°C.

Before using this buffer, 1x Protease Inhibitor (10 µl aliquots stored at -20°C; 100x mix, Amersham Biosciences) were added, vortexed and centrifuged briefly.

A.11 Acrylamide gels for second dimension: 12.5% gels

Gel cassettes (for 1.5 mm thick gels) were cleaned with methanol and air dried. The volume of gel-mix and therefore acrylamide (Acrylogel 2.6, 40% Solution; Electran, BDH) depended on which system was to be used. **Table A.11.1** summarises the volumes of each ingredient of the gel-mix depending on the number of gels to be cast.

No Gels	Final Volume	Acrylamide	Tris-HCl	H_2O	10% SDS	10% APS	TEMED (µl)
6	600 *	180	149.0	260.0	6	4.50	130.0
10	900 **	270	223.5	390.0	9	6.75	195.0
12	1,100 **	330	273.2	476.7	11	8.25	238.3

Figure A.11.1 2D-gel mix volumes for a different number of gels. All volumes are given in ml with exception of TEMED. * Six- and ** 14 gel-caster, respectively.

To the acrylamide, amberlite (2 g) was added and stirred for 20 min. The acrylamide was filtered through a 0.45 µm circular filter. Tris-HCl (1.5 M, pH 8.8; PlusOne, Amersham Biosciences) and milli-Q H_2O were added to complete the volume. This mix was de-gassed for 1 hour, with stirring. After this period, sodium dodecyl sulphate was added (SDS, Sigma), with stirring.

The cassettes were then assembled in the casting chamber using a plastic sheet between each cassette. Plastic sheets were added to level the casting cassette. Freshly prepared 10% ammonium persulphate $(NH_4)_2HO_8$ (APS, MW 228.20; PlusOne, Amersham Biosciences), and TEMED (N,N,N',N'-tetramethylethylenediamine; PlusOne, Amersham Biosciences) were added to the mix. The gel mix was stirred and immediately poured into the gel caster.

When using the 12/14-gel caster, it was necessary to make up 100 ml of displacing solution to fill up the balance chamber: 25 ml glycerol anhydrous (50% v/v; Fluka Biochemika), 25 ml 1.5 M Tris-HCl pH 8.8 (0.375 M), 25 ml milli-Q water and a

sprinkle of bromophenol blue. After pouring the gel mix, the funnel and feed tube were removed and the displacing solution was allowed to run in to displace the gel mix into the cassettes. The gels were immediately overlaid with water saturated butanol and left to set for a minimum of 2 hours. After polymerisation, the gel-casting cassette was dismantled, the butanol was poured off and the top of the gels were rinsed with milli-Q water. The gel cassettes were wrapped between damp tissues, and then the whole stack was wrapped in cling-film and stored at 4°C overnight if not used on the same day.

- **Running buffer for 10-DALT tank:** for 1x buffer, 60.5 g Tris (PlusOne), 288.0 g glycine (Fisher Scientific) and 20.0 g SDS were added straight to the tank and the volume was made up to 20 L with milli-Q water and left circulating for at least 3 hours.

- **Running buffer for 12-DALT tank:** 45.4 g Tris, 216.0 g glycine and 15.0 g SDS were added to a Duran bottle, made up to 1.5 L with water to give a 10x buffer. For the run itself: it was necessary to make up 7.5 L of 1x buffer for the lower chamber (left circulating for 2-3 hours), 250 ml 1x buffer for washing strips after equilibration and agarose mix, and 3x buffer for the upper chamber.

A.11.a Water Saturated n-butanol

Equal volumes of n-butanol (BDH) and milli-Q water were added to a Duran bottle, and mixed vigorously several times. The top layer was water-saturated n-butanol and the lower layer was n-butanol-saturated water.

A.12 Equilibration buffer for second dimension

Table A.12.1 summarises the recipe for this buffer. All ingredients were added to 400 ml of water and stirred for 2-3 hours. Once in solution, a few grains of bromophenol blue were added. The volume was topped up to 500 ml with milli-Q water and aliquots were stored at -20°C.

Reagent		Final concentration
Urea	180 g	6 M
Glycerol anhydrous	150 g	30% (w/v)
SDS	10 g	2%
1.5 M Tris pH 8.8	16.7 ml	0.05 M
Bromophenol Blue	few grains	
Milli-Q H_2O	To 500 ml	

Table A.12.1 Recipe for a 500 ml stock solution of equilibration buffer.

A.13 Mix for the agarose sealing solution

For 6 gels:

125 mg of agarose were added to 25 ml 1x running buffer, with a few grains of bromophenol blue and boiled prior to cooling before use. The final solution contains 25 mM Tris-HCl, 192 mM Glycine, 0.1% (w/v) SDS, Bromophenol Blue and 0.5% (w/v) agarose.

A.14 Trypsin for in-gel digestion of protein spots

250 µl of 0.1 % trifluoroacetic acid (TFA; Sigma-Aldrich) were added to bovine trypsin (25 µg/tube; Roche sequencing grade), and vortexed to dissolve the trypsin powder. When in solution, 15 µl aliquots were stored at -20 ^{o}C.

A.15 Western blot buffers

A.15.1 Radio-Immunoprecipitation Assay (RIPA)

Reagent	Final concentration
1.5 ml Sodium Chloride (5 M stock)	150 mM
0.5 µl NP-40 (Fluka)	1%
0.25 g Sodium deoxycholate (Sigma)	0.5%
0.05 g SDS	0.1 %
2.5 ml Tris-Cl (1 M, pH 7.4)	50 mM
500 µl Phosphatase 1	1x
500 µl Phosphatase 2	1x
5 tablets protease inhibitors (Complete)	1x

Table A.15.1 RIPA lysis buffer. All reagents were mixed and made up to a final volume of 50 ml wit milli-Q water. Aliquots were stored at -80^{o}C.

A.15.2 Bio-Rad and Invitrogen system transfer buffers

Reagent	Final concentration
5.82 g Tris-base	25 mM
0.375 g SDS	25 mM
2.939 g Glycine	1 mM
20% methanol	0.05 mM

Table A.15.2 Transfer buffer for semi-dry system. For the Tris-SDS transfer buffer all reagents were dissolved for 1 L final volume with milli-Q water.

Reagent	Final concentration
10.2 g Bicine (Fluka)	25 mM
31.3 g Bis-Tris (free base)	25 mM
0.75 g EDTA (Sigma)	1 mM
0.025 g Chlorobutanol (Alpha Aesar)	0.05 mM

Table A.15.3 Transfer buffer for wet system. To make up 20x NuPage transfer buffer, all regents were dissolved, the pH adjusted to 7.2 and the volume completed to 125 ml with milli-Q water.

1 Gel – 10% methanol		2 Gels – 20% methanol
50 ml	20 x transfer buffer	50 ml
100 ml	Methanol	200 ml
850 ml	Milli-Q water	750 ml
1000 ml	Total volume	1000 ml

Table A.15.4 NuPage buffer to transfer 1 or 2 gels. From the 20x stock buffer, 1x buffers were made up with different methanol concentrations to transfer 1 or 2 gels.

A.15.3 Tris-buffered saline (TBS) and TBST for immunoblotting

To the TBS buffer, 0.1% Tween-20 (Sigma) was added and thoroughly mixed. Blocking buffers were made with 5% non-fat dried milk (Marvel) or 5% Albumin from bovine serum (BSA; Sigma), depending on the antibody.

A.16 Restriction enzyme digests in general and transcription reactions

A.16.1 Enzyme digest: small/single, double and large scale

- Small scale digest: 1 µl DNA template (0.2 – 0.5 µg), 2 µl 1x restriction enzyme buffer (1/10 of the 10x concentrate), 0.2 µl BSA (1/10; Promega enzymes), 0.5 µl enzyme (5-10 Units), and the volume was made up to 20 µl with water. Digests were incubated for 2 hours at 37^{o}C.

- Double digest: same volumes and concentrations as above but 0.5 µl (5-10 Units) of each restriction enzyme. Digests were incubated for a minimum of 2 hours at 37^{o}C.
- Large scale digest: 5 - 10 µg DNA with 1x restriction enzyme buffer, 20 – 50 Units restriction enzyme, to a final volume of 50 – 200 µl. Digested for 2 hours at 37^{o}C.

Cut DNA and uncut DNA (for comparison) were run on 1% agarose gels. For other applications, gel concentration would depend on the size of the fragment.

Large scale digests were purified by making up to 100 µl with water and an equal volume of phenol-chloroform isoamyl alcohol mixture (24:24:1; i.e., 100 µl; Sigma), mixed and centrifuged for 2 minutes (13,000 rpm). The aqueous phase (top layer) was transferred to a clean tube and DNA was precipitated by adding 1/10 volume of 3 M sodium acetate and 3 volumes of absolute ethanol and incubating at -80 ^{o}C for 30 minutes. After this period, the tubes were centrifuged for 15 minutes at 13,000 rpm to pellet the DNA, the liquid phase was discarded and the pellet washed by addition of 500 µl 70% ethanol. After 5 minutes centrifugation at 13,000 rpm the pellet was air dried at room-temperature and dissolved in 20 µl of RNase/DNase-free water.

Restriction enzyme	10x Enzyme buffer	Experiment
AciI	NEB3 (New England BioLabs)	*Grhl3* C-21350T mutation assay
HindIII	E (Promega)	*Lmnb1* exon 1 polymorphism assay
EcoRI	H (Promega)	*Lmnb1* cloning (direction of insert)
PstI	H (Promega)	*Lmnb1* cloning (direction of insert)
HincII	React 4 (Invitrogen)	*Lmnb1* cloning (direction of insert)
NcoI	D (Promega)	*Lmnb1* anti-sense probe (linearization)
SpeI	React 4 (Invitrogen)	*Lmnb1* sense probe (linearization)
XhoI	D (Promega)	Full-length *Lmnb1* cloning fusion construct
KpnI	J (Promega)	Full-length and C-40 *Lmnb1* cloning fusion construct
XbaI	D (Promega)	C-40 *Lmnb1* cloning fusion construct
RsaI	React 1 (Invitrogen)	4-base cutter – for BAC localisation experiment
HaeIII	R (Fermentas)	4-base cutter – for BAC localisation experiment
BamHI	E (Promega)	6-base cutter – for BAC localisation experiment

Table A.16.1 Restriction enzymes, respective buffers and application (experiment).

A.16.2 Transcription of digoxygenin (DIG) labelled probes

Typically, 1 µg of linear DNA was used for transcription in a reaction mix containing: 2 µl DIG RNA Labelling Mix (10x concentrated; Roche), 2 µl transcription buffer (10x concentrate; Roche), 0.5 µl RNase inhibitor (Roche), 2 µl polymerase and RNase-free water to a final volume of 20 µl. This reaction was incubated for 2 hours at 37 ^{o}C. A sample of the product was then run on a 1% agarose gel.

Transcripts were purified with DEPC-water BD CHROMA SPIN columns (BD Biosciences) according to the manufacturer's instructions giving 100 µl probe ready for use for *in situ* hybridisation.

A.17 *In situ* hybridisation buffers

A.17.1 Pre-hybridisation mix

Reagents	**Volume (ml)**	**Final concentration**
Formamide (Sigma)	25.0	50%
20x SSC (pH 4.5)[a]	12.5	5x
25 mg/ml RNA from baker's yeast (S. cerevisae; Sigma)	0.1	50 µg/ml
10% SDS	5.0	1%
Heparin (10 mg/ml; FisherBiotech)	0.25	50 µg/ml
H_2O (DEPC-treated)	7.15	

Table A.17.1 Pre-hybridisation mix. (a) 20x SSC, pH 4.5 was prepared by dissolving 175.3 g of NaCl and 88.2 g sodium citrate (Sigma) in 800 ml DEPC-H_2O. The pH was adjusted to 4.5 before completion of the volume to 1 L**. (b)** 20x SDS was prepared as in **section A.5.d** but with DEPC-treated water.

A.17.2 Post-hybridisation washing solutions

Reagent	Volume (ml)	Final concentration	Reagent	Volume (ml)	Final concentration
Formamide	25.0	50%	Formamide	25.0	50%
20x SSC (pH 4.5)	12.5	5x	20x SSC (pH 4.5)	5.0	2x
10% SDS	5.0	1%	10% SDS	5.0	1%
H_2O	7.5		H_2O	15.0	

Table A.17.2 Post-hybridisation solutions. Solution 1 (black text) and solution 2 (blue text).

A.17.3 Tris-Buffered Saline (TBST) for *in situ* hybridisation

To make up a 1 L of 10x TBS 80 g of 5 M NaCl, 2 g of potassium chloride (KCl74.55g; Sigma) and 250 ml of 1 M Tris-HCl (pH 7.5) were mixed with milli-Q water to a volume of approximately 950 ml. The pH was adjusted to 7.0, and the volume made up to 1 litre with milli-Q water.

For the TBST working solution, 100 ml 10x TBS were added to 890 ml of water with 10 ml Tween-20 (to 1%), and 0.48 mg/ml levamisole (Sigma).

A.17.4 Sodium chloride/Tris/Magnesium chloride/Tween (NTMT) buffer

For 50 ml final volume the following reagents were added (**Table A.17.3**).

Reagents		**Final concentration**
5 M NaCl,	1 ml	100 mM
Tris-HCl (of the 1 M stock, pH 9.5)	5 ml	100 mM
Magnesium chloride ($MgCl_2$, of the 2 M stock)	1.25 ml	50 mM
Tween-20	0.05 ml	0.1%
Levamisole	0.024 g	
Milli-Q H_2O	42.7 ml	

Table A.17.3 NTMT buffer.

A.18 MEF Medium

To a 500 ml DMEM (high glucose, Gibco) were added:

10% fetal bovine serum (FBS; Invitrogen);

1/100 (v/v) L-Glutamine (200 mM; Gibco);

1/100 (v/v) Penicillin-Streptomycin (Gibco).

The media was mixed and stored at 4°C (stable for 10 days) and warmed to 37°C before use.

APPENDIX B – Primers

Primer name	Transcript region (bp)	Primer sequence	Size and T°
Mat2a_3UTRF Mat2a_3UTRR	2403 - 2639	5'- TGTATTCTGGGGTATGGCGT -3' 5'- CCAGCCAAGTCAGCTTTCTC -3'	237 bp 60˚C
Gart-T1_F3 * Gart-T1_R3	2396-2603	5'- GGGTGATAGGCAGTGTCGTT -3' 5'- TCCCGGGTGCTATCTATGAG -3'	208 bp 60˚C
Gart-T2_F2 * Gart-T2_R2	937 - 1105	5'- CAAAGATGGCCCAAAAGTGT -3' 5'- GGTTACGGCACTGTGGTTTT -3'	169 bp 60˚C
Ube2n_F3 Ube2n_R3	2382 - 2622	5'- GAAAGCCAGAGCTGCTCCTA -3' 5'- CAACCTCCACCTCAACCTGT -3'	241 bp 60˚C

Table B.1 Primers for qRT-PCR of candidate genes arising from 2-DE analysis. Region of the transcript amplified by the primers and sizes of product-fragments are given in base pairs (bp). T° indicates annealing temperature used for PCR amplification. Asterisk (*) indicates two different sets of primers. Transcript IDs: S-adenosylmethionine synthase isoform type-2 (*Mat2a*, ENSMUST00000059472); Trifunctional purine biosynthetic protein adenosine-3 (*Gart*, ENSMUST00000023684-1 and ENSMUST00000120450); ubiquitin-conjugating enzyme E2N gene (*Ube2n*, ENSMUST00000099329).

Primer name	Primer sequence	Size and T°
pTARBAC-R 327D13-R1	5'-GTCGACATTTAGGTGACACTA-3' 5'-TCACGTGGTCATCATTAGGG-3'	230 bp 54˚C
Grhl3_UF10 Grhl3_UR10	5'-TTGTATTTTCTTGCTTGAAACG-3' 5'- TCAGCGTAAGAAAGCTGTGG-3'	551 bp 54˚C

Table B.2 Primers for genotyping of transgenic mice. The first pair of primers were used to amplify a region of the BAC. The second pair (in green) were used to assay the C-21350T polymorphism. Sizes of product-fragments are given in base pairs (bp). T° indicates annealing temperature used for PCR amplification.

Primer name	Intron region	Primer sequence	Size and T°
Grhl3_Int2-3_F Grhl3_Int2-3_R	2-3	5'- tgcaggctgttagtgtctgg -3' 5'- cacagccctgaaaatgacct -3'	188 bp 60˚C
Grhl2_Int1-2_F Grhl2_Int1-2_R	1-2	5'- tggcaactggtttgttgtgt -3' 5'- ccctgaatcggggtagaaat -3'	158 bp 60˚C

Table B.3 Primers for genomic genotyping of transgenic mice. *Grhl3* intronic primer-pairs used to amplify genomic DNA by qG-PCR for genotyping of single and double transgenic embryos. *Grhl2* was used as reference gene **(**ENSMUST 00000022895**).** Sizes of product-fragments are given in base pairs (bp). T° indicates annealing temperature used for PCR amplification.

Primer name	Primer sequence
pTARBAC-R inverse	5'-TAGTGTCACCTAAATGTCGAC-3'
327D13-R1 inverse	5'-CCCTAATGATGACCACGTGA-3'
Chr18_F1 (18:3,005,256-3,005,276)	5'-TATCTTTGGCCACGCAGTGGT-3'
Chr18_F22 (18:3,005,098-3,005,119)	5'-ATAATGTAAGCAGCCCTGGCCG-3'
Chr18_F23 (18:3,005,050-3,005,072)	5'-CTCTCTCTCTCTCTCTTTCTTAA-3'
Chr18_R1 (18:3,005,603-3,005,621)	5'-TGGCTGGCCTTCATGTGA-3'
Chr18_R2 (18:3,005,653-3,005,671)	5'-GTGCATGTCAGCTATCTTG-3'
Chr18_R3 (18:3,005,757-3,005,776)	5'-AACACAGAAGGGAGGTGGTG-3'
Chr18_R4 (18:3,005,906-3,005,925)	5'-AGAAACCACCATGCAGCTCT-3'
Chr18_R5 (18:3,005,944-3,005,963)	5'-ATATACCTGCATGCCAGGAG-3'
Chr15_F15(15:74,916,886-74,916906)	5'-TGGTTGTGGTGGCAGAGGGA-3'
Chr15_R15 (15:74,917,756-74,917,776)	5'-CAATTGTGGATGGTAGTTCA-3'

Table B.4 Primers for sequencing for localisation of the BAC. Primers inverse to the ones in T**able B.1** were used to sequence genomic DNA for BAC localisation in transgenic embryos. Primers designed against chromosomes 18 and 15 were designed in an attempt to genotype transgenic embryos. Forward primers are indicated in grey and reverse primers in green. These primers were used at 58˚C annealing temperature for 35 cycles. The genomic region within each chromosome where the primer was designed is given in brackets.

Primer name	Primer sequence	Size and T°
LmnB1_F1ex1 LmnB1_R1in1	5'-AGCCCGAGAGGAAACAAAGT-3' 5'-CTGCGCACCTTATCGATGTA-3'	411 bp 55°C
LmnB1_F1in2 LmnB1_R1ex2	5'-GGCCTGTGGTTTGTACCTTC-3' 5'-GGCACCCCTGTTCAGTTCTA-3'	568 bp 55°C
Lmnb1_F1up Lmnb1_R1up	5'-CGCTCCCGTTTACTTTTGAA-3' 5'-GTACACGCACACTCGCAGAC-3'	551 bp 55°C
LmnB1_F2 LmnB1_R2	5'-CATGTGATGTGGGGAATGTC-3' 5'-ATGGTGGCTCACAACCATCT-3'	482 bp 52°C
LmnB1_F3 LmnB1_R3	5'-AACGGCCCCAAAGTTAAAAT-3' 5'-GACCAGCCTAGGCAACAGAG-3'	352 bp 60°C
LmnB1_F4* LmnB1_R4*	5'-GACAGGCACAGAGGTTGGTC-3' 5'-ATGCATGCAGACAAAACACC-3'	396 bp 60/55°C
LmnB1_F5 LmnB1_R5	5'-AGCGTGCTTTCCTGTTTCAT-3' 5'-TGTCTCATCTGGGACAAAAGA-3'	367 bp 60°C
LmnB1_F6 LmnB1_R6	5'-AAGAGCTAGAGCTCCTTTAGGG-3' 5'-AGAGCAGTCCTAAAATAATGGAGA-3'	454 pb 60°C
LmnB1_F7 LmnB1_R7	5'-ACATGGTGAGGGACCTCTTG-3' 5'-GCATCCAGAAGACGGATAGC-3'	409 bp 60°C
LmnB1_F8 LmnB1_R8	5'-TCTGGGGTCATGGATTTGAT-3' 5'-GCCTCCCTCTTCTGGAGTGT-3'	301 bp 60°C
LmnB1_F9 LmnB1_R9	5'-AAGCAGCTGGACAGAGTCGT-3' 5'-TGTGGTGTGTCCGTTTTCTC-3'	370 bp 60°C
LmnB1_F10 LmnB1_R10	5'-TCGAAGGTCTACTAACTGCTGCT-3' 5'-GAAACGGTAAAGGGCTACCA-3'	400 bp 60°C
LmnB1_F11_p1 LmnB1_R11_p1	5'-AGGTGTGAGCTGGCTCATTT-3' 5'-GGACACGCAGTGGTTTTCTT-3'	511 bp 60°C
LmnB1_F11_p2 LmnB1_R11_p2	5'-CCCTCAAGTTTTTGGCATTT-3' 5'-TTAAAAGGGCCAGTCACCTC-3'	621 bp 55°C

Table B.5 Primers used for sequencing of *Lmnb1* genomic DNA. All primers are flanking coding regions of the respective exons. Sizes of product-fragments are given in base pairs (bp). T° indicates annealing temperature used for PCR amplification.

Primer name	Transcript region (bp)	Primer sequence	Size and T°
B1TrsF1 B1TrsR1	265 - 802	5'-GGCCTGTGGTTTGTACCTTC-3' 5'-TCAGATCCTCCAAGTCTCCCT-3'	538 bp 55˚C
B1TrsF2 B1TrsR2	726 - 1286	5'-ACTAAACTCTAAGGATGCGGC-3' 5'-AGCATGTCCTCCAATTCCTG-3'	561 bp 60˚C
B1TrsF3 B1TrsR3	1082 – 1934	5'-ACAAGGAAGAGCTGGAGCAG-3' 5'-TGCTTCTCTGAGCAACC-3'	852 bp 60˚C
B1TrsF4 B1TrsR4	1421 – 2081	5'-AGATCAGCGCCTACAGGAAG-3' 5'-AGCTTGAGGAAGATCGACCA-3'	680 bp 55˚C
B1TrsF5 B1TrsR5	1917 – 1451	5'-GGTTGCTCAGAGAAGCA-3' 5'-CACCCATCTAGGGAGGCAA-3'	535 bp 60˚C

Table B.6 Primers used for sequencing of *Lmnb1* transcript. Pairs of primers: 1, include regions of exons 1 and 2; 2, exons 2-6; 3, exons 4-10; 4, 6-11; and 5, 10-11. Sizes of product-fragments are given in bp. T° indicates annealing temperature used for PCR amplification.

Primer name	Primer sequence	Size and T°
RT_B1_F2 RT_B1_R2	5'- CAGGAATTGGAGGACATGCT -3' 5'- GAAGGGCTTGGAGAGAGCTT -3'	221 bp 60˚C
Gapdh_F Gapdh-R	5'- ATGACATCAAGAAGGTGGTG-3' 5'- CATACCAGGAAATGAGCTTG-3'	177 bp 60˚C

Table B.7 Primers used for qRT-PCR of *Lmnb1* and *Gapdh*. *Lmnb1* and *Gapdh* primers were designed to cross exons 6 -7 boundaries.

Primer name	Primer sequence	T°
FL_Lmn_F	5'-CTAGCTCGAGTGTGGTTTGTACCTTCGGTC-3'	56°C
FL_Lmn_R1	5'-CTGAGGTACCATGTCTTGACAAGTTCAC-3'	
mC40_F2	5'-GCACCCGGTACCACCATACCCGAGGAG-3'	60°C
mC40_R	5'-CTAGTCTAGACAAGTTCACATAATGGCACAGCT-3'	

Table B.8 *Lmnb1* primers for production of fusion-constructs. Primers were for cloning of full-length (FL) and mouse C40 (mC40) constructs. Random sequence is in purple. Red sequence denotes *XhoI*, green indicates *KpnI* and blue indicates *XbaI* restriction sites. The random sequences will be excised upon restriction digest.

Primer name	Primer sequence	T°
Sp6	5'-TATTTAGGTGACACTATTAG-3'	55 - 60°C
T7	5'-TAATACGACTCACTATAGGG-3'	55 - 60°C
R_pcDNA3.1	5'-TAGAAGGCACAGTCGAGG-3'	60°C

Table B.9 Vector primers. Sp6 and T7 primers were used when cloning with pGEM-TEasy vector and the R_pcDNA3.1 reverse primer was used with the pcDNA3.1 vector.

Primer name	Primer sequence	Size and T°
D18Mit36_L	5’- CTTGTATCCATGAATCCATCCA -3’	147 bp
D18Mit36_R	5’- TTCTTCCATGCTGTATACAAGGC -3’	58/60˚C
D18Mit44_L	5’-AGGAGTTGCAGAACGGAGAA -3’	145 bp
D18Mit44_R	5’- AACTGCCCATTACTTCAATAGAGG -3’	58/60˚C
D18Mit50_L	5’- TCCCTAAATCACTCTTTCCATTG -3’	156 bp
D18Mit50_R	5’-AACTCGGGGACTTTGACATG-3’	58˚C
D18Mit56_L	5’-ACATGCCTGACCTCCCTG-3’	251 bp
D18Mit56_R	5’-AAGAGAGCCAATTCCCACAA-3’	58/60˚C
D18Mit58_L	5’-GAAGGAACTTGATTATTGTTCACA -3’	184 bp
D18Mit58_R	5’-GATCATCCACAGATAGTCCAAGC-3’	58˚C
D18Mit81_L	5’-TCTCATCATAAAGTTAGGCTTCCA-3’	148 bp
D18Mit81_R	5’-GGTCAGCATACTTTTTGTTGTAGC-3’	58/60˚C
D18Mit103_L	5’-GGCCTATGCCTACAGTAACTGG-3’	113 bp
D18Mit103_R	5’-CCAAAACAAACAACACGCAC-3’	58˚C
D18Mit141_L	5’-CTAAAATGTTGGCAGATTTTAAATG-3’	94 pb
D18Mit141_R	5’-ATACAGTAGATTTAGTTCTCTGGCACC-3’	58˚C
D18Mit158_L	5’-TCTGACACTGGCTTCTGTGG-3’	276 bp
D18Mit158_R	5’-GGCTTGCCATGACACATATG-3’	58˚C
D18Mit172_L	5’-TGGGGTCCTATCCTTCTGC-3’	106 bp
D18Mit172_R	5’-AGTGATACTTACTTTATCACACATGCG-3’	58˚C
D18Mit180_L	5’-CTGGCTCTGTGTGGGCTT-3’	109 bp
D18Mit180_R	5’-TAATAAAAAGAAAAAGAAAACCACACA-3’	58/60˚C
D18Mit185_L	5’-ACAATAAATGGTTGGGAATATAACG-3’	79 bp
D18Mit185_R	5’-CTGACTGACGGAAGTGCAAA-3’	58/60˚C
D18Mit194_L	5’- CCACCACATAAGGGAGGAAA -3’	125 bp
D18Mit194_R	5’- GTTTGTTGTTGTTCTATTTTCAAACA -3’	58/60˚C
D18Mit209_L	5’- AAGTTGACAACCAAGATTAACTCTAGC -3’	125 bp
D18Mit209_R	5’- AGACCACCTTTGTAAATGTCTGTG -3’	58˚C
D18Mit237_L	5’- CTGAACACTTATTATATAACCCCTGTG -3’	87 bp
D18Mit237_R	5’- ACAGTGTCCCTGAGGAGGC -3’	58/60˚C
237746_L	5’-CATGGAACGCTTAAAGCACA-3’	~ 300 bp

237746_R	5’-GGGCTCTCAGATGTTCTTGC-3’	60˚C
AV259382_L	5’-GATTTTTACATGTTTCTTTTTGAGGA -3’	97 bp
AV259382_R	5’-GAAAAGCACATGAATGAGCAA-3’	60˚C
BB384708_L	5’-CGGGTTTTGACAATGAGTTG-3’	97 bp
BB384708_R	5’-TGCACATTAGCTGGTCACAA-3’	60˚C
D18Mit25_L	5’-CTGGAAATAAAACCTGGGCA-3’	125 bp
D18Mit25_R	5’-TTTAGCCTAACTGAGTTCCAGACC-3’	60˚C
RH126430_L	5’-CTAGAAAAATATTGGTTAGATAAGGC-3’	203 pb
RH126430_R	5’-GTAGCTTCAAGACATTCTTTAAAAAT-3’	60˚C
RH130816_L	5’-TTGAAATCAGGGAATGGTTCTG-3’	175-200 bp
RH130816_R	5’-CTAGCAGCTGTGGAACCTGTGT-3’	60˚C
RH136284_L	5’-ATTTATTGCCTCCCAAACCA-3’	175-200 bp
RH136284_R	5’-CTTGAGATCTGCCTGCCTTC-3’	60˚C
Ttr_L	5’-CTCACCACAGATGAGAAG-3’	< 175 bp
Ttr_R	5’-GGCTGAGTCTCTCAATTC-3’	60˚C
224716_L	5’-TGGCCATGTGGACTTGTAGA-3’	~ 200 bp
224716_R	5’-AGAAGCAGAAGGGCAAACAA-3’	60˚C
237730_L	5’- CGCAAAGACTAAAAGAACCTGC -3’	200-250 bp
237730_R	5’- CATCAGAAGTCTGTGGAGCG -3’	60˚C
D18Mit171_L	5’- AATTAGAACAACCCTATTTATCCTGC -3’	110 bp
D18Mit171_R	5’- AGGAAAGCAAGGGGAAGAAA-3’	60˚C
D18Mit21_L	5’-GCCCAGTCAAGGCATTTTAA-3’	131 bp
D18Mit21_R	5’-CCATCCAGGAACTCTTTGGA-3’	60˚C
D18Mit66_L	5’-AAACAAAACCAGAACAATAGAGCA -3’	160 bp
D18Mit66_R	5’-TAAGTTCCTCTCATTTTCTGACCC-3’	60˚C
D18Mit82_L	5’-AGTAGTTCTTGGAGGTCTGAAATAGG-3’	135 bp
D18Mit82_R	5’-CATGACACACATGCATTCACA-3’	60˚C
D18Mit88_L	5’-TCTTCTGGCCTCCACATACC-3’	140 bp
D18Mit88_R	5’-GCAATGCTGCTTTAATTGCA-3’	60˚C
D18Mit146_L	5’-ATGTCCCTCTGCTCTTTAGTTACC-3’	144 pb
D18Mit146_R	5’-GGACCACAGAGTCATTCCGT-3’	60˚C
D18Mit167_L	5’-AATGTAACCATGGAAACCAAGC-3’	102 bp
D18Mit167_R	5’-AGGTGTTCACACATTACTTCAACTT-3’	60˚C

D18Mit196_L	5’-GGGCTACATGATAACCTCTCTCA-3’	117 bp
D18Mit196_R	5’-AAATTCAGAACAGTACAGATGACCC-3’	60˚C
D18Mit213_L	5’-ATGTTATCCTCTGGCTCCATATG-3’	125 bp
D18Mit213_R	5’-ATCCAGTTTCTTTTAAAATTATTTCCC-3’	60˚C
D18Mit215_L	5’-TCACATTCTGCATTACTTTGTATAGA-3’	189 bp
D18Mit215_R	5’-TCACACTGTGTCATGCATGTG-3’	60˚C
D18Mit219_L	5’- TGTAAGACAATGTTTAACAATCATTCA-3’	164 bp
D18Mit219_R	5’- AAAAACATACATATTCATGCTACACAT -3’	60˚C
D18Mit221_L	5’- TCAGAGGACCCAGTGCTTTT -3’	123 bp
D18Mit221_R	5’- TCTTGTGTATGAATGCCTTTGC -3’	60˚C
D18Mit231_L	5’- TCTCTGATCTGCACACACACC -3’	119 bp
D18Mit231_R	5’- GGCACTGCTTAAAAACTTAGAAGC-3’	60˚C
D18Mit3_L	5’-TTCCCTATCCAGTTGTGTGC-3’	104 bp
D18Mit3_R	5’-AGCAGAGAATGCACCACCTC-3’	60˚C
D18Mit8_L	5’-TTTGGAATCTGGCATGTTAC -3’	77 bp
D18Mit8_R	5’-GTCTGAAATGAAGTGCCTGC-3’	60˚C
D18Mit47_L	5’-CTTCTTCTTCCCAACCAGACC-3’	100 bp
D18Mit47_R	5’-CTAGCACATTTTTATAAGCAACCC-3’	60˚C
D18Mit84_L	5’-ATCACAACCCCCCTACTTCC-3’	141 bp
D18Mit84_R	5’-TCACGTGTTCTGTCTCCAGTG-3’	60˚C
D18Mit108_L	5’-AGACAGAAGTGGGCTGGAGA-3’	122 pb
D18Mit108_R	5’-CAGTGTTGATAATTGAATCAAGGC-3’	60˚C
D18Mit118_L	5’-ACAGTGAGTTCCACTACAAGATGC-3’	188 bp
D18Mit118_R	5’-TATGATGCGCTCTGCAGG-3’	60˚C
D18Mit148_L	5’-GTGTTTATGGGGTAGAAGAACTGC-3’	117 bp
D18Mit148_R	5’-TCTGTGGGCATCTGAACTCA-3’	60˚C
D18Mit200_L	5’-TTTAATTGTGTGAATGTTTGAGCA-3’	120 bp
D18Mit200_R	5’-AATTCCATGGGCATGTCACT-3’	60˚C
D18Mit210_L	5’-TGGGCAGAAGTATAACTAAATCCA-3’	119 bp
D18Mit210_R	5’-TTCAAACCGTATGCCTTTCC-3’	60˚C
D18Mit227_L	5’- GCAAGCCCATCAGCATACTT-3’	122 bp
D18Mit227_R	5’- TAGTGAACTCAAATGGGGGC -3’	60˚C
RH125196_L	5’- CTGGTGGAATCGTGAGC -3’	279 bp

RH125196_R	5’- ACACTGTGGCGGTAACAATC -3’	60˚C
260951_L	5’- GATGAGCTTGGGTTCCGAGTAG -3’	< 200 bp
260951_R	5’- CCACGCAAGGACTCACAGAG-3’	60˚C
AA763521_L	5’-TATGTAAGAACGCCAGCCAC-3’	92 bp
AA763521_R	5’-GGATTAGGGCAGAATTTCCA-3’	60˚C
AW120568_L	5’-TGCTCTGACGTCCCTTTGTA -3’	175-200 bp
AW120568_R	5’-TTGTCTAAAGGCAGCAGTGG-3’	60˚C
G67025_L	5’-CTTTCCCTGCCATGACCTTA-3’	469 bp
G67025_R	5’-CTACCGTTGAATTGGCAGGT-3’	60˚C
D18Abb2e_L	5’-CAGGTGAAGGAAGGAACCAA-3’	170 bp
D18Abb2e_R	5’-TTCCTAGACAGTGAGACAGG-3’	65˚C
D18Dev1_L	5’-CTGCTATTCCATTCAGTAGCTG-3’	~ 300 bp
D18Dev1_R	5’-CACCCAAATAACTCAGTGAG-3’	60˚C
D18Mit186_L	5’-AAGTGTTGGGCAAAGGCTAA-3’	125 bp
D18Mit186_R	5’-CTTTAGTATAGTGTGCATGAGTGTGA-3’	60˚C
D18Wsu70e_L	5’-TGTGGTACAGTCAATGTGT-3’	250-300 bp
D18Wsu70e_R	5’-TCTGTGGGCATCTGAACTCA-3’	60˚C

Table B.10 Chromosome 18 microsatellite markers. 57 markers were used to compare the *SWR* and $+^{ct}/+^{c}$ strains. All PCR products were run on 4-5% agarose gels.

Primer name	Transcript region (bp)	Primer sequence	Size and T°
Matr3_F1 Matr3_R1	518 - 689	5'- TGTCTTCTCAACACCGTGGA -3' 5'- GGGCCTTCTTCAGTTCTCCT -3'	172 bp 60°C
Isoc1_F Isoc1_R	418 - 646	5'-TGTGGGACAGAGACTGTTGC-3' 5'- CACGTGCGTTTCTACTCCAA -3'	229 bp 60°C
A730017C20Rik_F A730017C20Rik_R	247 – 451	5'- CTGAGAGTCCTCCAGCATCC-3' 5'- TACGTATCCCCCAACCAAAA-3'	205 bp 60°C
Tcof1_F1 Tcof1_R1	747 – 977	5'-GATCCTCCAGCAAGAACAGC-3' 5'- TCTGACATGGGGACCTTTTC -3'	231 bp 60°C
Grpel2_F Grpel2_R	482 – 706	5'-ACCAAGCATGGCCTAGAGAA-3' 5'- GGTTTGGTTCCAGTGACCTG -3'	225 bp 60°C
Apcdd1_F Apcdd1_R	983 - 1177	5'-AAGCAGTATCCCCACCACAG-3' 5'- TATGGGAGGGTGGTGTTCAT-3'	195 bp 60°C
Tubb6_F Tubb6_R	413 - 651	5'- TGAGCATTGCGACTGTCTTC -3' 5'-TGTCGATGCAGTAGGTCTCG -3'	239 bp 60°C

Table B.11 Primers for qRT-PCR of selected genes on chromosome 18. Gene: *Matrin 3* (*Matr3*, ENSMUSG00000037236), *Isochorismatase domain containing 1* (*Isoc1*, ENSMUSG00000024601), RIKEN cDNA *A730017C20* gene (*A730017C20Rik*, ENSMUSG00000050875), *Treacher Collins Franceschetti syndrome 1*, homolog (*Tcof1*, ENSMUSG00000024613), *GrpE-like 2*, mitochondrial (*Grpel2*, ENSMUSG00000024580), *Adenomatosis polyposis coli down-regulated 1* (*Apcdd1*, ENSMUSG00000071847), *Tubulin, beta 6* (*Tubb6*, ENSMUSG00000001473).

APPENDIX C – Identified peptides for protein spots analysed by mass spectrometry

Differentially abundant proteins on 2-DE, with a fold-change in abundance of 1.5 fold or greater were considered for analysis by mass spectrometry. Protein identity (ID) was obtained by matching of LC-MS/MS data on peptides using the MASCOT search engine. Peptides in bold represent those with a MASCOT score of 35 or greater which is considered significant for identification purposes. Peptides with a score lower than 5 are also annotated for proteins which already had one or more scores of significance. Abbreviations: Progenesis SameSpots number (PSS No); Mascot score; Accession number (No).

PSS No	Matched peptides	Score	Accession No	Protein ID
7	**ASAPATPLSPTR** **LAVYIDKVR** **ALYETELADAR** **RALDDTAR** **FKAEHDQLLLNYAK** **AEHDQLLLNYAK** **ESDLSGAQIK** **DAALATALGDKK** **CQSLTEDLEFR** KNMYEEEINETR **LVEVDSGR** **LAQALHEMR** **LYKEELEQTYHAK** **LSSEMNTSTVNSAR** **IESLSSQLSNLQK** NTSEQDQPMGGWEMIR **KIGDTSVSYK** **NQNSWGTGEDVK** **NSQGEEVAQR** **AKLQIELGK**	**47** **54** **59** **61** **39** **36** **46** **79** **68** 33 **44** **35** **47** **73** **75** 24 **54** **54** **40** **54**	P14733	Lamin B1
8	**KESDLSGAQIK** **LVEVDSGR** **LSSEMNTSTVNSAR** **KIGDTSVSYK** **IGDTSVSYK** **NSQGEEVAQR**	**67** **40** **55** **49** **49** **41**	P14733	Lamin B1
20	**SLETENSALQLQVTER** **ALYETELADAR** **IESLSSQLSNLQK**	**68** **35** **77**	P14733	Lamin B1
36	**ALYETELADAR** RALDDTAR **DAALATALGDKK** LSSEMNTSTVNSAR	**68** 32 **76** 29	P14733	Lamin B1

	LVEVDSGR **LAQALHEMR** **LSSEMNTSTVNSAR** **KIGDTSVSYK** **NSQGEEVAQR**	**39** **54** **45** **58** **63**		
41 *	LAQSPQVK ILSGPFVR	29 29	Q64737	Trifunctional purine biosynthetic protein adenosine-3 *
42	**ALELEQER** APDFVFYAPR	**40** 11	P26041	Moesin
47	LAQSPQVK AVQEIMQEK **FGDPECQVILPLLK** CFGPTAQAAQLE SSKK AFTNPEDACSFITSANFPALVVK	31 17 **67** 13 15	Q64737	Trifunctional purine biosynthetic protein adenosine-3
52 **	ALGGEDVR	28	P29699 **	Alpha-2-HS-glycoprotein precursor **
59	EILFYDR **GAEQLAEGGR** **TLLTQENPFFR** DGQWFADWHEVPQGR	34 **40** **36** 28	Q1HFZ0	tRNA (cytosine-5-)-methyltransferase NSUN2
60	SAECPGPAQK FMETATESLAK **IISVTCSFFNSQAPTPR** SEGSSCALESPGSVPVGICHGSLG EPQGNQGK	6 15 **37** 11	Q9QXC1	Fetuin-B
61	**QSPDEPLR** FTEYETQVK TSDLIVLGLPWK **FGGNPGGFGNQGGFGNSR**	**35** 26 34 **61**	Q921F2	TAR DNA-binding protein 43
63	EILFYDR **GAEQLAEGGR** FYALDPSFPR TLLTQENPFFR LFEHYYQELK DGQWFADWHEVPQGR LAQEGIYTLYPFINSR LSSPCIMVVNHDASSIPR	19 **42** 23 31 30 28 23 14	Q1HFZ0	tRNA (cytosine-5-)-methyltransferase NSUN2
71	**AIGVKPPR** **KGDIFLVR** ESIESEIR DVDLEFLAK **LAGESESNLR** **GILLYGPPGTGK** LAGESESNLRK **WALSQSNPSALR** **LDQLIYIPLPDEK** IVSQLLTLMDGLKQR VRLGDVISIQPCPDVK **NAPAIIFIDELDAIAPK** **QAAPCVLFFDELDSIAK** **QAAPCVLFFDELDSIAKAR** **LIVDEAINEDNSVVSLSQPK** ELQELVQYPVEHPDKFLK **ETVVEVPQVTWEDIGGLEDVK** **R** KAFEEAEKNAPAIIFIDELDAIAP K	**48** **65** 33 24 **71** **39** 25 **72** **48** 21 27 **56** **73** **83** **59** 31 **142** 32 **98** 19	Q01853	Transitional endoplasmatic reticulum ATPase

	AFEEAEKNAPAIIFIDELDAIAP **KR** MDELQLFR GGNIGDGGGAADR **QAAPCVLFFDELDSIAK** **NAPAIIFIDELDAIAPKR** EVDIGIPDATGRLEILQIHTK **ETVVEVPQVTWEDIGGLEDVK** **R** **LADDVDLEQVANETHGHVGA** **DLAALCSEAALQAIR** **VSLAVLNPYIK** LVRPPVQVYGIEGR	25 **48** **39** 25 **140** **42** **59** 12	Q9DB20	ATP synthase subunit O
72	HVGDLGNVTAGK DGVANVSIEDR **VISLSGEHSIIGR** AVCVLKGDGPVQGTIHFEQK	22 30 **86** 8	P08228	Superoxide dismutase
75	**LSQETEALGR** DLELLIQTATR YLQEVINVLETDGHFR	**59** 34 11	Q02819	Nucleobindin-1
76	AAIDYQK **TGMILLAGEITSR** TQVTVQYMQDR DLDLKKPIYQR **FVIGGPQGDAGLTGR** HLQLAIR **VTIAQGGVLPNIQAVLLPK** **VALTGLTVAEYFR** **SLQD** **IIAILGMDELSEEDKLTVSR**	22 **36** 6 22 **63** 16 **87** **36** **45**	Q3THS6 Q8CGP5 Q3U774	S-adenosylmethionine synthase isoform type-2 Histone H2A ATP synthase subunit beta
81	GSPLVVISQGK **IVLEDGTLHVTEGSGR**	27 **64**	O08553	Dihydropyrimidinase-related protein 2
86	**VAVSADPNVPNVIVTR** LTLVCSTAPGPLELDLTGDLESF KK	**55** 13	Q99PT1	Rho GDP-dissociation inhibitor-1
88	DYDDMSPR NLPLPPPPPR IDEPLEGSEDR IILDLISESPIK TDYNASVSVPDSSGPER **ILSISADIETIGEILKK**	8 20 25 22 20 **36**	P61979	Heterogeneous nuclear ribonucleoprotein K
96	LLAEPVPGIK **TNEAQAIETAR**	21 **59**	P61089	Ubiquitin-conjugating enzyme E2
1, 9, 10, 23, 24, 30, 35, 37, 39, 46, 51, 54, 55, 56, 58, 62, 73, 74, 78, 79, 82, 83, 85, 87, 91, 92, 93, 94				No ID

Table C.1 Proteins identified from 2-DE analysis of caudal regions at the 28-29 somite stage. Spots 41* and 52** were also considered to be likely identities, other spots for the same proteins were identified with significance Mascot scores: 47, Trifunctional purine biosynthetic protein adenosine-3, and 8, Fetuin-A (Alpha-

2-HS-glycoprotein precursor; 30-31ss analysis). In addition, there are other Fetuin-A spots identified by random collection (**Table C.4**). Last row are the numbers of unidentified spots.

PSS No	Matched peptides	Score	Accession No	Protein ID
8	**ALGGEDVR** TPIVGQPSIPGGPVR	**52** 7	P29699	Alpha-2-HS-glycoprotein precursor
12	LVEVDSGR LAQALHEMR **LSSEMNTSTVNSAR** **KIGDTSVSYK** **NSQGEEVAQR**	23 33 **54** **55** **55**	P14733	Lamin B1
20	**ASAPATPLSPTR** **LAVYIDKVR** **SLETENSALQLQVTER** SLETENSALQLQVTEREEVR **ALYETELADAR** ALYETELADARR RALDDTAR **ESDLSGAQIK** **LREYEAALNSK** **DAALATALGDKK** **LVEVDSGR** **LSSEMNTSTVNSAR** **IESLSSQLSNLQK** **DQMQQQLSDYEQLLDVK** **IGDTSVSYK** **NSQGEEVAQR**	**63** **54** **77** 26 **56** 31 22 **59** **62** **60** **41** **56** **62** **56** **49** **62**	P14733	Lamin B1
158	**QQLQTTR** YIAENGTDPINNQPLSEEQLIDIK ATVLTTER	**36** 8 15	Q99KP6	Pre-mRNA-processing factor 19
168	**VLDLDLFR** **LLIDEAIQK** LLIDEAIQK	**35** **36** 33	P26638	Seryl-tRNA synthetase
7, 15, 18, 19, 21, 27, 40, 46, 57, 65, 66, 67, 72, 74, 75, 76, 77, 85, 91, 97, 106, 109, 110, 112, 116, 122, 126, 127, 129, 130, 133, 135, 137, 138, 140, 141, 143, 147, 148, 149, 150, 151, 152, 153, 155, 156, 157, 160, 161, 164, 165, 166, 169				No ID

Table C.2 Identification of differentially abundant protein-spots from 2-DE analysis of caudal regions from 30-31 somite stage embryos. Last row are the numbers of unidentified spots.

Spot No	Matched peptides	Score	Accession No	Protein ID
S10	**EQFLDGDAWTNR** FYGDLEKDK DKGLQTSQDAR FYALSAK LFPSGLDQK KVHVIFNYK VHVIFNYK **CKDDEFTHLYTLIVRPDNTYEVK** **IDNSQVESGSLEDDWDFLPPK** **IDNSQVESGSLEDDWDFLPPKK** IKDPDAAKPEDWDER QIDNPDYK SGTIFDNFLITNDEAYAEEFGNETWGVTK **FYGDLEKDKGLQTSQDAR**	**47** 23 24 32 33 24 23 **40** **65** **36** 30 30 20 **88**	P14211	Calreticulin
S11	**HTLNQIDSVK** **K.ALGGEDVR.V**	**39** 28	P29699	Alpha-2-HS glycoprotein (Fetuin-A)
S60	R.SNVTAVHK.A **R.NVTAIQGPGGK.W** **R.IAEFAFEYAR.N** R.ENTEGEYSGIEHVIVDGVVQSIK.L K.IEAACFATIK.D	23 **47** **61** 17 23	P47955	Isocitrate dehydrogenase [NAD] subunit alpha
S79	**AAVPSGASTGIYEALELR**	**130**	P17182	Alpha-enolase

Table C.3 Identification of protein spots collected from 2-DE gels for reference. These spots were collected at random from different areas of silver-stained gels to confirm correlation of pH range and protein pI values.

APPENDIX D

D.1 Sequence assembly of the BAC 327D13 BAC vector insertion site (230 bp).

The PCR product generated using the pTARBAC-R (in the BAC vector end) and 327D13-R1 (in the genomic DNA insert), was sequenced using the pTARBAC-R and 327D13-R1 primers. Primer sequences are underlined and the *BamHI* site highlighted (bold, six-base cutter). Sequence in black text corresponds to the BAC vector and red text corresponds to genomic sequence (chromosome 4).

GTCGACATTTAGGTGACACTATAGAA**GGATCC**AAGATGTCCTTGTTTTGAC
ACCAATCACACAGAGATGATAGGCGATTACTAATGAGCCATCTCGAGGGGA
GTCTTTGCAGTCTGGTGTGTATCTGCTCTATGCAGCCTGCCTTAAGTTTGGA
TCAGTCAAGTTTCCAGGGCTGATTGTGGATACTCTCTTGGTCATGCTGTTCT
AGAATGTTCCCCTGGAATAGCTGGACCCTAATGATGACCACGTGA

D.2 BAC localisation – primer design

>18 dna:chromosome:NCBIM37:18:3004060:3007000:1

TATTATTTTTTT	Region upstream of BAC insertion site
*	Chr18:3,005,382: putative insertion site
CTCTCTCTCTCT	Forward primers
TCACATGAAGGC	Reverse primers

1 CTGTCTGTCTGTCTGTCTTCTGTCTGTCTGTCTTTCTTTCTTTCTTCTGTCTTTCTTTCT
TCTTTCTTTCTTTCTTTCTTTCTTTCTTTCTTTCTTTCTTTCTTTCTCTCTGTCTGTCTT
TCTATTTTTTTTTCGTTTTTTCTGAGATATGGTTTCCTAGCCCTGGCTGACTTGTAAGCC
AGGGTGACCTTGAACACAGAAATCTGCCTGAGGTTAAAGGTGTGTTCCACAATTGCCCCA
GCTCTACTCTAATTCTCTTTAAAAAAAATGTGTATGTATATATGTATATATAGAGGTAAT
ATTAATCCGTTAATATCTTTTTTCCTAAAATTCATGTCTTTCTTTCTCTCTCTTTCTCTC
TCTCTCTTTCTCTCTCTCTCTTTCTTTCTTTCTGTCTGTCTGTCTGTCTTTCTGTCTTTC
TATTATTTTTTTCGTTTTTTTTCTGATATATGATTTCTCTAGCCCTAGCTGACTTGTAAG
TCAGGGTGACCTTGAACGCAGAAATCTGCCTGAGGTTGAAGGTGTGTTCCACAATTGCCC
CAGCTCTACTTTAATTCTCTTTTTAAAAATTGTGTGTATGTTTGTATGTATATATGTATA
TATAGAAGTAATATTAATCCATTAATATCTGTTTCCTAAAATTCATGTCTTTCCTTCTCT
CTCTCTCATTCTTCTTTCTTTCTTTCTTTCTTTCTTTCTTTCTTTCTGTCTGTCTGTCTT
TCTTTCTGTCTTTCTATTATTTTTTTCGTTTTTTCTGAGATATGGTTTCTCTAGCCCTAG
CTGACTTGTAAGCCAGGGTGACCTTGAACGCAGAAATCTGCCTGAGGTTAAAGGTGTGTT
CCACAATTGCCCCAGCTCTACTCTAATTCTCTTTTTAAAAATGTGTGTGTGTATATATGT
ATATATGTATATATAGAAGTAATATTAATCCATTAATATCTGTTTCCTAAAATTCATGTC
TCTCTCTCTCTCTCTCTCTCTCTCTCTCTCTCTTTCTTAAATTTATTC F23bp
TTTTCATACATAGTTTCATAATGTAAGCAGCCCTGGCCGTCTTGAAGACACTTTGTAGGC F22bp
CTCAATCCTGTAAGAGCCTTCCTCTGCTTATCAAATGCTGCCATGAATGTTGTACCTCAC
TATGACTGGCTGAGATTCTCACCTTTTCTTCCCCCCCCCTTTCTTTTTATGATTCTATCT F1
TTGGCCACGCAGTGGTGGTGGTGGTGGCAGAGGGAGGTGGATCACTGTAACTTTGCAGCT
AGCTTAGTCTTCAGTCTGATTTACTCGAAAGGAGTTCCAAGAAGACTGGTTATATTTTTC
AT*TTATTATGCATTTTAATTAAAATTTAATTAAACCCAAAGAATTTAGACTGACCAATTC

AGAGTCTGCCATTTAAAAGCATAAGGAAAAAGTAGGAGAAAACGTGAGGCTGTCTGTGGA
TGGTCGAGGCTGCTTTAGGGAACCTCCTCACCATTCTGCACTTGCAAACCGGGCCACTAG
AACCTGGTGAAGGGAGAAACCAAAGTGACCTGAAACAATAGGTCACATGAAGGCCAGCCA R1
CCATCTTGTTGTGCAGGTGGTCAGTTAGCAGACAAGATAGCTGACATGCACATGTTGTCT R2
TTCATCTTGGTGAGGTCAATGTGCAACCGAGTGACAGGACAAGGAAGTAGACATGCAGAC
AACAGACATGCAGGTGCACCACCTCCCTTCTGTGTTTGTATAAAACACACACAAAAATTT R3
TCATTATTTACAGTAAGCCTTAAAAAGCACTCTGACAGCCTCGCATATATCTACATTCTA
TGTGATTAGAATTTCCTTTTTTTGTTGTTTTTTAATTTATTCTCAAGAGCTGCATGGTGG R4
TTTCTCCTAGGTTCTGTTGCTCTCTCCTGGCATGCAGGTATATACACAGCAGATAAAGCA R5
CAAACACACATTTACATTGAAAAATAATTGTAATAAGAATGAAAGAAAGAAAGAAAGAAA
GAAAGAAAGAAAGAAAGAAAGAAAGAAAGAAAGAAAGAAAGAAAGAAAGAAAGGAA
GGAAGGAAGGAAGGAAGAAACAAAGATCCTAACTTTGGCCCGGCTGTGTGGGTGGCAGAA
GGAGGCAGGCAGGTAGGCAGAGAGGACCTCTCTGAGTTTGAGGTTACCAAAGCCTACAAA
GGAAGTTCCAGGCAGGGATGCCAGGGCTACACCGAGAGAAACCCTATCTTGGGGAAAAAG
AAAACAAAAGCAGAAAAAGTTCTGGCTTTTACTTTCAGACATATGATTCTTCTAGTACTA
TTGACTATCTAATTTTGATCATGAAGGCACATTGGATTTTATGACAGTGTGTGTGTGTGT
GTGTGTGTGTGTGTGTGTGTAATATTTCTACTGTGATTGTGGTAACTTGCACCCTAGTGG
GCTTATGTTTGATTTCTGTAATCTTTTTTCTAATTCTTTTTCATTTATATTTTTATTTTA
TTTTATTTTGGGTTTTTTGTTTGTTTGTTTGTTTTGTTTTGTTTTTGTTTGTTTGTTTGT
TTTTGAGACAGGGTTTCTCCATATAGCCCTGGCTGTCCTGGAACTCACTGTGCTGACCAT
GACCATGATGGCCTTGAATTCAGAAATCCTCCCATCCCTGCCTCTCTAGGGCTGGGATTA
AAGGCTTGAGCCACCACTCCCAGCTACTTTTTAATTTTTTAATTTTTTAATTTTATATAT
TTAGTTTATTTTTGTTTTCTTCTTTCTGTCTTTCTTTCTCTCTCTCTCTCTCTCTCTC
TCTCTTTCTTTCTTTCTTTCTTTCTTCCTTTCTTTCAGTCTTTCTATTATTTTTTTCGTT
TTTTCTGAGATATGGTTTCTCTAGCCCTAGCTGACTTGTAAGTCAGGATGACCTTGAAAG
CAGAAATCTGCCTGAGGTTGAAGGTGTGTTCTGTTGGGAGCTATTAAGACAGCCCTTGAT
C 2941 letters

D.3 Sequence 'tag' generated by sequencing genomic DNA of a transgenic sample with R4 primer

CTGTGGATGGT	Tag
TCTCACCAGCC	BAC sequence
GGCC	*HaeIII* sites

BAC -
AGAGCAGTCGGGTGCTCTTACCCACTGAGCCATCTCACCAGCCCTTATTATG
CATTTTAATTAAGATTTAATTACACCAAAAGAATTTAGACTGACCAATTCAG
AGTCTGCCGTTTAAAAGCATAAGGAAAAAGTAGGAGAAAACGTGAGGCTGT
CTGTGGATGGTCGAGGCTGCTTTAGGGAGCCTCCTCACCATTCTGCACTTGC
AAACCGGGCCACTAAAACCCGGTGAAGGGAGAAACCAAAGCGACCTGAAA
CAATAGGTCACATGAAGGCCAGCCACCTCCATCTTGTTGTGCGGGAGTTCA
GTTAGCAGACAAGATGGCTGCCATGCACATGTTGTCTTTCAGCTTGGTGAGG
TCAAAGTGCAACCGAGTGACAGAACAAGGAAGTAGACATGCAGACAACAG
ACATGCAGGCGAACCATCTGCCTTCTGTGTTTGGATAAAAGACACACAACA
ATTTTCATTACTTACACTAAGCCTTAAAAAGCACTCTGACAGCCTTGCATAT
ATCTACATTCTATGTGATTAGAATTTCCTTTTTTGTTGTTTTTTCATTTATTCT
CAAGAGCTGCATGGTGGTTTCT R4

Chapter 3

Two-dimensional protein gel electrophoresis analysis of a mouse model for neural tube defects

3.1 Introduction

As described in **Chapter 1**, *curly tail* is one of the most extensively characterised mouse models of NTDs, with resemblance to the multifactorial etiology and pathogenic features of human NTDs (Copp and Bernfield, 1994; Van Straaten and Copp, 2001). The penetrance of the *ct* mutation is strongly dependent on genetic background and influenced by environmental factors (Neumann et al., 1994; Van Straaten and Copp, 2001). *Curly tail* also provides a model in which NTDs are unresponsive to folate but preventable by inositol (Greene and Copp, 2005).

Previous studies revealed that prevention of NTDs in *curly tail* embryos by inositol depends on downstream activity of protein kinase C (PKC), specifically the PKCβI and PKCγ isoforms, with a lesser requirement for PKCζ (Greene and Copp, 1997; Cogram et al., 2004). In order to build on these findings, one next step would be the identification of key target proteins that are phosphorylated by PKC in inositol treated embryos. As a precursor to such an approach it was decided to compare the proteome profile of *curly tail* mouse embryos with wild-type embryos that do not develop NTDs. These studies were intended to reveal proteins that are abnormally represented in the *curly tail* proteome. In this context abnormal would mean that proteins are present at reduced or excess abundance or are abnormally modified. These protein changes could be directly involved in development of spina bifida and be indicative of downstream effects of *Grhl3* (**Figure 3.1**).

Differences between cellular states are reflected in changes in gene expression that typically manifest themselves at the level of both the message (mRNA) and the final protein products. While mRNA based approaches such as microarray allow many genes to be analysed in an experiment, it was decided to use a protein-based, 'proteomic', approach in this project. Analysis of proteins provides sensitivity to differences in both abundance and post-translational modification, the latter being particularly relevant if subsequent studies are to address the downstream phosphorylation events following inositol treatment of embryos. In addition, it can be the case that protein abundance can be altered without changes in mRNA level, due to changes in translational regulation.

Since proteins are more likely to affect biological functions, studies at the protein level may therefore provide insight that mRNA based studies are not sensitive to.

In one separation procedure, 2-DE technique is capable of simultaneously resolving thousands of proteins depending on the amount of sample, the apparent molecular weight, and the amount of each protein. The process requires stringently controlled steps of sample preparation, protein separation, image detection and analysis, followed by spot identification. Proteins are separated according to two independent properties in two discrete steps. The first-dimension step, isoelectric focusing (IEF), separates proteins according to their isoelectric point (pI). This is followed by the second-dimension step, sodium dodecyl sulphate-polyacrylamide gel electrophoresis (SDS-PAGE), which separates proteins according to their molecular weight (MW). Gels are then stained and each spot on the resulting two-dimensional gel corresponds to a single protein species. The 2-DE method used in this project is based on the method developed by A. Görg and colleges (Gorg et al., 1985; Gorg et al., 1998), which utilises a first dimension separation method with precast immobilised pH gradient (IPG) with gel strips supported by a plastic film backing. The method is described in **Chapter 2**, **section 2.5**, and summarised in **Figure 2.4**.

A proteomics approach has previously been used in mouse embryos to investigate the molecular events underlying the processes occurring at the stage of neural tube closure (Greene et al., 2002). The analysis revealed a number of developmentally regulated proteins whose abundance changes between E8.5 and E10.5 and which were identified by mass spectrometry (MS). This study encouraged the view that 2-DE and MS analysis could be applied to mouse embryonic samples for global analysis of the proteome at specific developmental stages. Therefore, in this study of a mouse model of spinal neural tube defects, a 2-DE approach was used to compare *curly tail* and wild-type embryos.

3.2 Results

3.2.1 Two Dimensional Protein Gel Electrophoresis (2-DE) on neurulation stage mouse embryos

The initial approach of this project was to identify candidate proteins which are abnormally represented in the *curly tail* proteome. A genetically matched wild-type ($+^{ct}/+^{ct}$) strain was previously generated by successive backcrossing (four generations) from an initial cross between *ct/ct* and SWR inbred strain. *Grhl3* expression is reduced in *curly tail* (*ct/ct*) embryos compared to wild-type ($+^{ct}/+^{ct}$) embryos at the stage of PNP closure (Gustavsson et al., 2007). A *Grhl3*-transgenic *curly tail* line ($ct/ct^{TgGrhl3}$) exhibits elevated expression levels of *Grhl3* and hemizygous embryos do not develop spinal NTDs.

Embryos of the *ct/ct* strain, $+^{ct}/+^{ct}$ strain and the $ct/ct^{TgGrhl3}$ line were collected at E10.5, during posterior neuropore (PNP) closure, and allocated to groups according to somite number, 26-27, 28-29 and 30-31 (**Chapter 2**, **section 2.1**). Initial experiments focussed on comparison of *ct/ct* and $+^{ct}/+^{ct}$ samples, and $ct/ct^{TgGrhl3}$ samples were included at a later stages of the project.

The 2-DE method was first optimised for mouse embryos, using samples at the stage of PNP closure (26 – 31 somites; **Chapter 2**, **section 2.5**). The main elements that were varied were the amount of tissue used for sample preparation, the staining method, the pH range used for isoelectric focussing and the gel analysis software. In initial experiments, gels were generated using different amounts of tissue to determine the amount of protein that was the limiting factor in producing gels. Optimal sample quantity produces representation of spots across the gel, and without over-loading that, results in adjacent spots becoming indistinguishable (**Fig. 3.2**). Initially whole embryos were used for 2-DE. However, since the major interest was in the spinal defect, embryos were cut at the level of somites 14-15 to separate the caudal from the cranial region (**Chapter 2**, **Fig. 2.4 A**). Use of the caudal region provided the opportunity to identify differences in the neuroepithelium as well as the hindgut in which the proliferation defect is localised, and gave sufficient material to use one embryo per 2D gel.

Whole embryo 2-DE was performed using 18 cm IEF gels (350 µl total volume loaded). In order to increase resolution of proteins with similar isoelectric point (pI) values, a range of different pH gradients (4-7, 3-5 and 6-9) was tested to increase coverage of the whole *ct/ct* proteome (from very acidic proteins to more basic ones). In some cases pH 3.0-5.6 gels were used to provide coverage of acidic proteins and to improve separation of spots of interest from the acidic end of pH 4-7 gels. Different stains were also tested, owing to their possible differences in labelling and linearity for quantification (**Chapter 2**, **section 2.5.4**): silver, Sypro Ruby stain and Deep Purple stain. **Table 3.1** summarises how many gels were run for samples from each strain at different somite stages. **Figure 3.1** shows examples of 2D gels using different pH ranges for first dimension separation and the different protein amounts used in this study.

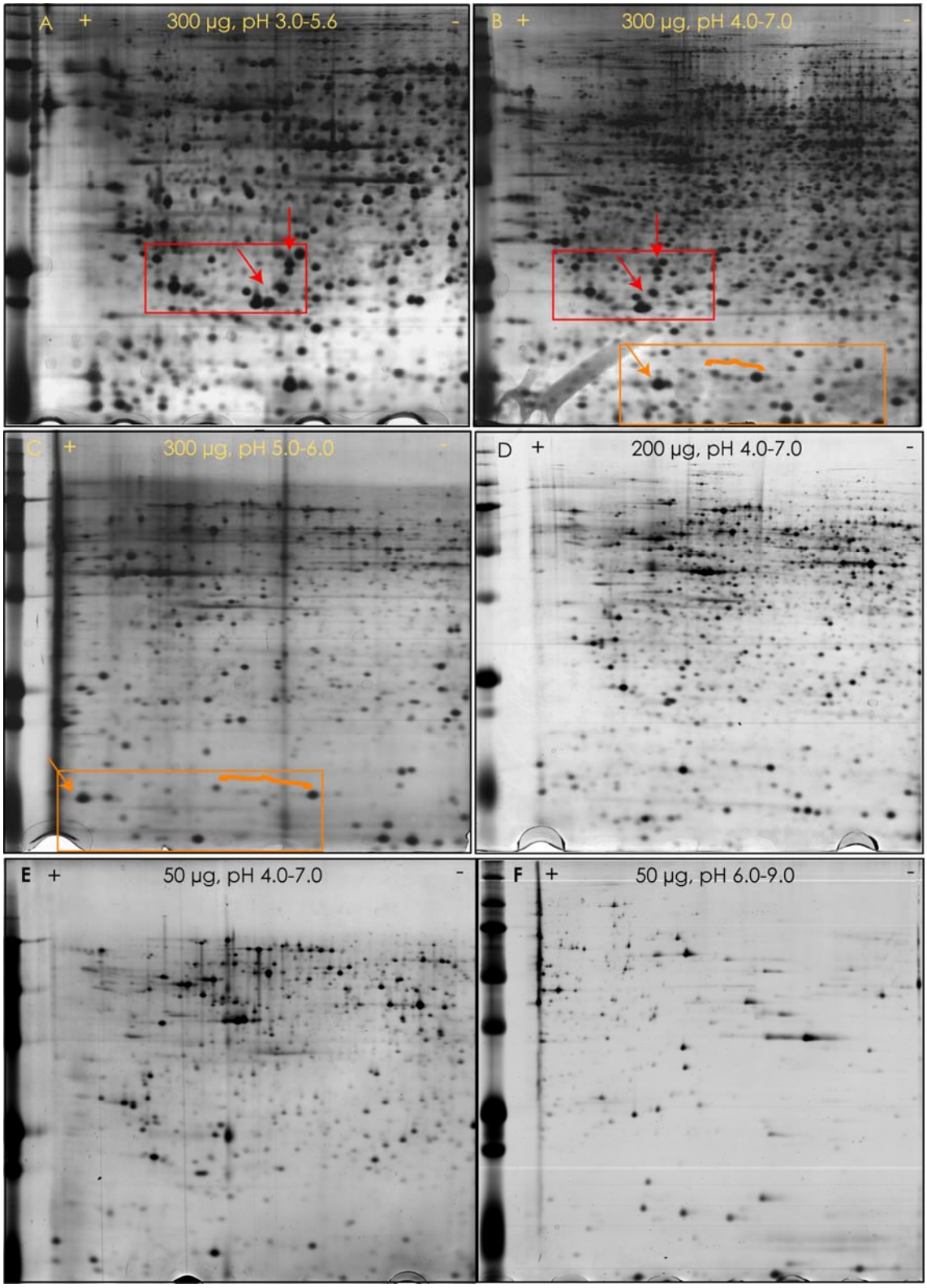
A + 300 µg, pH 3.0-5.6 -
B + 300 µg, pH 4.0-7.0 -
C + 300 µg, pH 5.0-6.0 -
D + 200 µg, pH 4.0-7.0 -
E + 50 µg, pH 4.0-7.0 -
F + 50 µg, pH 6.0-9.0 -

Figure 3.1 2D gels. (A-C) Typical 2D gels generated from whole embryo samples loaded on 18 cm gels for IEF in pH range 3.0-5.6 **(A),** 4.0-7.0 **(B)** or 5.0-6.0 **(C)**, followed by SDS-PAGE on 12% gels and silver staining. These gels have a relatively high loading of 300 μg protein. **(D)** 2-DE using 200 μg of protein from the cranial region of an embryo at E10.5, with IEF on pH 4.0-7.0 gel. **(E-F)** 2-DE generated from isolated caudal regions using 50 μg protein loading with IEF on (E) pH 4.0-7.0 or (F) pH 6.0-9.0 gels. Gels with greater loading had more visible protein spots (**B**, approximately 5,000 spots) than gels loaded with the 50 μg proteins although on the latter still a large number of proteins (**E**, approximately 2,000 spots) are readily detectable. Gels on pH 3.0-5.6 have a better separation of spots compared to pH 4.0-7.0 (red arrows within red box, **A-B**); and even better separation is achieved with pH 5.0-6.0 (orange arrow and orange bracket within orange box, **B-C**). +, indicates acidic side, and -, the basic side.

Gel analysis was performed with the Progenesis SameSpots software (**Chapter 2**, **section 2.5.6**), which processes the gel images to match the image pattern across different gels and then to detect the spots and quantitate the spot volumes. Images were then separated into groups (*ct/ct*, $+^{ct}/+^{ct}$, $ct/ct^{TgGrhl3}$) for comparison. Differences between mean spot volumes for the different experimental groups (genotypes) were ranked on the basis of the p value for the One Way ANOVA analysis and by maximum fold change, based on the normalised volume (total pixel intensity within the spot area) of the spot across all the groups being compared.

Spots that showed statistically significant variation ($p<0.05$) and a fold change of 1.5 or greater were excised from gels. Manual in-gel digestion (**Chapter 2**, **section 2.5.7**) was performed and proteins were identified by electrospray-liquid chromatography tandem mass spectrometry (LC-ESI-MS/MS) on a QTof mass spectrometer (performed by Dr Kit-Yi Leung).

Tissue	Somite stage (ss)	Strain	pH range	No. gels	Staining
Whole embryo	26-31	*ct/ct*	3.0-5.6 4.0-7.0 5.0-6.0	8† 5† 1†	Silver
		$+^{ct}/+^{ct}$	3.0-5.6 4.0-7.0 5.0-6.0	4† 3† 1†	
Cranial region	27-30	$ct/ct^{TgGrhl3}$	4.0-7.0	5†	Silver
Caudal region	28-31	*ct/ct*	4.0-7.0 6.0-9.0	17 + 6* 2	Silver Sypro* Ruby
		$+^{ct}/+^{ct}$	4.0-7.0 6.0-9.0	11 + 4* 2	
		$ct/ct^{TgGrhl3}$	4.0-7.0	13	

Table 3.1 Summary of 2D gels generated for comparison between strains. The major focus of software based differential analysis between strains was whole embryos and isolated caudal-regions of embryos at somite stages 28-29 and 30-31. † Some gels were not included in the full analysis but were used to confirm patterns for spots of interest. * A total of 10 gels were stained with Sypro Ruby.

3.2.2 2-DE analysis

3.2.2.1 Analysis of whole embryos

Initial analysis was performed to compare the protein profile of *ct/ct* and $+^{ct}/+^{ct}$ samples on 2-DE using pH ranges 3.0-5.6 and 4.0-7.0, and silver staining. The number of gels and spots that were found to `significantly differ in abundance between genotypes is shown in **Table 3.2**, while a representative gel, showing the position of varying spots is shown in **Figure 3.2**. Overall, relatively few spots were found to significantly differ in abundance between genotypes. This may reflect in part the relatively small number of gels included in the analysis of whole embryos. It was decided to focus on the isolated caudal region in subsequent experiments, in order to increase the likelihood of detecting differences specific to posterior neuropore closure.

Strains	pH	No. gels	No. differentially abundant spots
ct/ct	3.0-5.6	4	19
$+^{ct}/+^{ct}$	3.0-5.6	5	
ct/ct	4.0-7.0	2	23
$+^{ct}/+^{ct}$	4.0-7.0	2	

Table 3.2 Analysis of whole embryo samples by 2-DE for comparison of *ct/ct* and $+^{ct}/+^{ct}$ embryos. The number of gels included in the analysis for each strain is indicated. Spots were considered to be differentially abundant where $p<0.05$ and there was 1.5-fold or greater difference in mean spot volume.

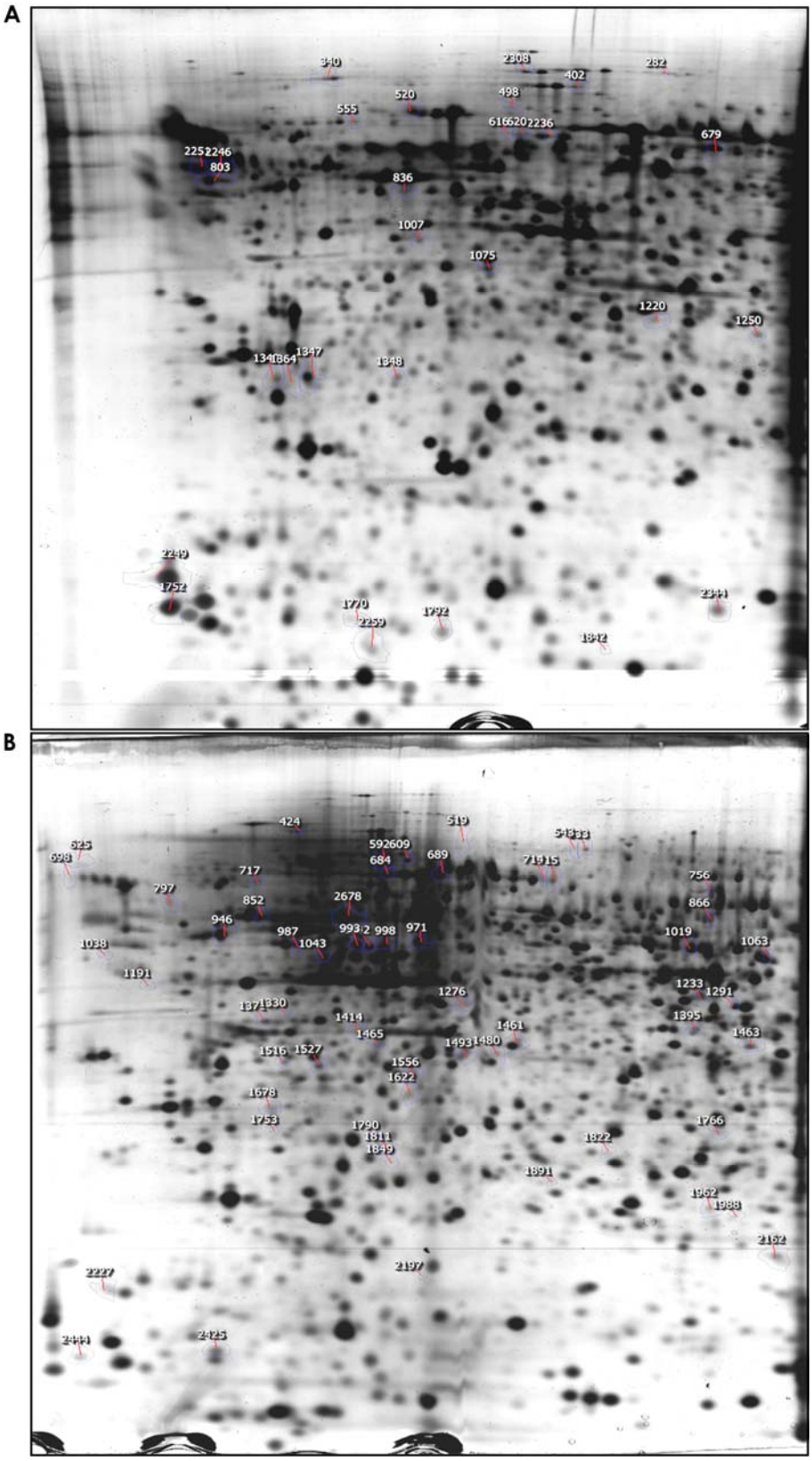

Figure 3.2 Analysis of *ct/ct* and $+^{ct}/+^{ct}$ whole embryos by 2-DE. (**A**) Typical silver-stained *curly tail* 2D gels generated using pH gradient of (**A**) pH 3.0-5.6 or (**B**) pH 4.0-7.0. The position of spots that were differentially abundant between genotypes is indicated (with their unique spot number).

3.2.2.2 Analysis of the caudal region of *ct/ct* and $+^{ct}/+^{ct}$ embryos by 2-DE with Sypro Ruby stain

Following 2-DE analysis of whole embryo samples it was decided to focus on the isolated caudal region of embryos at the stage of PNP closure. This approach was expected to provide possible additional sensitivity to protein changes that only occur in this region, with the disadvantage that an individual caudal region only contains enough protein for production of a single gel. In the first study, staining of the gels was performed using Sypro Ruby stain, followed by laser scanning. This is a fluorescent stain which provides as least as much sensitivity as silver stain but has the advantage of enhanced dynamic range, such that in 16-bit scanned images it is possible to represent up to 65536 levels of intensity. Gels were generated for embryos at the 28-29 somite stage, when failure of PNP closure is first apparent in *ct/ct* embryos. The experimental groups are summarised in **Table 3.3**, and a typical Sypro Ruby stained gel is shown in **Figure 3.3.** Although fluorescent stains give a higher dynamic range than silver stained gels, and a number of variant spots were identified, this stain causes characteristic background speckling. In some cases speckles were recognised as spots by the analysis software such that there was an increased requirement for manual editing to eliminate these "spots" from the analysis.

Strain	pH range for isoelectric focussing	Replicates	Differentially abundant spots (P<0.05)
ct/ct	4.0-7.0	5	13
$+^{ct}/+^{ct}$	4.0-7.0	5	

Table 3.3 Experimental groups for 2-DE analysis of *ct/ct* and $+^{ct}/+^{ct}$ embryos, using Sypro Ruby Protein Gel stain. Each replicate is a separate gel generated from an individual sample. Spots were considered differentially abundant spots if the mean volume differed by 1.5 fold or greater (and $p<0.05$, ANOVA).

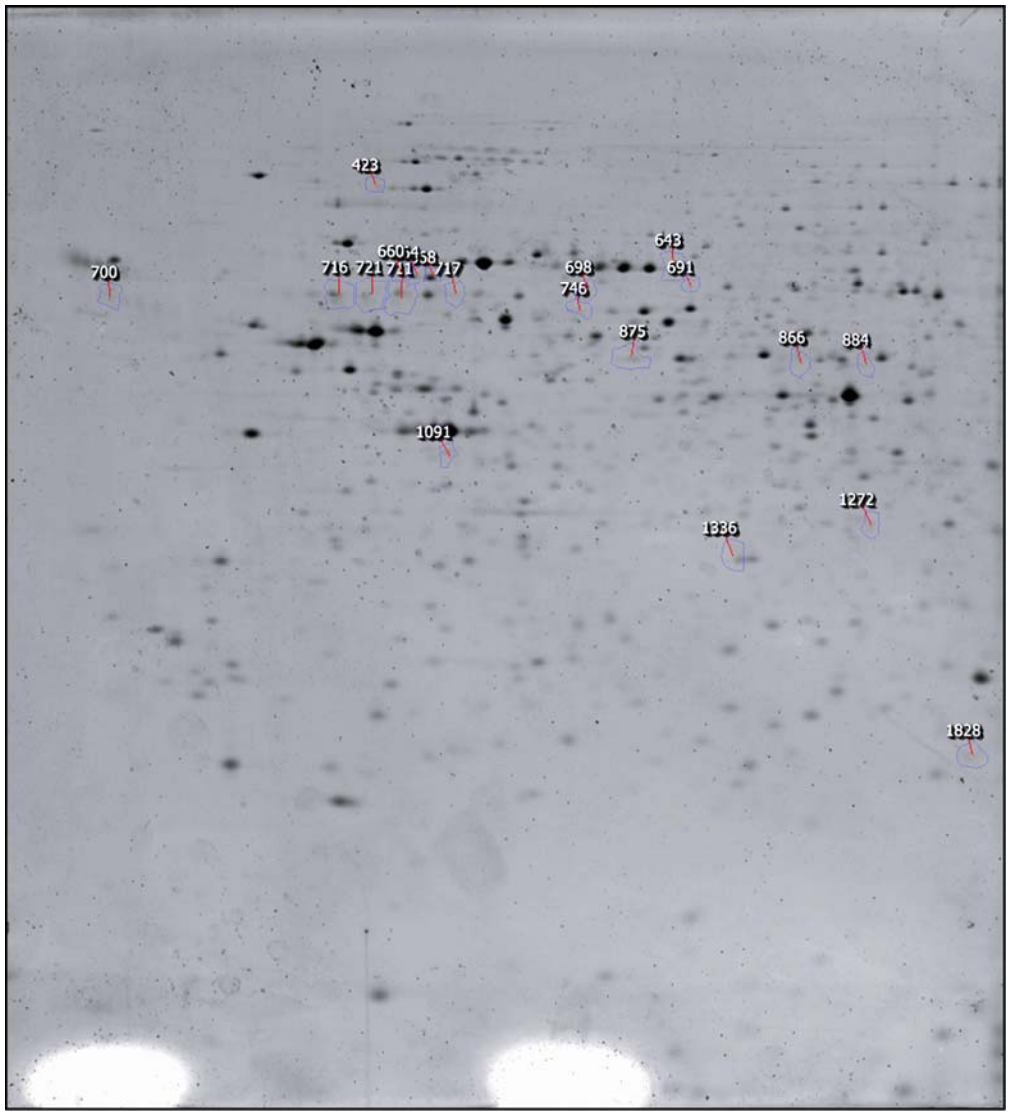

Figure 3.3 Typical appearance of 2D gel from a *ct/ct* caudal region (50 µg) sample following staining with Sypro Ruby Protein Gel Stain. The example shows the reference gel from comparison of $+^{ct}/+^{ct}$ and *ct/ct* samples at the 28-29 somite stage, using pH 4.0-7.0 for first dimension separation. Differentially expressed spots indicated by numbers.

3.2.2.3 Analysis of the caudal region of *ct/ct* and $+^{ct}/+^{ct}$ embryos at the 28-29 and 30-31 somite stages by 2-DE with silver staining

Two further experiments were designed in order to compare the proteome profile of isolated caudal regions at the 28-29 somite stage, while the PNP is gradually shortening in wild-type embryos, and at the 30-31 somite stage, when the PNP is undergoing final

closure or just closed in wild-type embryos but remains open in affected *curly tail* embryos. These are the stages at which diminished expression of *Grhl3* and a reduced cellular proliferation rate are detected in *ct*/ct embryos (Gustavsson et al., 2007; Copp et al., 1988a). The pH range chosen for isoelectric focussing was pH 4.0-7.0 based on preliminary studies that showed representation of spots across the gel and good separation of spots. In this case silver staining was used, which has a detection limit as low as 0.1 ng of protein per spot, but limited dynamic range compared with fluorescent stains. The advantage of silver staining was the ability to pick differentially abundant spots directly from gels for subsequent identification. The number of gels and variant spots is summarised in **Table 3.4** and typical 2D gels for each stage are show in **Figure 3.4**.

Strain	No. of somites	Replicates	No. spots significantly varying in abundance
ct/ct	28-29	3	
$+^{ct}/+^{ct}$	28-29	2	48
$ct/ct^{TgGrhl3}$	28-29	2	
ct/ct	30-31	3	
$+^{ct}/+^{ct}$	30-31	2	58
$ct/ct^{TgGrhl3}$	30-31	2	

Table 3.4 2-DE analysis of the caudal region of *ct/ct*, $+^{ct}/+^{ct}$ and transgenic embryos using silver staining. Spots were considered to significantly vary where $p<0.05$ (ANOVA) and mean volume differs by 1.5-fold or greater.

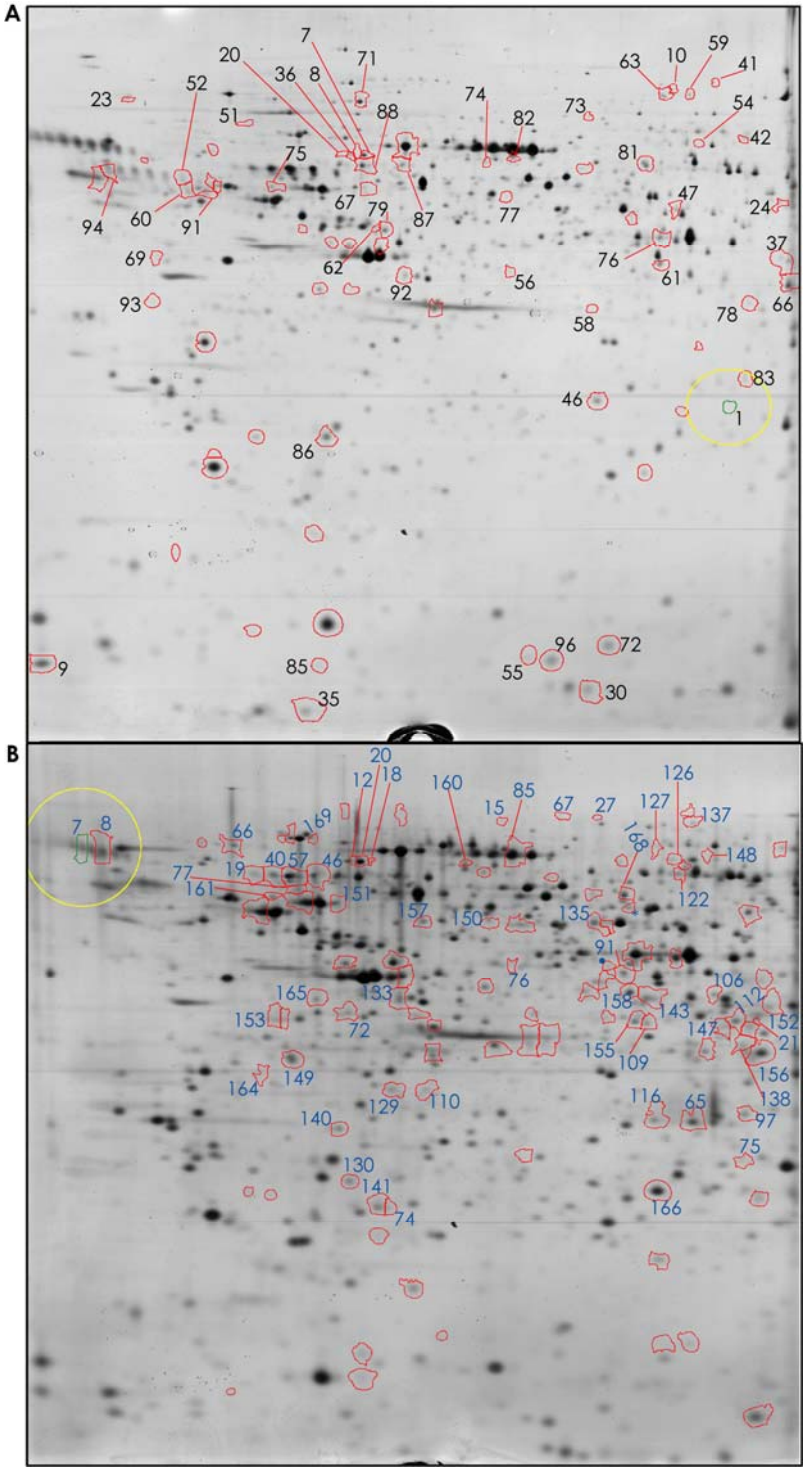

Figure 3.4 Silver stained gels following 2-DE of samples generated from caudal region of *ct/ct* embryos. Samples were from embryos at (**A**) the 28-29 somite stage and (**B**) 30-31 somite stage. A pH 4.0-7.0 gradient was used for isoelectric focussing and gels were silver stained. Spots that differed in abundance between *ct/ct*, $+^{ct}/+^{ct}$ and $ct/ct^{TgGrhl3}$ gel are indicated by red outlines. Numbers indicate spot number allocated by the software. Outlined spots without numbers, are differentially abundant spots ($p<0.05$) with a fold change lower than 1.5.

Overall, a number of protein spots were found to differ in abundance between genotypes at both stages examined (**Fig. 3.4 A-B**). Among a total of approximately 1,315 spots analysed on 2D gels generated from embryos at the 28-29 somite stage, 114 significantly differed in abundance between strains ($p<0.05$, One Way ANOVA). Following manual inspection (to confirm that detected spots were not gel artefacts), and application of a 1.5-fold change cut-off, 48 spots were considered to represent possible genuine differences of potential biological relevance. Overall, among these spots, 26 were detected at greater abundance in wild-type than *curly tail* samples and 12 were at greater abundance in *curly tail* than wild-type samples while 8 spots were differentially abundant in *Grhl3*-transgenic embryos (details of numbers of spots which fit into different expression profiles are given in **Table 3.5**).

At the 30-31 somite stage, 193 spots were found to significantly differ in abundance between strains ($p<0.05$, One Way ANOVA) out of approximately 1,675 spots detected on gels. Following manual inspection and application of the 1.5-fold change cut off, 58 spots were considered to be of potential interest. Among these spots 16 were at greater abundance in wild-type than *curly tail* samples and 28 were at greater abundance in *curly tail* than wild-type samples while 12 spots were differentially abundant in *Grhl3*-transgenic embryos (**Table 3.5**).

Although a large number of gels were run for each genotype (**Table 3.1**), some gels were not considered ideal for the overall analysis (which uses the entire gel for 'in-gel' normalisation of values) owing to small areas of abnormal migration (**Fig. 3.5**). These gels were useful for visual inspection to evaluate spots that were indicated to vary between genotypes in the software-assisted analysis.

Profile	No. differentially abundant spots 28-29ss analysis	No. differentially abundant spots 30-31ss analysis
1) $+^{ct} > ct > ct^{TgGrhl3}$	3	4
2) $+^{ct} > ct \equiv ct^{TgGrhl3}$	16	5
3) $ct \equiv ct^{TgGrhl3} > +^{ct}$	7	8
4) $ct > +^{ct} \equiv ct^{TgGrhl3}$	4	12
5) $+^{ct} \equiv ct^{TgGrhl3} > ct$	4	6
6) $ct^{TgGrhl3} > ct > +^{ct}$	3	6
7) $ct^{TgGrhl3} > +^{ct} \equiv ct$	5	5
8) $+^{ct} > ct^{TgGrhl3} > ct$	3	1
9) $+^{ct} \equiv ct > ct^{TgGrhl3}$	2	2
10) $ct > +^{ct} > ct^{TgGrhl3}$	1	6
11) $ct > ct^{TgGrhl3} > +^{ct}$	0	2
12) $ct^{TgGrhl3} > +^{ct} > ct$	0	1
Total no of spots	**48**	**58**

Table 3.5. Differentially abundant spots on 2-DE among samples of *curly tail* (*ct*), wild-type ($+^{ct}$) and transgenic ($ct^{TgGrhl3}$) embryos at the 28-29 and 30-31 somite stages. The total number (no.) of differentially abundant spots is indicated for each stage, as well as details of the relative abundance between strains. The Profile Number corresponds to that used in **Figure 3.8**.

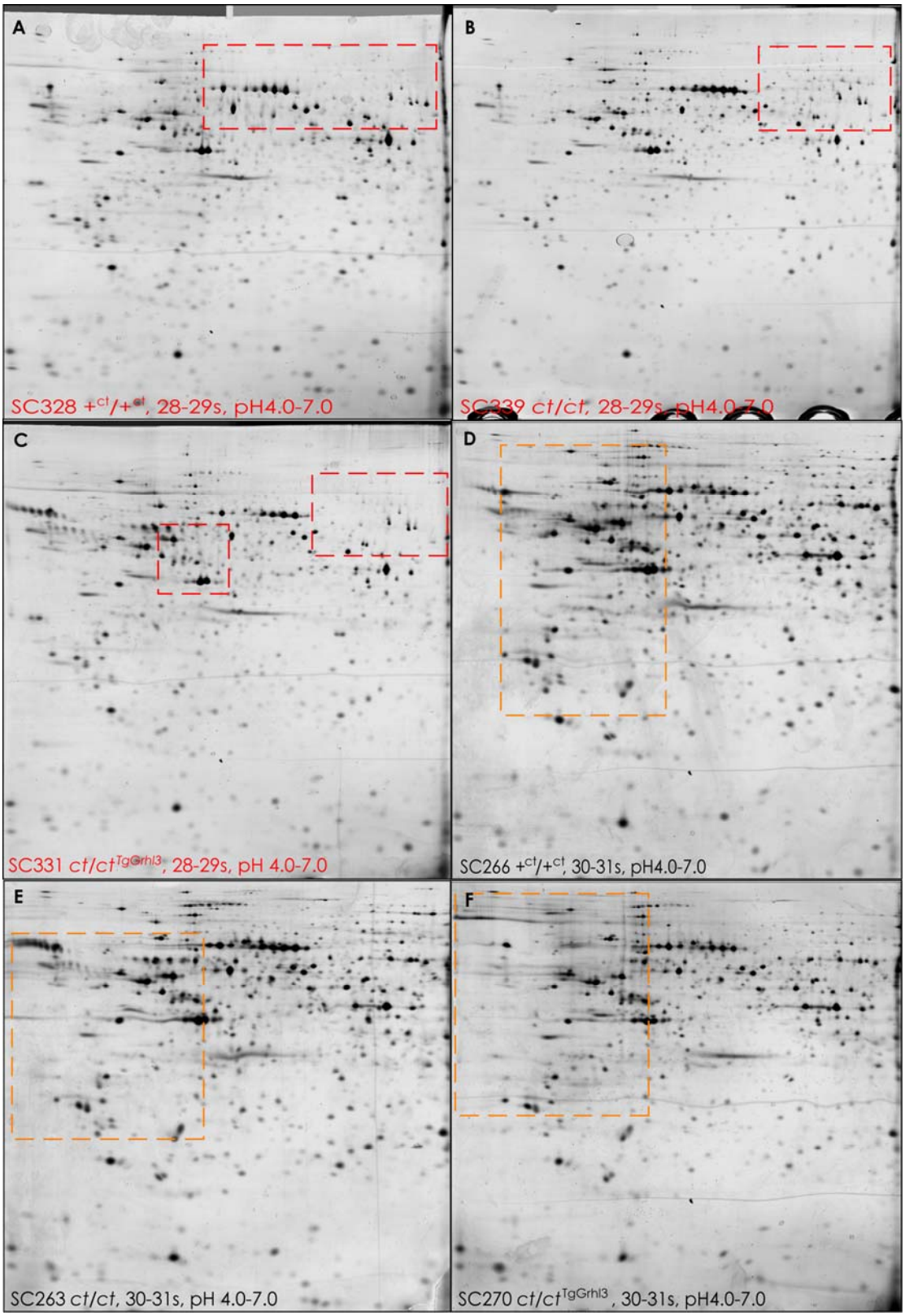

Figure 3.5 Examples of 2D gels excluded from the caudal region analyses, of $+^{ct}/+^{ct}$, *ct/ct*, $ct/ct^{TgGrhl3}$ strains, pH4.0-7.0. (**A-C**) Gels of the 28-29 somite stages analysis (red squares indicate bad areas). (**D-F**) Gels of the 30-31 somite stages analysis (orange squares indicate bad regions).

3.2.3 Peptides and spots/protein identification

Spots of interest, that were differentially abundant on gels from different genotypes, were excised from a gel or pooled from different gels (in case of very small or weaker spots). Spots were subjected to in-gel digestion by trypsin and sent for identification by electrospray ionisation liquid chromatography tandem mass spectrometry (ESI-LC-MS/MS). The MS/MS approach generates sequence data for fragmented peptides, and interrogation of protein databases allows protein identification (**Chapter 2**, **section 2.5.7.2**). The matched peptides for each spot are shown in **Appendix C**. Some spots were not abundant on the 2D gels despite production of additional gels with increased protein content (400 µg protein loading for spot excision). Thus, some spots that were found to significantly vary on 2-DE by Progenesis SameSpots analysis were not identified. Among spots which exhibited statistically significant differences in abundance between groups ($p<0.05$ ANOVA; 1.5 fold-change), the identified proteins are listed in **Table 3.6.** Reference gels showing the location of identified protein spots are shown in **Figures 3.6** and **3.7.**

PSS No	Mean Spot Volume	Fold Change	No. MP	Score	Acc. No.	Protein ID
8	8,239,964 3,192,257 1,335,020	6.2	2	52	P29699	Alpha-2-HS-glycoprotein precursor – *Ahsg*, *Fetuin-A*, *Fetua*; *countertrypin*
7	147,210 742,463 881,136	6.0	20	1022	P14733	Lamin B1*
8	1,048,049 292,823 181,853	5.8	6	301	P14733	Lamin B1*
12	942,028 197,702 349,901	4.8	5	220	P14733	Lamin B1*
20	440,175 1,387,622 1,858,381	4.2	16	836	P14733	Lamin B1*
20	283,280 100,262 72,549	3.9	3	180	P14733	Lamin B1*
36	75,628 209,056 219,517	2.9	9	464	P14733	Lamin B1*
41	182,216 110,613 68,344	2.7	2	58	Q64737	Trifunctional purine biosynthetic protein adenosine-3

42	297,065 144,495 112,763	2.6	2	40	P26041	Moesin
47	836,263 372,571 538,918	2.2	5	143	Q64737	Trifunctional purine biosynthetic protein adenosine-3
52	503,573 775,073 365,906	2.1	1	28	P29699	Alpha-2-HS-glycoprotein precursor
60	535,295 814,396 438,187	1.9	4	69	Q9QXC1	Fetuin-B
61	1,639,971 882,975 1,504,074	1.9	4	156	Q921F2	TAR DNA-binding protein 43
59 63	400,067 214,428 237,702 798,581 438,128 534,891	1.9 1.8	4 8	138 210	Q1HFZ0	tRNA (cytosine-5-)-methyltransferase NSUN2
71	1,996,354 1,152,346 1,274,760	1.7	26 2	1385 59	Q01853 Q9DB20	Transitional endoplasmatic reticulum ATPase ATP synthase subunit O
72	1,268,203 1,708,057 2,148,528	1.7	4	146	P08228	Superoxide dismutase
75	448,305 524,152 734,653	1.6	3	59	Q02819	Nucleobindin-1
76	2,551,689 1,565,114 2,408,714	1.6	5 2 2	149 87 81	Q3THS6 Q8CGP5 Q3U774	S-adenosylmethionine synthase isoform type-2 Histone H2A ATP synthase subunit beta
81	1,822,433 1,143,352 1,210,995	1.6	2	64	O08553	Dihydropyrimidinase-related protein 2
86	1,818,534 2,112,241 2,747,851	1.5	2	55	Q99PT1	Rho GDP-dissociation inhibitor-1
88	2,628,033 1,963,683 1,747,780	1.5	6	131	P61979	Heterogeneous nuclear ribonucleoprotein K
96	1,674,772	1.5	2	59		Ubiquitin-conjugating

	1,982,083 2,436,848				P61089	enzyme E2
158	1,061,683 1,619,735 1,571,230	1.5	3	36	Q99KP6	Pre-mRNA-processing factor 19
168	1,078,953 1,311,369 1,577,263	1.5	3	104	P26638	Seryl-tRNA synthetase

Table 3.6 Identity of protein spots that statistically differed in abundance in $+^{ct}/+^{ct}$, *ct/ct* and *ct/ct*^{TgGrhl3} samples. The Progenesis SameSpots software (PSS No) gives a unique identifier allowing localisation on the 2D gels. The mean normalised spot volume (MNSV; arbitrary units) is given for each group and is colour coded as $+^{ct}/+^{ct}$, *ct/ct* and *ct/ct*^{TgGrhl3}**.** MP indicates the number of matched peptides that were identified for that spot and the identified protein. Score from Mascot analysis is also indicated with scores of ≥35 considered sufficient for confident identification. The protein database accesstion number (Acc. No.) and protein names (ID) are also indicated. Proteins are listed in order of the magnitude of the fold-change in abundance between the highest and the lowest mean volumes. * A difference in lamin B1 spots between *ct/ct* and $+^{ct}/+^{ct}$ was evident on every gel analysed. Text colour indicates whether the spot difference was observed in the analysis of caudal regions at the 28-29 somite stage (black) or the 30-31 somite stage (blue).

In some cases a protein spot was found to correspond to more than one protein identity. For example, PSS71 included transitional endoplasmatic reticulum ATPase, and ATP synthase subunit O. This probably results from co-migration on 2-DE owing to very similar molecular weight and pI of the proteins. In these cases it is possible that use of narrow range pH strips for isoelectric focussing would allow separation of the spots to allow determination of which one differs in abundance between groups. In addition, some proteins were identified from more than one spot. For example, PSS 59 and 63 both correspond to tRNA (cytosine-5-)-methyltransferase NSUN2, and are likely to correspond to different isoforms or post-translationally modified variants.

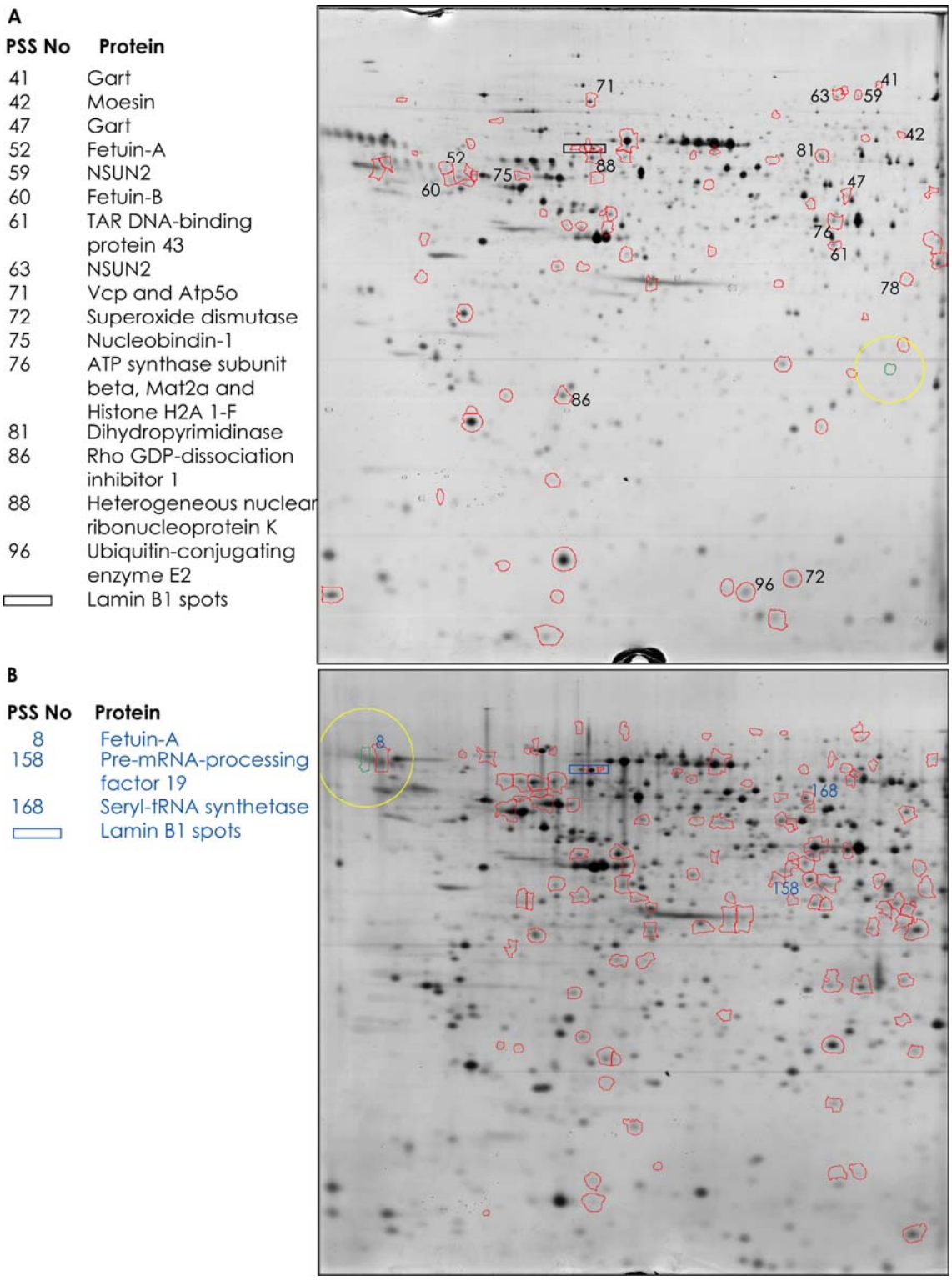

Figure 3.6 Representative 2D gels of embryo caudal regions showing the location of identified proteins at the 28-29 (A) and 30-31 (B) somite stages. Isoelectric focussing was performed on a pH4-7 gradient (acidic side on left of gel image). Numbered spots (PSS No., Progenesis Spot Number) are indicated.

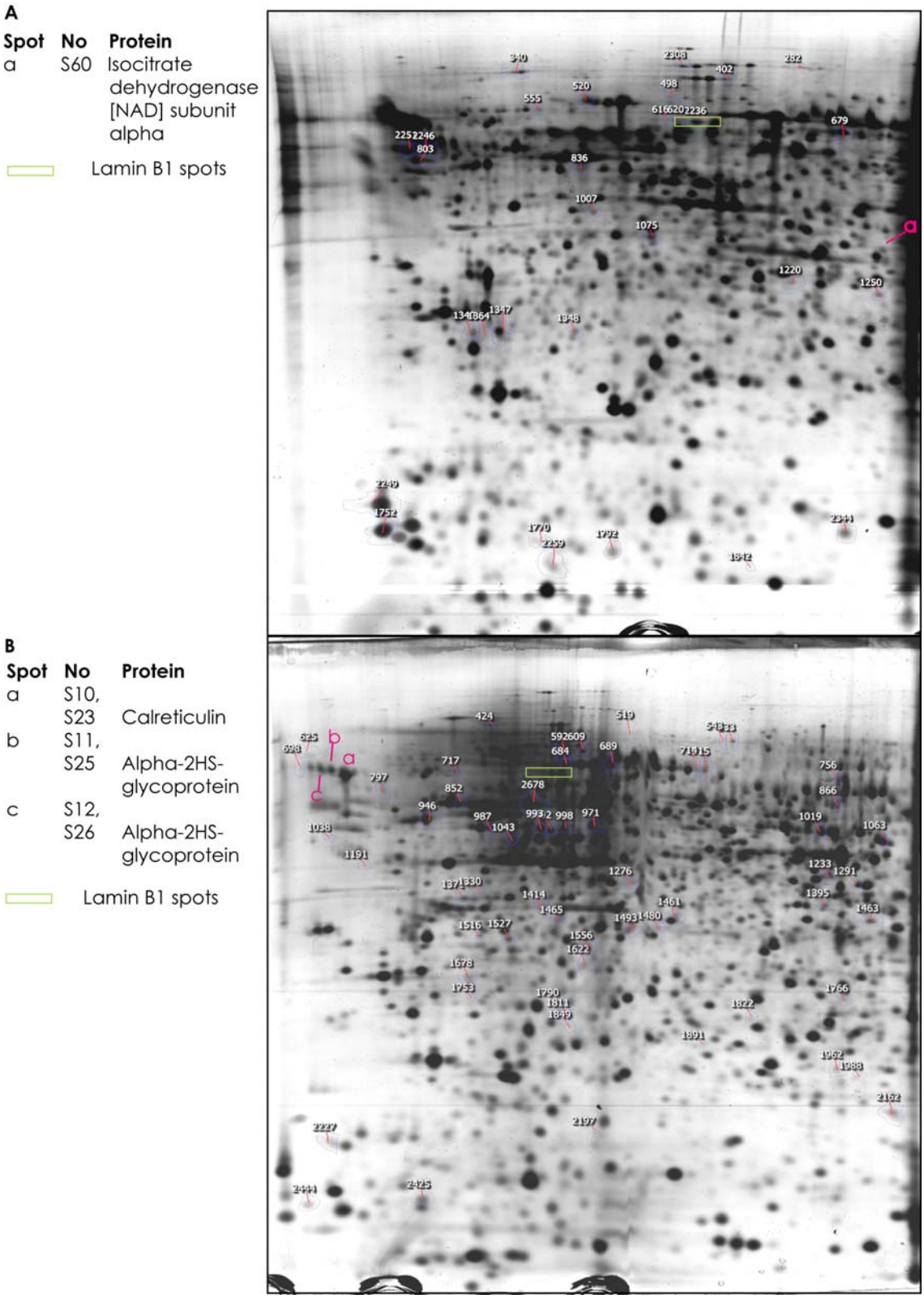

Figure 3.7 Location of additional proteins identified by mass spectrometry on pH 3.0-5.6 (A) and pH 4.0- 7.0 (B) 2D gels. Gels were generated from whole embryo samples at E10.5.

3.2.4 Protein profiles

The proteins which were identified by mass spectrometry can be broadly divided into profiles according to their differences in relative abundance between experimental groups. A graphical representation of each possible profile is shown in **Figure 3.8** and **Table 3.7** lists the proteins that correspond to each profile. The graph bars correspond to the colour codes used in **Table 3.6.**

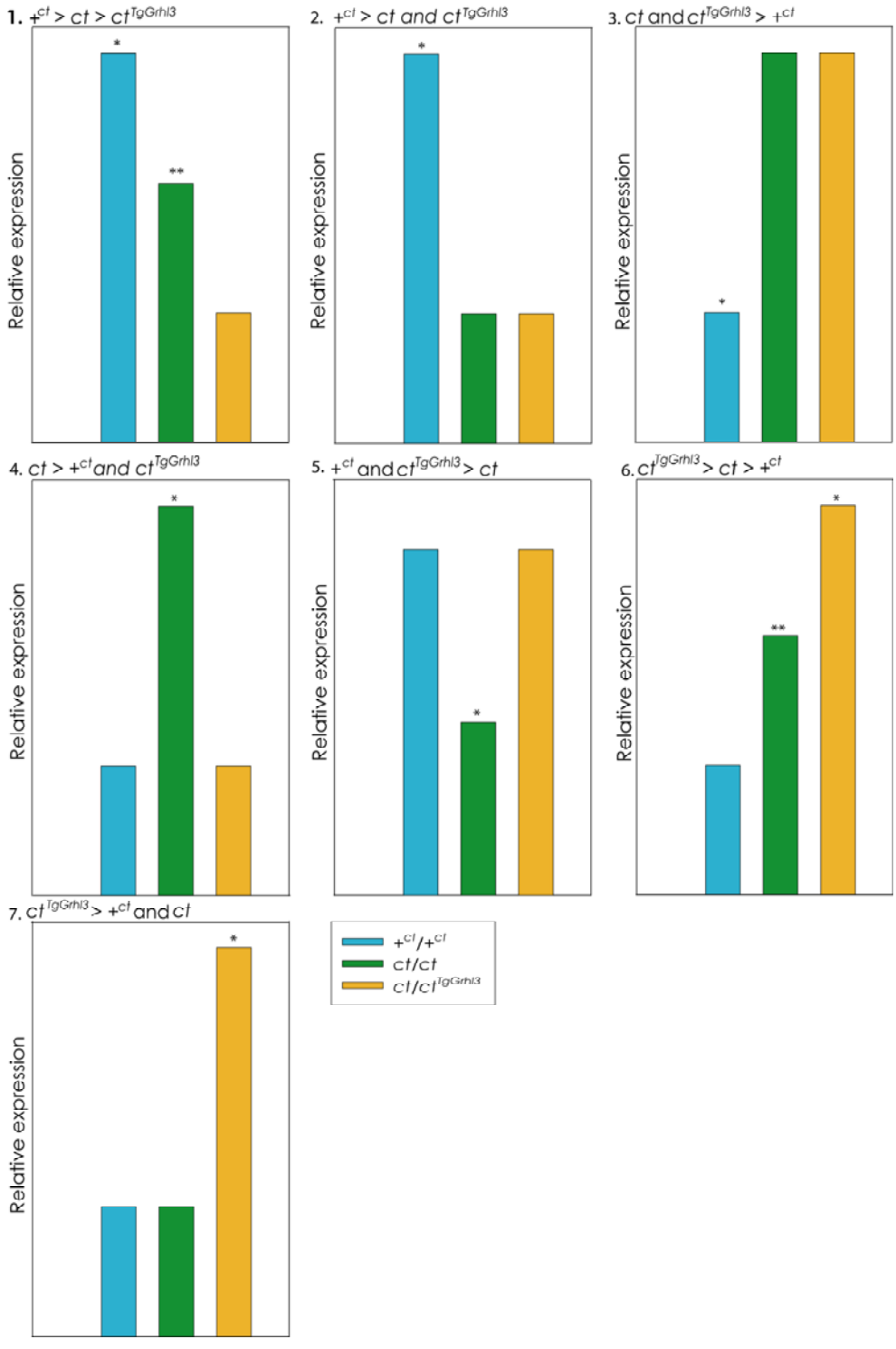

Figure 3.8 Profiles of protein abundance for identified spots that are differentially represented between experimental groups. Graphical representation of the relative expression observed in the three strains. * Spots that are significantly more abundant (Profiles 1, 2, 4, 6, 7) or less abundant (Profiles 3, 5) than in the other two strains. ** Spots that are significantly more abundant than in the strain with lowest abundance (Profiles 1, 6). Note that, profiles 5 and 7 represent proteins whose abundance is positively correlated with the expression level of *grainyhead like-3*, whereas profile 4 represents proteins whose abundance is negatively correlated with the expression level of *grainyhead like-3*. Profiles 1, 2, 3 and 6 could represent proteins whose abundance is influenced by the small differences in genetic background between *ct* (and $ct^{TgGrhl3}$) on the one hand and $+^{ct}$ strain on the other.

PSS No	Protein – Gene Symbol	Function
1) $+^{ct}/+^{ct} > ct/ct > ct/ct^{TgGrhl3}$		
8	Fetuin-A	Development-associated regulation of calcium metabolism and osteogenesis
2) $+^{ct}/+^{ct} > ct/ct \equiv ct/ct^{TgGrhl3}$		
8, 12, 20	Lamin B1 – *Lmnb1*	Nuclear envelope protein – control of cell cycle and nuclear shape
41, 47	Trifunctional purine biosynthetic protein adenosine-3 - *Gart*	Purine metabolism
42	Moesin - *Msn*	Belongs to the ERM (ezrin/radixin/moesin) protein family. Regulates epithelial organisation by linking membrane-associated proteins to the actin-cytoskeleton
59, 63	tRNA (cytosine-5-)-methyltransferase NSUN2 – *Nsun2*	Control of cell cycle
71	Transitional endoplasmic reticulum ATPase – *Vcp* or *p97*	Role in nuclear envelope assembly and proliferation
71	ATP synthase subunit O – *Atp5o*	ATP synthase involved in oxidative phosphorylation
81	Dihydropyrimidinase-related protein 2 – *Dpysl2*	Necessary for signaling by class 3 semaphorins and subsequent remodelling of the cytoskeleton. Substrate of Rho kinase in the brain
88	Heterogeneous nuclear ribonucleoprotein K - *Hnrpk*	RNA/DNA-binding protein – gene expression and signal transduction

3) ct/ct ≡ ct/ct^{TgGrhl3} > +^{ct}/+^{ct}		
7, 20, 36	Lamin B1 – *Lmnb1*	Nuclear envelope protein – control of cell cycle and nuclear shape
158	Pre-mRNA-processing factor 19 –*Prpf19*	Acts as a structural component of the nuclear framework
168	Seryl-tRNA synthase - *Sars*	Catalyses the attachment of serine to tRNA

4) ct/ct > +^{ct}/+^{ct} ≡ ct/ct^{TgGrhl3}		
52	Fetuin-A	Development-associated regulation of calcium metabolism and osteogenesis
60	Fetuin-B	Like fetuin-A, mRNA level is down-regulated in recovery phase of acute inflammatory response

5) +^{ct}/+^{ct} ≡ ct/ct^{TgGrhl3} > ct/ct		
61	TAR DNA-binding protein 43 – *Tardbp* or *Tdp-43*	DNA and RNA-binding protein - regulates transcription and splicing
76	S-adenosylmethionine synthase isoform type-2 – *Mat2a*	Role in the methylation cycle – synthesis of S-adenosylmethionine from methionine and ATP
76	Histone H2A – *Hist1h2af*	Transcription regulation, DNA repair, DNA replication and chromosomal stability
76	ATP synthase subunit beta – *Atp5b*	ATP synthase

6) ct/ct^{TgGrhl3} > ct/ct > +^{ct}/+^{ct}		
72	Superoxide dismutase – *Sod1*	Antioxidant enzyme defence mechanism to minimise cellular damage by reactive oxygen species (ROS)
86	Rho-GDP-dissociation inhibitor-1 – *Gdi1*, *Arhgdia*	Regulates the GDP/GTP exchange reaction of the Rho dissociation proteins
7) ct/ct^{TgGrhl3} > +^{ct}/+^{ct} ≡ ct/ct		
75	Nucleobindin-1 – *Calnuc*, *NucB1*	Major calcium-binding protein of the Golgi.
96	Ubiquitin-conjugating enzyme E2 – *Ube2n*	Mediates transcriptional activation of target genes. Controls progress of cell cycle and differentiation

Table 3.7 Protein profiles. Identified proteins were allocated into broad profiles (see **Fig. 3.8**) according to the mean spot volume of each strain seen in **Table 3.6**. For example, spot 41 (Gart protein), is in the profile $+^{ct} > ct \equiv ct^{TgGrhl3}$ as there was no statistically significant difference between the mean spot volume in *ct/ct* and *ct/ct*^{TgGrhl3} strains, whereas both statistically differ from the wild-type strain.

3.2.5 Evaluation of differentially abundant proteins from 2-DE analysis

After evaluation of all the proteins which exhibited differential abundance, certain proteins were chosen for further validation **(Table 3.8**). Proteins were selected on the basis of several considerations including the magnitude of the fold change, whether the spot was found to vary in different analyses (e.g. using different gel conditions or embryonic stages), information from a microarray-based expression analysis recently performed in the laboratory (in a parallel project; N. Greene personal communication) and possible functional relationship to NTDs or the known cellular defect in *curly tail* embryos. In order to attempt to validate the findings of 2D gel analysis these proteins were analysed further by Western blot and/or real-time quantitative polymerase chain reaction (RT-qPCR).

One approach to evaluate findings of 2-DE analysis is Western blotting to investigate the total abundance of a protein of interest. A protein whose abundance differs between strains on a 2-DE spot may also differ on Western blot, thereby validating the 2-DE result. However, this may not be an informative approach in every case since an individual isoform or post-translational variant of a protein may differ in abundance, apparent on a 2D gel, while the overall abundance (i.e., all isoforms pooled) is unaltered.

Protein	Gene, chr	pI	MW (kDa)	Comments
Lamin B1	*Lmnb1*, 18	4.92, 5.11	66.7	Strains differ by presence or complete absence of spots, detectable in all analyses
Trifunctional purine biosynthetic protein adenosine-3	*Gart*, 16	6.25	107.3	Involved in folate one-carbon metabolism; two different spots vary; differential expression in microarray
Transitional endoplasmic reticulum ATPase	*Vcp*, 4	5.14	89.3	Involved in nuclear envelope assembly and cell proliferation
S-adenosylmethionine synthase isoform type-2	*Mat2a*, 6	6.02	43.7	Involved in folate one-carbon; altered methylation cycle detected in *ct/ct* embryos; differential expression in microarray
Alpha-2-HS-glycoprotein precursor	*Fetuin-A*, 16	5.26	38.4	High fold change; two different spots differ on 2D gels
Fetuin-B	*Fetuin-B*, 16	5.59	52.6	Paralogue of *Fetuin-A*
Ubiquitin-conjugating enzyme E2	*Ube2n,*10	6.13	17.1	Ubiquitin related enzymes implicated in NTDs

Table 3.8 Proteins selected for further validation from 2-DE data. Gene symbol and mouse chromosome, isoelectric point (pI) and molecular weight (MW) are given, as well as information that indicates the reason for further analysis.

3.2.5.1 Proteomic analysis of Lamin B1 in *curly tail* embryos

2D gels generated from *ct/ct* and $+^{ct}/+^{ct}$ embryos, at the 26-27, 28-29 and 30-31 somite stages (ss), allowed picking and identification of proteins that were differently expressed between the two strains (**Table 3.1**). A row of spots, each of which was identified as lamin B1 showed an interesting difference in migration on *ct/ct* and $+^{ct}/+^{ct}$ gels (**Fig. 3.9 A-B**). Three spots present on $+^{ct}/+^{ct}$ gels were not detected on *ct/ct* gels whereas three spots detected on *ct/ct* gels were not present on $+^{ct}/+^{ct}$ gels. Examination of the gel patterns showed that these differences are due to a shift of the lamin B1 spots to a more basic position on *ct/ct* gels compared to the lamin B1 spots on the $+^{ct}/+^{ct}$ gels (**Fig. 3.9 B**). This same difference in pattern of lamin B1 spots was detected using samples of whole embryos, cranial or caudal regions alone, large or small PNP. Immunoblots of 2D gels were carried out using an antibody raised against a peptide mapping at the C-terminus of the lamin B1 protein. This allowed further confirmation that the gel spots correspond to lamin B1 (**Fig. 3.10 A**), thereby complementing the mass spectrometry analysis.

Samples of the caudal region of *ct/ct*, $+^{ct}/+^{ct}$ and $ct/ct^{TgGrhl3}$ strains, at somite stages 28-29 and 30-31 were used for this analysis (**Chapter 2**, **section 2.6**). Commercial antibodies (**Chapter 2**, **Table 2.11**) were acquired to validate lamin B1 and the other seven proteins in **Table 3.8**. Blots were scanned and target protein expression was normalised to β-tubulin and/or Gapdh, by adjusted volumetric measurement (with background subtraction), in order to compare the samples (**Chapter 2**, **section 2.6.5**).

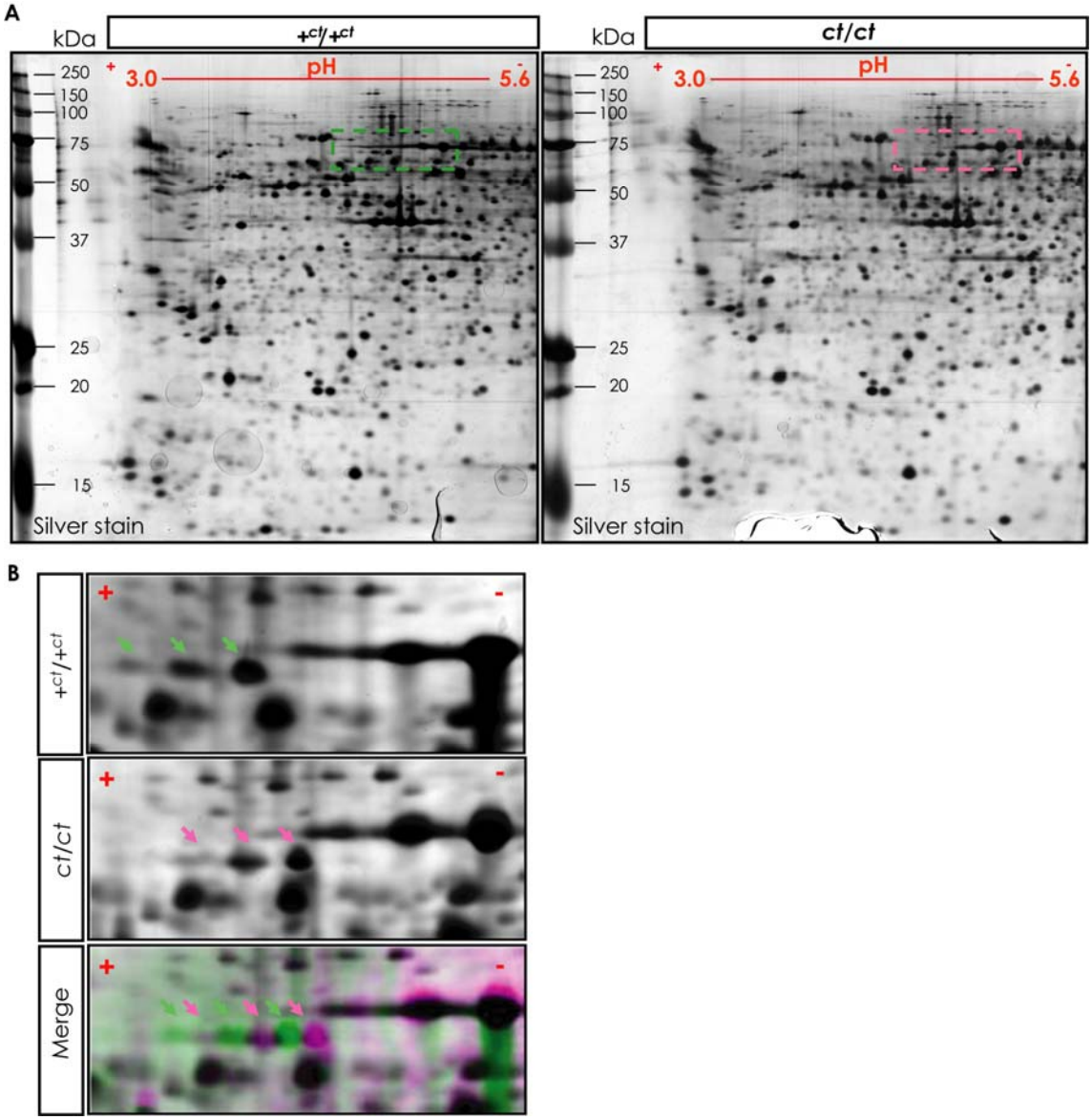

Figure 3.9 Difference in lamin B1 protein migration on 2D gels of $+^{ct}/+^{ct}$ and *ct/ct* samples. (**A**) Silver stained 2D gels, with isoelectric focussing on pH 3.0 to 5.6, generated from $+^{ct}/+^{ct}$ and *ct/ct* embryo samples. Coloured rectangles indicate the region encompassing lamin B1 protein spots. (**B**) Higher magnification of the lamin B1 region in $+^{ct}/+^{ct}$ and *ct/ct* gels (indicated by the green and pink rectangles on gels in A), respectively, with a merged and pseudo-coloured image below. The spots on the *ct/ct* gel (indicated by the pink arrows) migrate differently from the spots on the $+^{ct}/+^{ct}$ gel (indicated by green arrows). The merged image most clearly shows this difference.

Lamin B1 spots on 2D gels generated from *ct/ct* and $+^{ct}/+^{ct}$ samples appeared at similar intensity, and western blots of 2D gels suggested that additional lamin B1 spots were not present elsewhere on the gels (**Fig. 3.10 A**). Western blotting analysis on 1D gels was also performed to examine the hypothesis that there may be a difference in total abundance of lamin B1 between *ct/ct*, $+^{ct}/+^{ct}$ and $ct/ct^{TgGrhl3}$ samples. Lamin B1 was detected on immunoblots as a band at 67 kDa as expected (**Fig. 3.10 B**). Overall there were no differences between the $+^{ct}$ and *ct* strains in the total abundance of lamin B1, normalised to β-tubulin (**Table 3.9**).

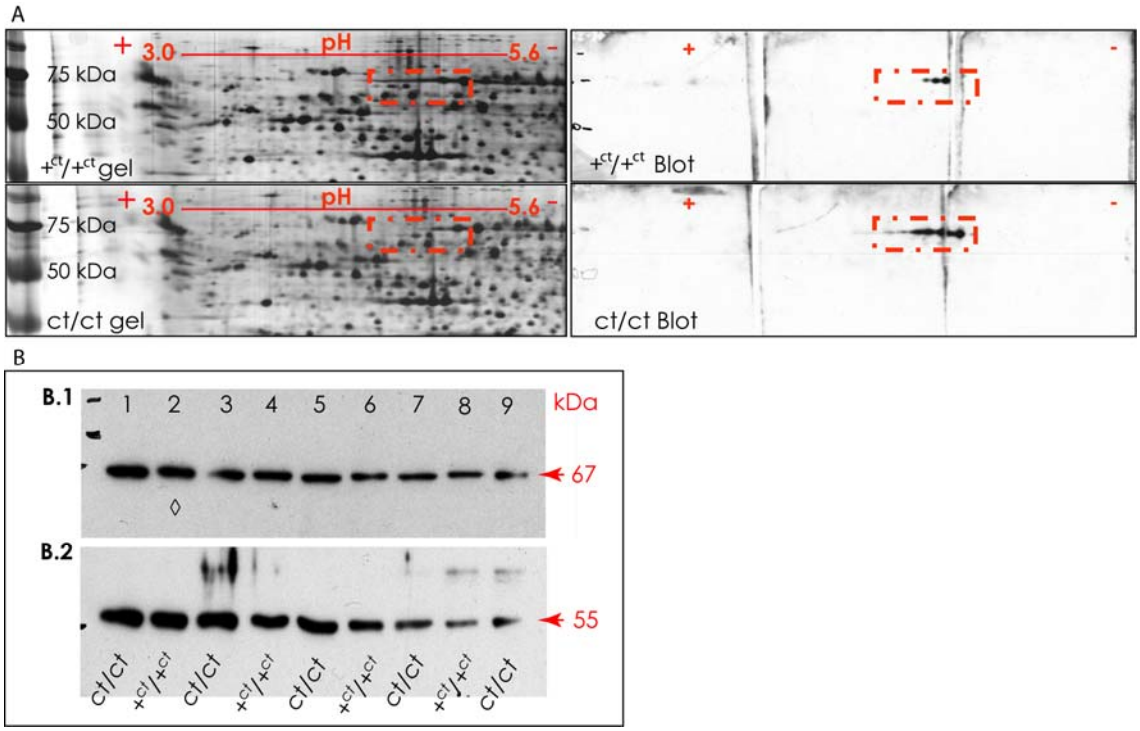

Figure 3.10 Western blots of lamin B1 on 2D and 1D gels. (**A**) Blotting of 2D gels with an antibody to lamin B1 confirmed the identity of the spots identified as lamin B1 by mass spectrometry. The number of detectable isoforms varies between experiments with three to five spots present on different blots (no consistent difference between the number of isoforms detected for each strain was apparent). (**B**) Western blots at the 28-29 (**B.1-2**) somite stages were used to compare lamin B1 abundance in $+^{ct}/+^{ct}$ and *ct/ct* samples generated from isolated caudal regions. The lamin B1 antibody recognises a 67 kDa band. Blots were stripped and re-probed with an antibody to ß-tubulin for normalisation (55 kDa band in **B.2**). In each experiment, ratios were calibrated relative to a wild-type sample (◊, value 1.0).

<table>
<tr><th colspan="6">Protein</th></tr>
<tr><td rowspan="4">Lamin B1</td><td rowspan="2">2D-gel</td><td colspan="2">Stage and Spot number</td><td>Fold change</td><td>Profile</td></tr>
<tr><td colspan="2">28-29SS: S8, S20, 30-31SS: S12</td><td>5.8, 3.9, 4.8</td><td>$+^{ct} > ct \equiv ct^{TgGrhl3}$</td></tr>
<tr><td colspan="2">28-29SS: S7, S36, 30-31SS: S20</td><td>6.0, 2.9, 4.2</td><td>$ct \equiv ct^{TgGrhl3} > +^{ct}$</td></tr>
<tr><td rowspan="3">Western blots</td><td colspan="2">N</td><td>Volume</td><td>Comments</td></tr>
<tr><td>$+^{ct}$</td><td>8</td><td>2.24 ± 0.92</td><td rowspan="2">1.1 fold
$+^{ct} \equiv ct$
(No difference)</td></tr>
<tr><td>ct</td><td>8</td><td>2.23 ± 0.37</td></tr>
</table>

Table 3.9 Western blot results for lamin B1 protein. Lamin B1 spots, in contrast to other differential abundant proteins on 2-DE, migrated differently in *ct/ct* (and $ct/ct^{TgGrhl3}$) and $+^{ct}/+^{ct}$ 2D-gels. The spots fit into two different profiles for both stages (28-29 and 30-31 somite stage). Western blot analysis comparing the two strains at the 28-29 somite stage did not show any difference in the expression of lamin B1. Volume indicates the band volume normalised to the volume of the corresponding β-tubulin band for that sample (arbitrary units) and is given as the mean and standard error. Fold change is between the highest and the lowest values.

3.2.5.2 Proteomic analysis of Gart in *curly tail* embryos

The 2-DE analysis revealed two spots that varied between *curly tail* and wild-type samples and were identified as trifunctional purine biosynthetic protein adenosine-3 (Gart): S47 (approximately 65 kDa; **Fig. 3.11 A**) and S41 (approximately 110 kDa). In *ct/ct* and $+^{ct}/+^{ct}$ samples, the antibody against Gart recognised three different band sizes: at around 45 kDa, 65 kDa and 110 kDa (the latter is the expected size according to the manufacturer; **Fig. 3.11 B.1**). The 65 kDa band detected on Western blot showed a similar greater abundance in wild-type than in *curly tail* samples, as detected for the 65 kDa spot on 2D gels (**Table 3.10**). However, with the sample size used this apparent difference was not statistically significant. No difference in intensity of the 110 kDa band was observed in comparison of the two strains.

Quantitative Real Time RT-PCR (qRT-PCR) was also performed (as described in **Chapter 2**, **section 2.7)** using two different sets of primers designed against the *Gart* transcripts (**Appendix B**, **Table B.1**). The mRNA expression level appeared very similar in the *ct* and $ct^{TgGrhl3}$ strains while expression was slightly lower in the $+^{ct}$ strain but not to a significant degree (**Table 3.10**). Therefore, differences in Gart protein profile appear unlikely to be a direct consequence of transcriptional misregulation.

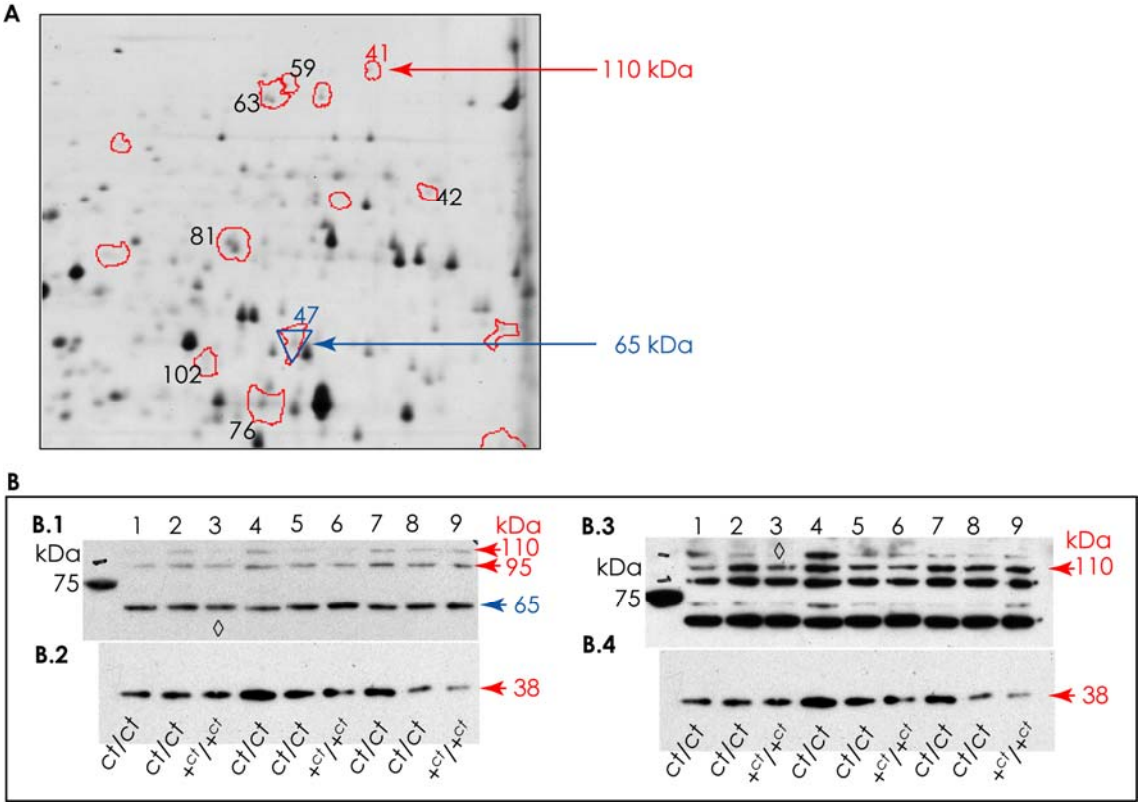

Figure 3.11 Evaluation of Gart protein abundance by Western blot. (**A**) High magnification of the region on a 28-29 somite stage 2D-gel image where Gart spots are localised: S41 (~110 kDa, red arrow), and S47 (~65 kDa, blue arrow). (**B**) Western blots for Gart on protein samples from 28-29 somite stage *ct/ct* and $+^{ct}/+^{ct}$ embryos. This antibody recognises three major bands (65, 95 and 110 kDa; **B.1**). To measure the volume of the bands for the 110 kDa size-band, the blot had to be exposed for a longer period (**B.3**). Samples were normalised to Gapdh protein (38 kDa; **B.2, B.4**). In each experiment, ratios were calibrated relative to a wild-type sample (◊, value 1.0).

<table>
<tr><td colspan="8">Protein</td></tr>
<tr><td rowspan="15">Gart</td><td rowspan="3">2D-gel</td><td colspan="2">Spot</td><td>Fold change</td><td colspan="3">Profile</td></tr>
<tr><td colspan="2">S41</td><td>2.7</td><td colspan="3">$+^{ct} > ct \equiv ct^{TgGrhl3}$</td></tr>
<tr><td colspan="2">S47</td><td>2.2</td><td colspan="3">$+^{ct} > ct \equiv ct^{TgGrhl3}$</td></tr>
<tr><td rowspan="5">Western blot</td><td colspan="2">N</td><td>Volume</td><td colspan="3">Comment</td></tr>
<tr><td colspan="6">110 kDa ≡ S41</td></tr>
<tr><td>$+^{ct}$</td><td>4</td><td>0.44 ± 0.19</td><td colspan="3" rowspan="2">1.2 fold
$+^{ct} > ct$ (Not significant)</td></tr>
<tr><td>ct</td><td>7</td><td>0.36 ± 0.13</td></tr>
<tr><td colspan="6">65 kDa ≡ S47</td></tr>
<tr><td rowspan="7">qRT-PCR</td><td>$+^{ct}$</td><td>4</td><td>0.83± 0.18</td><td colspan="3" rowspan="2">2.0 fold
$+^{ct} > ct$ (Not significant)</td></tr>
<tr><td>ct</td><td>7</td><td>0.42 ± 0.11</td></tr>
<tr><td colspan="6">Gart - Primer set 1</td></tr>
<tr><td colspan="2">$+^{ct}$</td><td>3</td><td>1.01 ± 0.08</td><td colspan="2" rowspan="3">1.5 fold
$ct \equiv ct^{TgGrhl3} > +^{ct}$
(Not significant)</td></tr>
<tr><td colspan="2">ct</td><td>3</td><td>1.48 ± 0.28</td></tr>
<tr><td colspan="2">$ct^{TgGrhl3}$</td><td>3</td><td>1.40 ± 0.17</td></tr>
<tr><td colspan="6">Gart – Primer set 2</td></tr>
<tr><td colspan="2">$+^{ct}$</td><td>3</td><td>1.05 ± 0.13</td><td colspan="2" rowspan="3">1.4 fold
$ct \equiv ct^{TgGrhl3} > +^{ct}$
(Not significant)</td></tr>
<tr><td colspan="2">ct</td><td>3</td><td>1.46 ± 0.20</td></tr>
<tr><td colspan="2">$ct^{TgGrhl3}$</td><td>3</td><td>1.52 ± 0.12</td></tr>
</table>

Table 3.10 Gart protein validation. Gart spots, S41 and S47 (110 and 65 kDa, respectively), were both found to be more abundant in $+^{ct}$ than *ct* on 2D-gels. Western blot analysis of Gart in $+^{ct}$ and *ct* samples shows a similar profile to 2-DE. Although the strain differences were not statistically significant (t-test), the western blot analysis appears to support the 2-DE data. The relative expression of *Gart* mRNA, as determined by qRT-PCR, was very similar in *ct* and $ct^{TgGrhl3}$ strains but lower in the $+^{ct}$ strain although these differences were not statistically significant (One Way ANOVA). Both pairs of primers gave similar results. Volume indicates the volume of the band on the western blot normalised to the volume of the corresponding Gapdh band for that sample (arbitrary units) and *Gart* relative expression in the RT-qPCR is given as the mean and standard error. Fold change is between the highest and the lowest values.

3.2.5.3 Proteomic analysis of Vcp in *curly tail* embryos

Transitional endoplasmic reticulum ATPase or Valosin-containing protein (Vcp), was found to be more abundant in $+^{ct}$ than *ct* samples on 2D gels. This protein migrates at approximately 89 kDa, and the same size was recognised by the antibody in Western blots (**Fig. 3.12 A-B**). Vcp total protein expression revealed no difference in abundance

between the three strains (1.3 fold difference between $+^{ct}$ and *ct*), unlike the 2-DE analysis which showed a 1.7 fold change for spot S71 ($+^{ct} > ct \equiv ct^{TgGrhl3}$; **Table 3.11**).

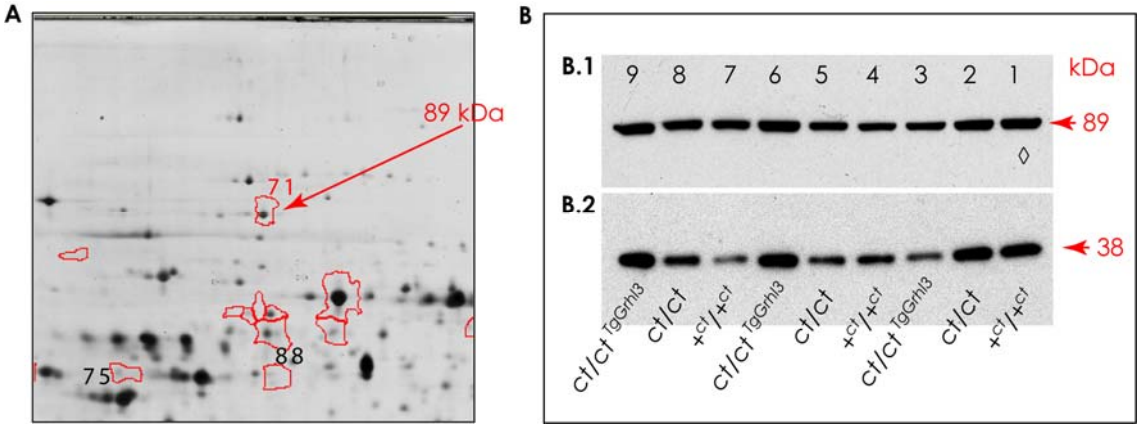

Figure 3.12 Validation of Vcp protein by Western blot. (**A**) High magnification of the region where the Vcp spot localises on 2D-gels: S71 (red arrow). (**B**) Western blot of Vcp in protein samples from *ct/ct*, $+^{ct}/+^{ct}$ and $ct/ct^{TgGrhl3}$ embryos at the 28-29 somite stage. Protein abundance was normalised to Gapdh protein using the same blot (38 kDa; **B.2**). In each experiment, ratios were calibrated relative to a wild-type sample (◊, value 1.0).

Protein				
Vcp	**2D-gel**	**Spot**		**Profile**
		71	1.7 fold	$+^{ct} > ct \equiv ct^{TgGrhl3}$
	Western blot			
		N	**Volume**	**Comment**
		$+^{ct}$ 3	1.74±0.62	1.3 fold $+^{ct} > ct \equiv ct^{TgGrhl3}$ (Not significant)
		ct 3	1.33±0.23	
		ct^{Tg} 3	1.35±0.54	

Table 3.11 Western blot results for Vcp protein. Total Vcp protein expression did not significantly differ between strains on western blot (One Way ANOVA) although it was noted that there was a slightly higher apparent abundance in $+^{ct}$ than in *ct* samples (the same profile as was observed on 2-DE). Normalised band volumes (determined using Gapdh bands as **Table 3.10**) are given as the mean and standard error (arbitrary units). Fold change refers to the difference between the highest and the lowest mean values.

3.2.5.4 Proteomic analysis of Fetuin-A in *curly tail* embryos

In separate 2-DE analyses, two spots corresponding to Fetuin-A (Fetu-A) were found to differ in abundance; spot S52 which migrates at approximately 60 kDa, and differs at the 28-29 somite stage, and S8, which migrates at approximately 65 kDa (different at the 30-31 somite stage; **Fig. 3.13 A-B**). Both spots were found to be at lower abundance in $ct^{TgGrhl3}$ samples than the other strains. In samples at the 28-29 somite stage, the antibody recognises two bands at around 45 kDa and the expected 59 kDa, corresponding to spot S52 (**Fig. 3.13 C.1**). The latter band was more abundant in *ct* than in $ct^{TgGrhl3}$ samples as found for 2-DE spot S52, further suggesting that there is a difference in protein level between the strains. However, there was major variation between individual samples within experimental groups such that this result should be treated with caution (**Table 3.12**). A band corresponding to the same molecular weight as spot S8 was not detected by western blot (**Fig. 3.13 C.3**).

It was previously found there are other isoforms of Fetuin-A present on 2-DE (**Fig. 3.7**). Therefore, it is unclear whether western blot analysis will be of use to validate any differences in one or a few Fetuin A spots. Narrow range 2D-gels could be run in order to better separate these spots and allow investigation of whether there is a different representation of Fetuin-A isoforms in the different strains.

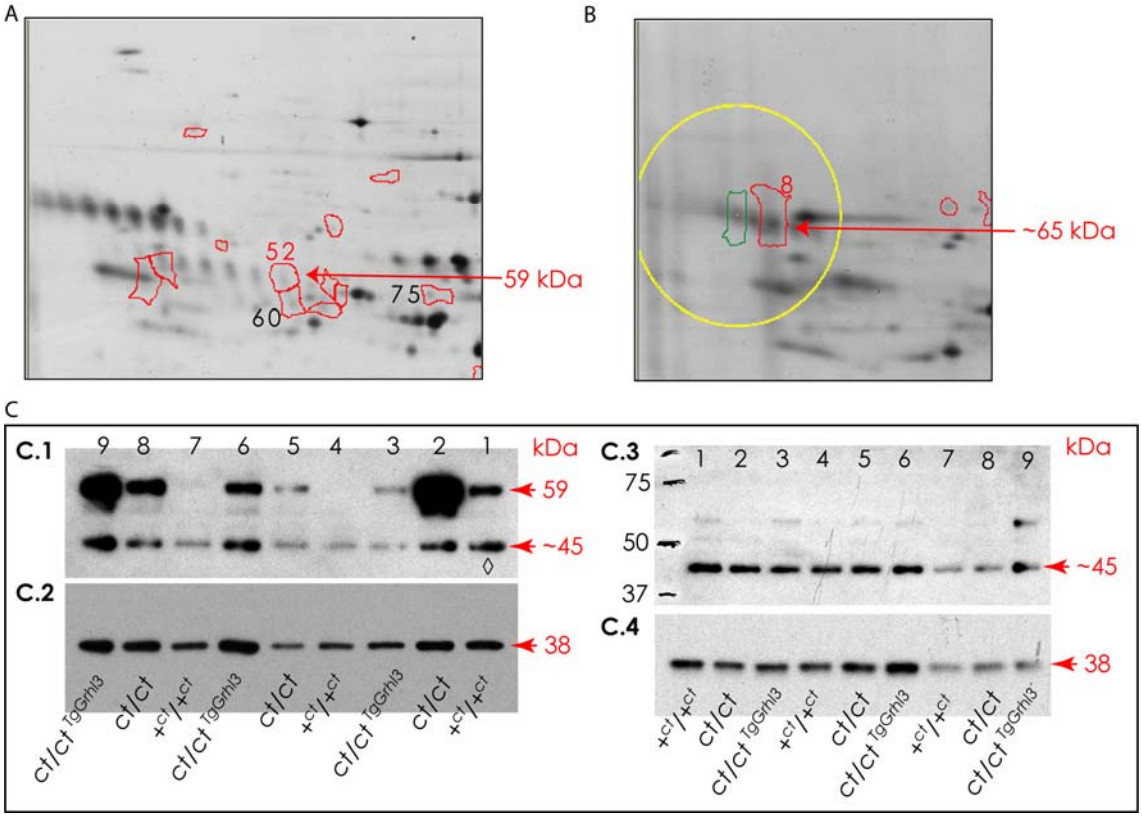

Figure 3.13 Analysis of Fetuin-A protein by 2-DE and Western blot. (**A-B**) High magnification of regions of 2D gel that contain spots identified as Fetuin-A on 2D-gels: S52 (28-29 ss, 59 kDa; **A**), and S8 (30-31 ss, 65 kDa; **B**). (**C**) Western blot of Fetuin-A in samples from *ct/ct*, $+^{ct}/+^{ct}$ and $ct/ct^{TgGrhl3}$ embryos at the 28-29 somite stage (**C.1**). The antibody recognises two bands, at ~ 45 kDa and the expected 59 kDa. In embryos at the 30-31 somite stage (C.3), the antibody recognises a main band ~ 45 kDa with the higher molecular weight band only faintly apparent. Therefore, the altered abundance of spot 8 on 2-DE could not be validated. The blots were stripped and re-probed with the antibody to Gapdh for normalisation (**C.2, C.4**). Normalised band volumes (determined as described in Table 3.9) were calibrated relative to a wild-type sample (◊, value 1.0).

Protein					
Fetuin-A	2D-gel	Spot		Fold	Profile
		52		2.1	$ct > +^{ct} \equiv ct^{TgGrhl3}$
	Western blot				
		N		Volume	Comment
		$+^{ct}$	3	0.30±0.35 *	2.1 fold $ct > ct^{TgGrhl3}$ (Not significant)
		ct	3	5.95±4.13	
		$ct^{TgGrhl3}$	3	2.86±2.26	

Table 3.12 Western blot results for Fetuin-A protein. A band corresponding to the same molecular weight as Spot 52 (59 kDa), identified as Fetuin-A protein, showed a difference between the *ct* and $ct^{TgGrhl3}$ strains with the same magnitude of difference as observed on the 2-DE analysis. However, there was considerable inter-sample variation (with correspondingly high standard errors) and the difference was not significant (One Way ANOVA). Normalised band volumes (determined using Gapdh bands as described in Table 3.9) are given as the mean and standard error (arbitrary units). The indicated fold change is that between the mean volume for *ct* and $ct^{TgGrhl3}$ samples. * In some cases $+^{ct}$ samples on the Western blot gave a barely detectable band with the Fetuin-A antibody and the quantitative data were not considered reliable.

3.2.5.5 Proteomic analysis of Fetuin-B in *curly tail* embryos

A paralogue of Fetuin-A, Fetuin-B (S60), was also identified as differentially abundant on 2D gels (Spot S60). Fetuin-B was detected at 28-29 somite stage as S60 which migrated at approximately 55 kDa (**Fig. 3.14 A**). This spot was found to be at lower abundance in $ct^{TgGrhl3}$ samples than in the other strains. In samples from embryos at the 28-29 somite stage, the antibody recognises a band at around 55 kDa (**Fig. 3.14 B.1**). A first analysis showed the opposite result than predicted i.e., the Fetuin B band was apparently more abundant in $ct^{TgGrhl3}$ than in the *ct* and $+^{ct}$ strains (1.5 fold difference; **Table 3.13**). However, as observed for Fetuin-A, there was a major variation between individual samples within experimental groups (i.e., more abundant in *ct* sample 2 or less abundant in *ct* sample 3 and $+^{ct}$ sample 7; **Fig. 3.14 B.1**). To further investigate this result, another Western blot was performed to compare $+^{ct}$ and *ct* individuals only (**Fig. 3.14 B.3**). A similarly variable result was obtained, e.g., *curly tail* samples 7 and 8, and wild-type sample 9 contained higher levels of this protein than the other samples

of the same strains (**Fig. 3.14 B.3**). In this experiment, $+^{ct}$ seems to express more Fetuin-B at the total protein level, compared to *ct* (1.9 fold; **Table 3.13**). Overall, western blot analysis of the fetuin proteins (A and B) did not provide evidence that there is a consistent difference in abundance of these proteins in the strains examined.

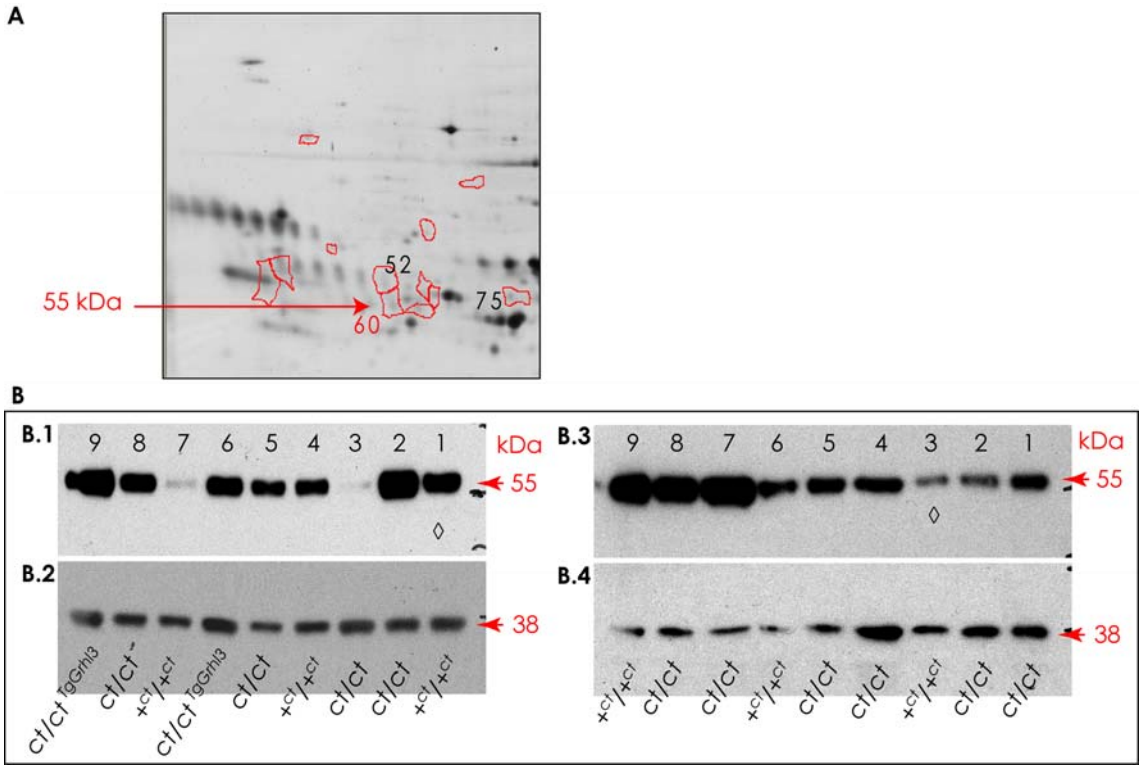

Figure 3.14 Evaluation of Fetuin-B protein by 2-DE and Western blot. (**A**) High magnification of the region of that contains spot S60, identified as Fetuin-B, on 2D gel generated from a 28-29 somite stage embryo. (**B**) Western blots of Fetuin-B in samples from 28-29 somite stage *ct/ct*, $+^{ct}/+^{ct}$ and $ct/ct^{TgGrhl3}$ embryos, with two different experiments shown (**B.1, B.3**). The antibody recognises a band at approximately 55 kDa. Similar to Fetuin-A, Fetuin-B is shows variable abundance (e.g. higher in samples 2 and 9 in **B.1**; and 7-9 in **B.3**) in individual samples independently of strain, rather than a general up- or down-regulation within a strain. The blots were stripped followed by re-probing with an antibody to Gapdh for normalisation (**B.2, B.4**). Normalised band volume ratios were calibrated relative to a wild-type sample (◊, value 1.0).

Protein					
Fetuin B	**2D-gel**	**Spot**		**Fold change**	**Profile**
		60		1.9 fold	$ct > +^{ct} \equiv ct^{TgGrhl3}$
	Western blot	WB - B.1-B.2			
		N		**Volume**	**Comment**
		$+^{ct}$	3	0.49 ± 0.28	1.5 fold - $ct^{TgGrhl3} > ct$
		ct	4	0.85 ± 0.35	2.5 fold - $ct^{TgGrhl3} > +^{ct}$
		ct^{Tg}	2	1.24 ± 0.56	(Not significant)
		WB - B.3-B.4			
		$+^{ct}$	3	31.38 ± 16.6	2.6 fold
		ct	6	11.96 ± 6.80	$+^{ct} > ct$ (not significant)

Table 3.13 Western blot analysis of Fetuin-B protein. Two different experiments were performed for this 55 kDa protein as shown in **Figure 3.14** (**B.1-B.2**, **B3-B4**). It should be noted that there was considerable variability in fetuin-B level between samples such that no differences between strains were statistically significant (One Way ANOVA). In contrast to observations on the 2D-gels, the total protein expression was apparently lower in *ct/ct* compared to $ct/ct^{TgGrhl3}$ (ct^{Tg}), and still lower in $+^{ct}$ (2.5 fold). As some *ct/ct* and $+^{ct}$ samples had undetectable levels of Fetuin-B, a second experiment was performed using only samples of these two strains. In this case, Fetuin-B seemed to be present at higher level in $+^{ct}$ than in *ct* samples (2.6 fold difference, although not statistically significant). Volume refers to band volume normalised to the Gapdh band (as in **Table 3.10**). Values are given as the mean and standard error. Fold change indicates the difference between the highest and the lowest volume values.

3.2.5.6 Proteomic analysis of Mat2a in *curly tail* embryos

A spot migrating at approximately 43 kDa (S76; **Fig. 3.15 A**) and corresponding to S-adenosylmethionine synthase isoform type-2 (Mat2a) protein was detected in the 2D analysis as being more abundant in the wild-type strain. On Western blots the antibody to Mat2a recognised a band of the expected size (43 kDa; **Fig. 3.15 B.1**) and this was present at 1.9 fold higher abundance in $+^{ct}$ compared to *ct* samples, apparently validating the 2-DE findings (**Table 3.14**). However, this difference was not statistically significant, probably owing to the small sample size and variability between samples, and the statistical test did not have sufficient power. Therefore, additional western blots would be necessary to establish whether the total Mat2a abundance truly differs

between strains. Surprisingly, Mat2a protein expression was apparently down-regulated in $ct^{TgGrhl3}$ (2.8 fold lower level than in $+^{ct}$). To further investigate the difference between the $+^{ct}$ and *ct* strains, the Mat2a antibody was used for western blot of 7 cm 2D gels, using a narrow pH range (6.1-7.0) for isoelectic focussing to better separate the protein spots (**Fig. 3.15 C-D**). Mat2a blots for both, *ct* and $+^{ct}$, show the antibody recognises more than one protein spot. These could represent either isoforms (e.g. with different post-translational modifications) or lack of specificity of the antibody. Consequently, there may be a difference between data obtained by Western blot, which detects total levels of protein expression, and 2-DE where one Mat2a spot was differently abundant

As another approach, qRT-PCR was performed using cDNA extracted from the caudal region of *ct/ct*, $+^{ct}/+^{ct}$ and $ct/ct^{TgGrhl3}$ embryos. A set of primers was designed to amplify part of the 3'UTR of *Mat2a* (**Appendix B**, **Table B.1**) and qRT-PCR was performed as described in **Chapter 2**, **section 2.7**. This did not show any significant difference in *Mat2a* expression between strains (**Table 3.14**). However, there was a trend towards lower expression in *ct* then in $+^{ct}$ samples, as observed on 2-DE. Given the relatively small fold-change detected in 2-DE analysis it may be necessary to analyse a much larger number of samples by qRT-PCR to test whether there is really a difference in expression at the mRNA level.

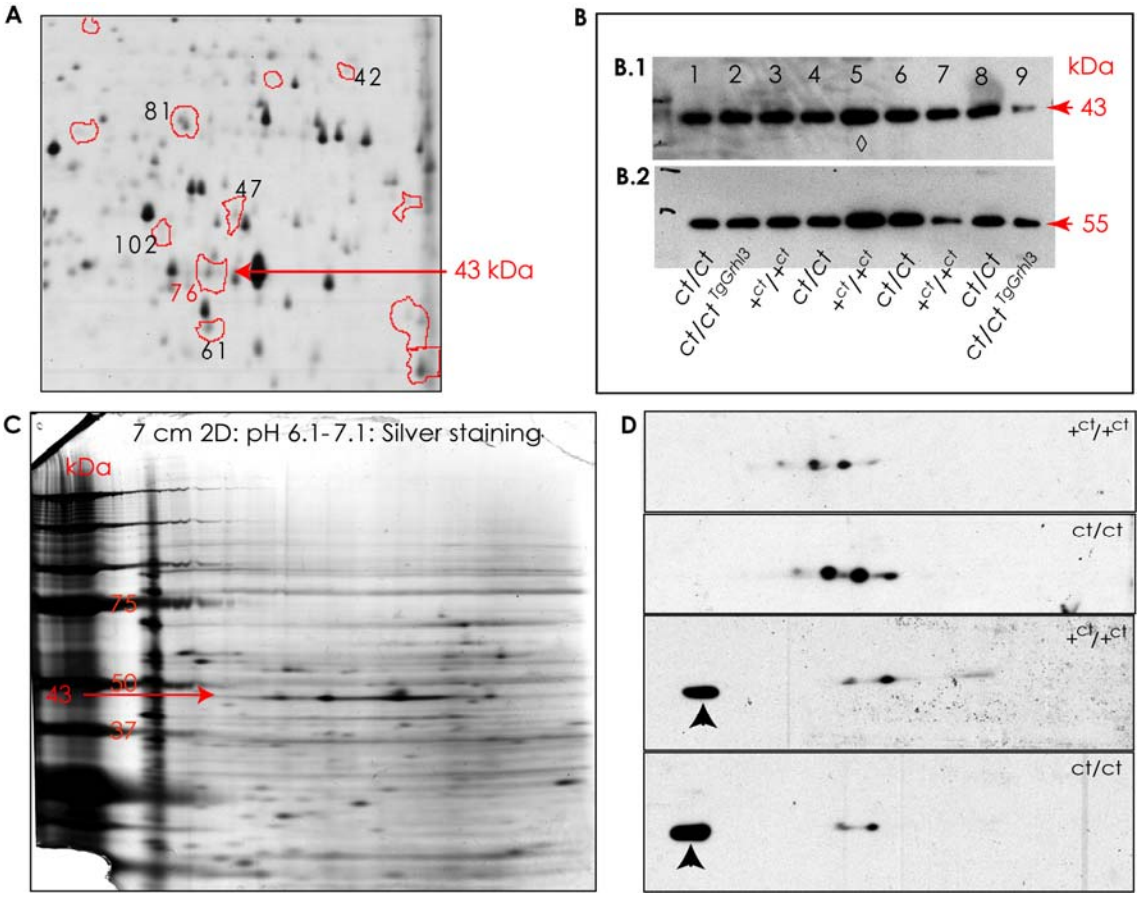

Figure 3.15 Evaluation of Mat2a protein abundance by Western blot and 2D-blots. (**A-B**) High magnification of the region of a 2D gel, generated from a 28-29 somite stage embryo, that includes the differentially abundant spot (S76) identified as Mat2a. (**B**) Western blot of Mat2a in samples from 28-29 somite stage *ct/ct*, $+^{ct}/+^{ct}$ and $ct/ct^{TgGrhl3}$ embryos. The antibody recognises a band at approximately 43 kDa. (**C**) Silver stained 7 cm-2D gel with first dimension separation on pH 6.1-7.1. The red arrow indicates molecular weight of Mat2a (43 kDa). (**D**) Four different 7 cm 2D gels generated from $+^{ct}/+^{ct}$ and *ct/ct* embryo samples and western blotted with the antibody to Mat2a. The black arrowhead indicates a parallel 1D lane on the gel which provides an indication of total protein loading. In all blots, the antibody detects two or more spots which may represent multiple isoforms of Mat2a.

Protein					
Mat2a	**2D-gel**	**Spot**			**Profile**
		76		1.6 fold	$+^{ct} \equiv ct^{TgGrhl3} > ct$
		N		**Volume**	**Comment**
	Western blot	$+^{ct}$	3	1.98 ± 0.82	2.8 fold $+^{ct} > ct^{TgGrhl3}$ (Not significant)
		ct	4	1.02 ± 0.12	
		ct^{Tg}	2	0.72 ± 0.69	
	RT-qPCR	**N**		**Relative expression**	**Comment**
		$+^{ct}$	2	1.14 ± 0.14	1.4-1.5 fold $+^{ct} > ct \equiv ct^{TgGrhl3}$ (Not significant)
		ct	6	0.80 ± 0.10	
		ct^{Tg}	3	0.77 ± 0.03	

Table 3.14 Western blot and qRT-PCR results for Mat2a. Mat2a was found to be down-regulated in the 2D gels from *ct* samples compared with the other strains. On Western blots total Mat2a protein level apparently differed between strains but these differences were not statistically significant (One Way ANOVA). Normalised band volumes (determined using ß-tubulin bands as **Fig 3.15**) are given as the mean and standard error (arbitrary units). Fold change refers to the difference between the highest and the lowest mean values. In addition, qRT-PCR was performed to investigate the possibility of a difference in *Mat2a* mRNA between strains level: the mean values are very similar in *ct* and $ct^{TgGrhl3}$ samples and overall lower than in the $+^{ct}$ strain but these differences are not statistically significant. Volume refers to the normalised band volume (arbitrary units) and both band volumes and relative expression levels in qRT-PCR are given as mean and standard error. Fold change describes the difference between the highest and the lowest values. These differences were not significant (One Way ANOVA).

3.2.5.7 Proteomic analysis of Ube2n in *curly tail* embryos

The Ubiquitin-conjugating enzyme E2 (Ube2n), is a low molecular weight protein migrating at approximately 17 kDa on 2D gels. This protein was present at higher abundance on $ct^{TgGrhl3}$ gels than gels for the other strains at the 28-29 somite stage. Unfortunately, after testing a commercially available antibody against Ube2n protein under different conditions, a specific band of the expected differential expression was not detected. Therefore, primers were designed for RT-qPCR amplification of a region of the *Ube2n* coding sequence. *Ube2n* mRNA expression analysis showed marginal up-

regulation in the *ct* strain compared to the other two strains, including $ct^{TgGrhl3}$ (**Table 3.15**). Hence, RT-qPCR did not reproduce the finding on 2D-gels.

Protein					
Ube2n	**2D-gel**	**Spot**			**Profile**
		96		1.5 fold	$ct^{TgGrhl3} > +^{ct} \equiv ct$
	RT-qPCR				
		N		**Relative expression**	**Comment**
		$+^{ct}$	3	0.84±0.19	1.6 fold $ct > ct^{TgGrhl3}$ (Not significant)
		ct	3	1.13±0.11	
		ct^{Tg}	3	0.69±0.09	

Table 3.15 Quantitative real time RT-PCR analysis of *Ube2n*. In contrast to findings on 2-DE, *Ube2n* mRNA levels were not higher in $ct^{TgGrhl3}$ samples than the other strains. In fact there was a trend towards higher expression in *ct* than in $ct^{TgGrhl3}$ samples, although this was not a statistically significant difference (One Way ANOVA). Relative expression is given as mean and standard error and the fold change refers to the difference between the highest and the lowest values.

3.3 Discussion

In order to perform proteomic analysis of *curly tail* embryos it was first necessary to optimise the 2-DE protocol for embryo samples using large format 10-gel and 12-gel tanks. Previous experiments on neurulation-stage mouse embryos had made use of gel equipment in another laboratory (Greene et al., 2002), and initial experiments suggested that modification of running conditions was necessary. Key considerations for production of high quality 2D gels were found to be avoidance of heating or bubbling of samples during the homogenisation step, concentration of CHAPS in lysis and rehydration buffers, and selection of second dimension electrophoresis conditions to allow maintenance of the buffer at 10°C. Finally, the silver staining conditions were changed to increase the incubation time for each step. These conditions resulted in 2D gels with approximately 4,000 well resolved proteins. In combination with use of software that provides semi-automatic gel alignment and for inter-gel calibration, the 2-DE analysis of *curly tail* embryos was sufficiently robust and sensitive to detect changes in abundance of spots and subtle shifts in migration.

Most 2D gels analysed in this study were silver-stained, which although time consuming, is a sensitive method, and suitable for manual picking of spots for proteolytic digestion and mass spectrometry analysis of the resulting peptides. Fluorescent stains such as SYPRO Ruby protein gel stain gave a very similar protein spot pattern to that observed with silver stain. Thus, SYPRO gave the same sensitivity as silver, but has the advantage of increased dynamic range for quantification of spot volume. The drawback with SYPRO Ruby stain was the creation of background speckles which were frequently detected as spots by the analysis software. An alternative approach could be the use of Deep Purple fluorescent stain, which is reported to have a dynamic range equivalent to SYPRO Ruby, similar sensitivity to silver staining, and does not give background speckles (Tannu et al., 2006). Alternativelly, a more accurate quantification would involve the use of 2D Fluorescence Difference Gel Electrophoresis (DIGE), in which protein samples are pre-labeled with different fluorophors, and a combined sample labelled with a third fluorophor for use as internal standard. The samples are then mixed prior to co-separation on the same gel, with visualisation by scanning with the gel still in the gel cassette. The co-separation and

absence of a separate staining step improves reproducibility, while the internal standard increases the accuracy of quantification. In addition, use of fluorophors offers the same advantages of sensitivity and dynamic range as fluorescent stains. In the latter stages of the project, DIGE was used to analyse samples from *curly tail* embryos treated *in vivo* with inositol compared with untreated *curly tail*. These preliminary experiments (not reported) suggest that DIGE will be a useful approach for detection of subtle changes in protein abundance or post-translational modification.

2-DE analysis at the 28-29 somite stage revealed more spots that show greater abundance in wild-type than *curly tail* samples than vice-versa. In contrast, at the 30-31 somite stage a greater number of spots showed higher abundance in *ct* gels than in the $+^{ct}$ and $ct^{TgGrhl3}$ gel strains. The reason for this difference is not known but it could be speculated that as PNP closure is nearly complete or complete in wild-type and transgenic embryos at the 30-31 somite stage, there may be associated changes in protein expression. A temporal analysis of closure within either of these strains might address this question. At both stages the abundance of a number of spots correlated with genetic background rather than predicted *Grhl3* expression level, for example, $+^{ct} > ct \equiv ct^{TgGrhl3}$ (Profile 2) or $ct \equiv ct^{TgGrhl3} > +^{ct}$. Alternatively, some of these spots may differ in expression due to a downstream effect of the reduced *Grhl3* expression in *curly tail* embryos that is not rescued in the transgenic, perhaps due to differences in the exact timing or level of *Grhl3* expression from the BAC compared to the endogenous locus.

Proteins were chosen for validation based on the possible relationship between their biological function and the cellular defect in *curly tail* and/or NTDs, parallel data from a microarray study and the magnitude of change in protein abundance. A difference in abundance of an individual 2D gel spot between samples could result from a corresponding alteration in the total abundance of that protein. Alternatively, a difference in the charge or mass of that protein, for example owing to post-translational modification, could alter protein migration with the result that a spot at a particular location shows differential abundance. Western blotting, using commercially available antibodies, was therefore used to evaluate total protein levels. In some cases, for example trifunctional purine biosynthetic protein adenosine-3 (Gart), a similar difference in protein abundance was observed between samples by 2-DE and Western blot. However, in other cases, such as lamin B1, major differences in abundance of

specific protein spots was not reflected in a difference in overall protein abundance. Inspection of 2D gels showed that this was due to a shift in migration of lamin B1 spots. In a few cases RT-qPCR was performed to test whether there was a correlation between the observed change in protein abundance and expression at the mRNA level. Such a change would be predicted if expression of the candidate protein was downstream of transcriptional regulation by *Grhl3*.

The proteomic analysis of *curly tail* and wild-type embryos by 2-DE in the present study revealed a differential abundance of proteins which can be broadly divided into functional groups: cell cycle, metabolic pathways, DNA repair, ubiquitination, cytoskeleton. In the current study one protein, lamin B1, has been investigated further in detail (**Chapter 4**). Other proteins are potentially of biological interest in the context of the development of NTDs in *curly tail* embryos, although not all 2-DE changes have yet been validated by Western blot.

The transitional endoplasmic reticulum ATPase (Vcp, or p97, or CDC48) and lamin B1 have been implicated in cell cycle function. They are both present in greater abundance in wild-type than *curly tail* samples ($+^{ct} > ct \equiv ct^{TgGrhl3}$). Other lamin B1 spots were found at greater abundance in *curly tail* than wild-type ($ct \equiv ct^{TgGrhl3} > +^{ct}$), and these reciprocal differences were later found to result from differential migration of lamin B1 spots rather than differences in total protein abundance. Vcp/p97 plays several roles, it is involved in cell cycle progression through mitosis and is necessary for the formation of a closed nuclear envelope and subsequent expansion of the nuclear envelope (Hetzer et al., 2001). *Vcp/p97* deficiency resulted in early embryonic lethality in null mutants showing that Vcp/p97 is an essential protein in early mouse development (Muller et al., 2007). On 2-DE analysis, Vcp was found to be down-regulated in *curly tail* embryos compared with wild-type. That is an interesting finding since the cellular defect in *curly tail* embryos is a cell-type specific proliferation defect. Western blot analysis also suggested that there is a difference between strains, although the magnitude of this change was smaller than that observed on 2-DE.

In the case of lamin B1, comparison of strains showed a difference in protein migration in *curly tail* and wild-type samples, rather than in total protein abundance. Lamin B1 belongs to the family of intermediate-type filament proteins, which are key structural

components of the nuclear lamina, a complex polymer underlying the inner nuclear membrane of the nuclear envelope (Stuurman et al., 1998). The nuclear envelope is thought to be important for nuclear stability, cell cycle regulation, chromatin organisation, DNA replication, cell differentiation, apoptosis and regulation of gene expression (Schirmer et al., 2001; Goldman et al., 2002; Hutchison, 2002b; Malhas et al., 2007; Malhas et al., 2009). Vertebrate lamins have been classified into A/C and B types based on primary sequences and biochemical properties, and four lamins (A, B1, B2, and C) are commonly found in mammalian somatic cells (Stuurman et al., 1998). Lamins are associated with the inner nuclear membrane (INM) of the interphase cell and just before mitosis starts, the nuclear envelope and nuclear lamina disassemble for chromosomal segregation. During this period, Lamin B1 remains attached to endoplasmic reticulum vesicles, while A-type lamins are dispersed as soluble proteins and later incorporated into the nuclear lamina during post-mitotic nuclear assembly (Hutchison et al., 1994).

Lamin B1 was the only protein for which a significant difference in abundance of protein spots corresponded to the presence or complete absence of a particular spot, and for which a likely shift in migration was apparent by comparison of gel patterns. The altered migration of lamin B1 in *ct/ct* samples represented the loss of a negative charge, since the spots shift to a more basic position on the gels compared to the $+^{ct}/+^{ct}$ lamin B1 (**Fig. 3.9 B**). Western blotting showed there was no significant difference in the total levels of the lamin B1 protein between the two strains. So what could be the cause of altered migration of the *ct/ct* lamin B1 protein and could this shift play a role in the pathogenesis of neural tube defects (NTDs) in *ct/ct* embryos? These questions will be investigated in **Chapter 4**.

Proteins involved in folate one-carbon metabolism and associated metabolic pathways (**Fig. 3.16**) are potentially of relevance to the study of the *curly tail* phenotype. NTDs in *curly tail* are not preventable by folic acid, or other related molecules (Van Straaten and Copp, 2001). On the other hand, dietary folate deficiency increases the frequency of cranial NTDs in both *ct/ct* and $+^{ct}/+^{ct}$ embryos (Burren et al., 2010), suggesting an interaction with the genetic background. Notably, the response of the methylation cycle (as shown by ratio of abundance of s-adenosylmethionine to s-adenosylhomocysteine) to folate-deficient conditions is atypical in *curly tail* embryos, showing an increase

rather than a decrease as observed in wild-type embryos (de Castro et al., 2010). Inhibition of the methylation cycle has previously been shown to cause cranial NTDs in non-mutant embryos (Dunlevy et al., 2006a). Thus, while diminished methylation cycle activity appears unlikely to be the cause of cranial NTDs in folate-deficient conditions, it is possible that there is an as yet undefined imbalance in folate one-carbon metabolism in *curly tail* embryos (de Castro et al., 2010).

Folate one-carbon metabolism plays several important cellular roles as it is required for nucleotide biosynthesis and provision of methyl units for methylation reactions as well as being interconnected with other metabolic pathways (**Fig. 3.16**). Proteins involved with both nucleotide synthesis and methylation reactions were found to be differentially abundant in the proteomic analysis in the current study.

For example, the trifunctional purine biosynthetic protein adenosine-3 (Gart) catalyses the synthesis of formylglycinamide ribonucleotide in the purine synthetic pathway, with donation of a one-carbon unit from 10-formyl-tetrahydrofolate (Deacon et al., 1985). Purine nucleotides function as precursors for RNA and DNA synthesis, coenzymes, and as substrates for mitochondrial ATP synthases, Atp5b and Atp5o. The diminished abundance of Gart in *curly tail* samples ($+^{ct} > ct \equiv ct^{TgGrhl3}$) raises the possibility that purine synthesis may be impaired, which could contribute to reduced cellular proliferation and/or sensitivity to folate deficiency.

The folate cycle supplies methyl units to the methylation cycle from 5-methyltetrahydrofolate. This is important for ensuring an adequate supply of S-adenosylmethionine which acts as a methyl donor in a wide range of methyltransferase-mediated reactions which result in methylation of DNA, RNA, lipids, hormones and proteins (Scott and Weir, 1994). Two proteins found to differ in abundance in the proteomic analysis of *curly tail* embryos function in the methylation cycle or methylation reactions. S-adenosylmethionine synthase isoform type-2 (Mat2a) catalyses the formation of S-adenosylmethionine from methionine and ATP. In this study Mat2a protein was present at lower level in *curly tail* than wild-type embryos ($+^{ct} \equiv ct^{TgGrhl3} > ct$) this correlated with a difference in mRNA expression level.

NSun2 (tRNA (cytosine-5-)- methyltransferase; Misu) is a methyltransferase acting on RNA and possibly DNA (Sakita-Suto et al., 2007), and its activity thus depends on supply of S-adenosylmethionine from the methylation cycle as methyl donor. A role for NSun2 in cell cycle progression has been suggested by studies showing that it acts downstream of c-Myc to regulate epidermal cell proliferation (Frye and Watt, 2006). This function appears to be mediated through stabilisation of the mitotic spindle (Hussain et al., 2009). Interestingly, NSun2 was another protein (like Vcp and lamin B1) that was differentially represented in the proteomic analysis and may be implicated in the proliferation defect observed in *curly tail* embryos ($+^{ct} > ct \equiv ct^{TgGrhl3}$).

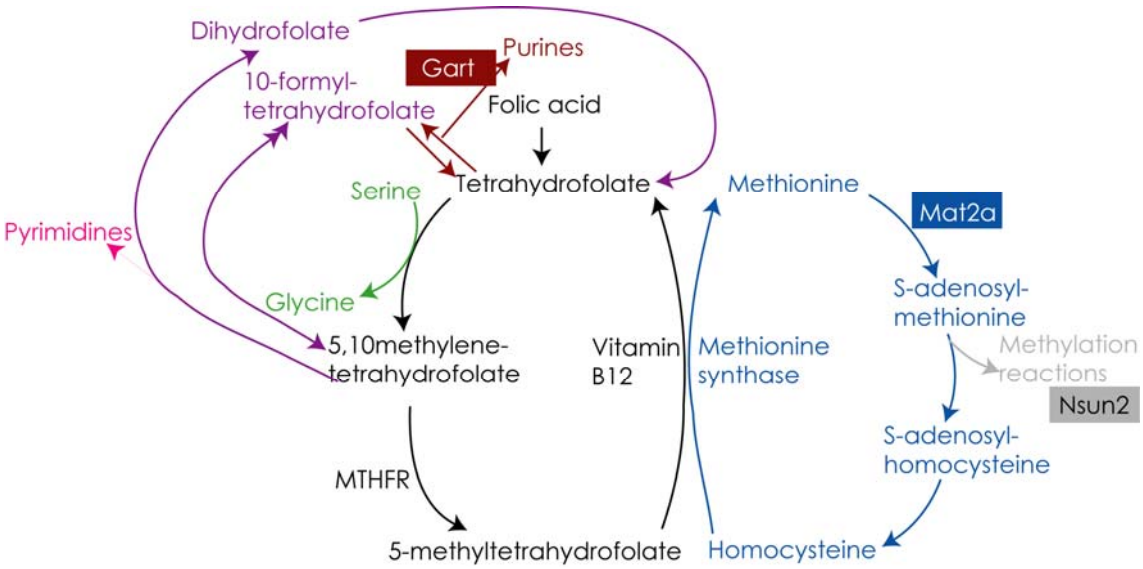

Figure 3.16 Diagrammatic summary of folate one-carbon metabolism. The main function of the folate cycle (in black) is to accept one-carbon units from donor molecules and pass them on via various biosynthetic reactions. 10-formyl-tetrahydrofolate donates C-2 and C-8 to the purine ring during **purine biosynthesis**, in reactions catalysed by Gart (in brown box). Folate is essential for the **DNA biosynthesis cycle** (cell replication; cycle in purple). The folate cycle is the methyl donor to the **methylation cycle** (cycle in blue). Methyl groups are donated from 5-methyltetrahydrofolate to remethylate homocysteine back to methionine in a reaction catalysed by methionine synthase. Methionine is converted to s-adenosylmethionine by the action of Mat2a (in blue box), which is the methyl donor for the various cellular methylation reactions (catalysed by methyltransferases such as NSun2). Abbreviation: MTHFR, 5, 10 - methylenetetrahydrofolate reductase.

Several varying proteins in the proteomic analysis have possible involvement in the response to cellular/oxidative stress including nucleobindin-1 (Nucb1), superoxide dismutase (Sod1), fetuin-A (alpha-2-HS-glycoprotein), and fetuin-B. Cellular stress conditions such as altered redox status, increased protein synthesis, expression of misfolded proteins, and perturbation of calcium homeostasis can induce an endoplasmic reticulum (ER) specific stress response (Teixeira et al., 2006). There are three signal transduction pathways involved: the inositol-requiring enzyme 1 (IRE1), activating transcription factor 6 (ATF6), and double-stranded RNA-activated protein kinase-like ER kinase (PERK). Nucleobindin-1 is the major calcium-binding protein of the Golgi and a repressor of the S1P (site-1 protease)-mediated ATF6 activation. *Nucb1* is an ER stress-inducible gene with the promoter region having functional *cis*-elements for transcriptional activation of ATF6. Knock-down of *NUCB1* by siRNA accelerates ATF6 cleavage during ER stress (Tsukumo et al., 2007).

Superoxide dismutase (*Sod1*) gene is expressed throughout mouse embryogenesis, including the neural folds and neural tube at E7.5-10.5 (Yon et al., 2008). Its main function is to destroy toxic free radicals which are normally produced within cells and have been implicated in diabetes-induced teratogenesis, which includes increasing risk of NTDs (Loeken, 2005). Correlating with oxidative stress, Sod1 activity was found to be elevated in embryos exposed to diabetic conditions (Dheen et al., 2009). Both Nucb1 and Sod1 are up-regulated in the transgenic strain (in relation to the wild-type strain, $ct/ct^{TgGrhl3} > ct/ct > +^{ct}/+^{ct}$, and $ct^{TgGrhl3} > +^{ct} \equiv ct$), perhaps suggesting that elevated *Grhl3* expression is associated with oxidative stress, a possibility which needs to be further investigated.

At the 28-29 somite stage, both fetuins A and B, were found to be up-regulated in *curly tail* embryos compared to the wild-type and transgenic strains ($ct > +^{ct} \equiv ct^{TgGrhl3}$). However, western blotting analysis showed considerable variation in abundance between individual embryos, even within strains, suggesting that the 2-DE differences may not represent a generalised differential expression. Fetuin-A is an abundant serum protein which acts as an inhibitor of spontaneous calcium phosphate precipitation, by forming soluble colloidal calciprotein particles that contain fetuin, calcium, and phosphate (Heiss et al., 2003). Other functions attributed to this protein include

inhibition of insulin receptor tyrosine kinase activity, and protease inhibitory activity in the recovery phase of acute inflammatory response (Olivier et al., 2000).

Most of the proteins identified to be differentially expressed in *curly tail* and wild-type strains by 2-DE analysis could be potential targets of protein kinase C (PKC) or be involved in the inositol phospholipid pathway. Since the normalising effect of inositol treatment on neural tube closure in *curly tail* embryos is mediated through activation of PKC (Greene and Copp, 1997), it is an interesting possibility that one or more of the key PKC targets could be proteins whose expression is misregulated in *curly tail.* For example, lamin B1 is both a substrate of PKC isoforms and a PKC-binding protein (Martelli et al., 2000; Tabellini et al., 2002), while moesin, an actin binding protein, is phosphorylated by PKC-θ in the actin-binding domain (Pietromonaco et al., 1998). Another differentially expressed protein, Vcp, binds phospholipids (preferably phosphatidylinositol mono-biphosphates) through its N-terminal domain (Waugh et al., 2003) and protein function could be affected by alterations in inositol phospholipid levels.

Overall, 106 spot-differences were detected in the 2D-gel analysis of the caudal region of *curly tail* embryos compared to background matched wild-type and *Grhl3*-transgenic *curly tail* strains (48 differences at the 28-29 somite stage and 58 at the 30-31 somite stage). Given that an average of 2000 total spots were detected on these gels, it does not appear that there are massive differences between the proteome of *curly tail* and wild-type caudal regions. This is perhaps to be expected since *curly tail* carries a hypomorphic, as opposed to completely null, allele of *Grhl3* which confers diminished *Grhl3* expression. In addition, the embryos were analysed at or immediately after the stage when defective neural tube closure becomes apparent, thereby minimising the possible detection of secondary changes owing to the presence of spina bifida. Finally the closely matched genetic background of the strains should minimise non-specific changes. Among the 106 differentially abundant protein spots, the fold-change in abundances were not dramatic (maximum two-fold), with the exception of the lamin B1 protein, perhaps suggesting that a combination of subtle changes in a few proteins might contribute to the neurulation defect. However, it is important to consider that spots identified on 2-DE represent the most abundant proteins in the sample and it is possible

that some of the undetected proteins change more significantly in abundance than the detectable ones.

Chapter 4

Studies of lamin B1 protein variants and their effect on development of neural tube defects

4.1 Introduction

Investigation of the possible causes of NTDs in *curly tail* embryos by two-dimensional gel protein electrophoresis revealed altered migration of lamin B1 protein in *curly tail* samples compared to wild-type samples (**Chapter 3**). In the studies described in this chapter, the variation in lamin B1 was further analysed and its possible involvement in the pathogenesis of NTDs was investigated.

Lamin B1 is a 67 kDa protein, comprising a central rod domain separated by flexible linker regions with globular head and tail domains (**Fig. 4.1 A**). The tail-domain harbours a nuclear-localisation signal sequence necessary for nuclear import and a CAAX-box motif (C, cysteine; A, any aliphatic amino acid; and X, any other residue), which is processed in a series of post-translational modifications (PTMs; **Fig**. **4.1 B**). First, the cysteine is subject to farnesylation, which is important for the peripheral localization and membrane association of the lamins. This process is followed by endoproteolysis, which removes the three C-terminal amino acids, and subsequent carboxymethylation increases the hydrophobicity of the carboxyl terminus and may stabilize the membrane association. Both endoproteolysis and carboxymethylation are dependent on farnesylation of the cysteine residue and are membrane-associated processing events (Dai et al., 1998; Otto et al., 1999). Consequently, lamin B1 remains stably associated with the lamina and with the inner nuclear membrane (Stuurman et al., 1998; Maske et al., 2003). Deficiency in endoproteolysis or in methylation processing results in loss of integrity and deformity of the nuclear lamina (Maske et al., 2003). Furthermore, deficiencies of CAAX processing enzymes result in severe phenotypic changes in mouse models. For example, *Rce1* (endoprotease)-deficient mice died during gestation or soon after birth (Kim et al., 1999). A more severe phenotype was observed in isoprenylcysteine carboxyl methyltransferase (*Icmt*) deficient mice and knockout embryos died by mid-gestation (Bergo et al., 2001).

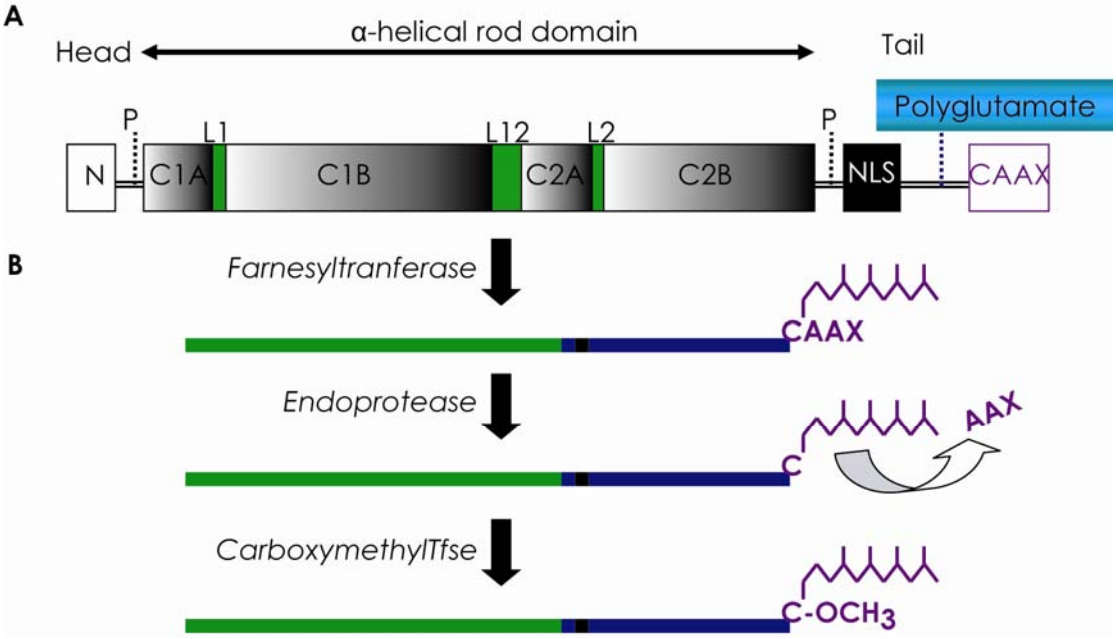

Figure 4.1 Schematic diagrams showing the structure and processing of the lamin B1 protein. (A) Lamin B1 has three domains. The head and tail domains mediate polymer assembly whereas the central rod, comprising four coiled-coil domains (C1A, C1B, C2A, C2B) separated by flexible linker regions (L1, L12, L2), mediates lamin dimerization. Phosphorylation sites (P) flank each end of the α-helical rod domain. Specific conserved serine (or threonine) residues are phosphorylated during mitosis, associated with disassembly of the nuclear lamina meshwork concomitant with NE breakdown. Importantly, the tail domain harbours a nuclear localisation signal (NLS) sequence necessary for nuclear import, and a CAAX box that is post-translationally modified. **(B)** The processing of lamin B1 protein to the mature form involves a series of posttranslational modifications of the CAAX motif. First, a farnesyl moiety is attached to the thiol group of the cysteine (C) by the protein farnesyltransferase (PFT). Next, the terminal three amino acids (AAX) are removed by the endoprotease *Rce1*. Finally, the carboxylate anion of the carboxyl-terminal farnesylcysteine is methylated by the isoprenylcysteine carboxyl methyltransferase (*Icmt*).

Lamins localised within the NE can interact with chromatin, nuclear pore proteins, and integral proteins of the inner and outer nuclear membranes (**Fig. 4.2**; (Glass and Gerace, 1990). The nuclear envelope derives its structural integrity from higher order lamin-lamin interactions mediated by the coiled-coil domains (McKeon et al., 1986; Heins and

Aebi, 1994). In addition, lamins and their associated proteins are proposed to have roles in large-scale chromatin organisation, the spacing of nuclear pore complexes (NPCs), the positioning of the nucleus in cells and the reassembly of the nucleus after mitosis (Gerace and Foisner, 1994; Gruenbaum et al., 2005).

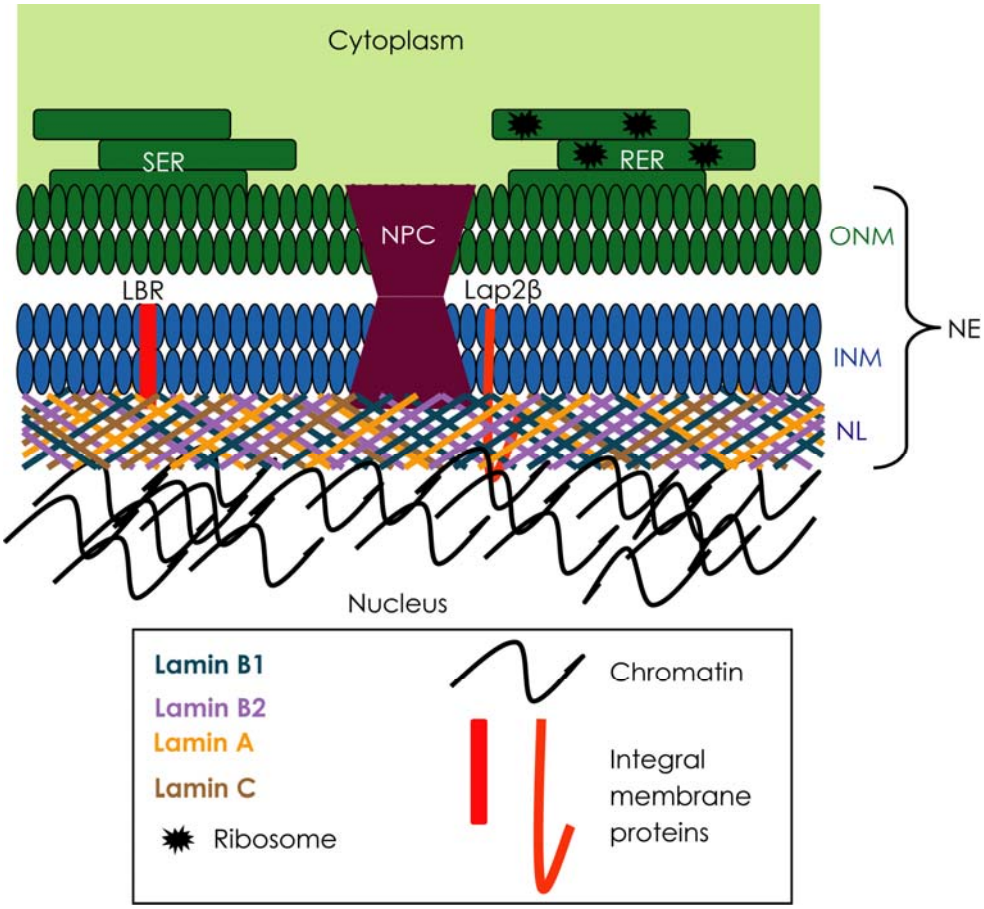

Figure 4.2 Schematic diagram of the nuclear envelope (NE). The NE consists of the inner (INM) and outer (ONM) nuclear membranes, nuclear pore complexes (NPC) and the nuclear lamina. The ONM is continuous with the smooth and rough endoplasmic reticulum (SER and RER). NPCs mediate trafficking of macromolecules between the cytoplasm and the nucleus. The nuclear lamina (NL), which is adjacent to the INM, is a fibrillar meshwork providing an attachment site at the nuclear envelope for interphase chromatin. The lamina consists of polypeptides called lamins (A, B1, B2, and C), members of the intermediate filament protein superfamily. Lamins interact not only with chromatin, nuclear pore proteins or NPCs directly, but also with integral membrane proteins (e.g., lamin B receptor, LBR; lamina associated polypeptide-2β, Lap-2β).

Essential nuclear functions also depend on lamins, notably DNA replication and RNA-polymerase-II-dependent gene expression (Moir et al., 1994). Interestingly, Malhas et al (2007) found that the stable association of the nuclear lamina with chromatin is important for regulation of gene expression. Their study showed that either absence of full-length lamin B1 or lack of the C-terminal processing affects gene expression and some of the dysregulated genes were clustered on certain chromosomes. Hence, loss of interaction with the nuclear lamina is thought to affect chromosome position within the nucleus, and therefore gene expression. Subsequently, interaction of lamins with chromatin and transcription factors has been shown to play a direct role in transcriptional regulation (Malhas et al., 2009). For example, sequestration of the octamer transcription factor 1 (*Oct-1*), at the nuclear periphery by lamin B1 might be a mechanism by which the nuclear envelope can regulate gene expression and contribute to the cellular response to stress, development, and ageing.

Dozens of disease-causing mutations in Lamin A (*LMNA*) have been catalogued (Capell and Collins, 2006; Worman and Bonne, 2007; Worman et al., 2009). In contrast only two diseases have been described as possible laminopathies of the B type lamins. Until recently it had been presumed that mutations in B-type lamins would result in embryonic lethality, because these lamins are primary components of the nuclear lamina in undifferentiated cells. Knockdown of either lamin B1 or lamin B2 with small interfering RNAs (siRNAs) in cultured cells inhibited cell growth and promoted apoptosis, suggesting that both genes are essential for viability, whereas reduced expression of the A-type lamins had no appreciable effect on cell growth (Harborth et al., 2001). However, rare novel mutations in *LMNB2* have been identified in patients with Barraquer-Simons syndrome, an acquired partial lipodystrophy (Hegele et al., 2006), and duplications in *LMNB1* have been found to cause the adult-onset demyelinating condition known as autosomal dominant leukodystrophy (ADLD, (Padiath et al., 2006; Meijer et al., 2008).

There are no reports of a possible involvement of lamins in neural tube closure. Mouse models of laminopathies, which model different human mutations in lamin A, resulted in progeria, muscular dystrophy and dilated cardiomyopathy (Stewart et al., 2007). *In vitro*, a deletion in the rod domain of lamin B1 resulted in nuclei becoming lobulated, associated with a patchwork accumulation of lamins, together with clustering of nuclear

pore complexes and other NE proteins (Schirmer et al., 2001). *In vivo*, mice that are homozygous for a gene-trap allele of *Lmnb1* survived embryonic development but died at birth with defects in the lungs and bone (craniofacial dysmorphology and a variety of skeletal abnormalities). In addition, fibroblasts from mutant embryos had grossly misshapen nuclei with frequent blebs, reduced replication rates, impaired differentiation, and premature senescence (Vergnes et al., 2004). However, the gene-trap allele may produce a truncated protein and a complete null allele for lamin B1, with no protein product at all, has not yet been generated and this could plausibly reveal further mutant phenotypes.

Although lamins have not been implicated in NTDs, loss of another NE component, Nup50, has been found to cause NTDs. Nup 50 is a nuclear pore protein involved in export of proteins and is expressed in the developing neural tube. Mice carrying a homozygous deletion in *Nup50* develop exencephaly with 100% penetrance (Smitherman et al., 2000).

In spite of the fact that a role for lamin B1 in neural tube closure has not been demonstrated to date, this protein has a number of functions which could be hypothesised to influence NTD risk. For example, it is possible that an alteration in lamin B1 function could affect the cell cycle, which is known to be dysregulated in *ct/ct* embryos. In addition, an effect on transcriptional regulation could potentially alter expression of genes which are required for neural tube closure such as *Grhl3* targets or other, perhaps unrelated, genes. Therefore I decided to investigate in detail the basis of the 2D gel change in lamin B1 migration and its possible functional consequences in *curly tail* embryos undergoing neural tube closure.

4.2 Results

4.2.1 Sequence analysis of genomic DNA and mRNA encoding lamin B1 in *ct/ct* and $+^{ct}/+^{ct}$ strains

The lamin B1 spots in *ct/ct* and $+^{ct}/+^{ct}$ 2D gels were differently charged, migrating to a more basic position in *ct/ct* gels than the equivalent spots in $+^{ct}/+^{ct}$ gels. This migration difference could be due to a difference in post-translational modification (PTM), such as phosphorylation, or a difference in amino acid sequence, either of which could cause a change in the isoelectric point (pI) of the protein. For instance, lamin B1 spots of *curly tail* 2D gels could be less phosphorylated (more basic) than the lamin B1 spots of the wild-type gels, which were more negatively charged (more acidic). To address this possibility, aliquots of individual *ct/ct* and $+^{ct}/+^{ct}$ embryo protein samples were digested with lambda protein phosphatase to remove phosphate groups. Another aliquot of each sample, was left untreated, to be used as a control. After incubation and protein purification, the phosphatase-treated and untreated aliquots were run on separate 2D-gels. If there was a phosphorylation difference in lamin B1 spots between *ct/ct* and $+^{ct}/+^{ct}$ samples it would be expected that spots in $+^{ct}/+^{ct}$ would become more basic after phosphatase treatment, and migrate like the spots on *ct/ct* gels. However, phosphatase treatment did not cause changes in the pattern of the lamin B1 spots either in *ct/ct* or $+^{ct}/+^{ct}$ gels (**Chapter 2**, **section 2.5.7**; **Fig. 4.3**).

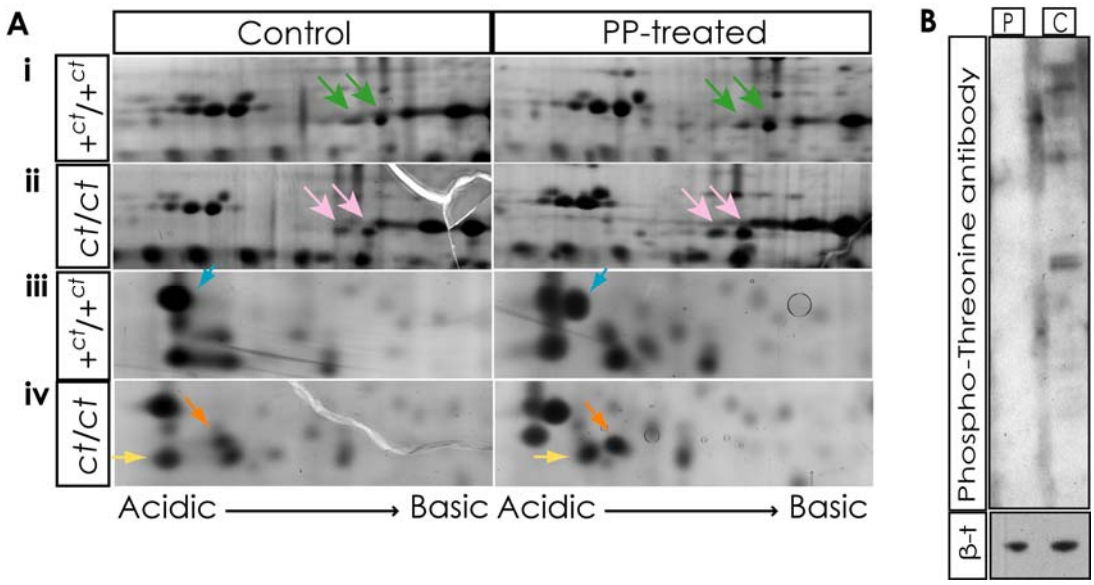

Figure 4.3 Phosphatase treatment suggests that lamin B1 protein spots are not phosphorylated. (**A**) Comparison of control and phosphatase-treated (PP) samples does not any alteration in the migration of lamin B1 spots in either (i) wild-type (green arrows) or (ii) *curly tail* (pink arrows) 2D-gels. Other spots shifted to more basic positions in the PP-treated gels compared with control gels generated from wild-type (blue arrow in iii) and *curly tail* (yellow and orange arrows in iv). These spots are predicted to correspond to phosphorylated proteins that are dephosphorylated by phosphatise treatment. (**B**) Validation of phosphatase activity by western blot using an anti-phospho-threonine antibody. Bands were detected in control (C) samples but not in phosphatase treated (P) samples. ß-tubulin (β-t) immunoblot was to show total protein sample loading.

In order to test whether a sequence change is present, primers were designed to amplify the genomic DNA and cDNA of the lamin B1 gene (*Lmnb1*, Ensemble NM 010721.1, ENSMUSG00000024590). The *Lmnb1* gene is located on mouse chromosome 18 and comprises 11 exons and 10 introns, covering 65.6 kilo bases (kb), encoding a 2.8 kb transcript (**Fig. 4.4 A**), and a protein of 588 residues (Maeno et al., 1995). The presumptive promoter region has high GC content suggestive of a typical housekeeping gene. Fifteen pairs of primers were designed to flank the coding regions at the genomic level, and five primer pairs were designed to amplify overlapping regions covering the cDNA (**Appendix B, Tables B.5 and B.6**). Genomic DNA was extracted for sequencing from E10.5 *ct/ct* and $+^{ct}/+^{ct}$ embryonic yolk-sac samples, using a standard

protocol (**Chapter 2, section 2.2**). To check the transcript sequence, mRNA was extracted from whole E10.5 embryos and used for synthesis of cDNA (**Chapter 2, section 2.7.1**). Genomic DNA and cDNA samples were amplified by PCR, and the products were purified and sequenced (**Chapter 2, section 2.8**).

Comparison of the *LmnB1* sequences of *ct/ct* and $+^{ct}/+^{ct}$ revealed two differences in the coding sequence of genomic DNA (summarised in **Fig. 4.4 B**), which were confirmed by sequencing the cDNA. In exon 1 a single base pair change, C612T, was detected that does not change the encoded amino acid, leucine 104, located in the coiled-coil domain of the protein. In exon 10 of *curly tail Lmnb1* there was a three base-pair deletion of one of a sequence of nine *GAG* repeats (nucleotides 1957 to 1983) which encodes a sequence of glutamic acid residues (Glu, E, position 553-561) in the wild-type sequence. Henceforth, the GAG variant will be denoted GAG $^{1957\text{-}1983\Delta}$ because it is not possible to identify which of the nine residues is deleted. The lamin B1 protein forms will be denoted 9E lamin B1 (wild-type protein) and 8E lamin B1 (*curly tail* protein), to describe the number of Glu residues. These Glu residues make up an acidic region of the tail domain of the protein, which could be involved in chromatin binding (http://www.uniprot.org/uniprot/P14733). The loss of a Glu was hypothesised to explain the migration change of the lamin B1 spots in *ct/ct* 2D gels, since Glu is a negatively charged residue.

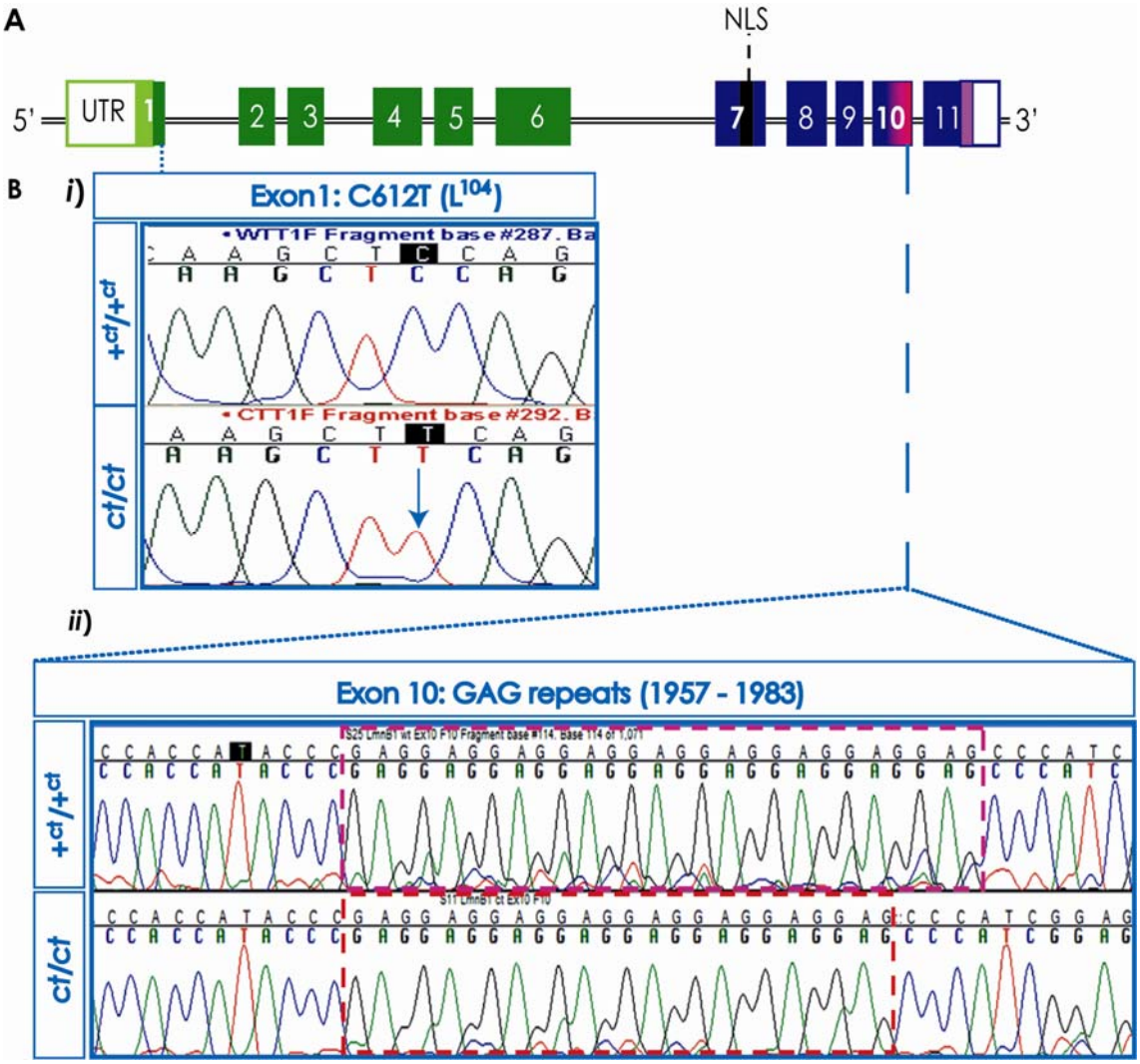

Figure 4.4 Diagram of *Lmnb1* gene and sequencing results. The *Lmnb1* gene comprises eleven exons and ten introns. Sequencing of *Lmnb1* revealed two sequence changes in *ct/ct* compared with $+^{ct}/+^{ct}$. In exon 1, a single cytosine to thymine nucleotide change (C612T, black arrow), does not change an amino acid. In exon 10, one of the nine GAG repeats (purple traced square) in $+^{ct}/+^{ct}$ is absent in *ct/ct* (red traced square).

4.2.2 Quantitative analysis and expression pattern of *Lmnb1* mRNA in $+^{ct}/+^{ct}$ and *ct/ct* embryos

It is possible that differences in *Lmnb1* sequence would result in alteration of transcription or translation in *ct/ct* and $+^{ct}/+^{ct}$ embryos. Analysis of total abundance of lamin B1 protein by western blot did not show any difference between $+^{ct}/+^{ct}$ and *ct/ct*

samples (**Chapter 3, section 3.2.5.1**). To check whether the sequence changes had any effect on levels of mRNA, reverse transcription quantitative real-time polymerase chain reaction (RT-qPCR) was performed.

RNA was extracted from the caudal region of E10.5 $+^{ct}/+^{ct}$ and *ct/ct* embryos and reverse transcribed for the generation of cDNA. A primer pair was designed to amplify a region of *Lmnb1* coding sequence (position 1267-1487 of *Lmnb1*-transcript; **Appendix B; Table B.7**), and tested in RT-qPCR (**Chapter 2, section 2.7.2**). Expression levels of *Lmnb1* were normalised to *Gapdh* (reference gene), and one $+^{ct}/+^{ct}$ sample was selected as a calibrator with an expression level of 1.0. No significant difference in *Lmnb1* mRNA abundance was observed between strains (mean relative expression levels were 0.74 ± 0.07 and 0.89 ± 0.08 in $+^{ct}/+^{ct}$ and *ct/ct* samples respectively).

The lamin B1 protein is reported to be present in almost all cell types (Stuurman et al., 1998). However, the spatial expression pattern of *Lmnb1* has not been investigated in *ct/ct* embryos. In order to examine the expression of *Lmnb1* mRNA, a 561 bp fragment (**Appendix B, Table B.6**) was cloned into pGEM-T Easy Vector for production of an anti-sense cDNA probe (**Chapter 2, section 2.9**). Using this probe, the expression pattern of *Lmnb1* was investigated by whole mount *in situ* hybridisation (WMISH; **Chapter 2, section 2.10**) in $+^{ct}/+^{ct}$ and *ct/ct* embryos (**Fig. 4.5 A-F**).

Initially, embryos were analysed at the stage of posterior neuropore closure (E10.5), revealing an mRNA expression pattern that was almost ubiquitous. However, no signal was observed in the heart or the surface ectoderm (**Fig. 4.5 A-B, D-E**). There were no apparent differences between $+^{ct}/+^{ct}$ (**Fig. 4.5 A, D**) and *ct/ct* (**Fig. 4.5 B, E**) embryos. The control sense probe gave no signal as expected (**Fig. 4.5 C, F**). The expression pattern in neurulation-stage embryos may be worthy of further investigation, and is supported by a limited number of studies of lamin B1 protein in human tissue (Broers et al., 1997; Ausma et al., 1996). These studies showed that Lamin B1 was not ubiquitously expressed but was negative in the muscle and connective tissue and reduced or absent in the skin.

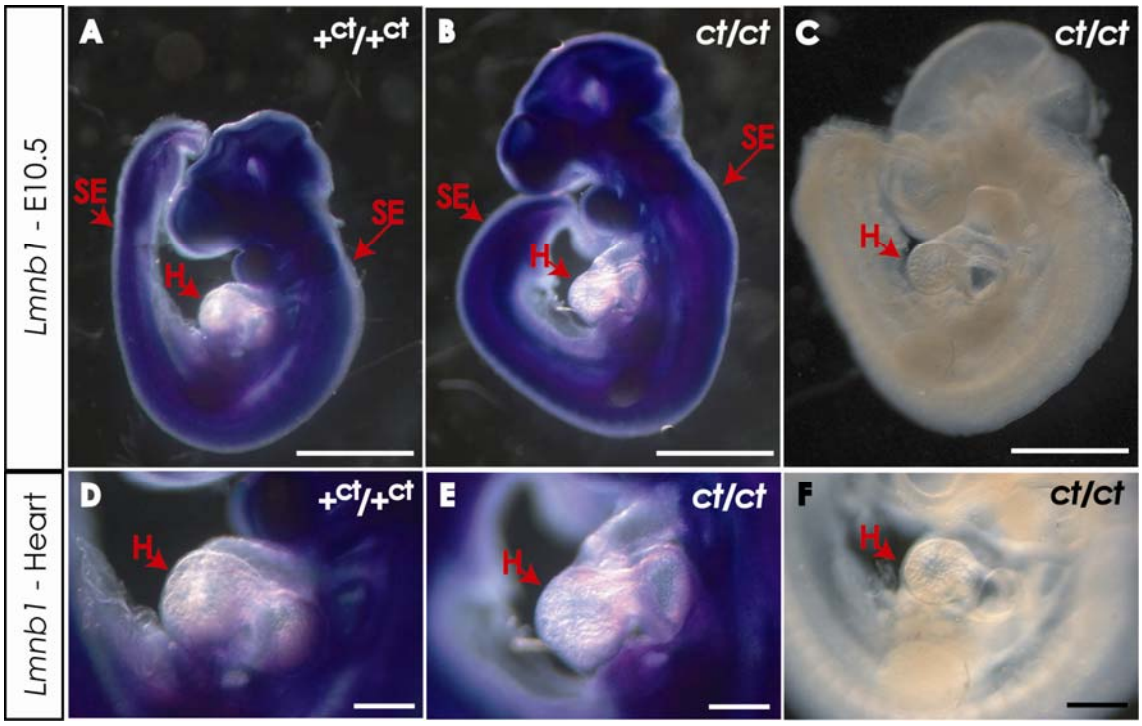

Figure 4.5 *Lmnb1* mRNA expression pattern. **(A-B)** Whole mount *in situ* hybridisation of $+^{ct}/+^{ct}$ and *ct/ct* embryos at E10.5. The expression was almost ubiquitous but appeared negative in the surface ectoderm (SE) and in the heart (H, seen at higher magnification in **D-E**). Overall, there were no apparent differences between $+^{ct}/+^{ct}$ **(A, D)** and *ct/ct* **(B, E)** embryos. **(C, F)** The control probe (sense) was negative as expected. Scale bars represent 1 mm in **A-C** and 0.5 mm in **D-F**.

To investigate this *Lmnb1* expression pattern a little further, I performed WMISH on embryos at earlier embryonic stages as well as on embryos with NTDs (exencephaly) to check whether the pattern was altered (**Fig. 4.6 A-M**). At all studied stages, *Lmnb1* had a very similar pattern, being expressed in almost all cell types with the exception of the heart and the surface ectoderm. This pattern was not different in embryos with forebrain or midbrain exencephaly (**Fig. 4.6 I, K-M**).

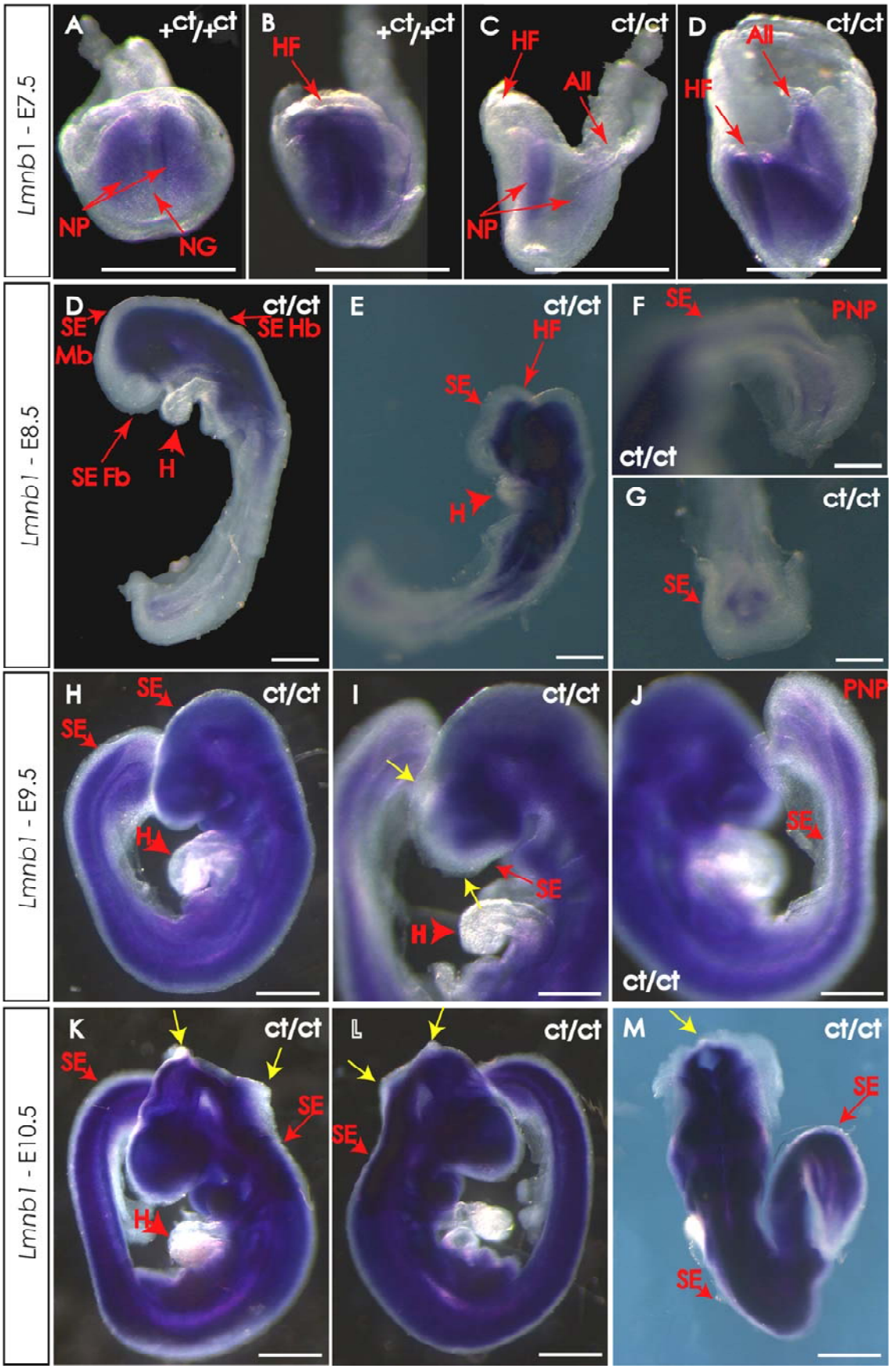
Lmnb1 - E7.5
A
+ct/+ct
NP
NG
B
+ct/+ct
HF
C
ct/ct
HF
All
NP
D
ct/ct
All
HF
Lmnb1 - E8.5
D
ct/ct
SE
SE Hb
Mb
SE Fb
H
E
ct/ct
HF
SE
H
F
SE
PNP
ct/ct
G
ct/ct
SE
Lmnb1 - E9.5
H
SE
ct/ct
SE
H
I
ct/ct
SE
H
J
PNP
SE
ct/ct
Lmnb1 - E10.5
K
ct/ct
SE
SE
H
L
ct/ct
SE
M
ct/ct
SE
SE

Figure 4.6 *Lmnb1* mRNA expression pattern at E7.5-10.5. **(A-D)** Whole mount *in situ* hybridisation for *Lmnb1* on $+^{ct}/+^{ct}$ and *ct/ct* E7.5 embryo. Dorsal view of an embryo, characterised by the neural groove (NG, **A**). *Lmnb1* expression is widespread in the neural plate (NP) but diminished in intensity caudally. Expression is not observed in extra-embryonic tissues such as the allantois (All) in either strain. **(D-J)** *Lmnb1* expression in *ct/ct* embryos between E8.5 and E9.5. Similar to expression observed at E10.5, *Lmnb1* is present in the cranial region and throughout the trunk, but is negative in the surface ectoderm (SE, red arrows) at all levels of the head folds (HF; forebrain, Fb; midbrain, Mb; hindbrain, Hb) and in the heart (**H**, red arrowheads). The same expression pattern was observed in embryos with forebrain **(I)** or midbrain **(K-M)** exencephaly (yellow arrows indicating level of defect). Other abbreviations: PNP, posterior neuropore level. Scale bars represent 1 mm **H**, **K-M**, and 0.5 mm **A-G**, **I-J**.

Analysis of sections through $+^{ct}/+^{ct}$ and *ct/ct* embryos confirmed that *Lmnb1* is not expressed in the heart (**Fig. 4.7 B1, C3, E2, F2**) or surface ectoderm (**Fig. 4.7**). Analysis of sections also confirmed the expression sites of *Lmnb1* in the cranial region (**Fig. 4.7 C1-C2, E1-E2, F1-F2**), in neuronal tissues, neural folds of the spinal region, notochord and the gut (**Fig. 4.7 B1-B4, C3-C4, E2-E4, F3**).

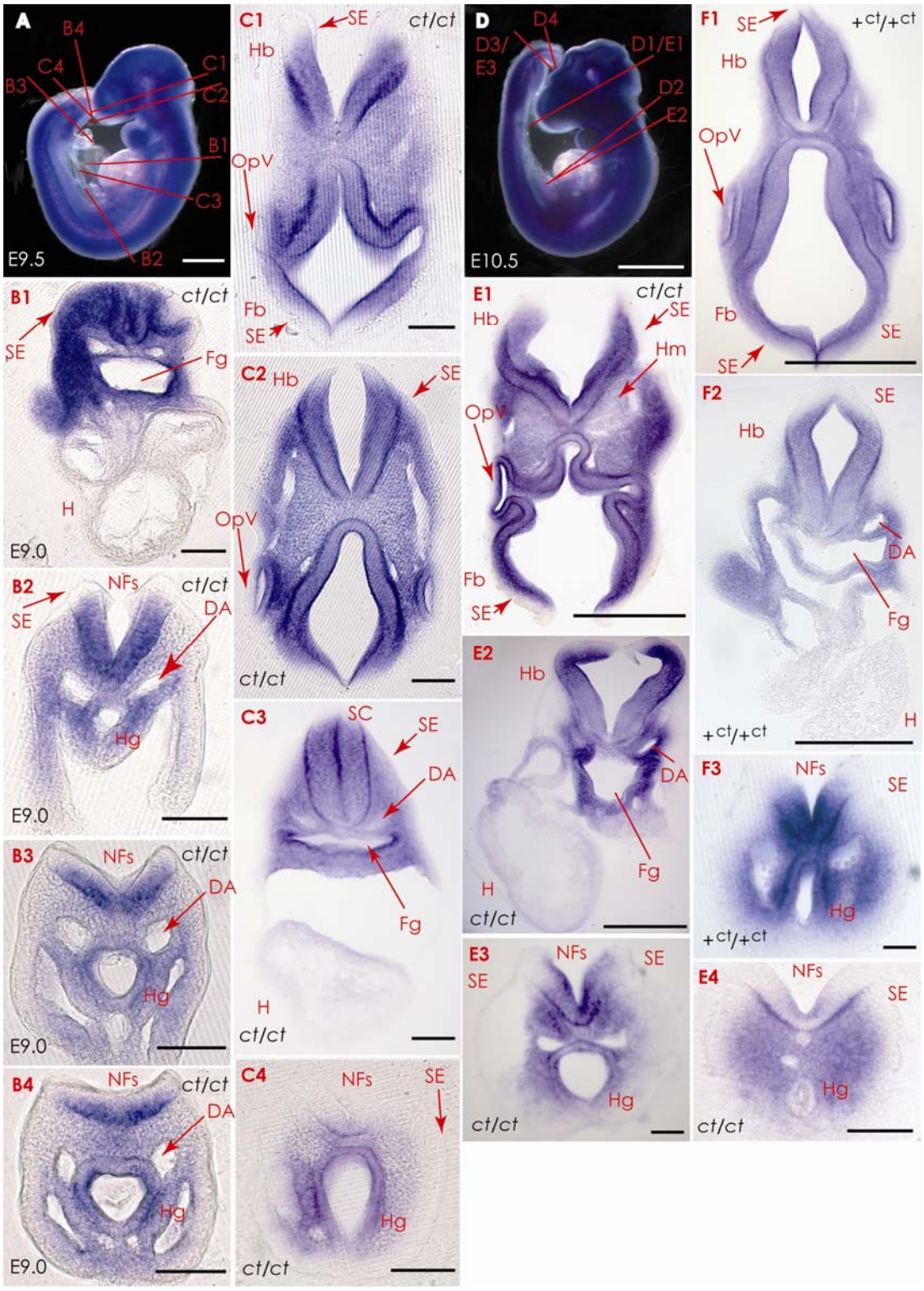
A
B4
C4
B3
C1
C2
B1
C3
B2
E9.5
C1
SE
ct/ct
Hb
OpV
Fb
SE
D
D4
D3/
E3
D1/E1
D2
E2
E10.5
F1
SE
+ct/+ct
Hb
OpV
Fb
SE
SE
B1
ct/ct
SE
Fg
H
E9.0
C2
Hb
SE
OpV
ct/ct
E1
ct/ct
Hb
SE
Hm
OpV
Fb
SE
F2
SE
Hb
DA
Fg
+ct/+ct
H
B2
NFs
ct/ct
SE
DA
Hg
E9.0
C3
SC
SE
DA
Fg
H
ct/ct
E2
Hb
DA
Fg
H
ct/ct
F3
NFs
SE
Hg
+ct/+ct
B3
NFs
ct/ct
DA
Hg
E9.0
E3
NFs
SE
SE
Hg
ct/ct
E4
NFs
SE
Hg
ct/ct
B4
NFs
ct/ct
DA
Hg
E9.0
C4
NFs
SE
Hg
ct/ct

Figure 4.7 *Lmnb1* WMISH sections. (**A, D**) E9.5 and E10.5 embryos show the level of sections cut for E.9.0-9.5 (**B1-B4**; **C1-C4**) and E10.5 (**E1-E4**) *curly tail* embryos, and E10.5 wild-type embryos (**F1-F3**). *Lmnb1* is expressed throughout the cranial region, neuroepithelium, head mesenchyme (Hm), and optic vesicles (OpV), even in embryos with open fore- and hindbrain (Fb, Hb; **E1**). Expression is also detected throughout the spinal cord (SC), including open neural folds (NFs) at lower spinal levels (**B2-B4**, **C4, E3-E4, F3**), to the level of the tail bud. At all levels the expression is absent in the surface ectoderm (SE), and it is also negative in the heart (H). Other abbreviations: BA, branchial arch; Da, dorsal aorta; Fg, foregut; Hg, hindgut. Scale bars: **A**, **E1-E2**, **F1-F2**, 0.5 mm; **B**, 1.0 mm; **B1-B4, C1-C4**, **E3-E4**, **F3**, 0.1 mm.

4.2.3 Dynamics of the lamin B1 variants within the nuclear envelope

Identification of the 8E variant form of lamin B1, lacking one glutamic acid in the polyglutamate tract (**Fig. 4.4**), in the *curly tail* strain raised the question of whether lamin B1 function may be altered in *curly tail* and whether this could contribute to development of NTDs. Loss of an amino acid could potentially affect lamin B1 protein conformation. For example, an alteration in the secondary structure of the protein (which is more conserved than the primary structure), might cause the 8E and 9E variants to fold differently. Using PSIPRED Protein Structure Prediction Server (http://bioinf.cs.ucl.ac.uk/psipred/psiform.html) bioinformatics tool, the predicted secondary structures of the two variants were analysed from their amino acid sequence. The region of the tail domain containing the glutamic acid repeat is predicted to consist of a helix region in both variants, suggesting that there is not a major effect of the 8E variant on protein conformation. The lamin B1 tail domain is also necessary for normal processing of the protein into its mature form (Maske et al., 2003). Therefore, an *in vitro* approach was taken to test if the variation in number of glutamic acid residues could have an effect on stability of the nuclear envelope

Expression constructs of green fluorescent protein fused with full-length *Lmnb1* (*GFP-Lmnb1*-FL) encoding the 8 and 9 glutamic acid variants were generated (**Chapter 2, section 2.13.1**). In order to investigate the dynamics of the nuclear lamina, these constructs were analysed using fluorescence loss in photobleaching (FLIP), in

collaboration with Dr Ashraf Malhas (Oxford University). This method, like fluorescence recovery after photobleaching (FRAP), can be used to measure the ability of a molecule to move around over time due to the capacity of fluorescent dyes which emit light of one wavelength (e.g., green) after they have absorbed light of another wavelength (e.g., blue). Nevertheless, if a high intensity blue light is delivered to the dye, it "photobleachs", i.e. the dye is unable to fluoresce (Lippincott-Schwartz et al., 2001). In the FRAP method a small area of a cell is rapidly bleached using a high-intensity laser pulse. The movement of unbleached molecules from the neighbouring areas is then recorded by time-lapse microscopy as the recovery of fluorescence in the bleached area. FLIP is based on the same principle, the difference is that while the area in the cell is repeatedly bleached, a different area is monitored. The loss of fluorescence in areas that are distant from the bleached one correspond to movement of molecules into the bleached area. FLIP largely eliminates the concern that the recovery properties are due to damage at the bleach spot, as all measurements are made in areas that are never bleached.

FRAP and FLIP can be used to investigate the stability and dynamics of the nuclear lamina. Within the lamina of interphase cells, lamins are relatively stable and that is revealed by their long recovery time during FRAP experiments. In this project FLIP was used to investigate the mobility of the 9E and 8E lamin B1 variants in the nuclear envelope in wild-type ($+^{ct}$) mouse fibroblast (MEFs, **Chapter 2, section 2.15**) following transfection with the full-length *GFP-Lmnb1* constructs. The two constructs did not show a difference in FLIP because the full-length protein has very stable interactions at the nuclear envelope.

Owing to the stability of the full-length lamin B1 protein in FLIP experiments truncated forms are commonly used to assess variant proteins and these provide more sensitivity in the assay. Expression constructs were generated for truncated forms of the two proteins, composed of forty amino acids upstream of the C-terminus (thirty nine for the 8E-lamin B1 variant), which includes the polyglutamic tract (thirty amino acids upstream). The cloning strategy used a plasmid containing a yellow fluorescent protein (YFP)-human *LMNB1* fusion construct (kindly provided by Dr Ashraf Malhas and used in Maske et al, 2003). The human *LMNB1*-C40 sequence was excised by restriction digestion. A PCR-generated fragment was then inserted containing the mouse coding

sequence encoding the 9E and 8E variants (**Chapter 2, section 2.13.2**) in frame with a nuclear localisation signal (NLS), necessary for nuclear import of lamins, fused to YFP. FLIP experiments were performed, by Dr Malhas, on wild-type MEFs transfected with the NLS-YFP-C40 constructs (9E and 8E variants). After photobleaching the YFP-8E protein showed a significantly greater loss of fluorescence intensity within the first 100 seconds than the YFP-9E protein (**Fig. 4.8**). This data shows that the 9E variant is less dynamic, indicative of a more stable interaction with the nuclear envelope than the 8E variant. Thus, the 8E lamin B1 variant present in the *curly tail* strain may confer altered stability and function of the nuclear envelope.

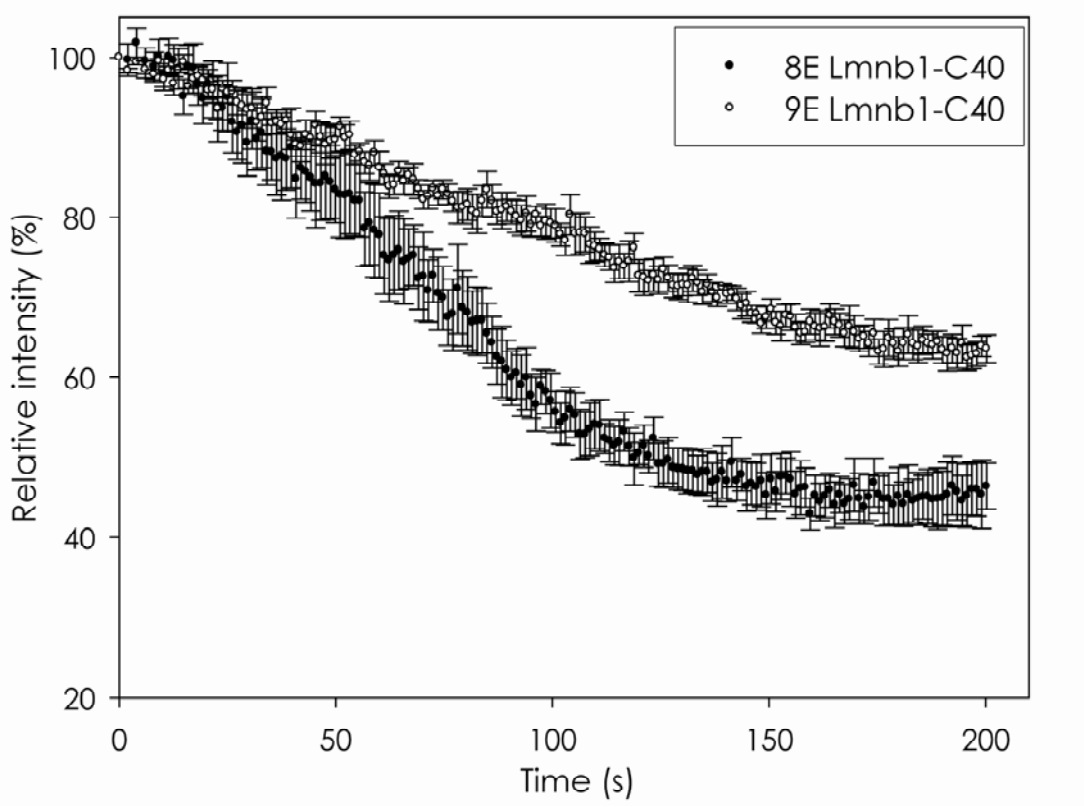

Figure 4.8 FLIP analysis of YFP-lamin B1 fusion proteins. FLIP was performed on wild-type MEFs expressing NLS-YFP-C40. Plot shows measurements of fluorescence loss after photobleaching (mean values ± SE) of the 9E and 8E NLS-YFP-C40 constructs. These results indicate that the 9E protein has more stable associations with the nuclear lamina than the 8E fragment, as shown by its slower loss of fluorescence.

4.2.4 Sequence analysis of *Lmnb1* in multiple species and mouse strains

Alignment of the mouse lamin B1 protein with lamin B1 of other species and the mouse lamins B2 and A using the Constraint-based Multiple Alignment Tool (COBALT), showed that the number of glutamic acid residues at the 8E/9E position varies between species **(Fig. 4.9).** Lamin B2 contains a 7E repeat while lamin A, has a combination of glutamic and aspartic acids (2E/4D).

N	Amino acid sequence
1	A Q R S T V F K T T I - - - P E E E E - E E E E E P I G V - A V E E E
2	A Q R S T V F K T T I - - - P - E E E - E E E E E A A G V - V V E E E
3	A Q R S T V F K T T I - - - P E E E E - E E E E E P I G V - P L E E E
4	A Q R S T V F K T T I - - - P - E E E - E E E E E A A G V - V V E E E
5	A Q R S T V F K T T I - - - P - E E E - E E E E E A A G V - V V E E E
6	A Q R S T V F K T T I - - - P - E E E - E E E E E A A E V - A V E E E
7	A Q R S T V F K T T I - - - P - E E E - E E E E E A P E V - V V E E E
8	A Q R S T V F K T T V - - - N - E G E - E E E E E G E E - - E I L E D
9	A Q R T T V Y T T T I - - - P - E E E L E E E M L E E - I T K E S H Y
10	A Q R T T V Y T T N I - - - P - E E E L E E E E E I F E E - T A K E S
11	A V R S T V F K T A V - - - E - D E D - D D E E E E K E A E V I E E R
12	A V R S T A F N T T V - - - E - - E - - E E E E E D A D V I E E R F F
13	A V K A A K H S S V Q G R E N G E E E - - E E E E E A E F G - - - E E D
14	A M R K L V R S L T M V - - - - - E D - N E D D D E D G E - - - - E L

1. NP_034851 Lamin B1 [Mus musculus] - Mouse (amino acid 541-575)
2. NP_005564lamin B1 [Homo sapiens] - Human (amino acid 540-574)
3. NP_446357lamin B1 [Rattus norvegicus] - Rat (amino acid 540-574)
4. XP_001158129PREDICTED: lamin B1 isoform 2 [Pan troglodytes] - Chimpanzee (aa 540-574)
5. XP_0010972340PREDICTED: lamin B1 isoform 1 [Macaca mulatta] - Rhesus monkey (aa 540-574)
6. NP_001096765lamin B1 [Bos taurus] - Cattle (aa 540-574)
7. XP_531892PREDICTED: similar to Lamin B1 [Canis familiaris] - Dog (aa 473-507)
8. NP_990617lamin B1 [Gallus gallus] - Chick (aa 539-573)
9. NP_989198lamin B1 [Xenopus (Silurana) tropicalis] (aa 540-574)
10. NP_001080053lamin B1 [Xenopus laevis] (aa 540-574)
11. NP_694504lamin B1 [Danio rerio] - Zebrafish (aa 541-575)
12. BAB32979lamin B1 [Carassius auratus] - Goldfish (aa 275-308)
13. NP_034852Lamin-B2 - Mouse (aa 549-583)
14. NP001002011Lamin-A/C - Mouse (aa 539-573)

Figure 4.9 Alignment of lamin B1 protein sequence at the region encompassing the glutamic acid repeat. The number of E residues (yellow shaded) varies between species. Mice and rats have a 9E repeat (**1, 3**); while humans, chimpanzee, rhesus, cattle, dog, and *Xenopus* have an 8E repeat (**2**, **4**, **5**, **6**, **7, 10**). The sequence is less similar in other species (**11**, **12**). Mouse lamin B2 contains a 7E repeat (**13**), while lamin A (**14**) contains a combination of aspartic acid (D) and glutamic acid residues. Shaded in grey are amino acids conserved between species. Amino acid (aa) number from the start of the sequence to the end, indicated in brackets.

Searches for annotated mouse single nucleotide polymorphisms (SNPs) in the online databases at http:\\www.ensembl.org/index.html, showed that the C216T single nucleotide change (exon 1) and the *GAG* variant (exon 10) had not yet been described. Therefore, I tested whether these sequence changes were present in other mouse strains. In later searches, I exported the full *Lmnb1* transcript sequence from the Ensembl website and performed a BLAST search against the NCBI-SNP Mouse Data Base (http://blast.ncbi.nlm.nih.gov/Blast.cgi), which revealed that C216T had been annotated as a SNP.

In order to test if the *Lmnb1* sequence changes identified in the *ct* strain were present in other mouse strains, methods were developed for genotyping. Exon 1 of *Lmnb1* was assessed for loss or creation of restriction sites using the online Webcutter 2.0 software (http://rna.lundberg.ru.se/cutter2/). The C612T base pair change results in the creation of a *HindIII* restriction site in the *ct/ct* sequence (**Fig. 4.10 A**). Therefore, amplification of a PCR product using primer pair *F1in2/R1ex2* (**Appendix B, Table B.5**), followed by digestion of the PCR product with *HindIII* enzyme resulted in different fragments for *ct/ct* and $+^{ct}/+^{ct}$ (**Fig. 4.10 A; Table 4.1**).

Strain	*HindIII* site	Fragment size (bp)
$+^{ct}/+^{ct}$	Absent	568
ct/ct	Present	225 and 343
Heterozygous	Present in one allele only	568, 225 and 343

Table 4.1 Restriction enzyme site difference between the wild-type sequence and the C612T nucleotide change at position 348 of *Lmnb1* exon 1.

For the $GAG^{1957\text{-}1983\Delta}$ variants, two pairs of primers (**Table 4.2**) were designed to amplify regions of exon 10, encompassing the nine GAG repeat (**Fig. 4.10 B**). In order to visualise the three base pair difference between *ct/ct* and $+^{ct}/+^{ct}$ samples, PCR products were run on 5% agarose gels. Both primer pairs produced products whose size difference between strains could be readily visualised.

Primer No	Sequence	Size of fragment (bp) – 9E; 8E
1 - Forward 1 – Reverse	5’ – AGACCACCATACCCGAGGA - 3’ 5’ – AAACGCTCCTCCTCCACAG – 3’	73; 70
2 – Forward 2 - Reverse	5’ – GACCACCATACCCGAGGAG – 3’ 5’ – TCCACAGCCACTCCGATG – 3’	58; 55

Table 4.2 Exon 10 *Lmnb1* primers for genotyping the $GAG^{1957\text{-}1983\Delta}$ deletion. The fragment size differentiates the wild-type (9E) and variant (8E) alleles.

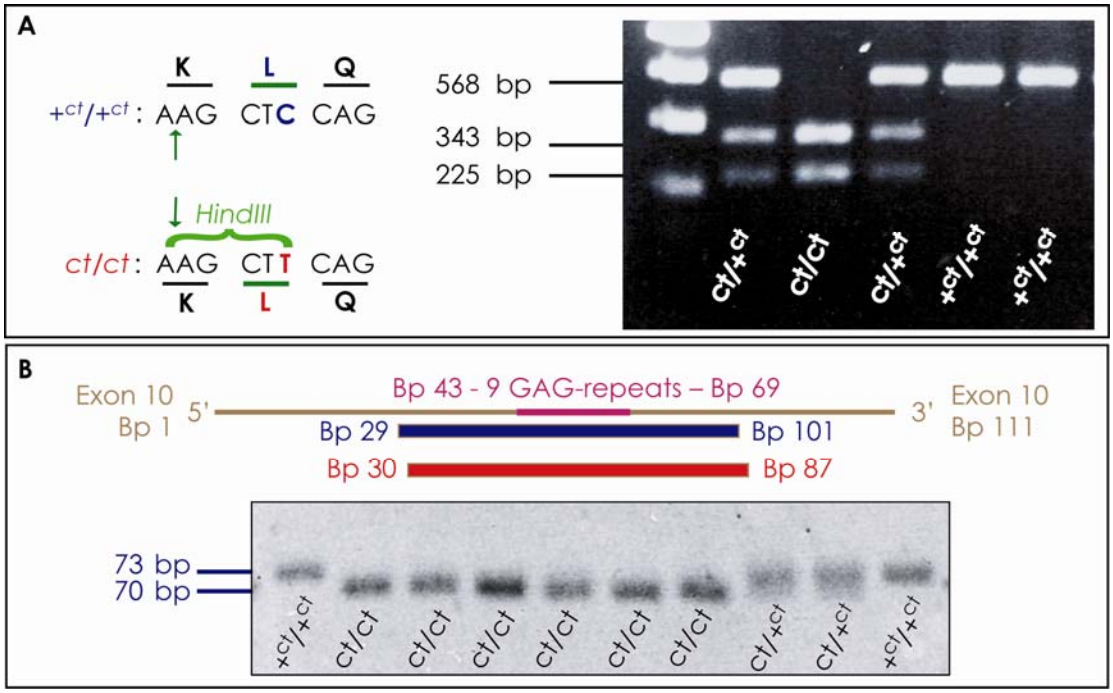

Figure 4.10 Diagrams of assays to genotype *Lmnb1* sequence changes. (A) The C612T single nucleotide in exon 1 (bold) change creates a *HindIII* site in *ct/ct* such that a PCR product encompassing this site can be digested by *HindIII* in *ct/ct* but not in $+^{ct}/+^{ct}$**.** The digested products were run on 1% agarose gels**,** where $+^{ct}/+^{ct}$ sample generate the undigested band (568 bp), *ct/ct* have two bands (225 and 343 bp) and heterozygous samples (*ct*/$+^{ct}$) have the three band sizes. **(B)** Schematic diagram of the PCR products amplified by primers designed specifically against exon 10 (111 bp length), amplified by PCR and run on 5% gels. For example, for primer 1, *ct/ct* samples generated a 70 base pair (bp) band, $+^{ct}/+^{ct}$ a 73 bp band and heterozygotes both bands. Green arrow in **A** indicates *HindIII* recognition site (a/agctt).

Having optimised these two assays as a means to genotype *ct/ct* and $+^{ct}/+^{ct}$ strains for *Lmnb1* polymorphisms, other NTD and inbred strains were genotyped for the same sequence changes (**Table 4.3**). This analysis showed that *splotch* (Sp^{2H}), another mouse model for NTDs, and the inbred strains *CBA/Ca* and *101* shared the same *Lmnb1* variants as *ct/ct.* Therefore, *Lmnb1* sequence changes in *ct/ct* and Sp^{2H} appear to be polymorphisms characteristic of the *CBA* inbred strain (one of the background strains of *ct/ct* and Sp^{2H}). Moreover, in the strains analysed these sequence differences always occurred together. The exon 1 and exon 10 polymorphisms have not been separated by

recombination, despite many generations of mouse breeding and thus appear to be in linkage disequilibrium.

Strains	Background/Inbred strain	Exon 1: C612T	Exon10: 9GAG/8GAG
Curly tail	*Curly tail*	C612T	8GAG
Congenic ***(+^{ct}/+^{ct})***	93.7% *Curly tail*	wt	9GAG
ct/ct^{TgGrhl3}	100% *Curly tail*	C612T	8GAG
C3H/HeJ	Inbred #	wt	9GAG
C57BL	Inbred	wt	9GAG
DBA/2J	Inbred #	wt	9GAG
SWR/J	Inbred #	wt	9GAG
SWR	Inbred	wt	9GAG
CAST/EiJ	Inbred #	wt	9GAG
CBA/Ca	Inbred	C612T	8GAG
CBA/J	Inbred #	C612T	8GAG
101	Inbred	C612T	8GAG
ct^{2J}/J	C57BL/6J #	wt	9GAG
Crsh	*BALB/c + C57BL*	wt	9GAG
Crc	*CBA/Ca + Circle tail*	wt	9GAG
Kumba	*C57BL*	wt	9GAG
Loop tail	*LPT/Le*	wt	9GAG
MTHFR KO	*BALBc*	wt	9GAG
Splotch	*CBA + C3H*	C612T	8GAG
Twist	*C57BL*	wt	9GAG

Table 4.3 *Lmnb1* sequence variations genotyped in inbred and other NTD mouse strains. Genomic DNA was extracted from in-house mouse strains or purchased from The Jackson Laboratory (indicated by #). Each strain was tested for the presence or the absence of the single nucleotide change in exon 1 (C612T or wt, wild-type) and whether exon 10 contained an 8 or 9 GAG repeat, using the genotype assays previously described.

More recently the Sanger Institute (Mouse Genomes Project,) provided sequence data for 17 mouse strains and this provided more extensive information on SNPs and INDELs (insertions and deletions), showing that both sequence changes were present in various mouse strains. The C/T is annotated as a synonymous coding SNP (18: 56868078), for the A/J, AKR/J and CBA/J strains. The GAG variant is annotated as

non-synonymous coding SNP (Deletion, 18: 56909394), with the 8E variant present in the A/J, AKR/J, CBA/J, PWK/PhJ and WSB/EiJ strains.

4.2.5 Investigation of *Lmnb1* as a potential modifier gene for NTDs in *curly tail*

Evidence from functional analysis of lamin B1 showed that the 8E variant could have an effect on the stability of the nuclear envelope. The analysis of different mouse strains suggested that this polymorphism is rare and insufficient to cause NTDs alone. For example, mice from the *CBA/Ca* inbred strain do not normally develop NTDs. However, the *CBA/Ca* genetic background may include risk factors, since both *curly tail* and *splotch* develop NTDs whose penetrance varies with genetic background. Studies have suggested the presence of modifiers for NTDs in the *ct* genetic background (Neumann et al., 1994; Letts et al., 1995). Therefore, I hypothesised that lamin B1 could act as a modifier gene, such that the frequency of NTDs caused by the *ct* mutation may be affected by the presence of the 8E or 9E variant. To test this hypothesis *ct* sub-strains carrying different combinations of the *Lmnb1* polymorphisms and the *Grhl3* mutation were generated in a two step breeding program (**Fig. 4.12**). At each step of this scheme, mice were selected on the basis of the *Lmnb1* polymorphisms (genotyping described on **section 4.2.4**) and for the presence of the *Grhl3* mutation (**Chapter 2, section 2.4.2**) and two polymorphic markers located on chromosome 4 on the opposite side of the gene to the mutation, *D4Bwg1551e* and *D4Mit204* (**Fig. 4.11**).

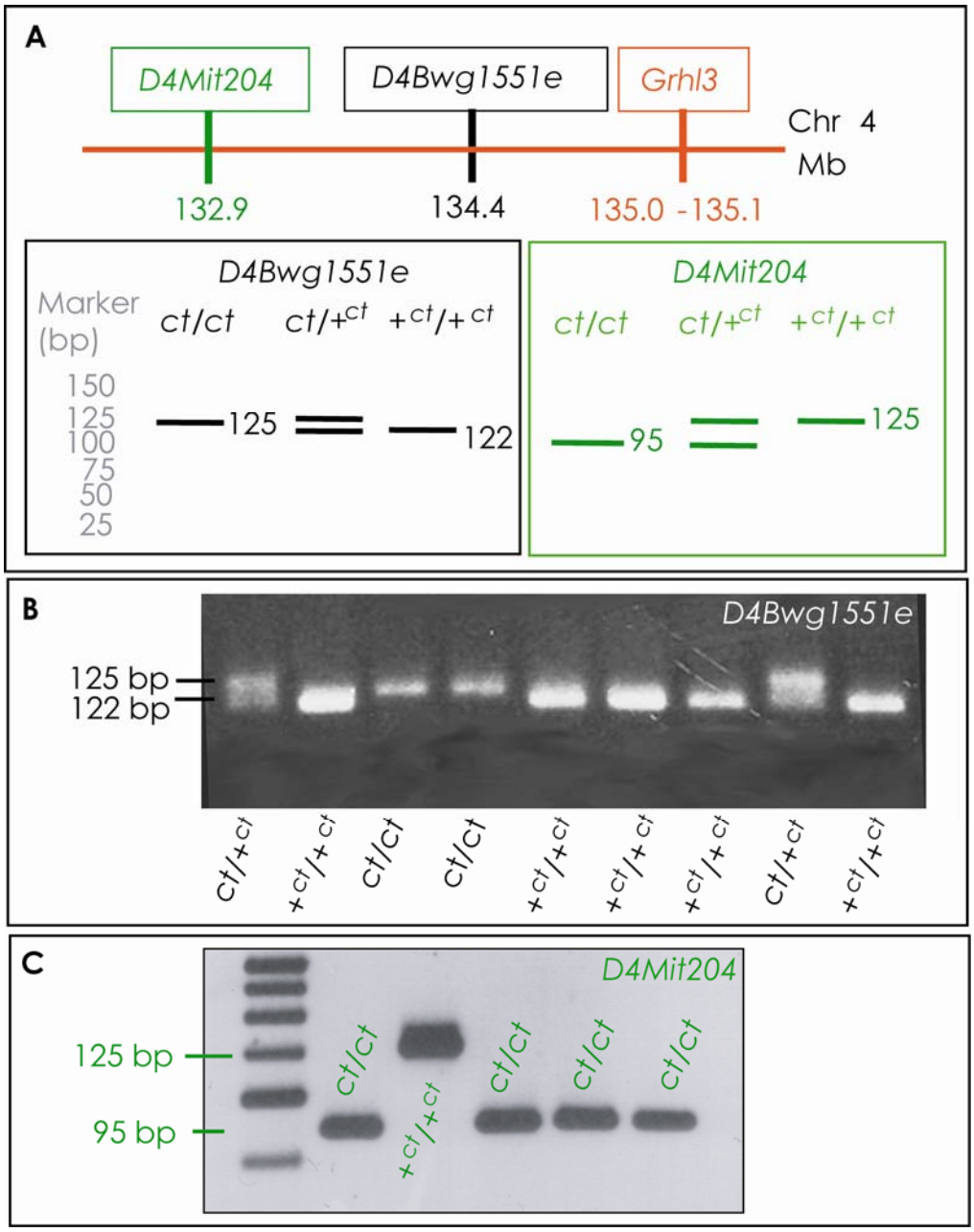

Figure 4.11 Schematic diagram of the genotyping using chromosome 4 polymorphic markers. (A) The *D4Bwg1551e* (black box) and *D4Mit204* (green box) microsatellites were used to distinguish between *ct/ct*, $+^{ct}/+^{ct}$ and heterozygous ($ct/+^{ct}$) samples. The diagram illustrates the position of the microsatellites in relation to the *Grhl3* gene on chromosome 4 and the expected product sizes upon PCR amplification. **(B-C)** Amplified samples were electrophoresed on 5% agarose gels.

Initially, *ct/ct* mice were crossed to $+^{ct}/+^{ct}$ mice to generate double-heterozygous offspring (**Fig. 4.12 A**). These mice were backcrossed to *ct/ct* mice (**Fig. 4.12 B**) to decrease genetic variability and from this backcross, double-heterozygotes were intercrossed (**Fig. 4.12 C**) to generate all the possible genetic combinations of the *Lmnb1* polymorphism on a *ct* background (**Fig. 4.12 D**). Henceforth the annotation for each *curly tail* strain will be as summarised on **Table 4.4**. Two strains were of particular interest for investigation of the possible effect of *Lmnb1* variants in determining risk of NTDs: ct^{9E} ($L^{9E/9E};G^{ct/ct}$) and ct^{8E} ($L^{8E/8E};G^{ct/ct}$).

Strain	Annotation	Genotype	Abbreviation
Curly tail	*ct*	$Lmnb1^{8E/8E};Grhl3^{ct/ct}$	$L^{8E/8E};G^{ct/ct}$
Curly tail – 8E	ct^{8E}	$Lmnb1^{8E/8E};Grhl3^{ct/ct}$	$L^{8E/8E};G^{ct/ct}$
Curly tail – 9E	ct^{9E}	$Lmnb1^{9E/9E};Grhl3^{ct/ct}$	$L^{9E/9E};G^{ct/ct}$
Wild-type – 8E	$+^{ct;8E}$	$Lmnb1^{8E/8E};Grhl3^{+/+}$	$L^{8E/8E};G^{+/+}$
Wild-type	$+^{ct}$	$Lmnb1^{9E/9E};Grhl3^{+/+}$	$L^{9E/9E};G^{+/+}$

Table 4.4 Annotation for *curly tail* strains after the generation of the *ct*-substrains.

Wild-type $(+^{ct}/+^{ct})$ embryos and mice develop normally, without tail flexion defects or NTDs. Following generation of wild-type mice carrying the 8E lamin B1 variant ($L^{8E/8E};G^{+/+}$; **Fig. 4.12**), these mice were twice backcrossed to *ct/ct* to increase the *ct*-background and to generate a colony of wild-type *ct*-strain carrying the 8E *Lmnb1* variant ($L^{8E/8E};G^{+/+}$), for comparison with the $+^{ct}/+^{ct}$ ($L^{9E/9E};G^{+/+}$) strain

The microsatellite markers *D4Bwg1551e* and *D4Mit204* were informative, distinguishing *ct/ct* from $+^{ct}/+^{ct}$ and heterozygotes ($ct/+^{ct}$). This complemented the genotyping of the putative *Grhl3* mutation which lies upstream of the gene (summarised on **Chapter 2, section 2.4.2**; **Fig. 2.3 C-D**). Therefore, if both the *C-21350T* mutation and the *D4Bwg1551e* and/or *D4Mit204* markers typed as *ct/ct* we could be confident that the *Grhl3* locus carries the *ct* mutation, and that a recombination event at the *Grhl3* locus had not arisen. The latter microsatellite was used for validation of the genotype obtained with *D4Bwg1551e* for the $+^{ct;8E}$ strain, since recombination at the *Grhl3* locus

occurred in some offspring, which were eliminated prior to establishment of a colony of $+^{ct;8E}$ mice.

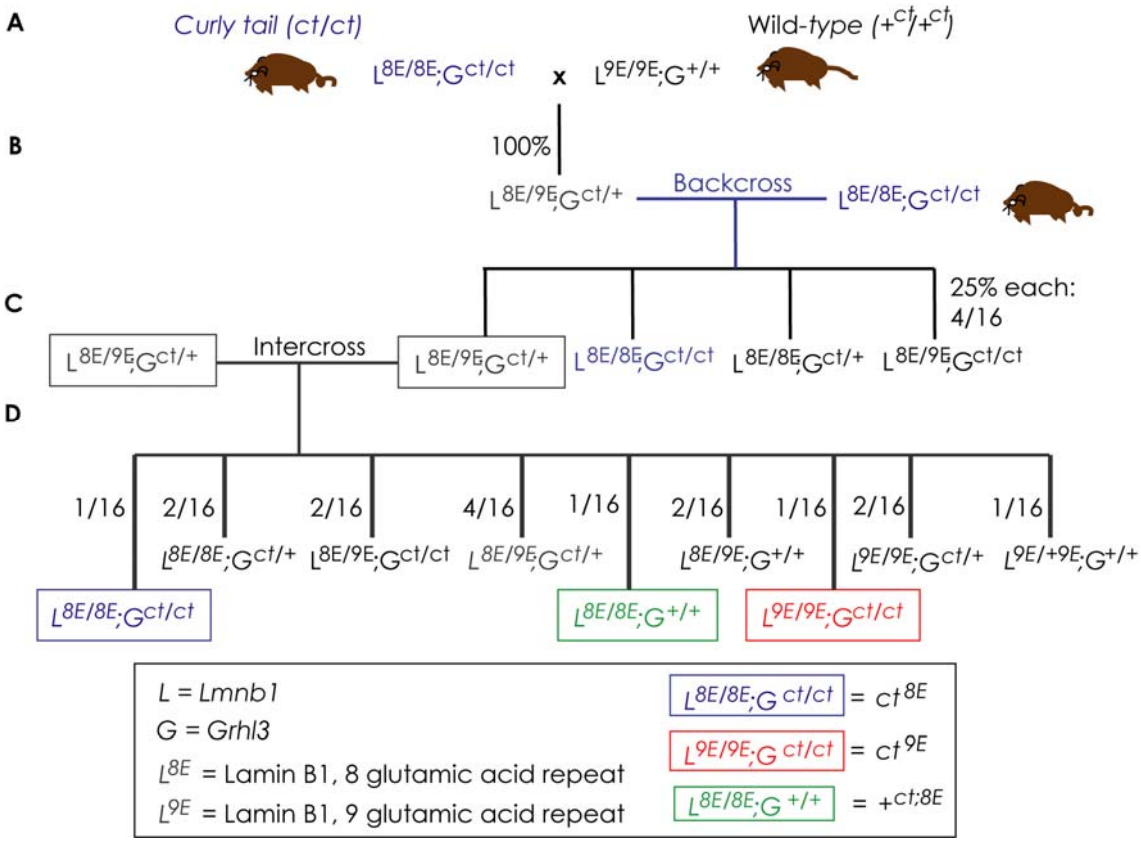

Figure 4.12 Schematic diagram of breeding programme to generate *Lmnb1* and *Grhl3* sub-strains of *ct/ct*. **(A)** Wild-type and *curly tail* males and females were crossed to generate double heterozygous offspring. **(B)** Double heterozygotes from initial crosses were backcrossed to *ct/ct*. **(C-D)** Intercrosses generated mice which were used to establish sub-strains for comparison. **(D)** The key strains of interest were ct^{8E} (same genotype as *ct/ct* at *Grhl3* and *Lmnb1*), and ct^{9E} which both carry the *Grhl3* mutation, but differ in *Lmnb1* sequence. A third strain, $+^{ct;8E}$, is wild-type for *Grhl3* but carries the 8E *Lmnb1* variant. The predicted frequency of each genotype is indicated.

Once mice of specific genotypes for *Grhl3* and *Lmnb1* had been generated, they were intercrossed to generate closed homozygous colonies. Mice and embryos of the *Grhl3/Lmnb1* sub-strains were analysed according to their phenotype: straight tail (ST) indicative of normal spinal development, tail defects (TD, such as kinked or bent tail,

BT, or curled tail, CT), and cranial (exencephaly, Ex) and/or caudal NTDs (spina bifida, SB; **Fig. 4.13**). Embryos were analysed at E11.5-E15.5, stages at which it is possible to clearly visualise spina bifida. The phenotypic appearance of tail flexion defects and/or NTDs was the same as in homozygous *ct/ct* embryos of the original strain. Thus, *ct* embryos carrying the 9E *Lmnb1* variant (**Fig. 4.13**) or the 8E *Lmnb1* variant exhibited straight, bent or curled tails or spina bifida accompanied by a curled tail. As in the original *ct* strain, spina bifida was always accompanied by a tail defect.

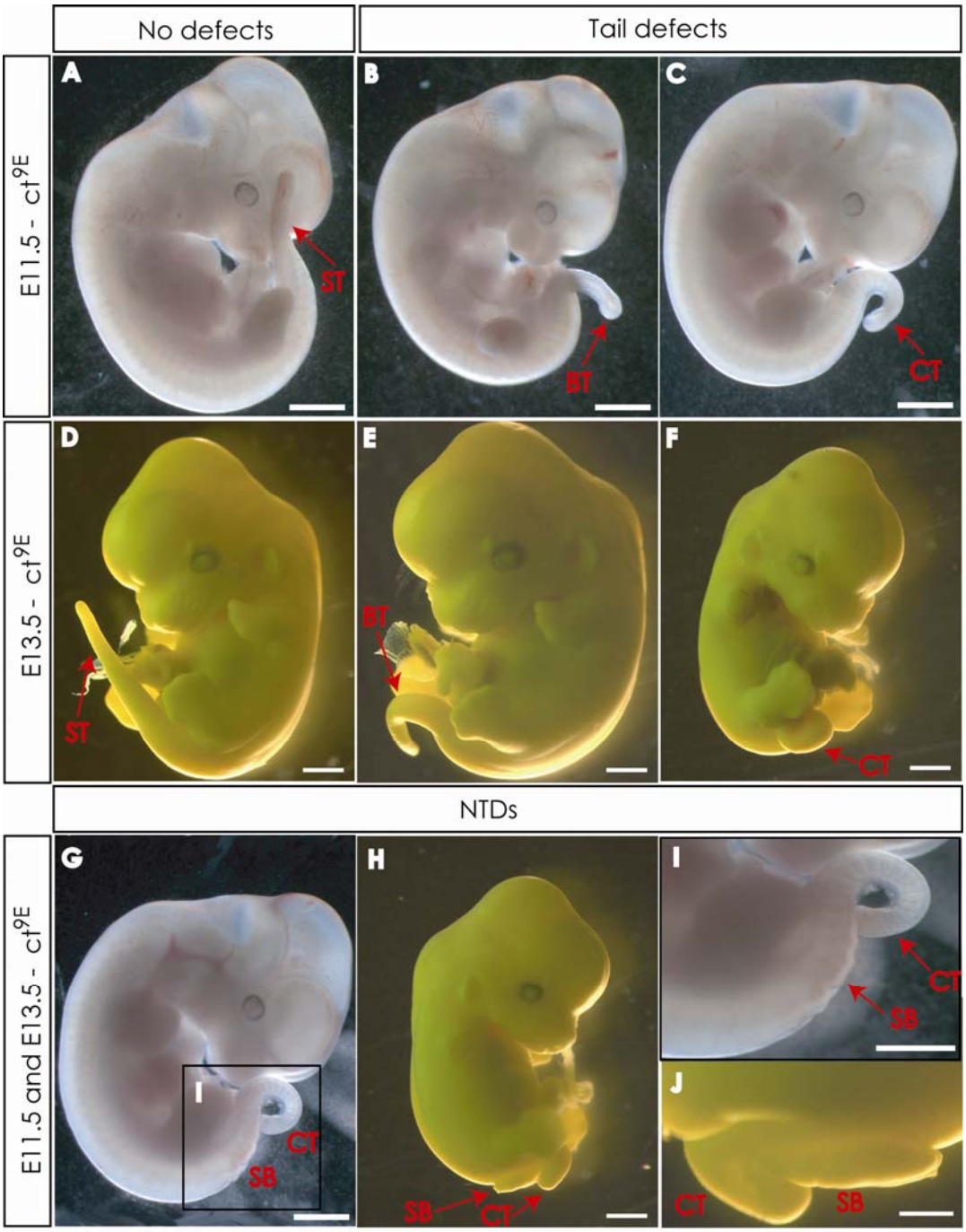

Figure 4.13 Phenotypes of *curly tail* ct^{9E} sub-strain. (A-C, D-F) Images of ct^{9E} embryos at E11.5 (**A-C, G, I**) and E13.5 (**D-F, H, J**) respectively, portraying the typical phenotypes observed in the ct^{9E} sub-strain**.** Typical examples of embryos displaying different categories of tail phenotypes: ST, straight tail; BT, bent tail; and CT, curled tail. (**G-J**) Embryos with NTDs, comprising spina bifida (SB) together with CT (**I** and **J**, higher magnifications of defects in embryos **G** and **H**). These phenotypes were observed at all developmental stages studied (E11.5 – E15.5) and do not differ from the phenotypes observed in *ct/ct*. Scale bars: 1 mm.

4.2.6 Frequency of NTDs in *curly tail* sub-strains expressing different *Lmnb1* variants

To investigate if the differing *Lmnb1* variants could influence the penetrance of the *curly tail* mutation, the frequency of defects was compared in the ct^{9E} ($ct^{9E/9E};G^{ct/ct}$) and ct^{8E} ($ct^{8E/8E};G^{ct/ct}$) sub-strains, the latter strain being equivalent genotype to the original *ct* strain. Embryos between E11.5 and E15.5 were then analysed for the presence of NTDs. The data for cranial and caudal defects are presented separately because exencephaly can occur in isolation or in combination with spina bifida and a curled tail or with tail defects alone and can be observed from E9.5.

A total of 224 ct^{9E}, 101 ct^{8E}, 113 $+^{ct}$, 105 $+^{ct;8E}$ and 113 *ct* embryos were collected for comparison (**Table 4.5; Fig. 4.14**). The frequency of SB in the ct^{8E} strain was similar to that in *ct*. This suggests that the out-cross to $+^{ct}$ has not resulted in loss of genetic modifiers that significantly affect frequency of NTDs. Only 5.8% of the ct^{9E} embryos developed SB compared to 15.8% of the ct^{8E} embryos. Thus, the frequency of SB was significantly lower in *ct/ct* embryos carrying the 9E *Lmnb1* variant compared with the 8E variant, equivalent to a 63% reduction in frequency. In contrast, the frequency of tail flexion defects did not differ between the two strains.

Strain	***ct*^{9E}**	***ct*^{8E}**	**+^{ct}**	**+$^{ct;8E}$**	***ct***
Genotype	$L^{9E/9E};G^{ct/ct}$	$L^{8E/8E};G^{ct/ct}$	$L^{9E/9E};G^{+/+}$	$L^{8E/8E};G^{+/+}$	$L^{8E/8E};G^{ct/ct}$
Embryos (n)	**224**	**101**	**113**	**105**	**113**
SB + CT	13 (5.8%)*	16 (15.8%)	0	0	16 (14.2%)
CT	121 (54.0%)	52 (51.5%)	0**	6 (5.4%)†	49 (43.4%)
No defects/ST	90 (40.2 %)	33 (32.7%)	113 (100 %)	98 (0.9%)	48 (42.5%)

Table 4.5 Frequency of tail flexion defects and spinal NTDs in *curly tail* sub-strains. Total number of embryos (n) collected for each strain (ct^{9E}, ct^{8E}, $+^{ct}$, $+^{ct;8E}$ and *ct*) is indicated. Embryos were scored for spinal NTDs (SB) and tail flexion defects (CT) compared to no defects (straight tail, ST). *Curly tail* embryos affected with spina bifida always have a curled tail (SB+CT). The frequency of SB is significantly lower in the ct^{9E} than in the ct^{8E} and *ct* strains (* $p<0.02$, χ^2). Spina bifida and tail flexion defects were never observed among $+^{ct}$ embryos (** $+^{ct}$ *versus* $+^{ct;8E}$; p=0.03, Z-test) but tail flexion defects did occasionally occur among $+^{ct;8E}$ embryos although at significantly lower frequency than among *ct* mutant embryos († $p\leq0.001$, χ^2).

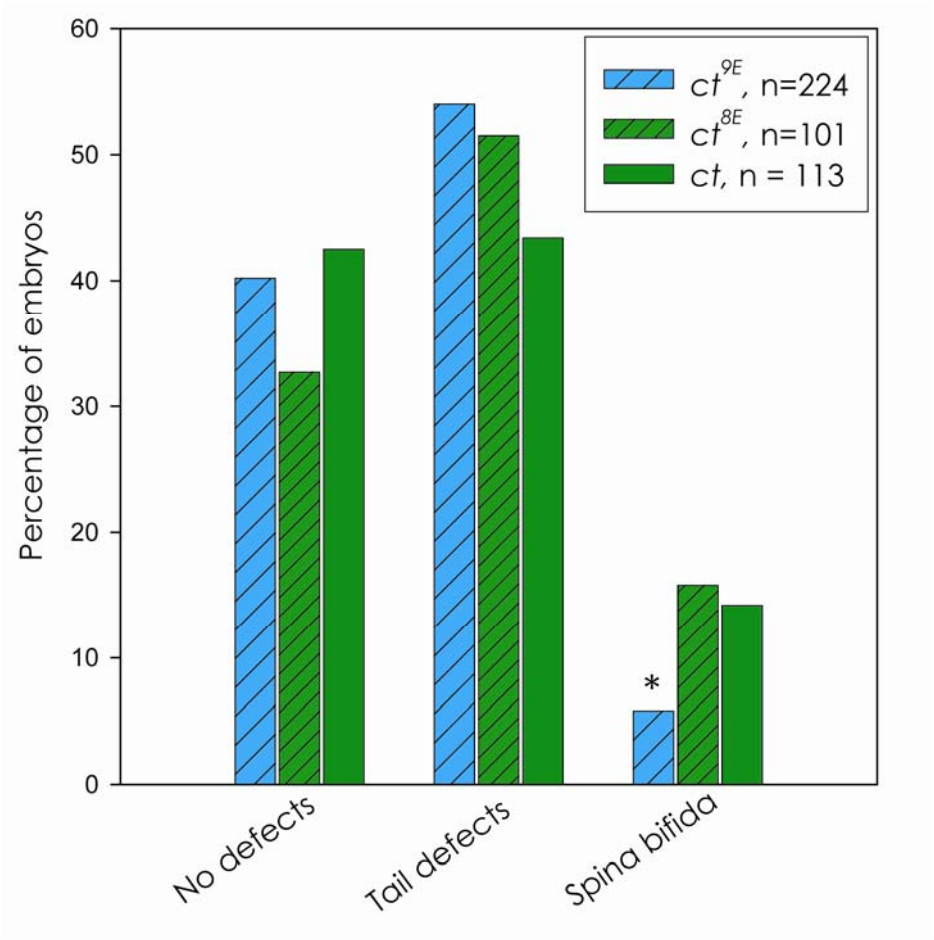

Figure 4.14 Frequency of tail flexion defects and spinal NTDs in *curly tail* sub-strains. Phenotypes were analysed at E11.5-E15.5. The frequency of spina bifida frequency is significantly lower in the ct^{9E} strain compared with ct^{8E} and *ct* (* p=0.02, χ^2).

All $+^{ct}$ embryos developed apparently normally. Most $+^{ct;8E}$ embryos developed normally, however, tail flexion defects were observed in a few cases. Nevertheless, the rate of tail defects was significantly lower than in *ct* (**Table 4.5**). Thus, in spite of the wild-type *Grhl3* allele, it appears that the presence of the 8E lamin B1 variant can affect the penetrance of tail defects in mice with a *ct* genetic background since $+^{ct}$ embryos were never observed to develop tail defects.

4.2.6.1 Analysis of posterior neuropore length within the *ct* sub-strains

An enlarged posterior neuropore (PNP) at the stage of spinal neurulation indicates delay or failure of closure, suggestive of the likelihood that a *curly tail* embryo will develop spina bifida and/or tail defect (Copp, 1985a). Since SB occurs at lower rate in the ct^{9E} strain, it was predicted that this would be reflected by a lower mean PNP length. However, it was unknown at what specific developmental stage PNP closure would begin to differ in *ct* and the sub-strains. Therefore, the PNP length was measured for a series of embryos at different somite stages to better understand at what stage (s) the PNP is enlarged and/or fails to close.

Examples of the different lengths of PNPs observed in these embryos are shown in **Figure 4.15**. Data for individual embryos were plotted (**Fig. 4.16**) and mean PNP lengths calculated for each stage (**Table 4.6**). Mean PNP lengths in embryos of both wild-type strains ($+^{ct}$; $+^{ct;8E}$) were significantly smaller than in the *ct* strains at all the stages examined (**Table 4.6**). This is particularly evident at the 30-31 somite stage where there is a major decline in PNP length in wild-types but not in the *curly tail* strains. The PNP length in $+^{ct;8E}$ was larger than in $+^{ct}$, particularly at the 26-27 somite stage, but this did not reach statistical significance (**Fig. 4.16**). The PNP lengths in the *ct* and ct^{8E} strains did not significantly differ. However, from somite stages 28-29 onwards the mean PNP length of embryos of the ct^{9E} strain was smaller than in the *curly tail* strains carrying the 8E lamin B1 variant (*ct* and ct^{8E}), and this difference was significant **Table 4.6**).

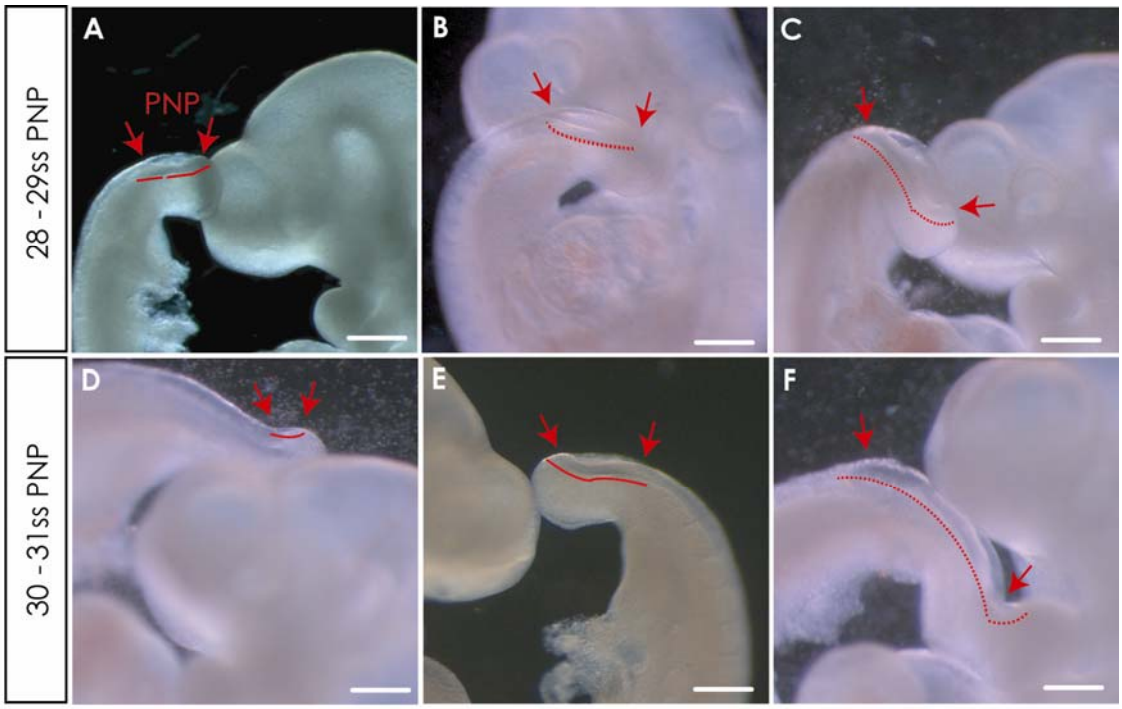

Figure 4.15 Typical appearance of different posterior neuropore (PNP) sizes during neural tube closure in *ct* sub-strains. Images of the PNP of embryos at E10.5, at the 28-29 (**A-C**) and 30-31 (**D-F**) somites stage (ss). A small PNP (SPNP; **A, D**), is characteristic of embryos in which the neural tube is closing normally. A medium (**B**, **E**) or large PNP (LPNP; **C, F**) is characteristic of embryos in which PNP closure is more likely to fail (**C**, **F**) or be delayed (**B**, **E**), leading to spina bifida and/or tail defects. PNPs are delineated by red-dotted lines and/or arrows for better visualisation **(A-F).** PNP length in μm: **A** = 375, **B** = 625, **C** = 800, **D** = 200, **E** = 500, **F** = 1050. Scale bar: 0.5 mm.

Strain	Somite stages					
	26-27		28-29		30-31	
	n	PNP (μm)	n	PNP (μm)	n	PNP (μm)
$+^{ct}$	10	307.5 ± 29.4 *	28	257.1 ± 21.6*, **	37	68.9 ± 18.9*, **,
$+^{ct;8E}$	16	385.9 ± 23.1*	15	286.7 ± 25.0*, **	14	75.0 ± 21.6*, **
ct^{9E}	5	490.0 ± 90.3	31	434.7 ± 28.8**, ‡	30	324.2 ± 55.1**, ‡
ct^{8E}	7	482.1 ± 59.7	26	478.8 ± 41.4 **	20	427.5 ± 50.3**
ct	12	581.3 ± 45.3*	64	540.2 ± 23.6*, ‡	66	453.8 ± 32.5*, ‡

Table 4.6 Mean PNP length of embryos of *ct* and the *ct*-substrains. Values are given as mean PNP length (μm) ± standard error. The somite stage intervals analysed correspond to the stage at which the PNP is closing. ANOVA (Holm-Sidak Method, p≤0.001): * at all stages, *ct* have larger PNPs than $+^{ct}$ and $+^{ct;8E}$ strains; ** from somite 28 to 31, both ct^{9E} and ct^{8E} strains also have larger PNPs than $+^{ct}$ and $+^{ct;8E}$; ‡ at somite stages 28-31, the mean PNP length of *ct* embryos is significantly larger than in the ct^{9E} strain.

Consideration of PNP lengths in individual embryos (**Fig. 4.16**) shows that in the wild-type strains ($+^{ct}$ and $+^{ct;8E}$) the PNP rapidly diminishes in length from the 28 somite stage onwards and closes in the majority of embryos at 30-31ss (25 out of 37). While the mean PNP length in the *ct* strains is larger than in the wild-type strains at the 26-27 somite stage the variation between embryos appears broadly similar. However, from the 28 somite stage onwards a considerably larger range of values is observed, particularly within the *ct* and ct^{8E} strains. Thus, at the 30 and 31 somite stages, *ct* and ct^{8E} embryos show a range of PNP lengths, from closed to as much as 1 mm long. This reflects the range of phenotypes observed in these strains. Overall, the mean PNP length observed in ct^{9E} embryos is lower than in the other *ct* strains from the 29 somite stage onwards. The distribution of PNP lengths also appears shifted to smaller values with few embryos showing very large PNP lengths, an observation which correlates with the lower frequency of spina bifida in the ct^{9E} strain compared with the *ct* and ct^{8E} strains.

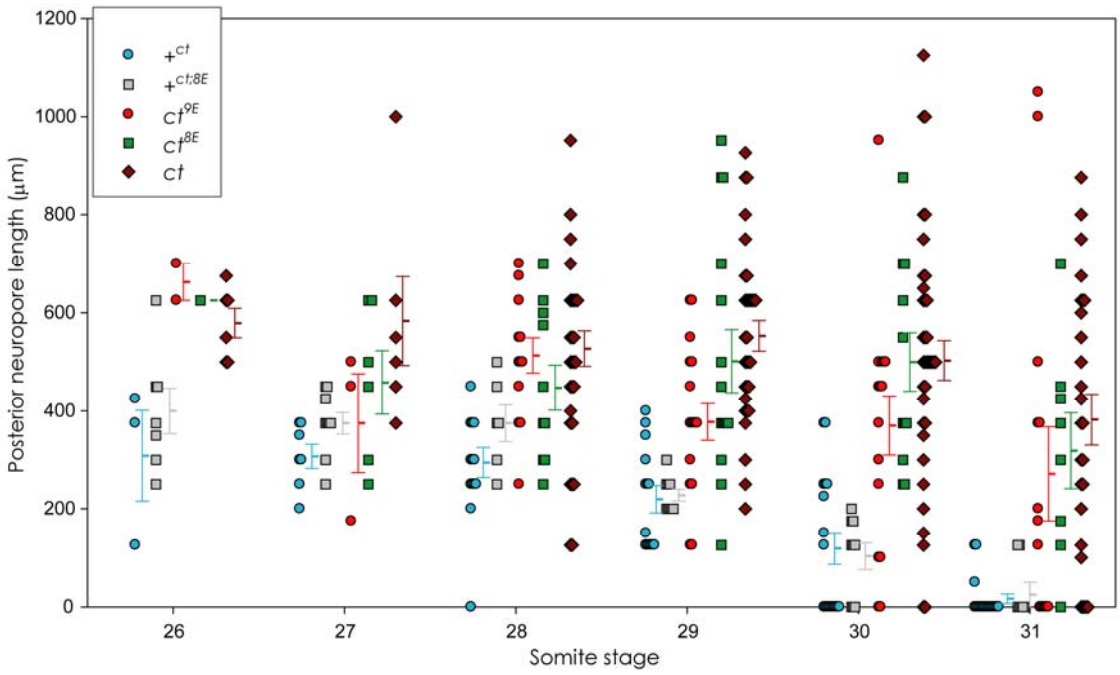

Figure 4.16 Plot of posterior neuropore length against somite stage for *ct* sub-strains. The data for individual embryos is shown, with the mean PNP length (and standard error) indicated for each strain at each stage. Number of embryos at the 26, 27, 28, 29, 30 and 31 somites stages are: for $+^{ct}$ 3, 7, 14, 14, 19, 18; for $+^{ct;8E}$ 7, 9, 6, 9, 9, 5; for ct^{9E} 2, 3, 13, 18, 16, 14; for ct^{8E} 1, 6, 11, 15, 12, 8; for *ct/ct* 6, 6, 32, 32, 39, 27.

4.2.7 Frequency of cranial NTDs in *curly tail* sub-strains

Exencephaly was observed amongst embryos of all the *ct* sub-strains. Since I was testing the hypothesis that *Lmnb1* variants can modify the frequency of NTDs in *ct*, it was of interest to investigate whether there is also an effect on the cranial defects. For that reason the frequency of exencephaly was compared among embryos collected at E10.5 of the ct^{9E}, ct^{8E} and $+^{ct;8E}$ strains (**Fig. 4.17**).

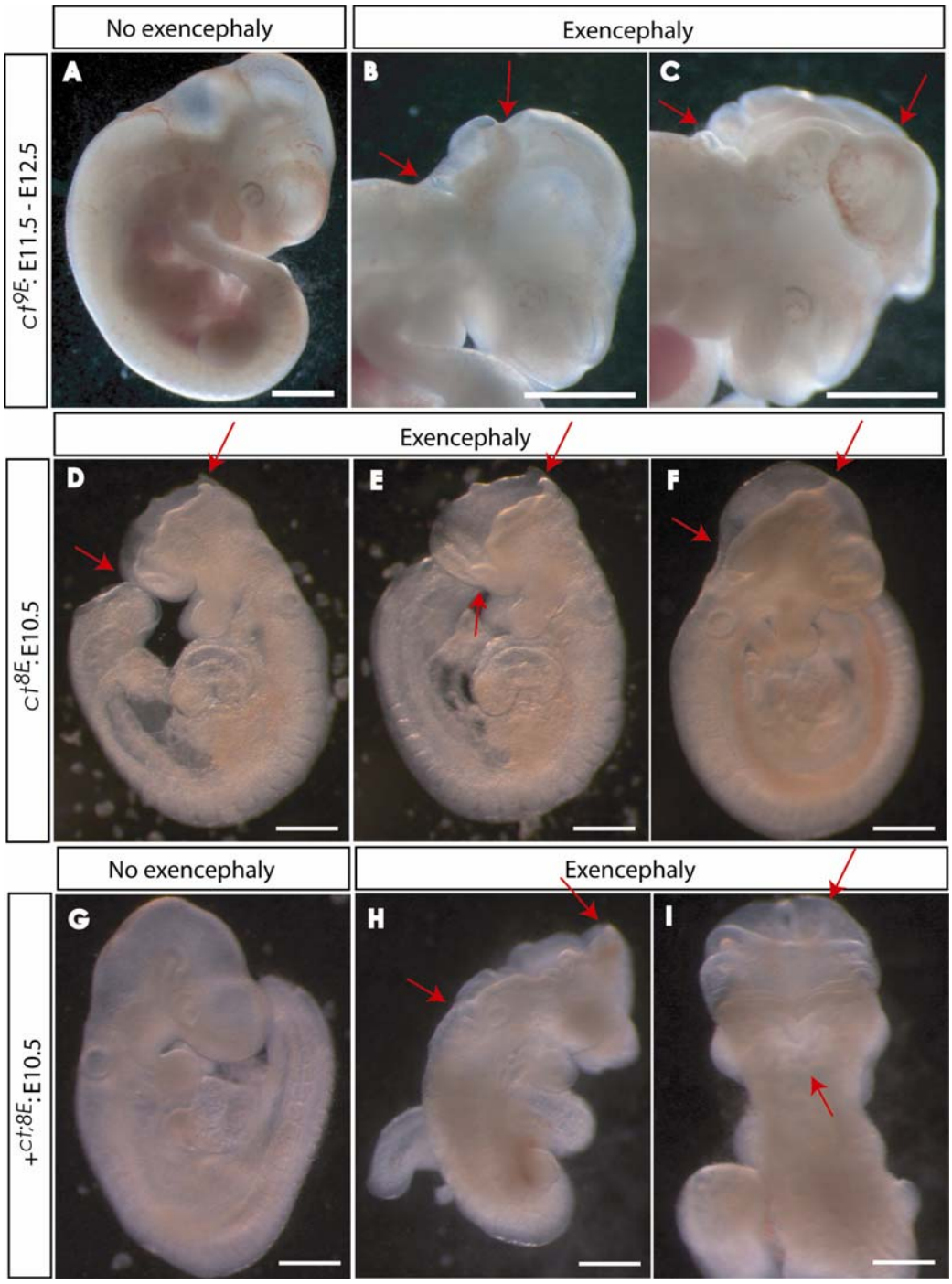

Figure 4.17 Appearance of exencephaly in *curly tail* sub-strains. (A-C) Side views of ct^{9E} embryos at E11.5-E12.5; **(D-F, G-I)** ct^{8E} and $+^{ct;8E}$ embryos at E10.5. The different types of exencephaly observed among embryos of the *ct* sub-strains reflect the range of phenotypes among *ct/ct* embryos. The neural folds may remain open in the hindbrain **(B)**, mid- and hindbrain **(C, F, H-I)** or fore- and midbrain **(D-E)** compared to normal neural tube closure (**A, G**). Panel **I**, is a back view of embryo in **H**. Red arrows indicate level and length of defect. Scale bars: 1 mm.

The ct^{9E}, ct^{8E} and $+^{ct;8E}$ strains exhibit a mix of types of exencephaly at different levels of the developing brain as summarised in **Figure 4.17**. Data collected for embryos of the *ct* sub-strains at E10.5-E15.5, showed that exencephaly occurred to some extent in each strain (**Fig. 4.18**). Exencephaly occurred at significantly lower frequency in ct^{9E} embryos (3%) compared with ct^{8E} (8.3%), representing a 63% reduction in exencephaly, similar to that observed for spina bifida. There is a small difference in the frequency of exencephaly between ct^{8E} (8.2%) and *ct* (6.4%) which was not statistically significant.

Surprisingly, 2.6% of the $+^{ct;8E}$ embryos also developed exencephaly suggesting that the presence of the 8E lamin B1 variant is sufficient to confer susceptibility to NTDs even in the absence of the *Grhl3* mutation **(Fig. 4.18).** Thus, in the context of the *curly tail* genetic background, the presence of either the *Grhl3* mutation or the 8E lamin B1 variant can cause cranial NTDs at approximately 3% frequency (ct^{9E} and $+^{ct;8E}$) while the presence of both together increases the frequency to around 6.5-8% (*ct*, and ct^{8E}) and if neither the mutation nor the 8E variant are present then cranial NTDs do not occur ($+^{ct}$).

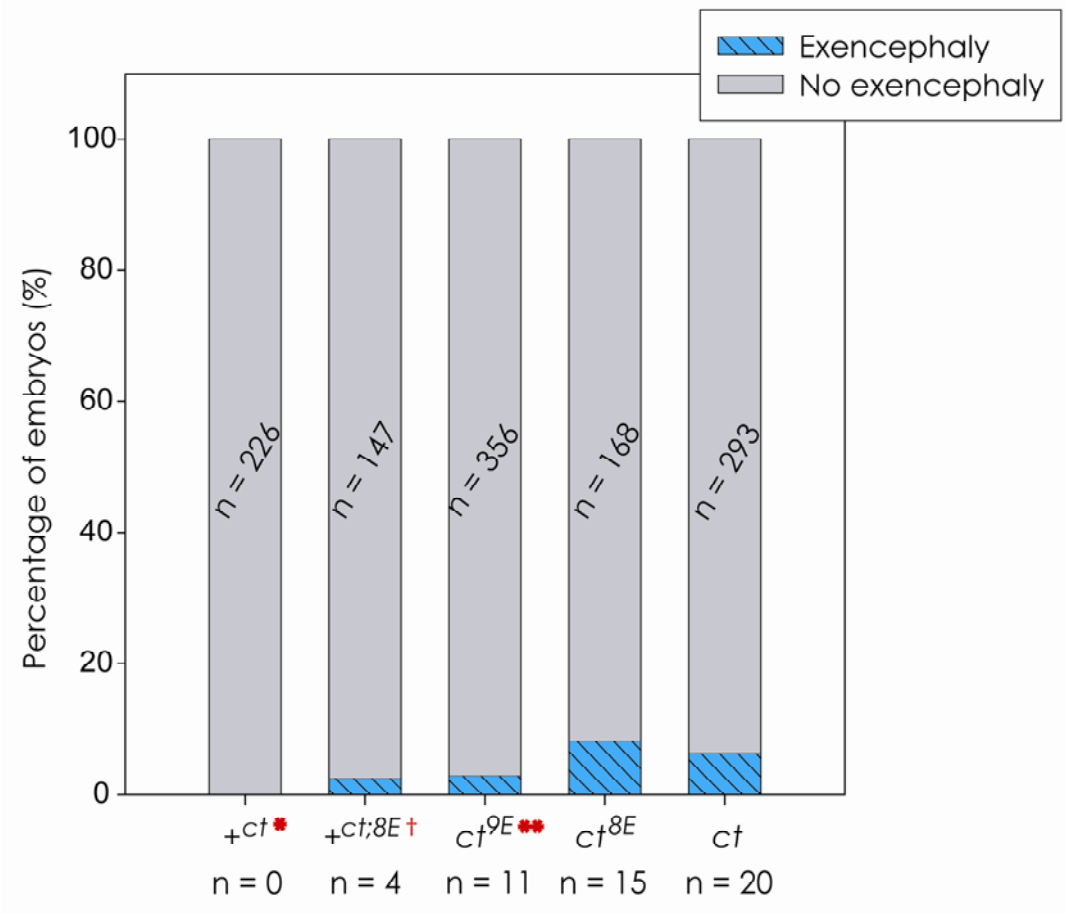

Figure 4.18 Frequency of exencephaly among embryos of the *ct* sub-strains. There is a significant variation in the frequency of exencephaly between the five strains ($p \leq 0.001$, χ^2). The frequency of exencephaly was significantly lower in $+^{ct}$, which does not develop exencephaly, compared with the other strains (* *Versus ct* and ct^{8E}, $p \leq 0.001$; *versus* ct^{9E}, $p = 0.02$, Z-test), but not with $+^{ct;8E}$. The frequency of exencephaly was significantly lower in ct^{9E} compared with ct^{8E} embryos (** p=0.01, Z-test). Exencephaly occurs at low frequency among $+^{ct;8E}$ embryos (2.6%) suggesting a possible effect of the 8E lamin B1 variant on cranial neural tube closure since exencephaly was not observed in the $+^{ct}$ strain**.** The frequency of exencephaly was significantly lower in $+^{ct;8E}$ than in ct^{8E} († p=0.049, Z-test). Number (n): underneath strain names are embryos with exencephaly; on the grey bar, n = embryos without exencephaly.

4.2.8 2D gels of ct^{9E} embryos

The analysis of *Lmnb1* polymorphisms in various mouse strains (inbred and NTD mouse models), showed that like *curly tail*, the *splotch* (Sp^{2H}) mouse strain also carries the 8 GAG repeat variant. In addition, the availability of a sub-strain of *curly tail* carrying wild-type *Lmnb1* (i.e., ct^{9E}) provided an opportunity to test if it is indeed the GAG deletion that causes the lamin B1 migration shift on 2D gels of *ct/ct* embryos (**Chapter 3, section 3.2.6.1**). Therefore, 2D gels were generated for *ct/ct*, $+^{ct}/+^{ct}$, $ct/ct^{TgGrhl3}$, ct^{9E}/ct^{9E} and $Sp^{2H}/+$ embryo samples and analysed using Progenesis SameSpots software to allow comparison of the migration of lamin B1 spots.

Lamin B1 spots on gels generated from $ct/ct^{TgGrhl3}$ and $Sp^{2H}/+$ embryos show the same pattern as on gels for *ct/ct* embryos (**Fig. 4.19**). Conversely, lamin B1 spots on gels for ct^{9E}/ct^{9E} embryos show the same migration pattern as $+^{ct}/+^{ct}$ samples. These analyses indicate that the migration pattern of lamin B1 corresponds to the presence of the 8E or 9E variant and provide further evidence that it is indeed the glutamic acid deletion which causes the shift of lamin B1 spots on the 2D gels of *ct/ct* embryos compared with $+^{ct}/+^{ct}$.

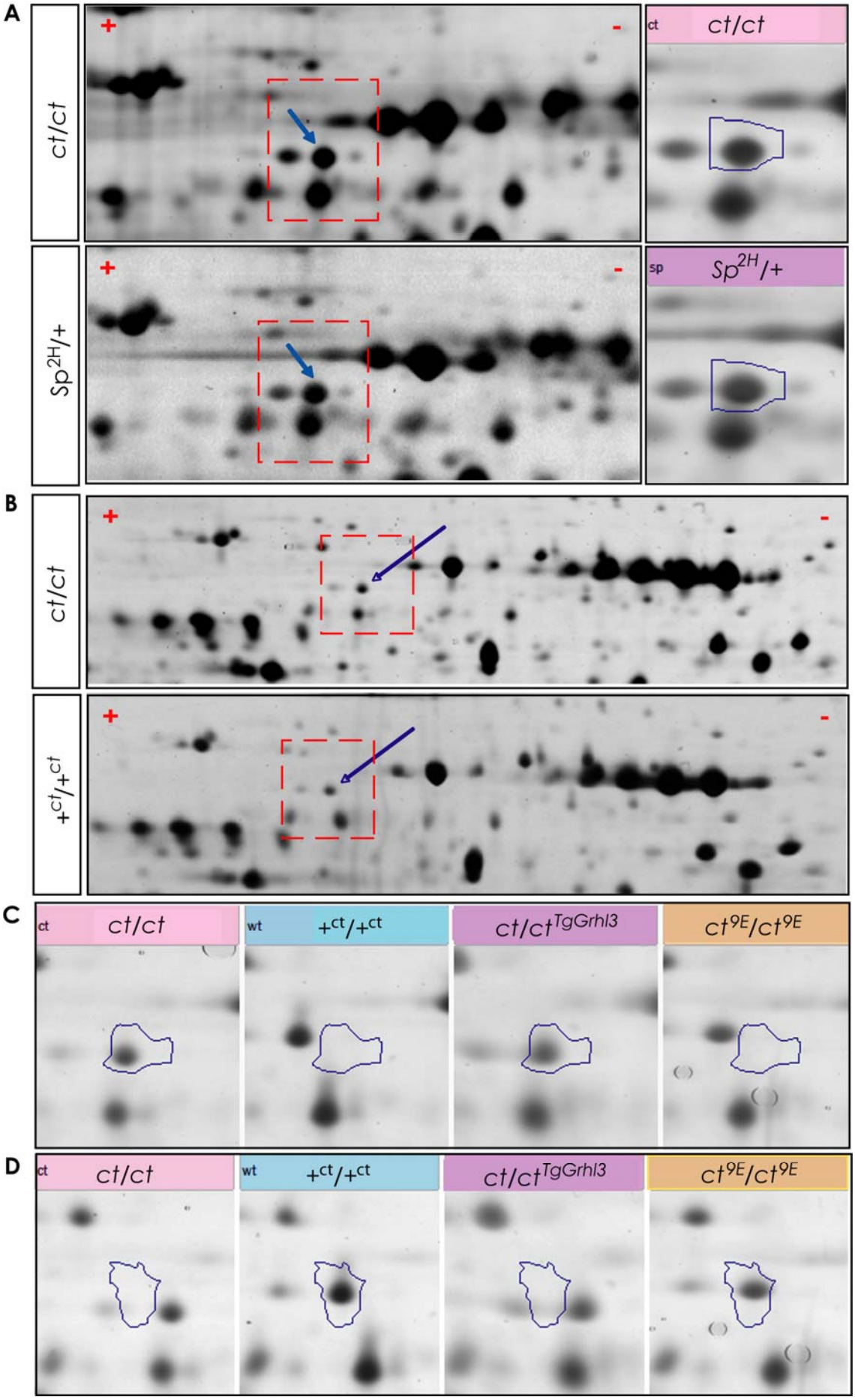
A
ct/ct
+
-
ct
ct/ct
Sp2H/+
+
-
sp
Sp2H/+
B
ct/ct
+
-
+ct/+ct
+
-
C
ct
ct/ct
wt
+ct/+ct
ct/ctTgGrhl3
ct9E/ct9E
D
ct
ct/ct
wt
+ct/+ct
ct/ctTgGrhl3
ct9E/ct9E

Figure 4.19 2D protein gel analysis of different lamin B1 variants. (**A**) 2D gels for *curly tail* (*ct/ct*) and heterozygous *splotch* (Sp^{2H}/+) embryos were generated for comparison of the spot pattern of lamin B1. Higher magnification of the area of lamin B1 spots (red boxes). Splotch embryos show the same lamin B1 pattern as *ct/ct* (blue arrow, and blue circle at higher magnification). (**B-D**) 2D gels were aligned against a *ct/ct* and a $+^{ct}/+^{ct}$ reference gel generated from embryo samples. (**B**) Enlarged region of *ct/ct* and $+^{ct}/+^{ct}$ gels in which the blue arrow indicates the most abundant lamin B1 spot (red boxes), shown circled in blue on panels **C-D. (C)** The lamin B1 spot aligns on *ct/ct* and $ct/ct^{TgGrhl3}$ gels but not with spots on gels for $+^{ct}/+^{ct}$ or ct^{9E}/ct^{9E} samples, which carry the 9E lamin B1 variant. **(D)** The lamin B1 spot (circled) aligns on $+^{ct}/+^{ct}$ or ct^{9E}/ct^{9E} but not with *ct/ct* and $ct/ct^{TgGrhl3}$ gels.

4.2.9 Lamin B1 protein localisation in the nuclei of mouse embryonic fibroblasts

It was therefore hypothesised that the mechanism by which lamin B1 variants influence risk of NTDs may relate to the apparent effect on stability of the nuclear envelope as shown by FLIP (**Section 4.2.3**). In order to further investigate the structure of the nucleus in the different mouse strains, mouse embryonic fibroblasts (MEFs) were generated from E13.5 embryos of various *ct* strains as well as the inbred strain C57BL/6.

These cells were stained by Dr Ashraf Malhas (Oxford University) with an anti-lamin B1 antibody to investigate its localisation by immunofluorescence (**Fig. 4.20**). The key finding was that *ct* nuclei showed a high degree of irregularity in terms of nuclear shape. Lamin B1 staining (green) on a proportion *ct* fibroblasts was discontinuous and even missing in certain cases (**Fig. 4.20 G-I**) reminiscent of cells with nuclear envelope abnormalities, such as from progeria models (Scaffidi and Misteli, 2005; Young et al., 2005). Staining for lamin A (**Fig. 4.20**, red) showed a similar distribution to lamin B1, indicating that the nuclear lamina as a whole is disrupted as opposed to solely an abnormality of lamin B1. This was perhaps to be expected since the nuclear lamina is a continuous meshwork so it is likely that disruption of one type of lamin will also affect the distribution of others.

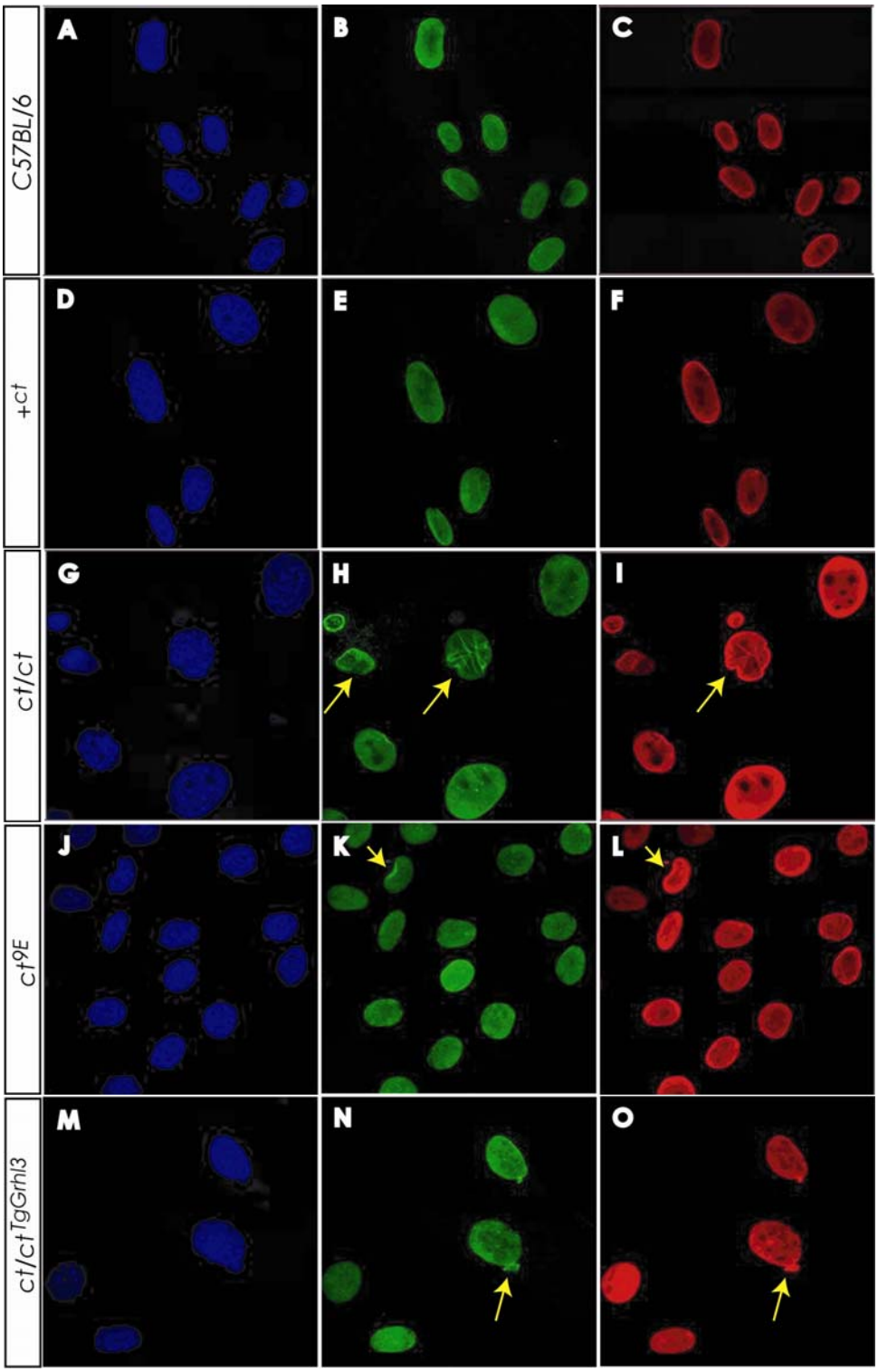

Figure 4.20 Lamin protein expression in mouse embryonic fibroblasts (MEFs). MEFs were stained with antibodies to lamins B1 (green) and A (red) and the nucleus was visualised by staining with DAPI (blue). Typical irregularities of lamin organisation are indicated by yellow arrows, and include lobulations (**H-L**), and herniations (**N-O**).

To provide a quantitative measure of the morphological observations, the contour ratio (CR = 4π x area/perimeter) of DAPI-stained nuclei (minimum 500 nuclei per strain) was analysed using MetaMorph software (by Dr Malhas, Oxford University). A lower CR indicates a more dysmorphic nucleus and a score of less than 0.7 is considered abnormal (Scaffidi and Misteli, 2005). These analyses showed statistically significant ($p<0.001$, One Way ANOVA) differences between strains. A greater proportion of *ct* strain MEFs have dysmorphic nuclei than all the other strains (**Fig. 4.21 A**), and the mean CR is correspondingly lower than for all the strains (**Fig. 4.21 B)**. These abnormalities are in association with the 8E lamin B1 variant and low *Grhl3* expression (summarised in **Table 4.7**).

In contrast to *ct* MEFs, nuclear envelope abnormalities were rarely observed among C57BL/6 cells, which were characterised by the lowest percentage of cells with CR <0.7 (**Fig. 4.20 A-C**), and the highest mean CR (**Fig. 4.21 B**). The ct^{9E} showed partial rescue of the phenotype compared with *ct* (**Fig. 4.20 J-L**), with similar proportion of abnormal nuclei and mean CR value to the $+^{ct}$ strain (**Fig. 4.21 A-B**). These results suggested that the lamin B1 variant plays a key role in determining nuclear envelope morphology. In addition these findings imply that in the presence of the wild-type form of lamin B1 (9E variant) low *Grhl3* expression does not have a major effect on nuclear structure (although still causing NTDs at a lower rate). Interestingly, the *Grhl3*-over-expressing transgenic line ($ct^{TgGrhl3}$; **Fig. 4.20 M-O**), exhibited more cells with abnormal nuclei than ct^{9E} and $+^{ct}$, in association with the presence of the 8E lamin B1 variant. However, nuclei were less abnormal than in the *ct* strain (**Fig. 4.21**), which has identical genetic background, perhaps suggesting a normalising effect of increased *Grhl3* expression on nuclear envelope integrity. Overall, these data suggest that the combination of 8E lamin B1 variant and diminished *Grhl3* expression has the most deleterious effect on nuclear morphology, which correlates with the highest risk of NTDs in embryos.

The finding of more frequent nuclear envelope abnormalities in each of the *ct* strains, including $+^{ct}$, than in C57BL/6 suggests that in addition to the lamin B1 variant there might be another underlying factor, characteristic of the *ct* genetic background, which compromises nuclear structure. Indeed, there is evidence that the genetic background

present in both $+^{ct}$ and *ct* strains includes factors that give susceptibility to folate-deficiency induced NTDs (Burren et al., 2010).

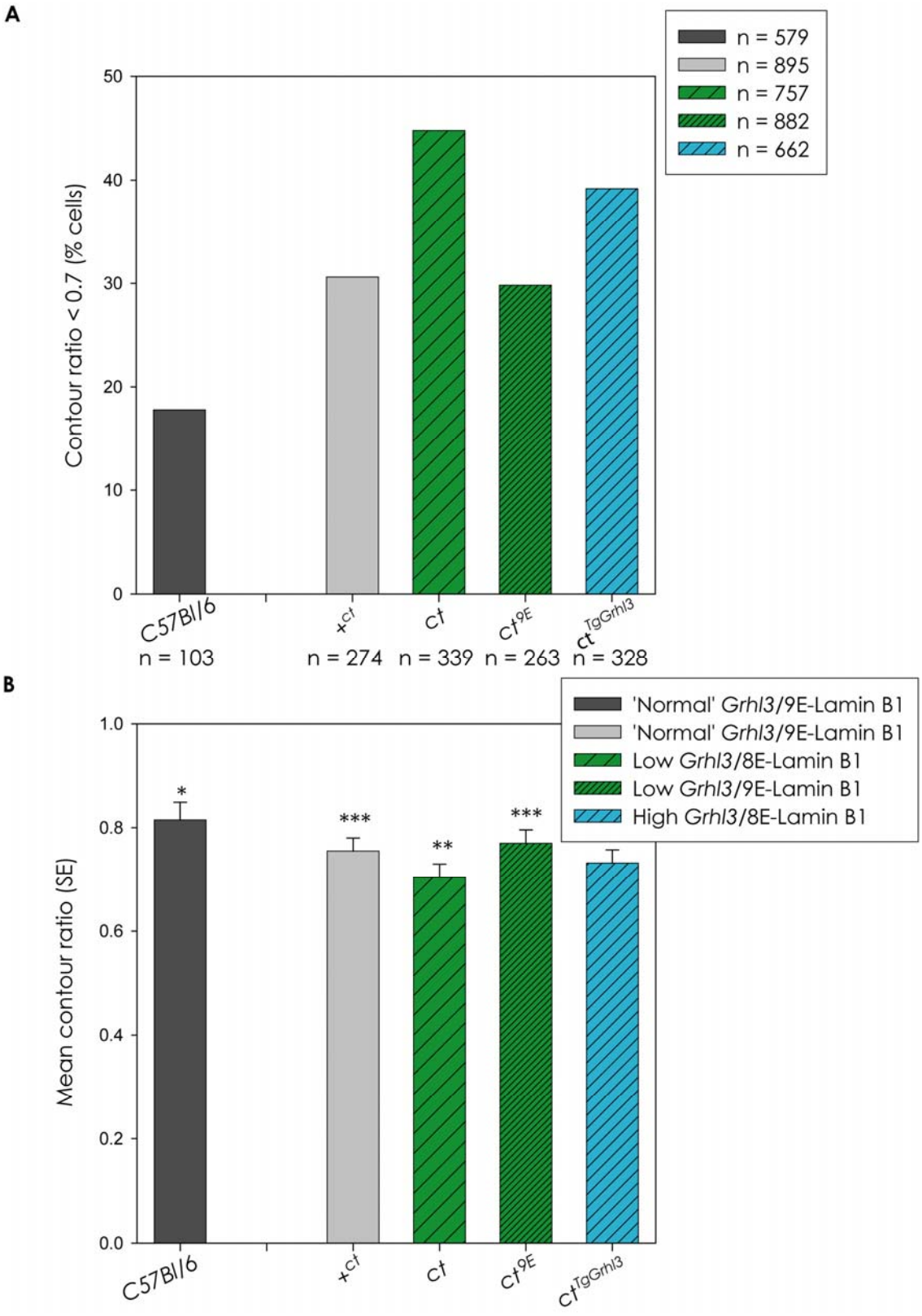

Figure 4.21 Contour ratio of nuclei in MEFs derived from mouse strains carrying 9E or 8E lamin B1 variants. (A) Analysis of the percentage of cells with contour ratio lower than 0.7 shows that the *ct* strain has significantly higher frequency of dysmorphic nuclei than all other strains (44.78%), whereas significantly fewer *C57BL/6* (17.79%) nuclei are dysmorphic compared with all other strains ($p \leq 0.001$, $\chi 2$). Frequency was calculated by dividing the number of cells with ratio <0.7 ("n=", underneath strain names) by the total number of cells (inset). **(B)** Mean contour ratio (CR) and standard error on MEFs. *C57BL/6* (*) have higher mean CR than all other strains whereas *ct* (**) have lower mean CR value than all other strains. Wild-type ($+^{ct}$, ***) and ct^{9E} (***) have higher mean CR than $ct^{TgGrhl3}$ MEFs. One Way ANOVA and Pairwise Multiple Comparison Procedures (Holm-Sidak method), $p \leq 0.001$.

Strain	**Lamin B1**	***Grhl3***	**Background**	**Nuclear morphology**
C57BL/6	9E	Normal	*C57BL*	*'Normal'*
$+^{ct}$	9E	Normal	*SWR/ct*	*Mildly dysmorphic*
ct	8E	Low	*ct*	*Highly dysmorphic*
ct^{9E}	9E	Low	*SWR/ct*	*Mildly dysmorphic*
$ct^{TgGrhl3}$	8E	High	*ct*	*Dysmorphic*

Table 4.7 Summary of nuclear morphology in relation to Lamin B1 variants, *Grhl3* expression and genetic background for strains for which mouse embryonic fibroblasts were generated.

4.2.10 Analysis of *Lmnb1* region on chromosome 18 in the *ct* strain

Sequencing of the *Lmnb1* gene revealed differences between the *ct* and the $+^{ct}$ strains. The *Lmnb1* gene is on a different chromosome to *Grhl3* and would therefore be expected to be the same sequence in the congenic $+^{ct}$ strain as in the *ct* strain owing to backcrosses to *ct* during the production of this strain (as explained in **Chapter 2; section 2.1.1**). However, it is possible that small areas of DNA from the SWR strain, from which the wild-type *Grhl3* allele was introduced, persist in the $+^{ct}$ background at

locations other than the *Grhl3* locus, which would explain how sequence differences in *Lmnb1* could be present. Hence, polymorphic markers on chromosome 18 upstream and downstream of the *Lmnb1* gene (**Fig. 4.22 A; Appendix B, Table B.10**) were typed to investigate how much of the *SWR* inbred strain persists in the $+^{ct}$ strain. Fifty seven microsatellite markers were tested of which fifteen markers were informative, in that the microsatellite size differed between *SWR* and *ct* (**Fig. 4.22 B**). Eight of those differed between SWR and the $+^{ct}$ strains, showing that the *ct* sequence is present in $+^{ct}$ (**Fig. 4.22 B**). Thus, seven markers were informative and differed between $+^{ct}$ and *ct*, *D18Mit200*, *84*, *194*, *237*, *36*, *185* and *141*. These markers lie within a region from mega base (Mb) 32.47 to 73.8 (between markers *D18Mit88* and *D18Dev1*, respectively) including *Lmnb1* (at 56.59 Mb). This region of approximately 41 Mb encompasses the region on chromosome 18 that could differ between $+^{ct}$ and *ct*.

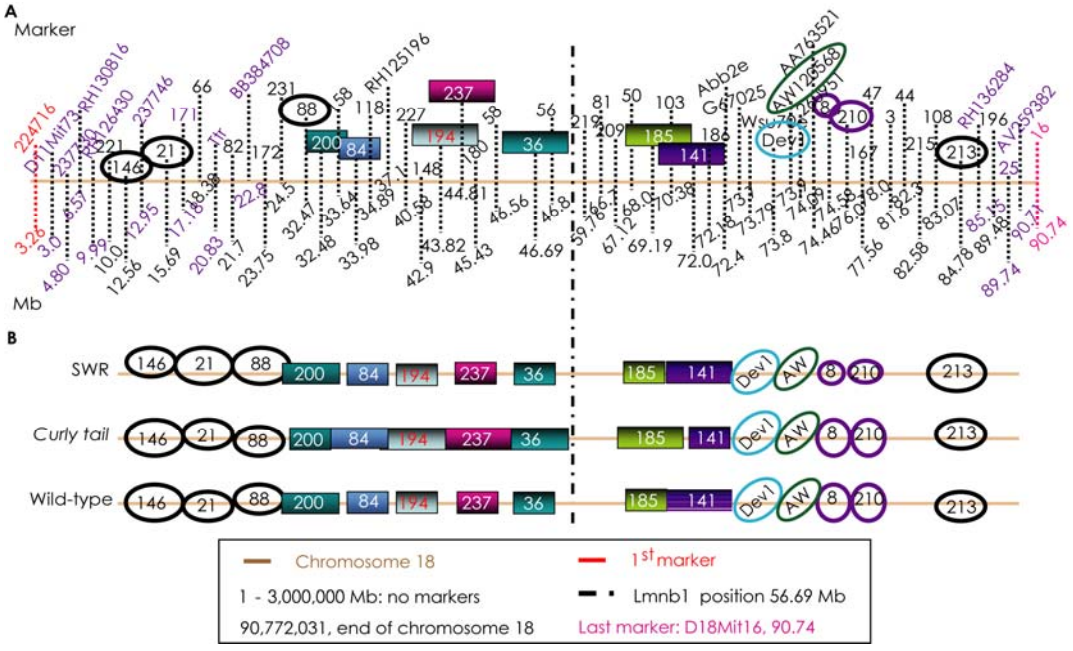

Figure 4.22 Schematic of chromosome 18 markers used to evaluate the contribution of SWR and *ct/ct* DNA in the $+^{ct}/+^{ct}$ strain. (A) The map positions of chromosome 18 microsatellites are shown in relation to *Lmnb1* gene (not to scale). The beige straight line demarks chromosome 18, with names of markers above the line (D18Mit… unless indicated), and the position on chromosome 18 in mega bases (Mb) underneath. **(B)** Of the fifty seven markers used, fifteen were informative, i.e., differed between *SWR* and the *ct/ct* strain. Eight markers differed between *SWR* and $+^{ct}/+^{ct}$ but were indistinguishable in $+^{ct}/+^{ct}$ and *ct/ct*: D18Mit146, 21, 88, Dev1, AW120568, D18Mit8, D18Mit210, and D18Mit213

(shown within circles). Seven markers differed between $+^{ct}/+^{ct}$ and *ct/ct*: D18Mit200, 84, 194, 237, 36, 185 and 141 (shown by the coloured squares). The first and the last chromosome 18 markers were not used in this analysis.

Further to this analysis (**Fig. 4.22**), I also used the same informative chromosome 18 markers to genotype *ct* sub-strains (**Fig. 4.23**). These analyses revealed that strains carrying the 8E lamin B1 variant like *ct* ($+^{8E;ct}$ and ct^{8E}) type for the same markers across this region, whereas the ct^{9E} strain shares the same 'SWR' regions as $+^{ct}$.

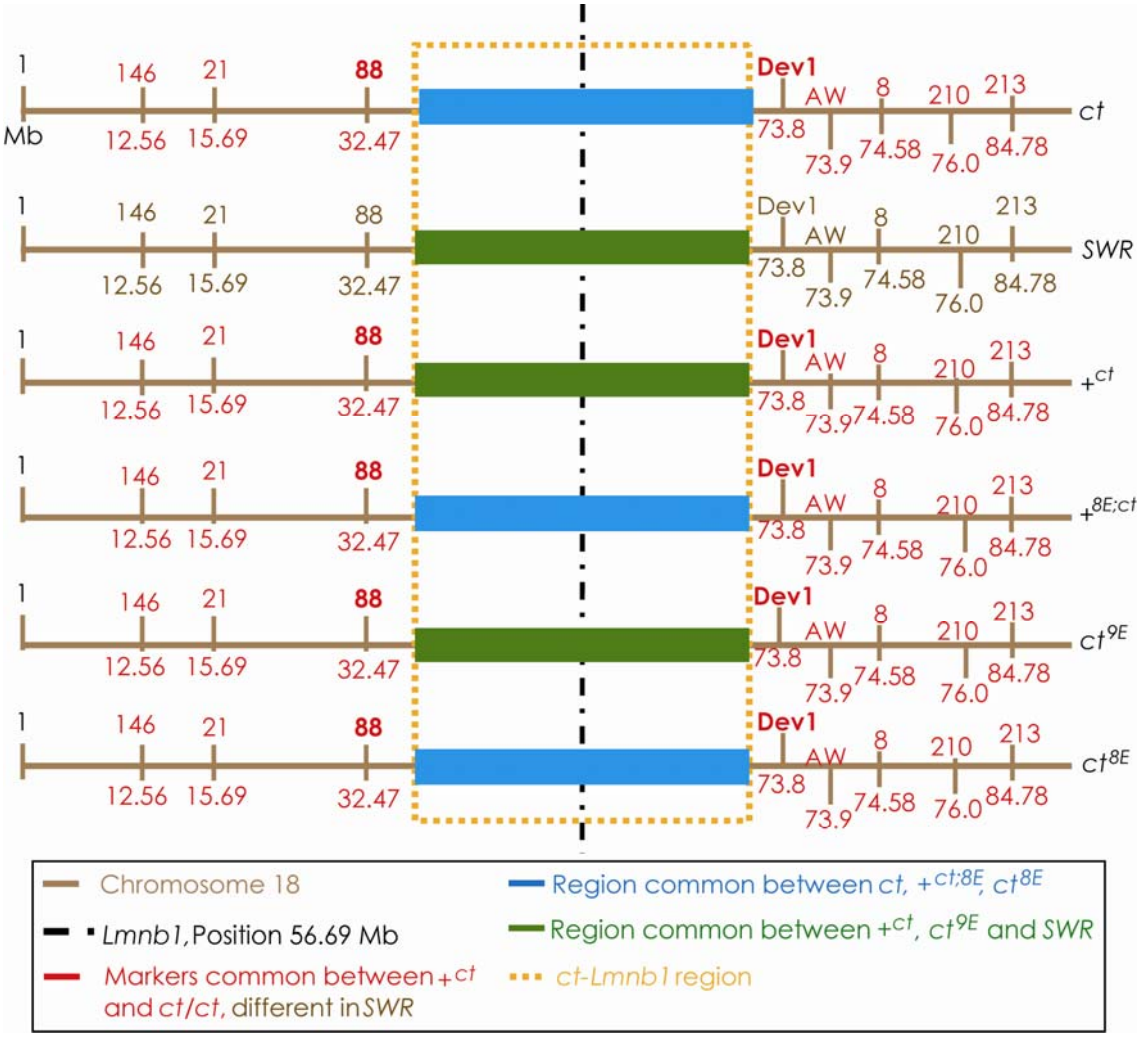

Figure 4.23 Schematic of the region of chromosome 18 encompassing *Lmnb1* in the *ct*-sub-strains. A 41 Mb region of chromosome 18 is shared by *ct,* $+^{8E;ct}$ and ct^{8E}. Conversely, this same region in $+^{ct}$ and ct^{9E} types as SWR.

One possible implication of the fact that a region of SWR genomic DNA on chromosome 18 is retained in the ct^{9E} strain is that modifier genes other than lamin B1 could also lay within this region. As a step towards addressing this issue the list of genes within the 41 Mb chromosome 18 region was used to interrogate data obtained from a microarray analysis of the caudal region of 28-29 somite stage *ct/ct* and $+^{ct}/+^{ct}$ embryos (Dr N. Greene, Personal Communication). It was reasoned that if genes from this region differ in expression between *ct* and $+^{ct}$ strains, this could be due to the fact they are downstream targets of *Grhl3*, or that this is a consequence of the local genomic sequence. In the latter case these genes would also be candidates to differ in expression between the ct^{8E} and ct^{9E} strains and potentially contribute to variation in the frequency of NTDs.

A list of genes within the 41 Mb of the chromosome 18 *Lmnb1*-region was downloaded from UCSC Genome Bioinformatics site (http://genome.ucsc.edu) and compared to a list of genes that differ in expression between *curly tail* and wild-type by 1.5-fold or greater ($p<0.05$). Nine genes were common between the two lists (**Table 4.8**).

Gene Symbol	Gene name	*Curly tail*	Array fold change	p-value
Matr3	*Matrin 3*	Down regulated	2.3	0.01
Rnf14	*Ring finger protein 14*	Up regulated	1.8	2.34E-05
Isoc1	*Isochorismatase domain containing 1*	Down regulated	3.5	0.02
A730017C20Rik	*RIKEN cDNA A730017C20 gene*	Down regulated	5.9	4.04E-05
Tcof1	*Treacher Collins Franceschetti syndrome 1, homolog*	Down regulated	1.7	0.007
Grpel2	*GrpE-like 2, mitochondrial*	Down regulated	1.9	0.006
Apcdd1	*Adenomatosis polyposis coli down-regulated 1*	Up regulated	1.5	0.04
Tubb6	*Tubulin, beta 6*	Up regulated	1.5	0.005
4930503L19Rik	*Putative uncharacterized protein*	Down regulated	1.7	0.04

Table 4.8 Genes from the chromosome 18-*Lmnb1* region that differ in expression between *curly tail* and wild-type. Microarray analysis was performed

using Affymetrix MOE430v2 arrays with data processing using GeneSpring (Version 11). Fold change indicates expression in wild-type relative to *curly tail* samples (for down-regulated genes) or vice-versa (for up-regulated genes).

Primers were designed for seven of these genes in order to investigate levels of expression by qRT-PCR using ct^{9E} and ct^{8E} cDNA as template (**Appendix B, Table B.11**). For each gene, the level of expression was normalised to a ct^{9E} sample. For the majority of these genes no statistically significant differences in expression were detected between ct^{9E} and ct^{8E}, suggesting that the expression difference between *ct* and $+^{ct}$ may be a consequence of difference in *Grhl3* expression (and may be worthy of further investigation in this context). However, there was a small but statistically significant down-regulation in ct^{8E} of the unannotated RIKEN EST, *A730017C20* (**Table 4.9**), which is predicted to encode a transmembrane protein. Given the small fold-change in expression level the biological significance of this finding is unclear.

Gene Symbol	Gene name	Ct^{8E}	Fold change	p-value
Matr3	*Matrin 3*	Down regulated	1.1	Not significant
Isoc1	*Isochorismatase domain containing 1*	Up regulated	1.1	Not significant
A730017C20Rik	*RIKEN cDNA A730017C20 gene*	Down regulated	1.2*	0.02
Tcof1	*Treacher Collins Franceschetti syndrome 1, homolog*	Down regulated	1.6	Not significant
Grpel2	*GrpE-like 2, mitochondrial*	Down regulated	1.1	Not significant
Apcdd1	*Adenomatosis polyposis coli down-regulated 1*	Up regulated	1.3	Not significant
Tubb6	*Tubulin, beta 6*	Up regulated	1.2	Not significant

Table 4.9 Comparison of expression of seven genes from the chromosome 18 *Lmnb1* region in ct^{9E} and ct^{8E} strains by qRT-PCR. Three individual embryo samples were used for each strain. None of the differences were significant with the exception of *A730017C20* (* $p<0.02$, t-test). Fold change indicates expression in ct^{9E} relative to ct^{8E} samples (for down-regulated genes) or vice-versa (for up-regulated genes).

4.3 Discussion

Lamin B1 represented a good candidate to play a role in influencing the risk of NTDs in *curly tail* embryos for several reasons. A defect in this protein could have an effect on its function in cell cycle progression and maintenance of nuclear shape and thereby contribute to the proliferation defect in *curly tail* embryos (**Section 4.1**). In addition, alteration of lamin B1 protein structure could affect its binding to chromatin or transcription factors, thereby affecting regulation of gene expression.

It was interesting to find that the migration change of lamin B1 protein on 2D gels of *ct/ct* embryos resulted from a genetic variation in the coding sequence of *Lmnb1*, resulting in the loss of a glutamic acid (E) in a region of nine repeats (polyglutamic acid tract) in the tail domain of the protein. The crystal structure of the mouse protein lamin B1 has not yet been described, but the crystal structure of human lamin-B1 was recently published (Protein Data Bank Japan, http://www.pdbj.org/pdb_nc/pdb3hn9.ent). However, the published structure does not extend beyond amino acid 548, whereas the E repeats are located at amino acids 552-559. It was therefore not possible to verify what type of 3D structure the eight glutamic acids would be present in, or to predict how the variation in number of Glu residues (as observed in different mouse strains) could affect tertiary structure. Having said that, polyglutamic acid tracts are known to become increasingly alpha-helical when interacting with phospholipid membranes. A tract length difference of one residue could therefore be important. It could induce local curvature owing to the almost hundred-degree rotational shift in the orientation of the distal portion of the protein sequence (Mori et al., 1977; Subramanian et al., 2000; Agresti et al., 2008). In lamin B1, the polyglutamic acid tract is situated in the tail domain of the protein, which is short and contains another strong membrane interactor (the farnesylcysteine) with a specific orientation. In consequence, a difference in tract length of a single residue (E deletion) could be hypothesized to lead to a dramatic loss of a stable membrane association. Functional testing of the lamin B1 variants by FLIP confirmed that the 8E variant could compromise stability of the nuclear lamina. The generation of *ct* sub-strains carrying combinations of the *Lmnb1* polymorphisms and the *Grhl3* mutation, strongly suggested that *Lmnb1* could act as a modifier gene which affects the risk of NTDs in *curly tail* (summarised in **Table 4.10**).

Strain	Lmnb1	*Grhl3*	Phenotype
ct	8E	Mutation	Spina bifida, tail defects
ct^{9E}	9E	Mutation	Less frequent spina bifida, tail defects
$+^{ct;8E}$	8E	Wild-type	Infrequent tail defects
$+^{ct}$	9E	Wild-type	No defects

Table 4.10 Phenotype of *ct*-substrains in relation to *Lmnb1* polymorphism and the *Grhl3* mutation.

Analysis of the frequency of NTDs observed in ct^{9E} and ct^{8E} embryos suggested that *Lmnb1* might be a major modifier, with an effect on the frequency of spina bifida as well as exencephaly. Although exencephaly occurs at much lower frequency than spina bifida, *Lmnb1* variation affected the penetrance of both defects to the same extent with a 63% reduction in frequency in ct^{9E}. Thus, although both the ct^{9E} and ct^{8E} strains carry the *ct* mutation which results in diminished *Grhl3* expression, a 'wild-type' Lmnb1 (9E) lessens the effect on neural tube closure. Even so, embryos carrying the *Grhl3* mutation can develop spina bifida even when wild-type *Lmnb1* (ct^{9E}-strain) is present. Conversely, reinstatement of *Grhl3* expression rescues spina bifida and tail defects independently of *Lmnb1*, since *Grhl3* transgenic ($ct^{TgGrhl3}$) embryos show the same lamin B1 2D gel pattern as *ct* (8E), but do not develop spinal NTDs (Gustavsson et al., 2007). On the other hand, embryos that are wild-type for *Grhl3* but which carry the *Lmnb1* polymorphism ($+^{ct;8E}$) can develop occasional tail flexion defects. It is therefore apparent that *Grhl3* is the major *curly tail* gene, but the penetrance of resulting NTDs is influenced by lamin B1 function. In summary, this study suggests that *Lmnb1* is a major modifier gene influencing the risk of NTDs in *curly tail* embryos.

Lamin B1 is known to play a role in the size and shape of the nuclear lamina during the cell cycle (Hutchison, 2002a). Lamin B1 plays a direct role in the reassembly of nuclear components after mitosis. In addition, differently from other lamins, this protein is stably associated with membrane vesicles even during mitosis (Hutchison et al., 1994). The *in vitro* studies described here are supportive of the hypothesis that disturbance of lamin B1 function can affect the nuclear lamina in general. I hypothesise that this could

lead to disturbances of the cell cycle and contribute to the proliferation defect which has been detected in the hindgut and notochord in *ct/ct* embryos (Copp et al., 1988a; Copp et al., 1988b). Studies on exencephaly in *curly tail* are suggestive of a temporary reduction in cell proliferation rate at the cranial level at the time of neural tube closure (Seller and Perkins, 1986). Fibroblasts generated from the *Lmnb1* gene-trap mouse mutant, a mutation which results in lack of a portion of the rod domain, the nuclear localisation signal and the CAAX motif, display striking nuclear dysmorphology and reduced proliferation (Vergnes et al., 2004). The mutant embryos ($Lmnb1^{\Delta/\Delta}$) are smaller and have abnormal curvature of the spine compared to their littermates, as well as abnormalities at the cranial level. It could be hypothesised that there would be an increase in the frequency of NTDs in double homozygous *ct/ct;*$Lmnb1^{\Delta/\Delta}$ compared to *ct/ct*.

Lamin B1 mutant MEFs ($Lmnb1^{-/-}$; Vergnes et al., 2004), which lack full-length lamin B1, have a higher proliferation rate than wild-type *Lmnb1* fibroblasts. It is not clear how this increased proliferation relates to the *in vivo* phenotype in which there appears to be diminished cell proliferation, with smaller pups that die perinatally. Unlike the *Lmnb1* mutant the levels of expression of *Lmnb1*/lamin B1 do not appear to be deficient in *curly tail* embryos. Nevertheless, in the future, it would be interesting to investigate cell cycle progression and the proliferation rate in the MEFs of the *curly tail* strains. An initial approach could involve culture of *curly tail* 9E and 8E MEFs, with counting of total cell number immediately after plating and then at twenty four hour intervals. Such an approach may reveal differences in proliferation rate or defects such as premature senescence. In another experiment, *curly tail* 9E and 8E MEFs could be treated with EdU (5-ethynyl-2'-deosyuridine) which allows detection of cells that are in S-phase. Quantification of stained cells may reveal differences in the proportion of cells in S-phase, indicative of differential proliferation rate.

Another possible mechanism by which the 8E lamin B1 variant could modify the *curly tail* phenotype might involve abnormal interaction between the lamin B1 8E variant and nuclear envelope binding partners. Weaker association between lamin B1 and chromatin and/or transcription factors could affect regulation of gene expression (Malhas et al., 2007; Malhas et al., 2009), and thereby contribute to disease pathogenesis. It is not known whether *Grhl3* interacts with lamin B1/*Lmnb1* or if they share interacting

partners. To date, the functional role and downstream mediators of *Grhl3* in neural tube closure are still undetermined. At present it is difficult therefore to predict: (**i**) whether *Lmnb1* mutations would alter expression of genes that are also *Grhl3* targets, or (**ii**) whether *Lmnb1* and *Grhl3* mutations would result in independent transcriptional effects that summate to enhance the cellular defects in *curly tail* embryos (**Fig. 4.24**).

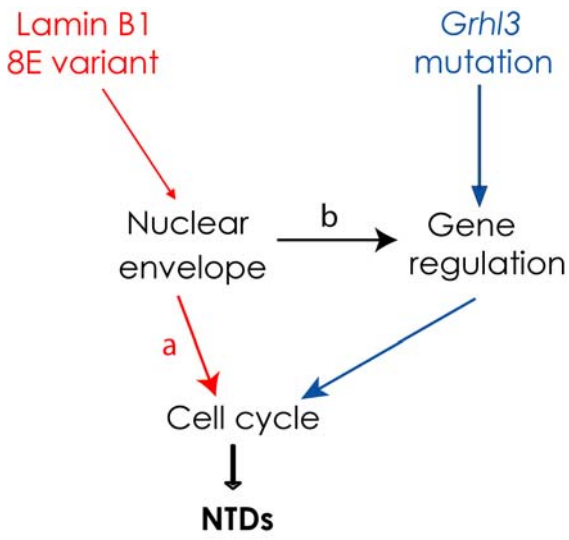

Figure 4.24 Summary. Diagram summarising possible mechanisms by which the 8E lamin B1 variant could modify risk of NTDs in *curly tail* mice. The *Grhl3* mutation is assumed to affect expression of downstream target genes, ultimately leading to reduced cell proliferation and NTDs. The lamin B1 8E variant could directly affect cell cycle regulation (a) owing to abnormal stability of the nuclear envelope. The lamin B1 8E variant could also result in defects of the nuclear envelope associations with chromatin or directly with transcription factors, leading to altered gene regulation (b) and enhancement of the *ct* phenotype.

Chapter 5

Over-expression of *Grainyhead-like-3* in mouse embryos

5.1 Introduction

Spinal NTDs occur in *Grhl3* null embryos, generated by gene targeting, and *curly tail* embryos, which carry a hypomorphic allele of *Grhl3* (Ting et al., 2003a; Gustavsson et al., 2007). Over-expression of *Grhl3* in *curly tail Grhl3*-transgenic mice ($ct^{TgGrhl3}$) prevents the development of spinal NTDs. These studies show that sufficient levels of *Grhl3* are essential for neural tube closure in the mouse.

In *Drosophila*, loss of GRH function causes late embryonic lethality, embryos have flimsy cuticles, grainy and discontinuous head skeletons and patchy tracheal tubes (Bray and Kafatos, 1991a). Moreover, a mutant lacking the GRH activation domain acted as a dominant-negative inhibitor of GRH activation in cultured cells, by forming inactive heterodimers with the full-length protein (Attardi et al., 1993). However, gain of function experiments, involving over-expression of GRH in the embryo or larva also suggest that excessive GRH is harmful during multiple stages of the *Drosophila* life cycle, resulting in 46% mortality, compared with 0% mortality in the wild-type control strain. In addition, over-expression of the dominant-negative protein (transgenic NΔ447) also had severe consequences, causing 83% mortality (as measured by unhatched embryos; Attardi et al, 1993). Transgenic embryos over-expressing full-length GRH that failed to hatch presented several defects including abnormal cuticle, and remained curved with failure to elongate during the dorsal closure stage of development (dorsal hole). The latter is a phenotype characterised by failure of contact and fusion of the epidermis at the dorsal midline. Interestingly, NΔ447 embryos did not develop these defects even though there was a high rate of mortality. Attardi et al (1993) concluded that over-expression of either the wild-type or dominant negative protein disturbed development by different mechanisms, resulting in the differences in the phenotypes of the two strains.

These observations raise the question of whether excessive expression of *Grhl3* might also have a deleterious effect in the mouse. In the literature, in the context of neurulation, the low-density lipoprotein receptor-related protein 6 (Lrp6, a coreceptor for Wnt ligands) is one example in which opposing changes in the gene function both cause NTDs during neural tube closure (Harris and Juriloff, 2007). *Lrp6* null mutant

embryos, with no protein function, exhibit exencephaly and/or spina bifida (Pinson et al., 2000). A hypomorphic mutation of *Lrp6*, *ringelschwanz* (*rs*), which retains partial protein function, results in spina bifida only (in approximately 70% of the homozygotes; (Kokubu et al., 2004). Conversely, *crooked tail* (*Cd*) mutant embryos, which carry a gain-of-function mutation in *Lrp6* develop only exencephaly (at 20-30% frequency; (Carter et al., 2005).

The $ct^{TgGrhl3}$ BAC transgenic mouse provides an opportunity to test the hypothesis that over-expression of *Grhl3* may have deleterious effects on embryonic development. To date, only embryos carrying a single copy of the BAC have been generated. Therefore, by intercrossing 'single' transgenic mice, with the BAC present at a single locus, it should be possible to generate embryos carrying double the dosage of the BAC. It was previously shown that $ct^{TgGrhl3}$ embryos express higher levels of *Grhl3* mRNA, by approximately 2-6 fold, than in *curly tail* embryos, at all stages examined (Gustavsson et al., 2007). Embryos with double the dosage of the BAC ($ct^{TgGrhl3}/ct^{TgGrhl3}$) would carry the BAC in homozygosity, and therefore be predicted to show double the level of *Grhl3* expression from the BAC compared to $ct^{TgGrhl3}$ embryos, in addition to expression from the endogenous *Grhl3* locus.

5.2 Results

5.2.1 Intercrosses between *curly tail*-transgenic mice to generate embryos that over-express *Grhl3*

To generate transgenic *Grhl3*-expressing mice, *curly tail* (*ct/ct*) mice were crossed to BAC positive ($ct/ct^{TgGrhl3}$) mice. In these crosses the BAC is present in hemizygous state (one insertion site; **Figure 5.1 A**), and embryos were always normal with respect to spinal neural tube development (as reported by Gustavsson et al, 2007). In order to investigate the effect of over-expression of *Grhl3*, male and female $ct/ct^{TgGrhl3}$ mice were intercrossed (**Fig. 5.1 B**).

Embryos were collected at stages between E10.5 and E18.5 and genotyped for the presence or absence of the BAC containing the intact *Grhl3* gene (**Chapter 2, section 2.4.1**). All samples were also genotyped for the C-21350T polymorphism in which transgenic embryos are expected to show both *ct/ct* and wild-type (from the BAC) genotypes, whereas non-transgenic samples only exhibit the *ct/ct* (T) allele (**Chapter 2, section 2.4.2**). The number of embryos collected at different stages of development is summarised in **Table 5.1**. At all stages the frequency of BAC-negative (*ct/ct*) and BAC-positive ($ct/ct^{TgGrhl3}$ and $ct^{TgGrhl3}/ct^{TgGrhl3}$) embryos did not significantly differ from the predicted Mendelian ratio, 1:3. Therefore, it appears unlikely that over-expression of *Grhl3* results in embryonic lethality (**Table 5.1**).

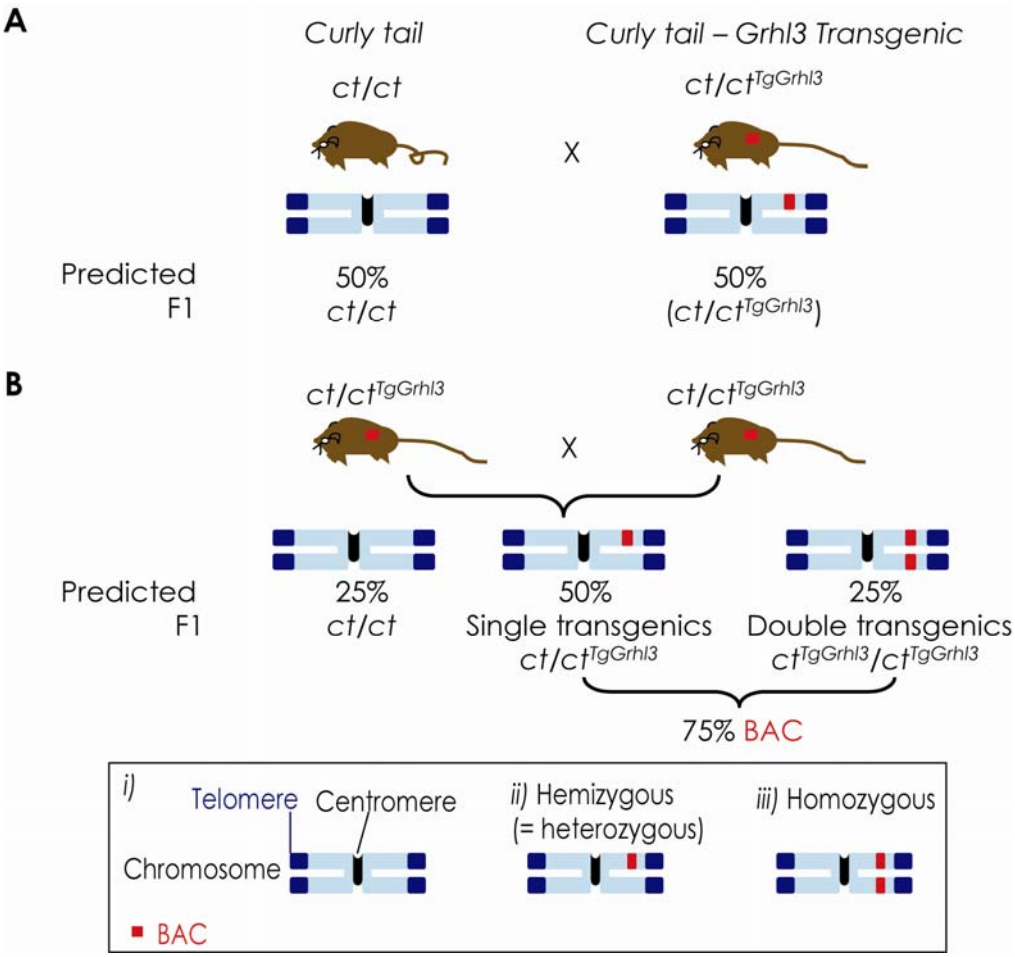

Figure 5.1 Schematic of the genetic crosses to generate *Grhl3*-homozygous transgenic embryos. (A) Diagram of genetic crosses between *ct/ct* and *ct/ct*^{TgGrhl3} mice to generate *Grhl3*-single transgenic mice. In these crosses the BAC is present in hemizygous state, and the expected proportion of F1 offspring is 50% *ct/ct* and 50% transgenic (1:1). **(B)** Diagram of genetic intercrosses between *ct/ct*^{TgGrhl3} mice to generate homozygous transgenics, the expected proportion of F1 offspring is: 25% *ct/ct*, 50% 'single' transgenic and 25% 'double' transgenic. Overall, it is expected that 75% of these mice carry the BAC (1:3, BAC-negative: BAC-positive).

Developmental Stage	No. Embryos	No. Bac^{-ve} embryos	Frequency	No. Bac^{+ve} embryos	Frequency
E10.5	316	81	25.6%	235	74.4%
E11.5 –E13.5	49	13	26.5%	36	73.5%
E14.5 – E16.5	109	30	27.5%	79	72.5%
E17.5 – E18.5	80	15	18.8%	65	81.3%
Total	**554**	**139**	**25.3%**	**415**	**74.7%**
Expected frequency			**25%**		**75%**

Table 5.1 Frequency of BAC negative and positive embryos collected from *Grhl3*-transgenic *curly tail* intercrosses. All embryos were collected between embryonic days 10.5 and 18.5, and scored for the presence or absence of the BAC.

5.2.2 Investigation of gross development abnormalities in embryos of the *Grhl3*-transgenic *curly tail* mice

Embryos generated by the intercross of *Grhl3*-transgenic mice were investigated for gross developmental abnormalities. The different phenotypes observed among embryos of the transgenic intercrosses are shown in **Figure 5.2**. Surprisingly, both exencephaly (**Fig. 5.2 A-B, I**) and spina bifida (**Fig. 5.2 D, F, H-L**) were observed among BAC-positive embryos. Spina bifida has not previously been observed among 'single' transgenic embryos, and it was therefore hypothesised that BAC-positive embryos which developed spina bifida corresponded to $ct^{TgGrhl3}/ct^{TgGrhl3}$. Spina bifida was accompanied by a straight, bent or curled tail. The spina bifida defect was itself variable in size with some embryos having larger defects (**Fig. 5.2 K**) compared to littermates also with spina bifida (**Fig. 5.2 J**). Predicted $ct^{TgGrhl3}/ct^{TgGrhl3}$ E10.5 embryos had enlarged PNPs (**5.2 A-B**). Embryos were scored according to the type of NTD (spinal and cranial) and presence of tail flexion defects. The penetrance of these defects was compared between BAC-negative (*ct/ct*) and BAC-positive embryos (**Table 5.2**).

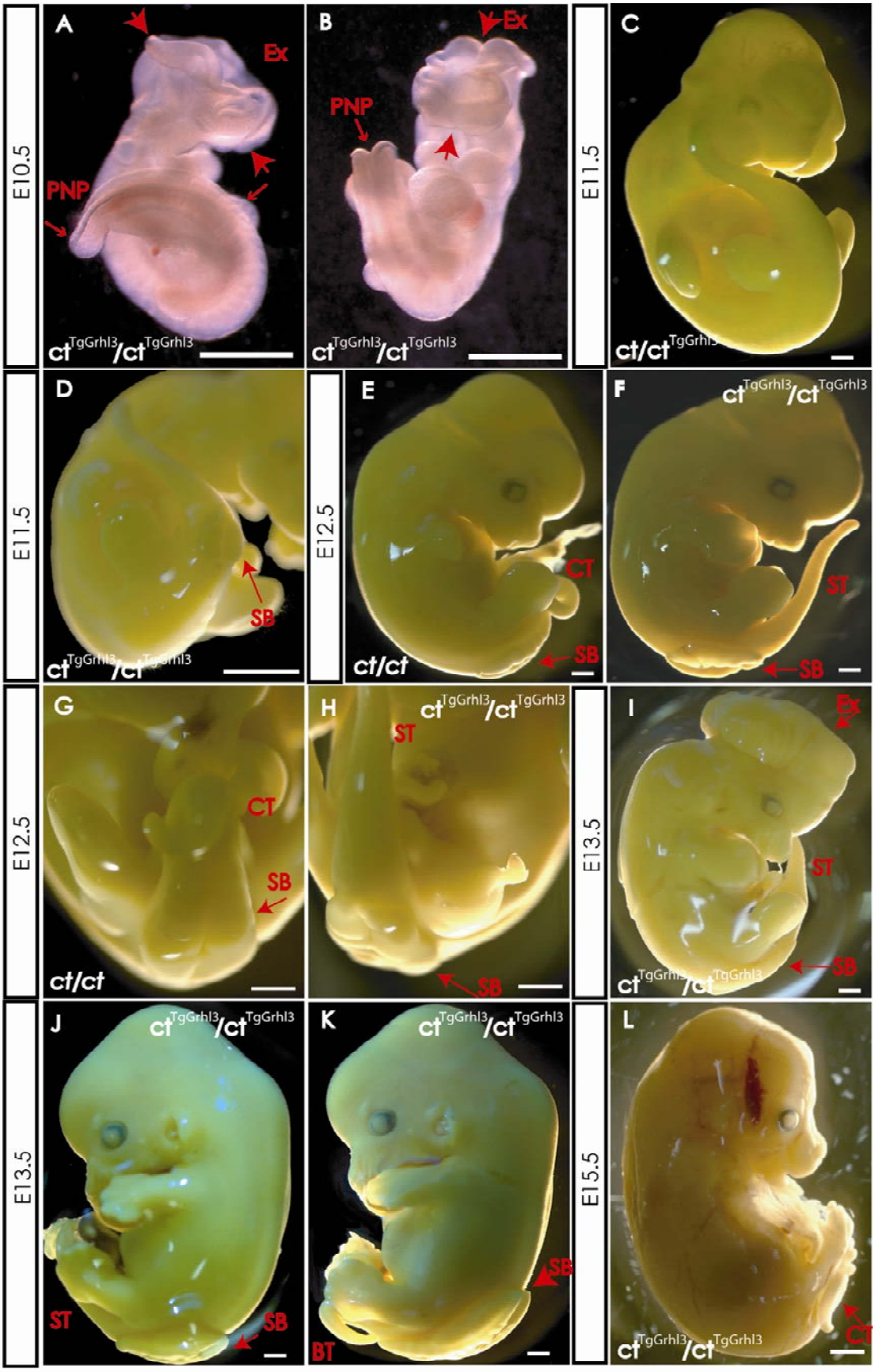
E10.5
A
Ex
PNP
ct^TgGrhl3/ct^TgGrhl3
B
Ex
PNP
ct^TgGrhl3/ct^TgGrhl3
E11.5
C
ct/ct^TgGrhl3
E11.5
D
SB
ct^TgGrhl3/ct^TgGrhl3
E12.5
E
CT
SB
ct/ct
F
ct^TgGrhl3/ct^TgGrhl3
ST
SB
E12.5
G
CT
SB
ct/ct
H
ct^TgGrhl3/ct^TgGrhl3
ST
SB
E13.5
I
Ex
ST
SB
ct^TgGrhl3/ct^TgGrhl3
E13.5
J
ct^TgGrhl3/ct^TgGrhl3
ST
SB
K
ct^TgGrhl3/ct^TgGrhl3
SB
BT
E15.5
L
CT
ct^TgGrhl3/ct^TgGrhl3

Figure 5.2 Phenotypes of embryos derived from transgenic intercrosses. (A-B) Predicted $ct^{TgGrhl3}/ct^{TgGrhl3}$ transgenic embryos at E10.5 exhibit forebrain-midbrain exencephaly (Ex, failure of closures 2 and 3) and an enlarged PNP. Both defects are characterised by open neural folds. **(C)** E11.5 $ct/ct^{TgGrhl3}$ embryo (known genotype) with normal spine. (**D**) Predicted $ct^{TgGrhl3}/ct^{TgGrhl3}$ embryo at E11.5 exhibiting spina bifida. **(E)** E12.5 *ct/ct* embryo with SB and a curled tail (CT; **G**) compared to (**F**) a predicted $ct^{TgGrhl3}/ct^{TgGrhl3}$ litter-mate with SB and a straight tail (ST; **H**). **(I)** Predicted $ct^{TgGrhl3}/ct^{TgGrhl3}$ embryo at E13.5 showing Ex, SB and a ST. At this stage, the nervous tissue of the brain bulges out and this will degenerate at later stages. (**J-K**) Predicted $ct^{TgGrhl3}/ct^{TgGrhl3}$ embryos at E13.5 showing differences in length of SB and with (**J**) straight and (**K**) bent tails. (**L**) E15.5 $ct^{TgGrhl3}/ct^{TgGrhl3}$ embryo exhibiting curled tail. Scale bar: 1 mm. Embryos shown in the figure are of known genotype.

Genotype	Total No.	Phenotype					
		Normal	Exen	Tail defect alone	Total SB	SB + BT/CT	SB + ST
BAC negative: *ct/ct*	58	29 ‡ (50.0%)	4 * (6.9%)	23 (39.7%)	2 (3.4%)	2 (100.0%)	0
BAC positive: $ct/ct^{TgGrhl3}$ or $ct^{TgGrhl3}/ct^{TgGrhl3}$	180	109 (60.6%)	13 † (7.2%)	11 (6.1%)	47 † (26.1%)	23 (48.9%)	24 (51.1%)

Table 5.2 Neural tube defects in embryos derived from *Grhl3*-transgenic *curly tail* intercrosses. E11.5 – E18.5 embryos were assessed for NTDs (spinal and cranial) and tail flexion defects (tail defect alone) or no defects (Normal). Exencephaly (Exen) can occur in isolation with straight tail (ST), or in combination with spina bifida (SB) and/or tail defects (bent, BT, or curled tail, CT). * Includes three embryos with exencephaly and tail defects. † Figures include three embryos with exencephaly and spina bifida accompanied by tail defects. Sub-types of spina bifida are indicated in blue and it should be noted that, in general, spina bifida in *curly tail* embryos is almost always accompanied by a curled tail. By comparison, among BAC positive embryos around half of the spina

bifida cases are accompanied by a straight tail. χ^2 test comparing the proportion of SB, tail defects and no defects shows a significant difference between the proportions in each category in *ct/ct* compared with BAC-positive embryos ($p \leq 0.001$).

A proportion of both *curly tail* and of BAC-positive embryos developed NTDs. BAC-positive embryos have a significantly higher percentage of spina bifida than *ct/ct* embryos ($p<0.001$, Z-test). On the other hand, the rate of isolated tail defects is the inverse: more frequent in *ct/ct* embryos than BAC-positive embryos. This finding suggests that excessive *Grhl3* expression predisposes to spina bifida but not tail defects. The frequency of spina bifida in *ct/ct* embryos within these litters is lower (3.4%) than usually observed among *ct/ct* (14-15%), but this may reflect the relatively small sample size (n = 58). Indeed, these differences are not significant by Z-test or χ^2 (spina bifida *versus* no spina bifida) when comparing *ct/ct* from double transgenic crosses (**Table 5.2**) to *ct/ct* from *ct* litters collected during a similar period (n = 113, 16 with spina bifida). In contrast, the frequencies of exencephaly and tail defects among *ct/ct* embryos from transgenic intercrosses are very close to those normally observed in *ct/ct* litters. Interestingly, both, *ct/ct* and BAC-positive embryos within these litters had similar rates of exencephaly (not significantly different).

It was hypothesised that transgenic embryos that developed spina bifida (26.1%) corresponded to those which carry double the copy number of the BAC ($ct^{TgGrhl3}/ct^{TgGrhl3}$). These were predicted to comprise 25% of the total number of embryos (one third of the BAC-positive). Thus, 60 of the 180 BAC-positive embryos are predicted to be $ct^{TgGrhl3}/ct^{TgGrhl3}$, of which 47 developed spinal NTDs, i.e. 75% of the predicted $ct^{TgGrhl3}/ct^{TgGrhl3}$ developed spina bifida (**Table 5.2**). Overall, these data suggest that the risk of spina bifida is higher in the predicted $ct^{TgGrhl3}/ct^{TgGrhl3}$ than in *ct/ct* littermates and that over- or under-expression of *Grhl3* can cause spinal NTDs

Interestingly, a proportion of the predicted $ct^{TgGrhl3}/ct^{TgGrhl3}$ embryos developed spina bifida with a straight tail (**Fig. 5.2 D, F, H-J; Table 5.2**), unlike the typical spina bifida with curly tail observed in *ct/ct* embryos. This phenotypic difference could be suggestive of possible variation in the mechanism underlying failure of neural tube

closure and development of spina bifida resulting from insufficient (*ct/ct*) or excessive (predicted $ct^{TgGrhl3}/ct^{TgGrhl3}$) *Grhl3* expression levels.

5.2.3 Investigation of *Grhl3* expression level in relation to posterior neuropore size

To further investigate the possibility that over-expression of *Grhl3* in $ct^{TgGrhl3}/ct^{TgGrhl3}$ embryos can result in NTDs, it was important to determine the relationship between *Grhl3* expression levels and PNP closure.

Using the same primers, *Grhl3_F6/R6*, as previously (Gustavsson et al., 2007); **Appendix B, Table B.2**), expression levels in the caudal region of stage-matched embryos undergoing PNP closure, were compared by quantitative RT-PCR. Expression of *Grhl3* was diminished in *ct/ct* embryos compared with transgenics, as previously observed (**Fig. 5.3 A**; Gustavsson et al, 2007). Transgenic embryos could be broadly divided into two groups on the basis of *Grhl3* expression level. One group exhibited expression levels approximately 2.7 fold higher than in *ct/ct.* These embryos were predicted to correspond to 'single' transgenic embryos as this degree of elevation of expression corresponds to that in known $ct/ct^{TgGrhl3}$ embryos from *ct/ct versus* $ct/ct^{TgGrhl3}$ crosses. In the latter case, data from two RT-qPCR experiments showed a mean fold change for *Grhl3* of 2.9 ± 0.70 for $ct/ct^{TgGrhl3}$ compared with *ct/ct.* A second group of samples showed expression elevation of up to 7.0 fold higher than *ct/ct*, and were predicted to correspond to $ct^{TgGrhl3}/ct^{TgGrhl3}$ embryos.

To investigate if there was a correlation between the expression levels of *Grhl3* and the length of the PNP, the mean PNP length of 26-31 somite stage embryos of different predicted genotypes were plotted (**Fig. 5.3 B**). A PNP larger than 500 μm at the 28-29 somite stage , is considered an indication of likelihood of developing spina bifida or a tail flexion defect (Copp, 1985). Comparison of mean *Grhl3* expression (**Fig. 5.3 A**) and mean PNP length (**Fig. 5.3 B**) for the same group of embryos showed that the embryos with the highest expression of *Grhl3* corresponded to the embryos with largest PNP (7.3 fold compared to *ct/ct*). The PNP in *ct/ct* embryos was larger than in $ct/ct^{TgGrhl3}$ but *Grhl3* expression was diminished (2.7 fold), albeit not significantly with this sample size. The predicted 'single' transgenics had small PNP sizes and higher *Grhl3* expression indicating rescue of the phenotype as shown previously (Gustavsson et al.,

2007). The small PNP size (200 μm) in *ct/ct*^{TgGrhl3} embryos reflects the fact that embryos of this genotype do not develop spina bifida.

These results indicate that the size of the PNP varies with expression level of *Grhl3* (**Fig. 5.3**). Overall, there seems to be a requirement for tight regulation of *Grhl3* expression, with insufficient or excessive expression both causing spinal NTDs. Wild-type and 'single' transgenic (*ct/ct*^{TgGhl3}) express *Grhl3* at a level that is compatible with normal spinal neurulation.

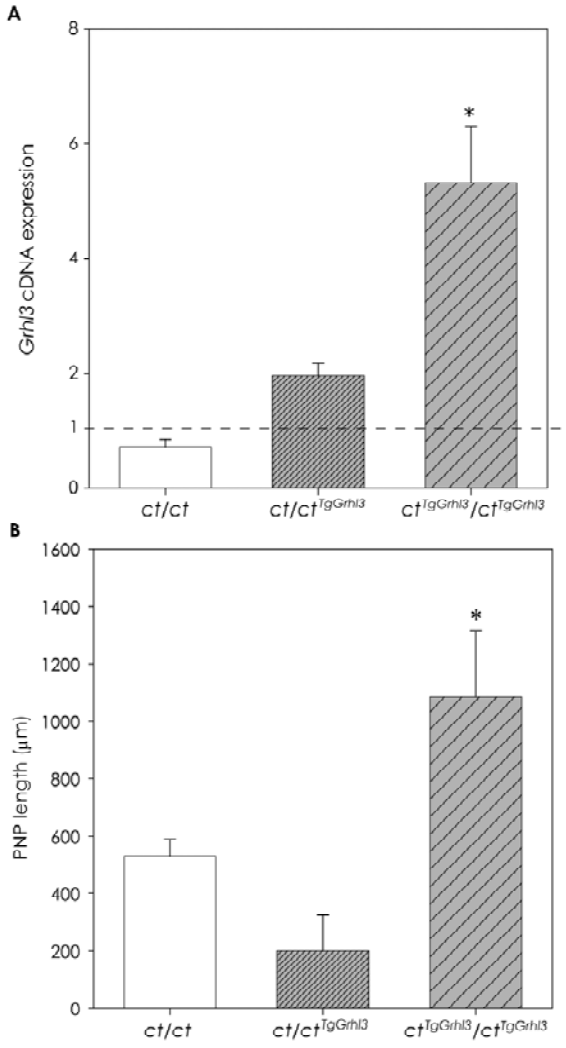

Figure 5.3 *Grhl3* mRNA expression *versus* posterior neuropore length. (A) *Grhl3* expression in *ct-Grhl3* expressing embryos (*ct/ct*, *ct/ct*^{TgGrhl3} and *ct*^{TgGrhl3}*/ct*^{TgGrhl3}) at the time of PNP closure (mean values ± SEM). *Grhl3* expression in predicted *ct*^{TgGrhl3}*/ct*^{TgGrhl3} embryos is significantly higher than expression in *ct/ct* (7-fold increase) and single transgenic (2.7-fold increase) embryos (* p = 0.0001, One Way ANOVA and Pairwise Multiple Comparison – Holm-Sidak Method). *Grhl3* expression is 2.7-fold elevated in single transgenics compared with *ct/ct.* A *ct/ct* sample was used as calibrator on the RT-qPCR analysis. Dotted line indicates expected wild-type level of expression. **(B)** The PNP lengths of the same group of embryos were plotted as mean ± SEM. In this experiment, predicted *ct*^{TgGrhl3}*/ct*^{TgGrhl3} transgenic embryos (n = 3) had significantly larger PNPs than single transgenics (n = 3) but not *ct/ct* (n = 4) embryos (* p = 0.011, One Way ANOVA and Holm-Sidak Method).

5.2.4 Genotyping of predicted 'double' transgenic embryos by quantitative real-time PCR of genomic DNA

In transgenic intercrosses (*ct/ct*^{TgGrhl3} *versus ct/ct*^{TgGrhl3}) embryos were genotyped for the presence or the absence of the BAC, and it was predicted that BAC-positive embryos with very large posterior neuropores (vLPNP) or spina bifida correspond to double transgenics. However, it was not possible to know for certain which of the embryos that carry the BAC are 'single' or 'double' trangenics. Moreover, it was not known whether all 'double' transgenic embryos develop such obvious phenotypes and whether defects are observable at earlier stages, such as E8.5 or E9.5. Therefore, it was necessary to develop a method to genotype embryos of the transgenic intercrosses without using qRT-PCR on embryo samples as this precludes use of the embryos for other analysis.

Primers for real-time quantitative genomic PCR (qG-PCR) were designed to amplify an intronic region of the *Grhl3* gene, as well as for the *Grhl2* gene, to be used as an internal control (**Appendix B**, **Table B.3**). Genomic DNA was extracted from the yolk-sac (E8.5 – E10.5) or from a limb (E11.5 – E18.5) and a 100 ng sample was used as template for qG-PCR based on the SYBR green method. Additional 'single' transgenics from *ct/ct versus ct/ct*^{TgGrhl3} crosses were used as controls since their genotype is known and expression levels were normalised to a *ct/ct* sample (**Chapter 2, section 2.7.3**).

Embryos with phenotype of predicted 'double' transgenics, i.e. spina bifida and/or tail defects (at E11.5 or later), or enlarged PNP (at E10.5) showed the highest *Grhl3* values compared to single transgenic-controls as well as to predicted 'single' transgenics (BAC-positive but no defects and/or small PNPs; **Fig. 5.4**). This method made possible the genotyping of transgenic embryos according to the abundance of *Grhl3* genomic DNA. With values normalised to a mean value of 1.0 for *ct/ct* samples (equivalent to the two copies of the endogenous gene), *ct/ct*^{TgGrhl3} samples had a mean value of 2.3 and *ct*^{TgGrhl3}*/ct*^{TgGrhl3} samples a mean value of 3.9 (**Fig. 5.4**). Therefore, it is possible to predict the genotype of embryos from transgenic intercrosses by qG-PCR.

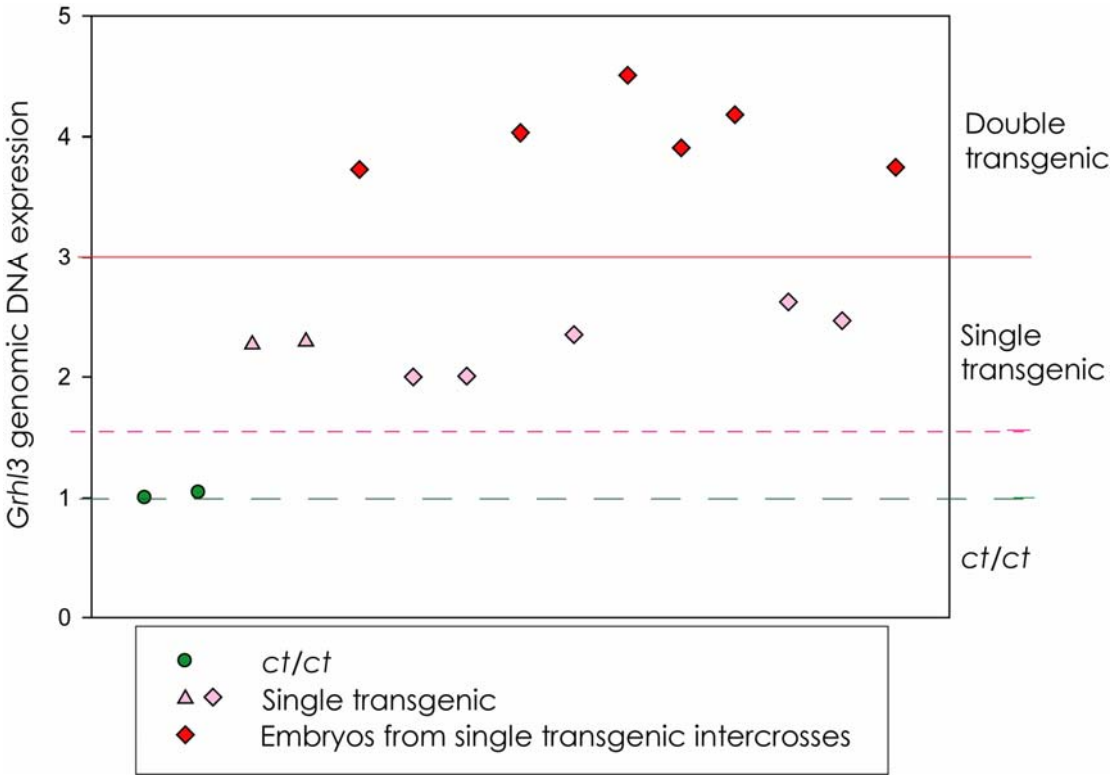

Figure 5.4 Predicted genotyping of *ct-Grhl3*-transgenic embryos. Symbols represent individual embryo samples (X axis) plotted against *Grhl3* genomic DNA level (Y axis). Known *ct/ct* (green circles) and single transgenics (pink triangles) fit within broadly consistent *Grhl3* levels. The genotype of double transgenic embryos (red diamonds) from transgenic intercrosses can be predicted on the basis of *Grhl3* qG-PCR with these embryos showing the highest values, whilst single transgenic embryos from the same crosses (pink diamonds) have comparable levels of *Grhl3* to known embryos of the same genotype (pink triangles).

5.2.5 Analysis of posterior neuropore length in double transgenic embryos

Following the observation of spina bifida among both *ct/ct* and *Grhl3*-transgenic *curly tail* embryos at E11.5 – E18.5, this phenotype was analysed at E10.5. It is known that the size of the PNP gives an indication of the likelihood of ensuing spina bifida. Enlargement of the PNP (LPNP) is associated with progression of spina bifida, whereas a small PNP (SPNP) predicts an unaffected embryo (Copp, 1985b). Consequently, the PNP was measured in a series of embryos (**Chapter 2, section 2.1.2**) and classified as

SPNP or LPNP. The typical appearance of large and small PNPs is shown in **Figure 5.5**.

Embryo images show the degree of severity of PNP enlargement in $ct^{TgGrhl3}/ct^{TgGrhl3}$ embryos. PNP lengths were measured at three somite stage intervals: 26-27, 28-29, 30-31 (**Table 5.3**). The mean PNP size of double transgenics is significantly larger than in all other strains. In contrast, single transgenic embryos have smaller PNPs throughout the period of closure. The PNP length of individual embryos and the mean value at each stage were plotted to allow visualisation of the pattern of closure through the 26-31 somite developmental period (**Fig. 5.6**). These data show a range of PNP sizes with progression of closure to completion in most wild-type ($+^{ct}/+^{ct}$) and single transgenic ($ct/ct^{TgGrhl3}$) embryos and failure of closure in most *ct/ct*, and double ($ct^{TgGrhl3}/ct^{TgGrhl3}$) transgenic embryos.

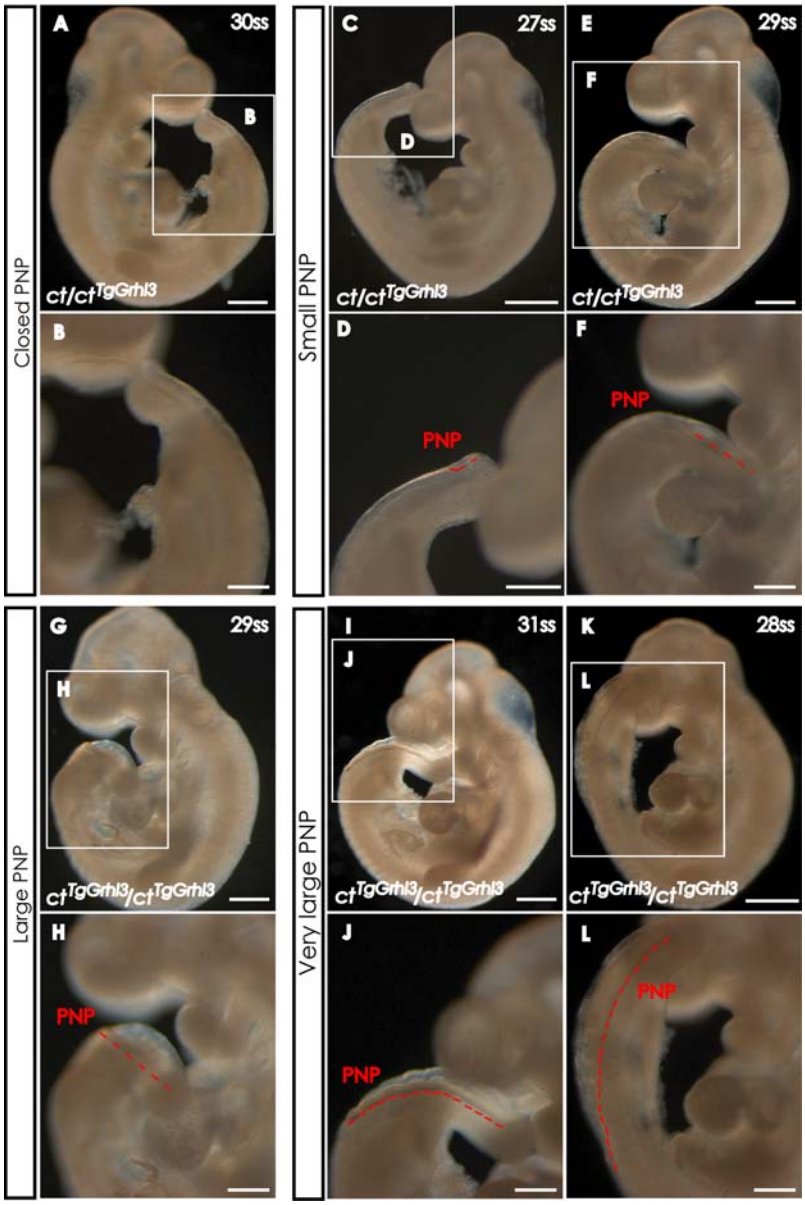

Figure 5.5 Differing appearance of posterior neuropore in E10.5 *Grhl3* transgenic embryos at the stage of PNP closure. **(A-B)** In some embryos, the PNP was closed (PNP=0), as is observed in wild-type embryos at this stage. **(C-F)** Embryos at the 27 and 29 somite stages with small PNPs, 125 μm (**C**, **D**) and 500 μm (**E**, **F**). **(G-H)** Enlarged PNP (875 μm) typical of affected *curly tail* embryos. **(I-L)** Two embryos with high levels of *Grhl3* showing very large PNPs, 1,550 μm (**I**, **J**) and 2,000 μm (**K**, **L**), larger than usually observed in *ct/ct* embryos. **B**, **D**, **F**, **H**, **J** and **L**, are enlargements of the indicated area in **A**, **C**, **E**, **G**, **I**, and **K**, respectively. Scale bars: **A**, **C**, **E**, **G**, **I**, and **K**, 1.0 mm; **B**, **D**, **F**, **H**, **J**, and **L**, 0.5 mm.

Closure of the PNP (length of 0 μm) occurs at the 30-31 somite stage in the majority of embryos expressing normal (wild-type, blue circles; **Fig. 5.6**) or moderately elevated (*ct/ct*^{TgGrhl3}, pink squares; **Fig. 5.6**) levels of *Grhl3*. From the 27 somite stage, the PNP length of *ct/ct* embryos, which were previously found to express reduced levels of *Grhl3*, is higher than in wild-type and single transgenic embryos (green diamonds; **Fig. 5.6, Table 5.3**). The PNP is severely enlarged at all stages in double transgenic embryos, which express high levels of *Grhl3* (purple triangles, and mean value higher than for the other three strains, **Fig. 5.6; Table 5.3**). Thus, PNP lengths are larger in double transgenics than even in *ct/ct* embryos (**Table 5.3**; **Fig 5.6**).

Since, PNP lengths are already enlarged in double transgenic embryos with 26 somites, it appears likely that PNP closure becomes abnormal in these embryos prior to this stage. For this reason, litters were collected at E9.5 and the PNP length was measured in a series of embryos at the 20-25 somite stages (**Table 5.4; Fig. 5.7**). Although the number of embryos is not large, it is apparent that the defect in PNP closure starts at the 20-21 somite stage (or even earlier) in double transgenic embryos.

Strain	**Number of somites**					
	26-27		**28-29**		**30-31**	
	n	PNP (μm)	n	PNP (μm)	n	PNP (μm)
Wild-type	10	307.5 ± 29.4	28	257.1 ± 21.6	37	68.9 ± 18.9
Single transgenic	10	332.5 ± 30.3	31	332.3 ± 23.0	43	73.8 ± 16.3
Curly tail	14	‡569.6 ± 41.5	78	‡536.9 ± 22.9	87	‡410.1 ± 29.2
Double transgenic	8	†1,150.0 ± 80.9	21	†1,236.9 ± 79.6	20	†1,408.8 ± 81.6

Table 5.3 Posterior neuropore (PNP) length of wild-type, *curly tail*, single and double transgenic embryos at E10.5. Mean and standard error values are given for the posterior neuropore length (PNP) within the 26-27, 28-29, and 30-31 somite stages. Double transgenics have significantly enlarged PNPs compared to all other strains at all stages examined (One Way ANOVA, and Holm-Sidak Method, $p \leq 0.001$†). Likewise, *curly tail* embryos have significantly larger PNP lengths than wild-type and single transgenic embryos but smaller PNPs than double transgenics (‡). There was no difference between the PNP length of single transgenics and wild-type embryos. Abbreviations: n, number of embryos of each

strain. Wild-type ($+^{ct}$) embryos are from the partially congenic wild-type (*curly tail*) strain.

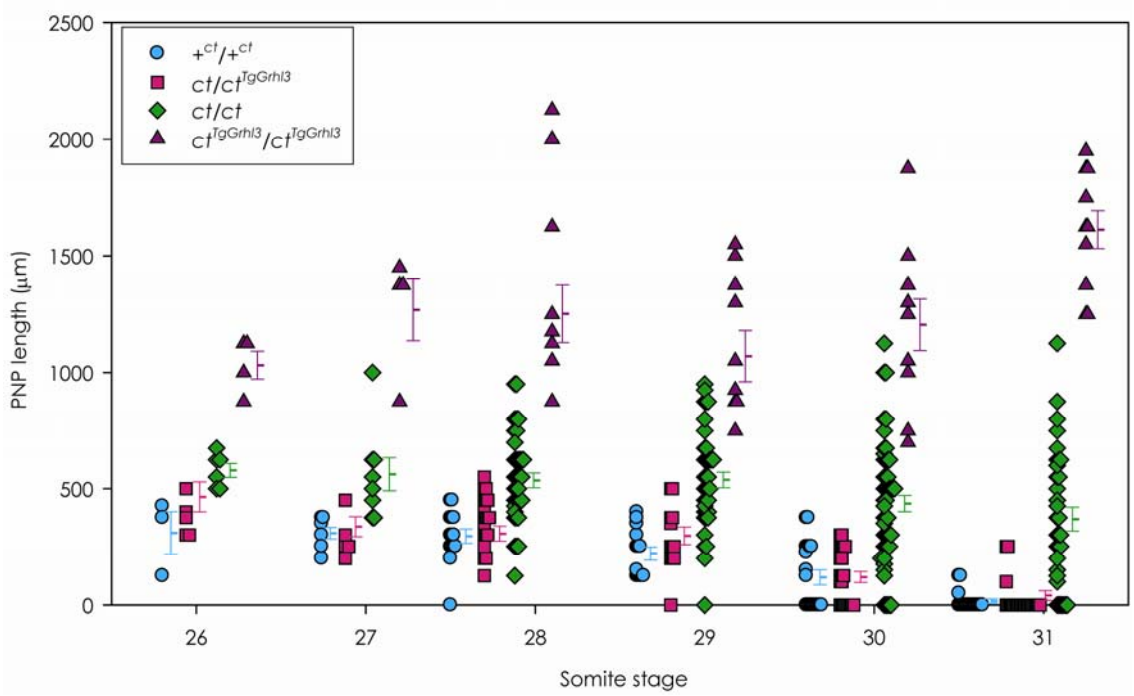

Figure 5.6 Variation in length of posterior neuropore with stage among embryos that differ in *Grhl3* expression level. The data for individual embryos is shown, with the mean PNP length (± SEM) indicated for each strain at each stage. Number of embryos at the 26, 27, 28, 29, 30 and 31 somites stages are: for $+^{ct}/+^{ct}$ 3, 7, 14, 14, 19, 18; for $ct/ct^{TgGrhl3}$ 5, 5, 19, 12, 22, 21; for *ct/ct*, 6, 8, 39, 39, 54, 33; for $ct^{TgGrhl3}/ct^{TgGrhl3}$, 4, 4, 12, 9, 10, 10.

Strain	Number of Somites					
	20-21		22-23		24-25	
	n	PNP (µm)	n	PNP (µm)	n	PNP (µm)
Curly tail	3	516.7 ± 16.7	1	375.0 ± 0.0	4	562.5 ± 47.3
Single transgenic	5	520.0 ± 12.2	6	475.0 ± 25.8	5	550.0 ± 30.6
Double transgenic	2	750.0 ± 0.0*	1	1,000.0 ± 0.0	4	887.5 ± 83.2*

Table 5.4 Posterior neuropore lengths of single transgenic embryos between somite stages 20 and 25. At 20-21 and 24-25 somite stages, double transgenics have significantly larger PNPs than single transgenic and *curly tail* embryos (* p

≤ 0.001 and p = 0.002, respectively; ANOVA – Holm-Sidak method). There was no significant difference in PNP length between single transgenics and *curly tails*. It was not possible to do statistical analysis at somite stage 22-23, owing to the small sample size (n).

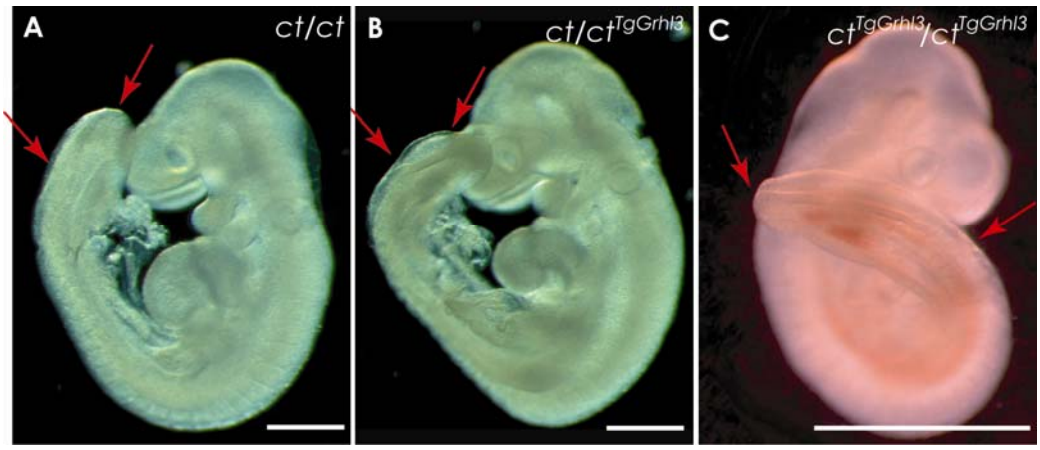

Figure 5.7 Posterior neuropore length of *curly tail* and *Grhl3* transgenic embryos at somite stage 20-25. The length of the PNP (between red arrows) does not apparently differ between *curly tail* and single trangenics but is greatly enlarged in double transgenics. PNP lengths: (**A**) 550 μm; (**B**) 500 μm; (**C**) 1125 μm. Scale bars: **A-B**, 0.5 mm; **C**, 1.0 mm.

Having established that the BAC-positive embryos which exhibit spinal NTDs correspond to the double transgenics, I next investigated whether *Grhl3* expression level also influences cranial neural tube closure. The presence of cranial NTDs (exencephaly) among embryos collected at E10.5 or later was compared between genotypes (**Table 5.5**). It is apparent that exencephaly occurs in both *ct/ct* and BAC-positive embryos, including known single transgenics, suggesting that reinstatement of *Grhl3* expression by the BAC is not sufficient to rescue these defects. The similar frequency of exencephaly between groups suggests that cranial neural tube closure is not exacerbated in a comparable manner to spinal closure in double transgenics.

Phenotype	No of Embryos	*Curly tail* *ct/ct* BAC negative	Transgenic $ct/ct^{TgGrhl3}$, $ct^{TgGrhl3}/ct^{TgGrhl3}$ BAC positive
E10.5	**316**	**81**	**235**
Exencephaly	18	6 (7.4%)	12 (5.1%)
Combined data			
E10.5 – E18.5	**554**	**139**	**415**
Exencephaly	34	10 (7.2%)	25 (6.0%)

Table 5.5 Cranial NTDs among embryos collected at E10.5-18.5. No significant differences were observed between groups.

Of the 25 BAC-positive embryos with exencephaly (**Table 5.5**), 22 were genotyped by qG-PCR, while the other 3 were undetermined (poor DNA quality). Among these embryos, 14 genotyped as single transgenics and 8 as double transgenics (including 3 embryos that showed both spina bifida and exencephaly). As an approximation, if one-third of the 415 transgenic embryos are double transgenics, 5.8% developed exencephaly (8 out of 137) compared to 5.1% of the single transgenics (14 out of 277). These data suggest that there is not exacerbation or rescue of exencephaly in double transgenics.

5.2.6 Examination of spina bifida in *ct/ct* and $ct^{TgGrhl3}/ct^{TgGrhl3}$

In the analysis of phenotypes and PNP sizes, some differences were noticed between spina bifida in *ct/ct* and transgenic embryos. In the double transgenics, not only do embryos develop spina bifida accompanied by a straight tail, as opposed to the association with curled tails in *ct/ct*, but the extent of the open defect also appears larger than in *ct/ct* embryos at least as indicated by PNP size (**Fig. 5.5**). To investigate the extent of the defect further, skeletal preparations were prepared from E15.5 embryos generated in the transgenic intercrosses (**Fig. 5.8**).

Curly tail and double transgenic embryos had the same number of ribs and vertebrae (**Fig. 5.8 A-G**). Comparisons were made between a *ct/ct* and double transgenic littermate, with curled tail (CT) and straight tail (ST) respectively (**Fig. 5.8**). Both fetuses exhibit lumbosacral spina bifida. In the *ct/ct* fetus the spina bifida lesion starts between lumbar vertebrae III and IV (**Fig 5.8 L**) and in the double transgenic between vertebrae II and III (**Fig. 5.8 M**). Variation in the extent of the defect likely reflects the size of the PNP and the axial level from which the neuropore remains open.

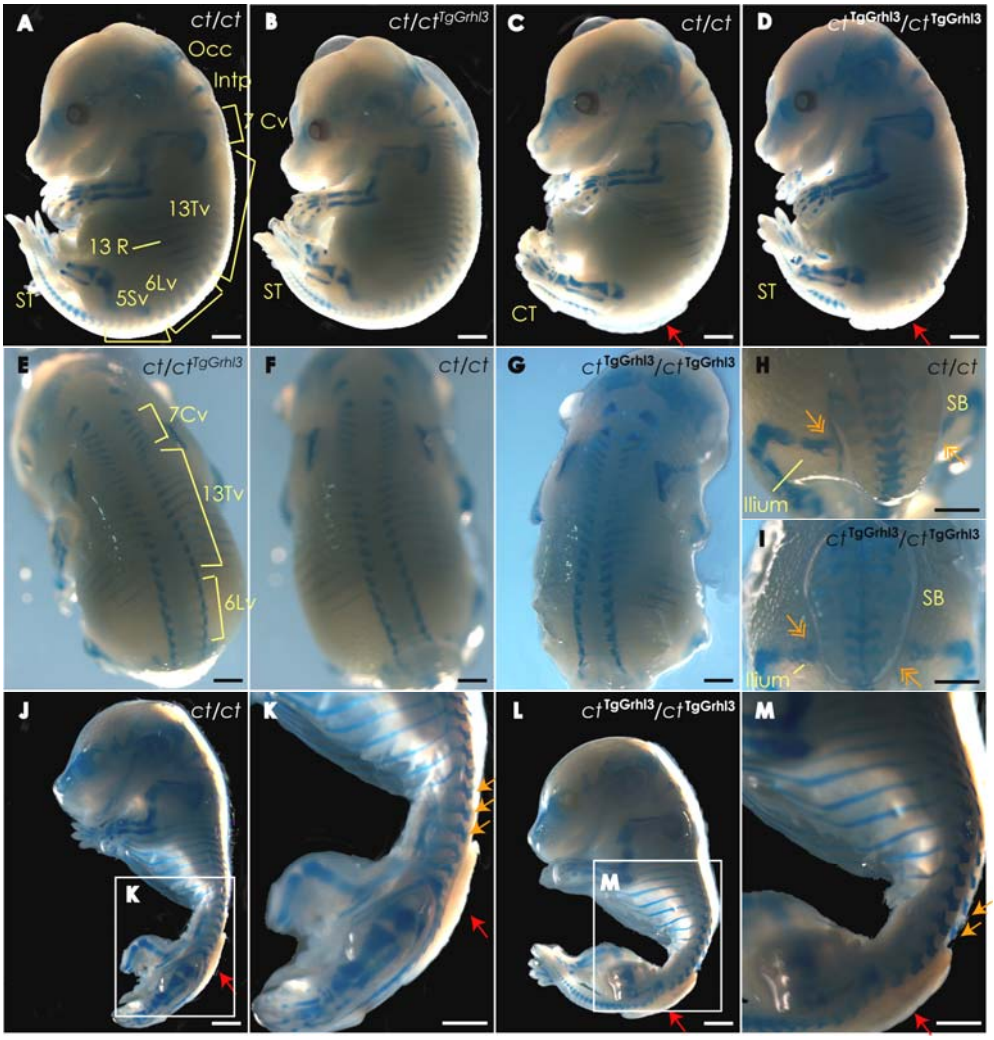

Figure 5.8 Alcian blue staining of E15.5 embryos from transgenic intercrosses. (A-G) Skeletal structure of *ct/ct* **(A, C and F),** *ct/ct*^{TgGrhl3} **(B, E)** and *ct*^{TgGrhl3}*/ct*^{TgGrhl3} **(D, G)** BAC-positive embryos**.** All studied embryos had 13 pairs of ribs (R) and equal numbers of vertebrae (v): 7 cervical (I-VII, Cv), 13 thoracic (I-XIII, Tv), 6 lumbar (I-VI, Lv), and 5 sacral (I-V, Sv). At the level of the iliac bone (double-headed arrows), it is noticeable that the level of spina bifida in *ct/ct* **(H)** differs from the double transgenic **(I).** To investigate this further, the internal organs of the embryos with spina bifida **(F, G)** were removed up to the diaphragm **(J, L)** and the lumbar and sacral vertebrae were counted (boxed areas at higher magnifications in **K, M**). In *ct/ct* the spina bifida starts between the LvIII and IV, and in the double-transgenic between Lv II and III. **H** and **I** are higher magnifications of **F** and **G**, respectively. Scale bar: 1 mm. Interpretation of skeletal structure was based on: (Menegola et al., 2001).

5.2.7 Localisation of the *Grhl3*-expressing BAC

In transgenic experiments, BAC transgenes usually insert randomly into the genome. This raises the possibility that, in the present study insertion of the *Grhl3* BAC could have disrupted another gene, and that the observed phenotype in double transgenic embryos could result from homozygous disruption of such a gene. For this reason, a strategy was designed to localise the BAC by inverse PCR in order to isolate genomic DNA adjacent to the BAC (**Fig. 5. 9**).

All transgenic embryos were genotyped for the presence of the BAC (**Chapter 2, section 2.4.1**) using primers 237D13-R1 (D13) and pTARBAC, within the genomic DNA insert (the region of chromosome 4 containing the *Grhl3* gene) and the BAC ends (vector). These primers allow PCR amplification of a 230 bp region which was sequenced, to confirm the position of the primers and presence of a six-base cutter restriction enzyme, *BamHI* (**Appendix D**, **section D.1**). Adjacent to the BAC end sequence lies the 'unknown genomic region' where the BAC is inserted (**Fig. 5. 9 A**). In principle, obtaining the sequence of this adjacent region and interrogation of the mouse genomic sequence should allow identification of the insertion site. Two enzymes within the BAC region were chosen to allow two independent experiments, to increase the chance of cutting the 'unknown genomic region' close to the BAC (**Fig. 5.9 B**). The four-base cutter restriction enzymes, *RsaI* and *HaeIII* that were not present within the 230 bp sequenced region, nor within the primer sequences, were selected for digestion of $ct^{TgGrhl3}$ genomic DNA.

After digestion with *RsaI* or *HaeIII* (**Chapter 2**, **section 2.14; Appendix A.16**), the reaction products were ligated to circularise the DNA fragments. A dilute reaction mixture was prepared to favour unimolecular ligation (440 µl of water, 50 µl ligase buffer and 10 µl T4 ligase). Following ligation, the DNA products were purified by ethanol precipitation and digested with *BamHI*, to linearise the fragments (**Fig. 5.9 C**). Finally, primers with the inverse sequence to D13 and pTARBAC were used (**Appendix B, Table B.4**) for PCR amplification of the intervening region of unknown genomic DNA (**Fig. 5.9 C**). The fragments were then sequenced (DNA Sequencing Service, The Wolfson Institute for Biomedical Research, UCL) using both inverse primers, i.e., for identification of the 'unknown region'.

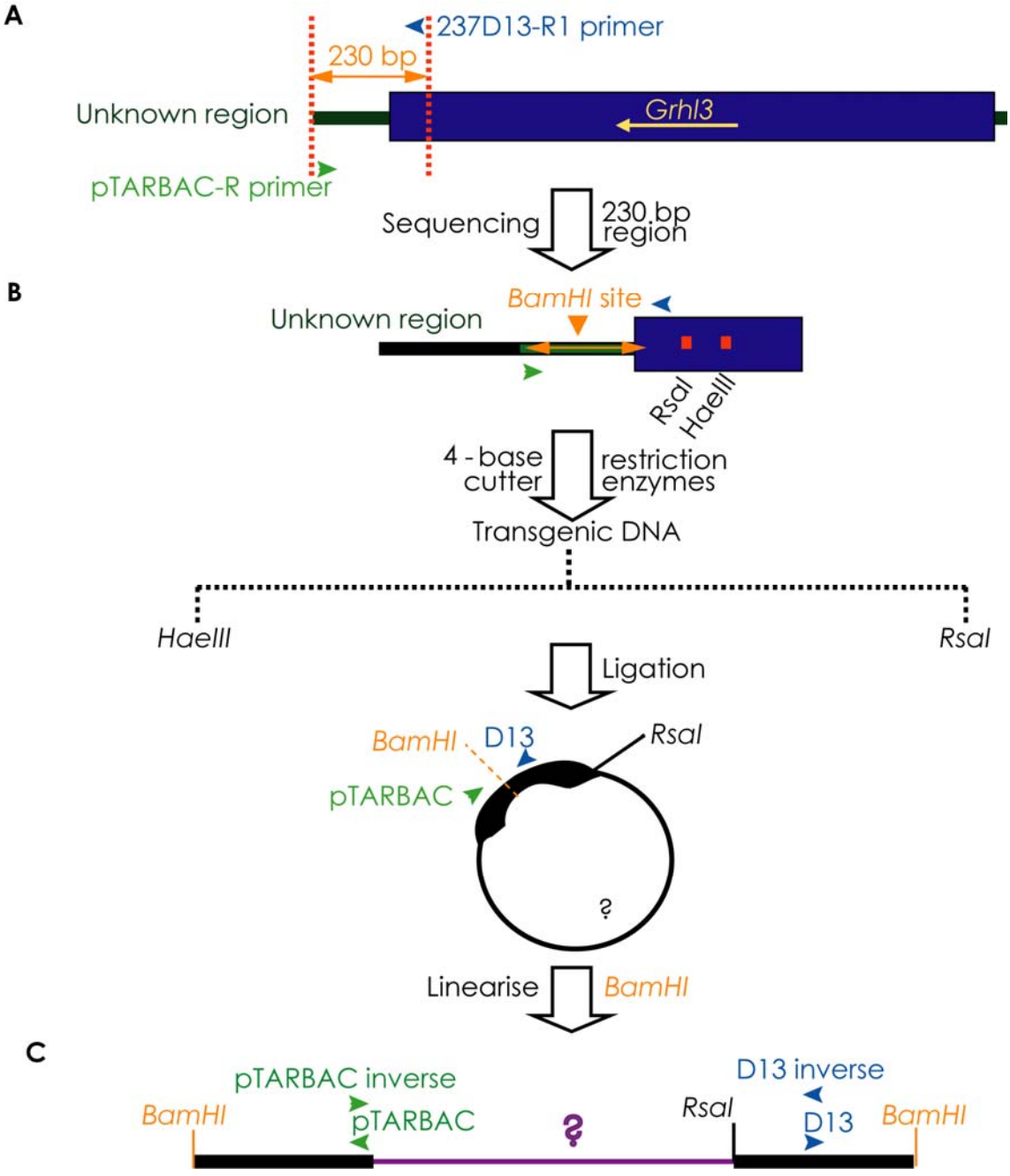

Figure 5.9 Diagram summarising the inverse PCR strategy used to localise the BAC. (A) The BAC insert (blue box) contains the intact *Grhl3* gene (yellow arrow indicates direction of transcription). The insert-BAC end junction encompasses a 230 bp region between genotyping primers 237D13-R1 (D13, blue) and pTARBAC (green), which was sequenced. This end junction is adjacent to an 'unknown region' of genomic DNA. **(B)** Sequencing of the 230 bp region revealed a 6-base cutter site, *BamHI*. Transgenic DNA was digested with the 4–base cutter restriction enzymes: *RsaI* and *HaeIII*. An *RsaI* site is known to lie upstream of the D13 primer site within the BAC but not between the D13 and

pTARBAC primer sites. It was predicted that an *RsaI* site would lie in the 'unknown' genomic region, close enough to generate a fragment that could be circularised. Hence, the digested samples were ligated to circularise the DNA fragments. **(C)** *BamHI* linearization should then result in a molecule whereby the 'unknown region' would be flanked by an *RsaI* site, and the sites for the D13 and pTARBAC primers. Inverse primers to D13 (D13 inverse) and pTARBAC (pTARBAC inverse) were therefore designed to amplify and sequence the 'unknown region'.

After sequencing, sequences were used to interrogate the mouse genome sequence using the BLAST feature of the ENSEMBL database (http://www.ensembl.org/Multi/blastview), followed by alignment of the hits. None of the sequencing hits from *HaeIII* fragments were informative since all corresponded to chromosome 4 (Chr 4:135,077,174 – 135,077,383 Mb). It appears likely that there is a *HaeIII* site close to the pTARBAC site, so that all sequencing reads went immediately into the BAC insert and this was confirmed on sequencing across the insertion site (see below). On the other hand, sequencing of fragments generated with *RsaI* produced matches to both BAC sequence (corresponding to chromosome 4) and novel sequence, adjacent to the BAC insertion site. Alignment of these sequences with genomic sequence, using BLAST revealed several possible chromosomal locations as summarised in **Table 5.6**.

Overall, the sequence fragments generated by inverse PCR did not allow definitive localisation of the BAC as none of them had a 100% match to a specific chromosomal localisation. This is presumably because the *curly tail* genomic sequence differs from the reference sequence in the database (C57BL/6). Moreover, the BAC appears to be inserted in a low complexity repeat region, such that several possible chromosomal locations were indicated. The sequencing alignment of the hits generated from the *RsaI* fragments suggested that chromosome 18, position 3,005,382, is the most likely site for the BAC position. The two primers generated sequence fragments that aligned to a contiguous region of chromosome 18 (**Fig. 5.10**), whereas this was not the case for possible locations on chromosomes 14 and 15. The only other regions for which both primers generated sequence fragments in close proximity were on chromosome 16.

However, the sequence identity and region of homology were lower for the possible insertion sites on chromosome 16 than for chromosome 18.

Primer	Chr	Alignment with genomic sequence (Mb)	% Identity	bp
pTARBAC inverse	14	9,119,164 – 9,119,375	96.73	214
	15	74,916,993 – 74,917,205	96.71	213
	18	**3,005,382 – 3,005,593**	**95.33**	**214**
	16	3,115,855 – 3,116,065	94.37	213
	16	3,350,523 – 3,350,733	93.93	214
D13 inverse	4	135,077,172 – 135,077,354	98.36	183
	18	3,005,889 – 3,006,013	94.40	125
	16	3,115,432 – 3,115,556	91.20	125
	16	3,351,034 - 3,351,158	91.20	125
	2	181,667,047 – 181,667,158	89.29	112
	19	61,341,681 - 61,341,786	88.99	109

Table 5.6 Chromosomal locations which align with sequence fragments generated by inverse PCR following *RsaI* digestion. Chromosome number (Chr.), the region of the alignment, percentage of identification (% identity) and length of homologous region (base pairs, bp) are indicated.

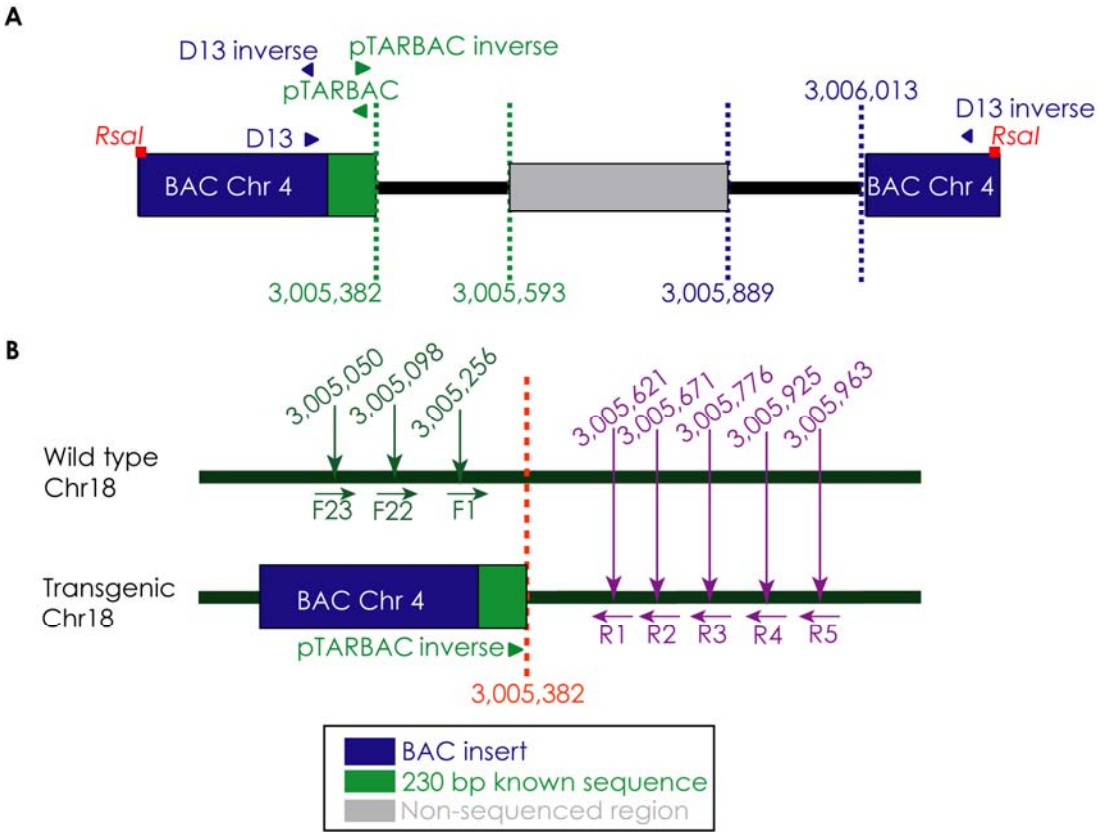

Figure 5.10 Diagram to possible localisation of *Grhl3*-containing BAC on chromosome 18, as indicated by inverse PCR using *RsaI*. (A) Schematic of predicted ligation product following *RsaI* digestion. The position of primers used for inverse PCR (pTARBAC-inverse and D13-inverse) are indicated. The same primers were used for sequencing of the inverse PCR product and the sequence fragments which align to chromosome 18 are indicated by black bars. **(B)** Diagram of putative BAC insertion site on chromosome 18. The position of primers used to further investigate the insertion site are indicated.

Despite the ambiguity of localisation based on sequencing data, one can deduce that in each possible location the potential insertion site of the BAC was at least 200 kb from the nearest gene. The closest gene to the putative insertion site on chromosome 18 (18: 3,005,382) is 260.8 kb away (**Fig. 5.11**), while the possible insertion sites on chromosome 16 lie 476.6 kb and 241.7 kb from the nearest gene. However, one of the possible insertion sites on chromosome 16 lies only 3.0 kb from a predicted non-coding mRNA (**Fig. 5.11**).

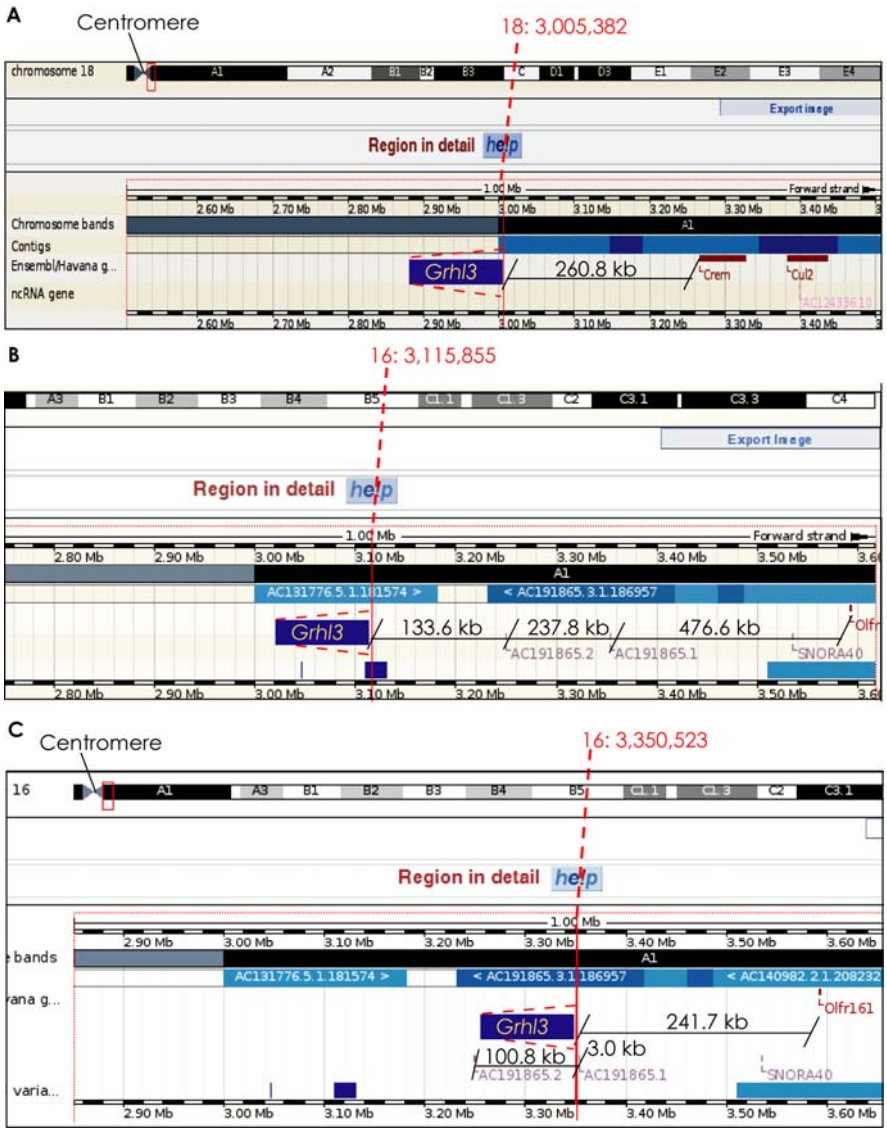

Figure 5.11 Possible chromosomal locations of the *Grhl3*-BAC as indicated by inverse PCR using *RsaI* digestion. (A) Putative insertion site on chromosome 18 where the closest known gene, *Crem*, is 260 kb from the BAC. (**B-C**) Putative insertion sites on chromosome 16 where the closest known gene, *Olfr1*, is 476.3 kb (**B**) or 241.7 kb (**C**) from the BAC. A predicted non-coding mRNA (AC191865.2) is located 133.6 kb from one possible insertion site (**B**) and 100.8 kb from the other site (**C**). Another predicted non-coding mRNA (AC191865.1) lies 237.8 kb (**B**) and 3.0 kb (**C**) from the possible insertion sites, respectively. Chromosome diagrams adapted from *ENSEMBL*.

In order to further investigate the potential sites for localisation of the BAC, primers were designed (**Appendix D**, **section D.2**; F1, F22, F23 and R1-R5; **Fig. 5.10 B**,

Appendix B, **Table B.4**), which could be used in pairs to amplify the wild-type genomic sequence. In addition, the reverse primers (R1-5) were also used in combination with the pTARBAC-inverse primer (**Figure 5.10 B)**. If the BAC is localised in the predicted region on chromosome 18 it was predicted that the reverse primers (Chr18_R1-R5) with pTARBAC-inverse primer should amplify genomic DNA of double and single transgenics, but not *curly tail* or wild-type samples, and this is indeed what was observed **(Fig. 5.12 A-C)**.

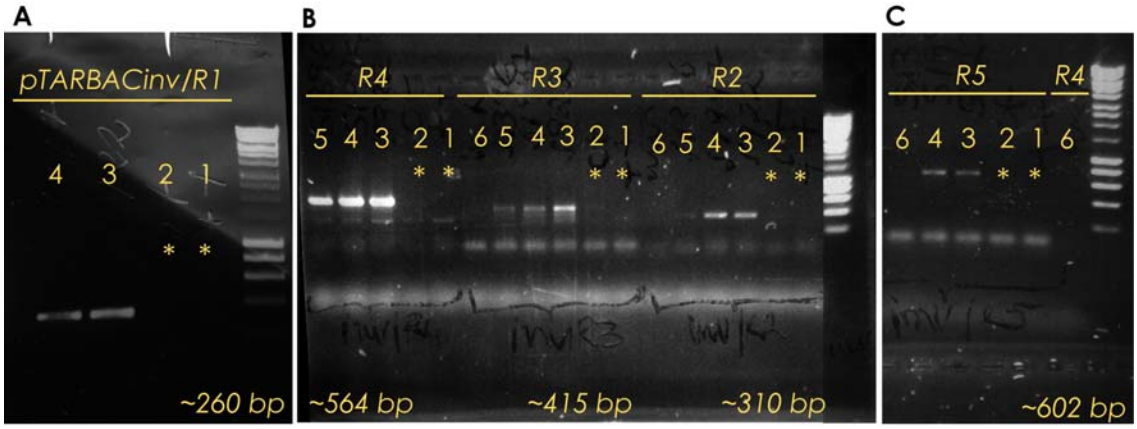

Figure 5.12 Genotyping using primers flanking the BAC region. (**A-C**) The pTARBAC-inverse primer used in combination with all reverse primers amplified the expected size products. DNA of single and double transgenic embryos amplified with R1-R5, whereas wild-type and *curly tail* samples did not amplify, as expected (*). Lanes: (1) $+^{ct}/+^{ct}$; (2) *ct/ct*; (3) $ct/ct^{TgGrhl3}$; (4) $ct^{TgGrhl3}/ct^{TgGrhl3}$; (5) $ct/ct^{TgGrhl3}$; (6) negative control.

Sequencing of the product amplified using pTARBAC-inverse with Chr18-R4, made it possible to sequence across the insertion site of the BAC and therefore to generate a 'tag' which corresponds to the chromosomal localisation (**Appendix D**, **section D.3**). Interrogation of the genomic database with this 'tag' sequence produced homology with several chromosomal locations (**Table 5.7**), all of which contained the *HaeIII* site.

Stats score	Chr	Location (Mb)	% ID	bp
422	18	3,005,382 – 3,005,924	94.32	546
374	15	74,916,993 – 74,917,205	94.24	486
342	16	3,115,521 – 3,116,065	90.55	550
332	16	3,350,523 – 3,351,069	90.04	552
249	14	9,119,164 – 9,119,444	97.15	281
139	19	61,299,655 – 61,299,967	85.76	323

Table 5.7 Chromosomal locations which align with sequence fragments generated by BLAST analysis of the sequence tag at the BAC insertion site. Chromosome number (Chr.), region of the alignment, percentage of identification (% ID) and length of homologous region (base pairs, bp).

Using CLUSTALW (http://align.genome.jp/), the genomic sequences corresponding to the sequence tag at the insertion site, plus 500 base pairs upstream and 500 base pairs downstream of it were aligned with chromosomes 18, 16 and 15 to search for regions that differ between these three chromosomes. This alignment allowed the design of a pair of primers that were unique to chromosome 15. The forward primer was designed 87 bp upstream of the putative insertion site and the reverse primer 241 bp downstream (Chr15_F15/R15; **Appendix B**, **Table B.4**). None of BAC-positive samples generated a PCR product using a combination of pTARBAC-inverse with the Chr15_R15 primer, suggesting that the BAC was not located on chromosome 15. The chromosome 15 primers did work in PCR since the F15/R15 primer pair amplified the expected 890 bp product (in all genotypes including $ct^{TgGrhl3}/ct^{TgGrhl3}$), while Chr_F15 generated a PCR product in combination with the non-chromosome specific primers R1-5, but with differing product size to that amplified using the chromosome 18-specific forward primer (see above, **Fig. 5.12**).

Ideally it would have been possible to design a chromosome specific forward primer upstream of the putative BAC insertion sites on chromosomes 16 and 18. In combination with the R1-R5 reverse primers, the primer corresponding to the insertion site would be expected to amplify a PCR product from wild-type, *curly tail* and 'single' transgenics but not from double transgenic genomic DNA. However, although several

primer combinations were tested (**Appendix B, Table B.4**), design of chromosome-specific forward primers was not possible owing to the low complexity repeat region in which the BAC is inserted.

5.2.8 *Grhl3* expression pattern in double transgenic embryos

The expression pattern of *Grhl3* has previously been characterised in *ct/ct* and single BAC-transgenic embryos (Gustavsson et al., 2007). In order to investigate whether *Grhl3* is expressed in ectopic locations in $ct^{TgGrhl3}/ct^{TgGrhl3}$ embryos, as well as at increased levels, whole mount *in situ* hybridisation (**Chapter 2, section 2.10**) was performed on embryos of each genotype at different stages of development during neural tube closure (**Figures 5.13 – 17**).

At embryonic days 8.0 to 8.5, *Grhl3* expression has been reported in the surface ectoderm adjacent to the tips of the neural folds (**Fig. 5.14 A-B,** and N. Greene, Personal Communication; (Ting et al., 2003a). In wild-type and *curly tail* embryos, whole mount *in situ* hybridisation for *Grhl3* requires a relatively long period of signal development, of up to one week. In the current study, the development of signal was stopped at the point when intense expression was observed among a subset of the embryos, which were presumed to correspond to transgenics (later confirmed by genotyping). Therefore, at E8.0 *Grhl3* expression was not detectable in *ct/ct* embryos (**Fig. 5.13 A-C**). Signal is observed along the lateral edges of the open neural folds in the caudal half of $ct/ct^{TgGrhl3}$ embryos (**Fig. 5.13 D-E**), which corresponds to the surface ectoderm expression previously reported in wild-type embryos (Ting et al., 2003a) and using a *Grhl3*-Cre knock-in allele in combination with a conditional lacZ reporter (Camerer et al., 2010a). A more intense signal in a similar location was observed in $ct^{TgGrhl3}/ct^{TgGrhl3}$ (**Fig. 5.13 G-M**) embryos. At E8.5, *Grhl3* expression was also observed in the anterior forebrain and at the lateral edges of the PNP in $ct^{TgGrhl3}/ct^{TgGrhl3}$ embryos (**Fig. 5.13 N, O**).

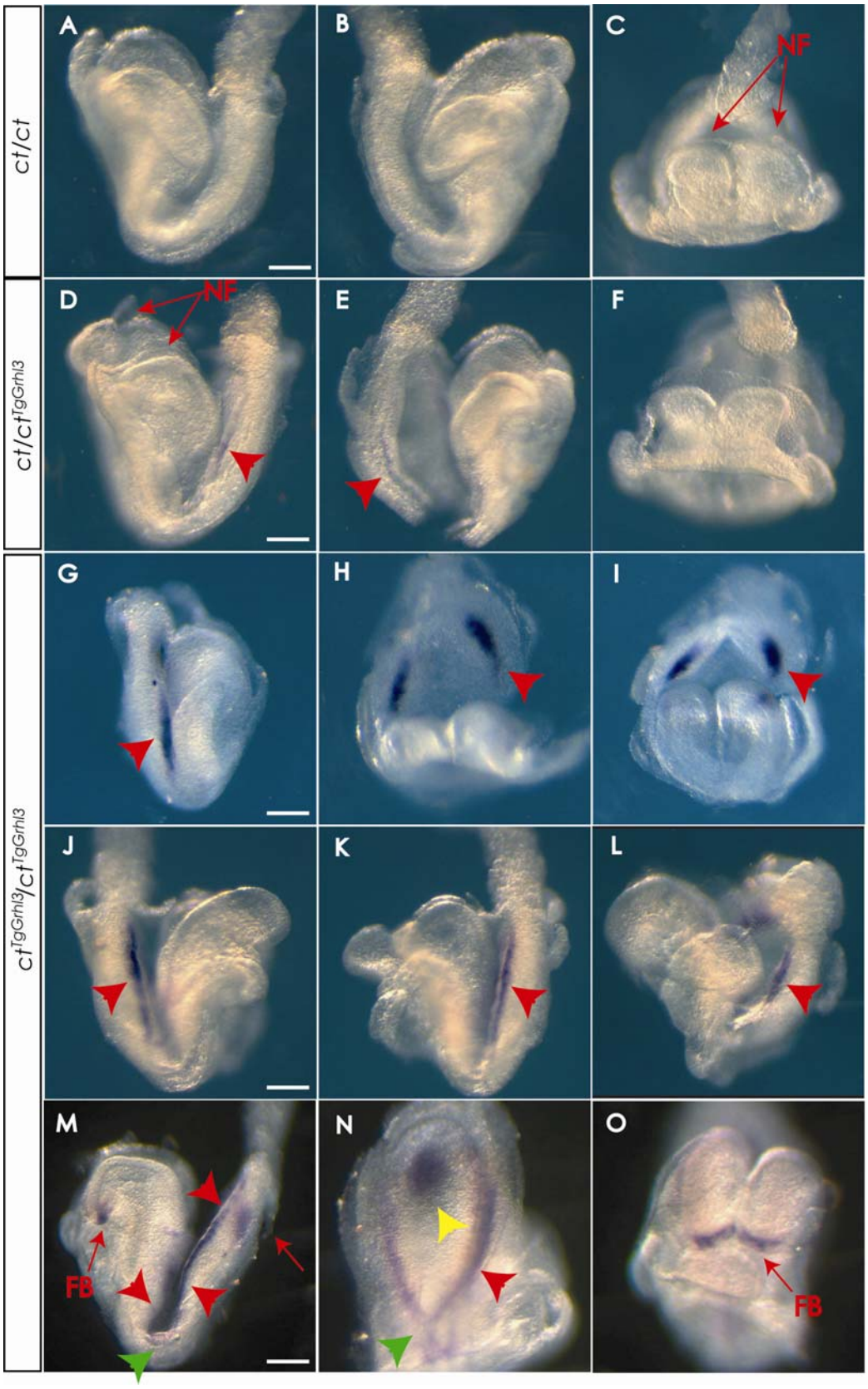
ct/ct
ct/ct^TgGrhl3
ct^TgGrhl3/ct^TgGrhl3
A
B
C
NF
D
NF
E
F
G
H
I
J
K
L
M
FB
N
O
FB

Figure 5.13 *Grhl3* mRNA expression in *curly tail* and *Grhl3* transgenic embryos determined by whole mount *in situ* hybridisation. (**A-L)** *Grhl3* expression at E8.0 in *ct/ct* (**A-C**), *ct/ct*^{TgGrhl3} (**D-F**), and *ct*^{TgGrhl3}/*ct*^{TgGrhl3} (**G-L**) embryos. At this stage, no signal is detectable in *ct/ct* embryos (see text) while expression was evident in a line (red arrowheads in **D**-**E**) at the lateral edges of the neural folds (NF) in *ct/ct*^{TgGrhl3} embryos with a stronger signal in *ct*^{TgGrhl3}/*ctTg*^{Grhl3} embryos (**G**-**L**). (**M-O**) *Grhl3* expression at E8.5 in a *ct*^{TgGrhl3}/*ct*^{TgGrhl3} embryo can be detected in the anterior forebrain (FB; **M, O**). Signal is also evident in the dorsal surface of the embryo (as seen from the side in **M**) and a ventral view (**N**) shows that this signal corresponds to the midline, thought to be the dorsal surface of the closed neural tube, (green arrowhead in **M** and **O**) and flanking the open neural folds in the posterior region (red arrowhead in **N**). Yellow arrowhead in **N** indicates expression in the primitive streak. Panels **A**, **B**, **D**, **E**, **G**, **J**, **K**, and **M**, side views; Panels **C**, **F**, **H**, and **O**, front views; Panels **I** and **L**, dorsal view; Panel **O**, ventral view. Scale bar: 0.1 mm.

To investigate the level of *Grhl3* expression further, E8.0 embryos were embedded in wax, sectioned and counter-stained with eosin (**Chapter 2, section 2.11.1**; **Fig. 5.14**). *Grhl3* is strongly expressed along the body axis of *ct*^{TgGrhl3}/*ct*^{TgGrhl3} embryos, in the surface ectoderm and neuroepithelium at the tips of the open neural folds **(Fig. 5.14 A.1-A.4).** Weaker expression in a similar pattern was observed in *ct/ct*^{TgGrhl3} **(Fig. 5.14 B1-B4)** but not detected in *ct/ct* **(Fig. 5.14 C.1-C.4)**. Expression of *Grhl3* has not previously been reported in the dorsal neuroepithelium, suggesting that there may be ectopic expression of *Grhl3* at the tips of the neural folds in *ct*^{TgGrhl3}/*ct*^{TgGrhl3} embryos at E8.0-8.5.

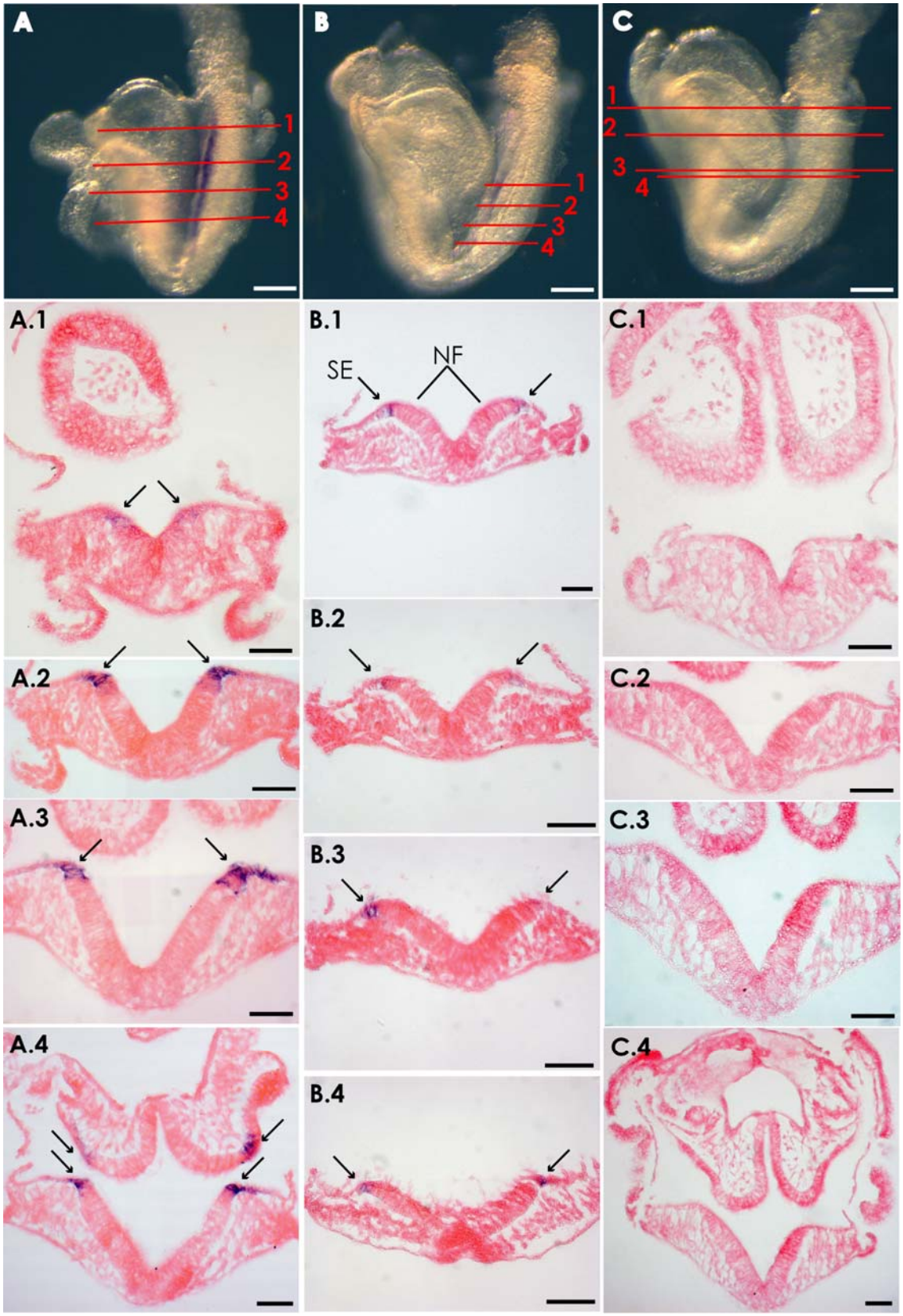
A
B
C
1
2
3
4
A.1
A.2
A.3
A.4
B.1
SE
NF
B.2
B.3
B.4
C.1
C.2
C.3
C.4

Figure 5.14 Sections of embryos at E8.0 following whole mount *in situ* hybridisation for *Grhl3*. Transverse sections through $ct^{TgGrhl3}/ct^{TgGrhl3}$ **(A.1-A.4)** $ct/ct^{TgGrhl3}$ **(B.1-B.4)**, and *ct/ct* (**C.1-C.4**) embryos at E8.0. The axial level of the sections is indicated in the whole mount images (**A-C**) and sites of *Grhl3* expression are indicated by black arrows. *Grhl3* is strongly expressed in the surface ectoderm (SE) and neuroepithelium at the tips of the neural folds (NF) of $ct^{TgGrhl3}/ct^{TgGrhl3}$. Expression in the surface ectoderm (and possibly the neural folds) was detected in $ct/ct^{TgGrhl3}$ transgenic embryos but was not in *ct/ct* embryos. Scale bars: 0.05 mm.

At E8.5 – E9.5 expression of *Grhl3* was less intense in *ct/ct* embryos than in $ct/ct^{TgGrhl3}$ and $ct^{TgGrhl3}/ct^{TgGrhl3}$ embryos where strong expression was observed (**Fig. 5.15**). In the three strains, *Grhl3* is expressed in the posterior neuropore (**Fig. 5.15 A-F**) as well as in the ventral forebrain (**Fig. 5.15 A, C, D**). At these stages, the sites and intensity of expression of *Grhl3* in $ct/ct^{TgGrhl3}$ and $ct^{TgGrhl3}/ct^{TgGrhl3}$ embryos seemed to be similar. Interestingly, expression was observed in a caudal region which may correspond to the primitive streak (or possibly the hindgut pocket), and also at later stages in the tail bud (**Fig. 5.15, F, L; 5.16**). Expression of *Grhl3* in the anterior forebrain was also observed throughout E9.5-E10.0 among embryos of all genotypes (e.g. $ct/ct^{TgGrhl3}$ embryos in **Fig. 5.16**). This expression was also observed in embryos that developed exencephaly (**Fig. 5.16 B**). Strong expression was also observed at the level of the posterior neuropore of the closing neural folds of a $ct/ct^{TgGrhl3}$ embryo (**Fig. 5.16 A-C**). In the caudal region of embryos later at E10.5, the most intense expression of *Grhl3* was observed in the hindgut and the expression in dorsal tissues and the tail bud is absent or very weak (**Fig. 5.17**).

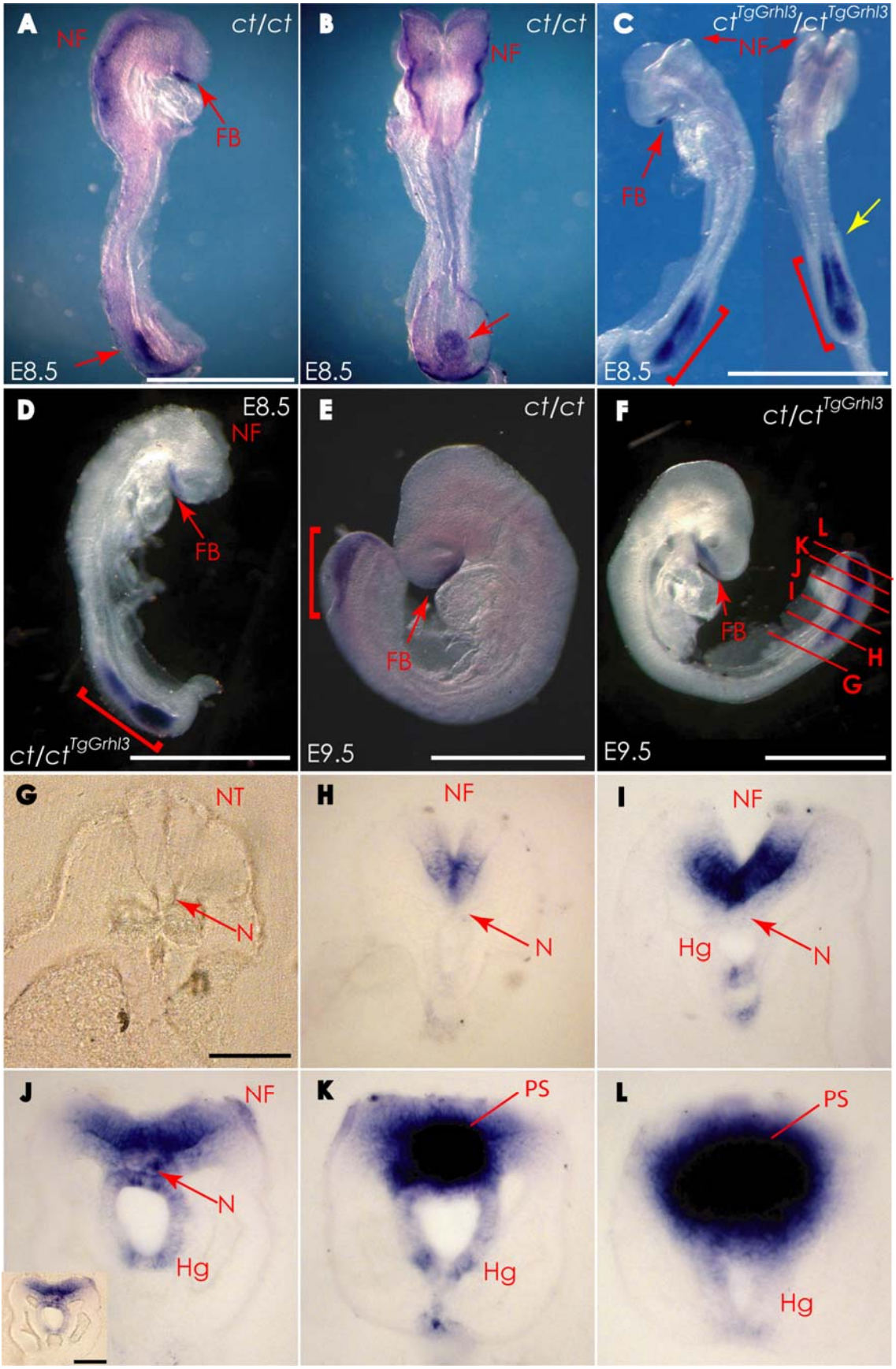
A
NF
ct/ct
FB
E8.5
B
ct/ct
NF
E8.5
C
ctTgGrhl3/ctTgGrhl3
NF
FB
E8.5
D
E8.5
NF
FB
ct/ctTgGrhl3
E
ct/ct
FB
E9.5
F
ct/ctTgGrhl3
L
K
J
I
FB
H
G
E9.5
G
NT
N
H
NF
N
I
NF
Hg
N
J
NF
N
Hg
K
PS
Hg
L
PS
Hg

Figure 5.15 *Grhl3* expression pattern amongst embryos at E8.5-E9.5 stages of development. (**A-B**) E8.5 *curly tail* embryo showing expression in the ventral forebrain (FB), the posterior region of the extending trunk (red arrow, **A**), surface ectoderm of the closing neural folds (NF) at the cranial level, posterior region and primitive streak or gut pocket (red arrow, **B**). (**C**) Lateral and dorsal views of a $ct^{TgGrhl3}/ct^{TgGrhl3}$ embryo at E8.5 (at slightly later stage than **A-B**), showing expression in the posterior region caudally from the forming somites (red bracket), and in the ventral forebrain (FB). Yellow arrow in **C** indicates most caudal somite. (**D**) E8.5 $ct/ct^{TgGrhl3}$ embryo with similar expression pattern to *ct/ct*, but with more intense staining which extends more rostrally staining in the posterior region, as in the $ct^{TgGrhl3}/ct^{TgGrhl3}$ embryo (red bracket). (**E**) A *ct/ct* embryo at early E9.5 shows expression in the anterior forebrain (FB) and posterior neuropore region (red bracket), as well as weakly in the tail bud. A comparable pattern is observed in a similarly staged $ct/ct^{TgGrhl3}$ embryo (**F**), but staining is more intense. (**G-L**) Sections through the caudal region of the embryo in **F**. (**G**) *Grhl3* is not expressed in the upper spine where the neural tube (NT) is closed. (**H-L**) Expression is observed in the open neural folds (NF, **H**), and notochord (N, **J**) with increased intensity in more caudal sections. The primitive streak (PS), remnant with the tail bud, is strongly positive (**K**, **L**). Panels: **A**, **C**, **D**, **F**, side views; **B**, D, **E**, back views. Scale bars: **A-F**, 1.0 mm; **G-L**, 0.1 mm.

To further examine the pattern of expression of *Grhl3* in the caudal region of *Grhl3* transgenics at E10-E10.5, transverse sections were cut through this region (**Fig. 5.16 D-F; Chapter 2, section 2.11.2**). Analysis of the sections confirmed that *Grhl3* expression in the caudal region was localised to the tail bud and neural folds. Weak expression in the hindgut endoderm was also apparent on sections at the level of the closed neural tube (**Fig. 5.16 D**).

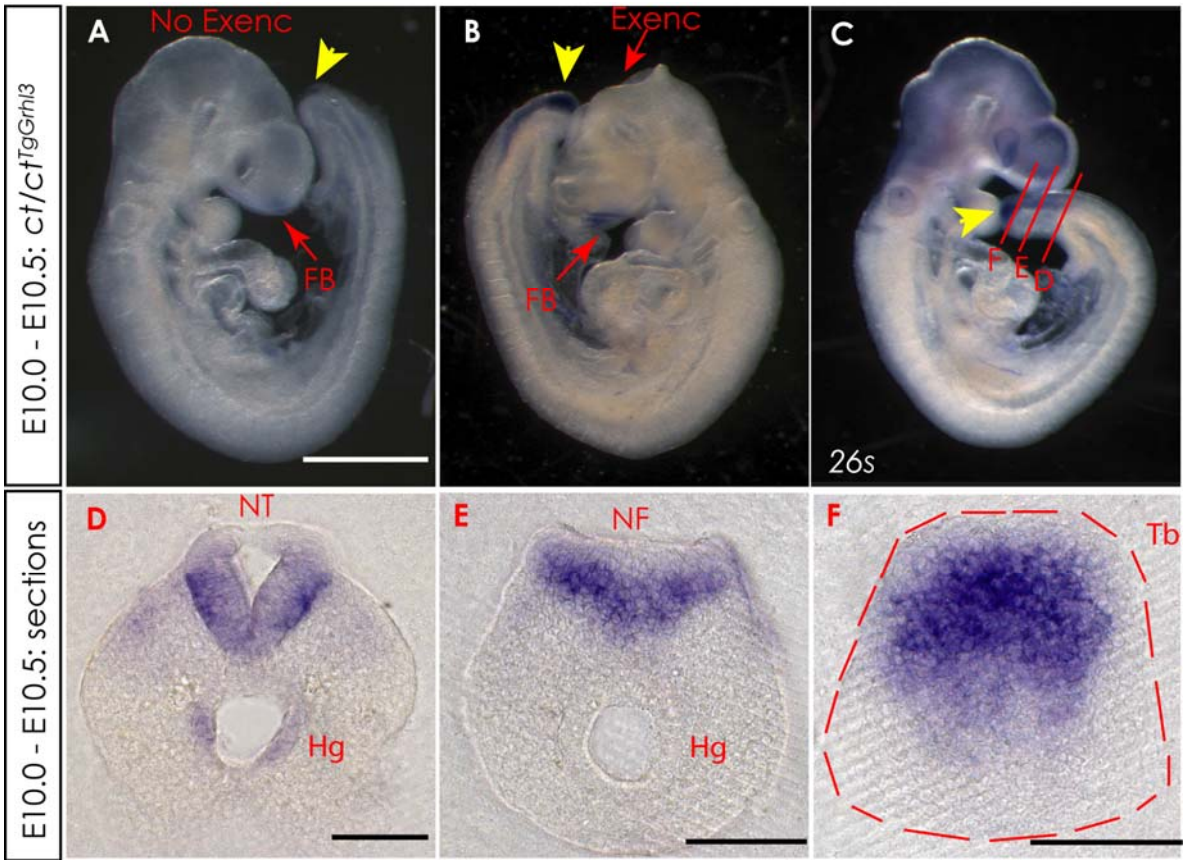

Figure 5.16 Expression of *Grhl3* in *ct/ct*^{TgGrhl3} embryos at E10.0-E10.5. At E10.0 (**A-B**) and early E10.5 (**C**) expression was detected in the ventral forebrain (FB), and in the neural folds of the closing posterior neuropore as well as the tail bud (yellow arrowhead). *Grhl3* expression is observed in embryos with exencephaly (Exenc, **B**), in a comparable pattern to embryos in which the cranial neural tube closed normally (**A, C**). (**D-F**) Sections of the caudal region of the embryo in panel C (at the levels indicated by the red lines). Expression is apparent in the neural tube (NT) and hindgut (Hg) at the level of the closed neural tube (**D**), in the open neural folds at the level of the posterior neuropore (**E**) and in the tail bud (**F**). Panels: **A - C**, side views. Scale bars: **A-C**, 1.0 mm; **D-F**, 0.1 mm.

The aim of the experiments described above was to characterise the *Grhl3* expression pattern in BAC-transgenic embryos. Colour development for *in situ* hybridisation was allowed to proceed for the same period of time for embryos of all genotypes, to avoid over-development of signal in transgenic embryos but to allow comparison with comparably-developed *ct/ct* embryos. Longer periods of signal development reveal the pattern of expression of *Grhl3* in *ct/ct* that was previously reported (Ting et al., 2003a; Gustavsson et al., 2008; Gustavsson et al., 2007). Analysis of embryos at intervals through the signal development process confirmed the elevated expression of *Grhl3* in transgenic embryos. For example, E10.5 embryos that were photographed after: 8 hours and 16 hours of development (**Fig. 5.17 A-F**), emphasised the much more intense expression of *Grhl3* in $ct/ct^{TgGrhl3}$ and $ct^{TgGrhl3}/ct^{TgGrhl3}$ embryos (**Fig. 5.17 B-C**), than in *ct/ct* embryos (**Fig. 5.17 A, D**). Sections through the caudal region of the "16-hour" embryos revealed expression of *Grhl3* in the hindgut of *ct/ct* (**Fig. 5.17 G**), but much more intense expression in the hindgut of transgenic embryos (**Fig. 5.17 H-I**). These sections also show the persistence of *Grhl3* expression in the neural folds of transgenic embryos but absence from *ct/ct*.

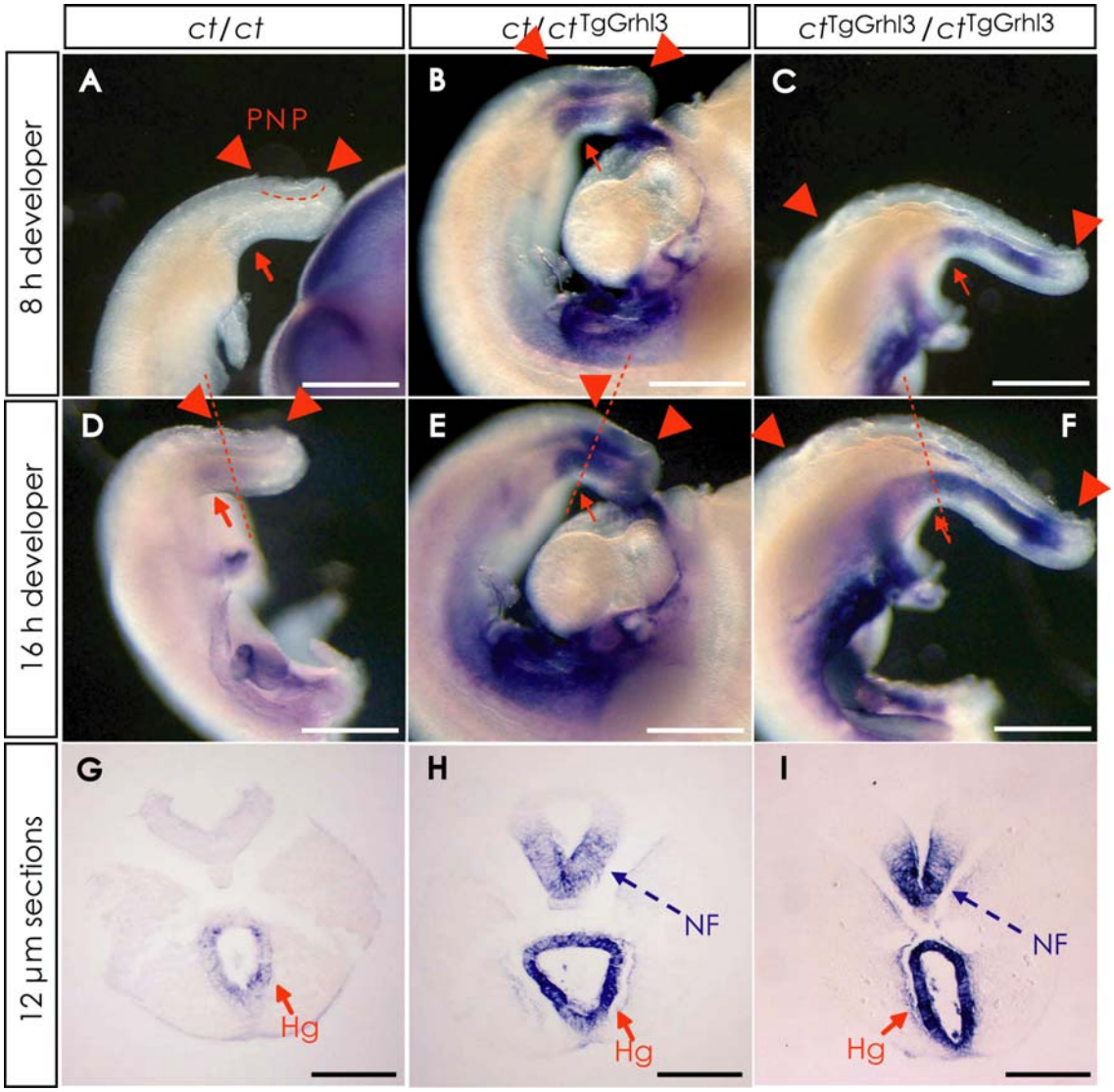

Figure 5.17 *Grhl3* expression at E10.5 at intervals of signal development. (**A-F**) *Grhl3* expression in the caudal region of E10.5 *ct/ct* (**A**, **D**), *ct/ct*^{TgGrhl3} (**B**, **E**) and *ct*^{TgGrhl3}/*ct*^{TgGrhl3} (**C**, **F**) embryos. (**G-I**) Transverse sections at the axial level indicated by the dotted lines in **D-F**. After 8 hours of signal development (**A-C**), *Grhl3* is faintly detectable in the hindgut of *ct/ct* embryos (arrow in **A**), while expression is already clearly evident in transgenic embryos (**B-C**). After 16 hours signal development expression is detected in the hindgut of *ct/ct* (arrow in **D**, **G**), as well as *Grhl3* transgenic embryos with stronger expression in *ct*^{TgGrhl3}/*ct*^{TgGrhl3} (**F**, **I**) than in *ct/ct*^{TgGrhl3} (**E**, **H**) embryos. *Grhl3* is expressed in the ventral neural folds (NF) of *Grhl3* BAC-transgenics but not in *curly tail* embryos. Red arrowheads indicate the extent of the PNP. Scale bars: 0.5 mm in **A-F**, 0.1 mm in **G-I**.

5.3 Discussion

The initial aim of this chapter was to investigate the possible effect of over-expression of *Grhl3* on neural tube closure, using the *Grhl3*-trangenic *curly tail* mice. These experiments show that over-expression of *Grhl3* can result in NTDs. Hence both, insufficient or excessive expression of *Grhl3* can prevent spinal neural tube closure. Interestingly, the defects in some of the embryos that over-express *Grhl3* differed markedly from those typically observed in *ct/ct* embryos. First, the double transgenic embryos have larger posterior neuropores than in *ct/ct* and this phenotype is apparent from an earlier developmental stage. Second, in approximately 50% of cases spina bifida was accompanied by a straight tail rather than curled tail. These factors suggest that there may be a different mechanism underlying the NTDs in these two strains.

Localisation of the BAC in *Grhl3* transgenic embryos by inverse PCR showed that it is present in a low complexity repeat region. While this made it difficult to determine precisely which chromosome carries the BAC, it is apparent that the BAC does not disrupt another gene. It also appears unlikely that regulatory regions distant from another gene are affected. However, one possible BAC-insertion site on chromosome 16 lies only 3 kb from a predicted non-coding mRNA, and the possible effect of this should be further investigated. Overall, it appears likely that NTDs in double transgenics result from over-expression of *Grhl3* rather than homozygous disruption of another locus. In support of this hypothesis, NTDs have recently been observed in *Grhl3* single transgenic embryos ($+/+^{TgGrhl3}$) on a BALB/c genetic background, where the *ct* mutation is absent (N. Greene, Personal Communication). Nevertheless, precise localisation of the BAC would potentially allow a genotyping method to be developed that would avoid the need for qG-PCR. Another way of confirming the localisation of the BAC would be by fluorescence *in situ* hybridisation (FISH). For this reason, mouse primary fibroblast cell lines were generated from single transgenic embryos and wild-type control strains for analysis of metaphase chromosomes (**Chapter 2, sections 2.15, and 2.15.1**). FISH will be performed in the near future, in collaboration with Dr. P. Gustavsson.

Use of quantitative real-time genomic PCR (qG-PCR) to evaluate the genomic copy number of *Grhl3* enabled the differentiation of transgenic embryo samples into single and double transgenics to be used in subsequent experiments. The gene copy number can be inferred through the level of *Grhl3* DNA using a *ct/ct* sample to normalise with a value of 1.0, equivalent to two *Grhl3* alleles and no BAC. Single transgenic embryos had a mean relative quantity of 2.5, which is predicted to correspond to the 2 endogenous alleles and 3 "copies" of the BAC in hemizygosity. The predicted double transgenic embryos had a qG-PCR mean value of around 4.0, which corresponds to the two endogenous *Grhl3* alleles and an estimated 6 "copies" of the BAC. Assuming that the chromosomal location of the BAC does not result in a higher apparent qG-PCR result, these data suggest that the BAC was inserted as a triplicate repeat.

The high levels of *Grhl3* expression in the double transgenic embryos and the fact they develop spina bifida, instigated an investigation of the expression pattern of *Grhl3* throughout stages of neural tube closure. Attardi et al (1993) demonstrated that the correct regulation of GRH is essential for proper development and viability in *Drosophila*, although it was unclear whether the defects induced by over-expressing full-length GRH resulted from abnormally high levels of GRH in cells in which it is normally present, expression of GRH in cells which it is not usually found, or both.

In the current study it is possible that spina bifida resulting from over-expression of *Grhl3* is due to excessive levels at the normal sites of expression. Alternatively, it is possible that expression also occurs at ectopic or temporally inappropriate sites. For example, *Grhl3* expression in the neural folds is normally seen at E9.0, but it was found to persist in the ventral neural tube to E10.5 in *Ghrl3*-transgenic *curly tail* embryos (Gustavsson et al., 2007).

In *curly tail* embryos, *Grhl3* expression has been reported in the surface ectoderm adjacent to the neural folds and the most anterior neural folds in the forebrain at E8.5 (Ting et al., 2003a; Gustavsson et al., 2007), although expression was barely detectable at E8.0 in this study. Between E9.0-E9.5, *ct/ct* embryos express *Grhl3* in the tail bud, the open neural folds of the PNP and the ventral forebrain (Gustavsson et al., 2007). The expression in the open neural folds is no longer detected at later stages (E10.0-10.5) but expression is evident in the hindgut (Gustavsson et al., 2007). In this project, *Grhl3*

expression in $ct^{TgGrhl3}$ embryos was clearly detectable in the surface ectoderm immediately lateral to the neural plate at E8.0-8.5. At later stages the expression pattern reproduced that observed in *ct/ct*, except that the signal was more intense and the expression in the ventral neural tube persisted until E10.5, the same stage at which *Grhl3* is expressed in the hindgut (**Fig. 5.13-5.17**, and (Gustavsson et al., 2007).

Expression of *Grhl3* in $ct^{TgGrhl3}/ct^{TgGrhl3}$ embryos was very similar to that observed in $ct/ct^{TgGrhl3}$ embryos but the signal was more intense. Interestingly, transverse sections through the neural folds of $ct^{TgGrhl3}/ct^{TgGrhl3}$ at E8.0, revealed expression of *Grhl3* not only in the surface ectoderm, as expected (Ting et al., 2003a; Camerer et al., 2010b), but also in the tips of the neural folds. Thus, there appears to be ectopic expression of *Grhl3* in the dorsal neuroepithelium of $ct^{TgGrhl3}/ct^{TgGrhl3}$ embryos at E8.0-8.5, as well as abnormally persistent expression of *Grhl3* in the ventral neuroepithelium at E10.0-10.5.

Expression of *Grhl3* in the tail bud has not been previously investigated and it is therefore not known whether altered expression in the tail bud relates to the development of tail flexion defects in *ct/ct* embryos. In addition, the biological function of *Grhl3* expression in the posterior primitive streak has not yet been addressed. It has been shown that genes expressed in regions of the streak continue their expression in subpopulations of the tail bud (Gont et al., 1993; Wilson and Beddington, 1996). Sagittal sections of the posterior region of whole mount *in situ* hybridisation E8.5 embryos could reveal the exact *Grhl3* expression sites compared to fate maps of the primitive streak already existent in the literature, such as the one published by Wilson and Beddington (1996). The use of lineage trace markers could also be applied to embryos in culture followed by in situ hybridisation to see if cells of the primitive streak co-express with sites of *Grhl3*.

In contrast to the rescue of spinal NTDs, transgenic embryos develop exencephaly with the same frequency as *ct/ct* embryos and there was no significant difference in the incidence of exencephaly between single and double transgenics. These data suggest that over-expression of *Grhl3* does not exacerbate cranial neural tube closure. On the other hand, a role for insufficient expression of *Grhl3* in the causation of exencephaly in *ct/ct* embryos cannot be ruled out as a low incidence of exencephaly has been reported in *Grhl3* null embryos (Ting et al., 2003a; Yu et al., 2006e). However, it also appears

likely that the *curly tail* genetic background predisposes to exencephaly as folate deficiency can induce exencephaly in $+^{ct}/+^{ct}$ embryos, but not in other wild-type strains (Burren et al., 2010). It will be necessary to analyse the expression level of *Grhl3* in the cranial region at E8.5-9.0, to further investigate the correlation with failure of cranial neural tube closure.

As described in **Chapter 1**, the cellular mechanism resulting in spina bifida and/or tail defects in *curly tail* embryos is a reduced proliferation rate in the hindgut and notochord, while normal proliferation occurs in the neural folds (Copp et al., 1988a; Copp, 1985a). In $ct/ct^{TgGrhl3}$ embryos, enhanced *Grhl3* expression correlates with an increased proliferation rate in the hindgut and consequent normalisation of neural tube closure (Gustavsson et al., 2007). It has not yet been investigated whether *Grhl3* expression in the neural folds, detectable at E9.5, is necessary for neural tube closure in the spinal region. However, expression is not detected in the spinal neural folds in *ct/ct* or wild-type embryos at E10.5, while it is present in $ct/ct^{TgGrhl3}$ embryos that develop normally. Whether this expression has any functional effect has yet to be determined. For example, it would be of interest to examine expression of dorso-ventrally restricted genes, such as the floor plate marker *sonic hedgehog* (*Shh*), to test whether the persistent expression of *Grhl3* in the ventral neural folds perturbs overall patterning.

The cellular basis of NTDs in $ct^{TgGrhl3}/ct^{TgGrhl3}$ embryos and indeed in *Grhl3* null embryos remains to be determined. The phenotype and earlier onset of PNP delay in double transgenic embryos suggest that the mechanism underlying NTDs could differ from *ct/ct* embryos, and it could be speculated that the over-expression of *Grhl3* in the neural folds plays a role. Excess *Grhl3* could potentially misregulate target genes in the neural folds, perhaps leading to an effect on proliferation. Given that *Grhl3* up-regulation in the hindgut stimulates proliferation, it is possible that there could be a similar effect in the neural folds. At E9.5-10.5, this expression is in the ventral neural folds and it could be hypothesised that a proliferation imbalance between the dorsal and ventral neural folds would hinder closure. Indeed, a similar mechanism has been suggested to underlie exencephaly in the *Phactr4* mutant mouse (Kim et al., 2007). Alternatively, a mechanism related to faulty fusion of the neural folds might be implicated. For example, the ectopic expression of *Grhl3* in the tips of the neural folds

in $ct^{TgGrhl3}/ct^{TgGrhl3}$ embryos, as well as in the overlying surface ectoderm, might exert a cellular effect that compromises the fusion process.

Would other defects, unrelated to NTDs, be expected in the $ct^{TgGrhl3}/ct^{TgGrhl3}$ embryos? *Grhl3* null embryos show defective skin barrier formation in addition to NTDs. In epidermal wound healing, Grainy head-like transcription factors (dGrh, Grhl3 in mammals) drive expression of proteins that participate in cross-linking of barrier components (Mace et al., 2005; Ting et al., 2005; Yu et al., 2006d). In a microarray analysis of skin at E18.8 (Yu et al., 2006c) there was a decrease in the expression of a large number of tight junction molecules, including claudin and occludin which may contribute to the barrier defect of the null-*Grhl3* mice. In addition, *Grhl3* mutant mice also have defective epithelial barrier formation in the bladder, resulting from failure of apical membrane specialization (Yu et al., 2009). *Grhl3* knockout mice have an open-eye phenotype at birth, thought to result from loss of the downstream effects of this gene in actin polymerisation and filopodia formation, required for migration and differentiation of epithelial cells at the leading edge during eyelid closure (Yu et al., 2006b; Yu et al., 2008). Whether there is an overall epidermal barrier and/or terminal differentiation effects in the same tissues in the *curly tail* transgenic embryos over-expressing *Grhl3,* in addition to failure of neural tube closure, has yet to be determined.

Key questions remain to be answered in relation to the development of spinal NTDs caused by over- or under-expression of *Grhl3*. What genes are direct targets of *Grhl3* during neural tube closure (activated or suppressed by *Grhl3*) and which of these are misregulated in association with development of NTDs? These questions have been addressed in two different ways, by 2D gel analysis (**Chapter 3**) and in a microarray comparing samples of the caudal region of the *curly tail*, wild-type, single and double transgenic strains (N. Greene, personal communication). In future, 2D gels will be generated using samples of double transgenic embryos in order to determine whether there are specific proteome changes in comparison to the three other strains. It is hypothesised that one or more of the *Grhl3* target genes are essential for the timing of the development of certain tissues in the mouse embryo (characterised by the dynamic spatio-temporal *Grhl3* expression). Faulty regulation of these target genes in *ct/ct* or double transgenic embryos is suggested to contribute to the NTD phenotype. Also, it is

possible that over-expression of *Grhl3* affects novel targets, or disrupts function of binding partners (Kudryavtseva et al., 2003; Yu et al., 2006a).

In conclusion, this chapter has identified a deleterious effect of over-expression of *Grhl3* that is analogous to the loss-of-function effect (neural tube closure failure) but is distinct in precise timing and phenotype. Further comparative analysis of this over/under expression phenomenon should significantly advance our understanding of the role of *Grhl3* in mouse neurulation.

Chapter 6

General Discussion

6.1 Identification of a polymorphism in lamin B1 that modifies risk of NTDs

In this project, investigation of possible abnormalities in the *curly tail* proteome by two-dimensional protein electrophoresis revealed several proteins whose differential abundance may be influenced by *Grhl3* expression level. However, the most striking difference between wild-type and *curly tail* was in migration of lamin B1 protein spots, which led to the identification of a polymorphism in lamin B1. Proteomic studies often focus on identification of proteins whose abundance differs under different conditions or in particular disease states. In contrast, few studies have used 2-DE and mass spectrometry to define the genetically encoded variations in proteins in related mouse strains. This information can be revealed, as in this study, by altered migration of proteins on 2-DE. In one study using large-scale 2D gels a comparison of the distantly related mouse strains, *Mus musculus* C57BL/6 and *Mus spretus*, found consistent differences in 1,000 of 9,000 detected proteins. Among these differences around one-third corresponded to variation in protein migration some of which were attributed to amino acid variation (Klose et al., 2002). In other cases genetic mapping of the protein phenotype implied that migration differences were secondary to polymorphism in other proteins. Another recent 2-DE based study of inbred mouse strains that differ in susceptibility to experimental autoimmune encephalomyelitis found missense variants in around 5% of proteins analysed (Mikkat et al., 2010). In the strains used in the current study it is anticipated the far fewer proteins will show sequence variation as the wild-type ($+^{ct}$) and *curly tail* strains are predicted to share more than 93.8% genetic background. Thus, while polymorphisms will be evident at the level of genomic or mRNA sequence, proteomic approaches may be useful to identify protein variants, particularly in strains for which full genomic sequence is not available.

The variation in length of glutamate repeat in lamin B1 (8 or 9 residues) appears to have a functional effect on the stability of lamin B1 within the nuclear envelope and to influence morphology of the nucleus. Notably, the lamin B1 variants influenced the penetrance of NTDs in the *curly tail* mouse, suggesting that lamin B1 is a modifier gene for NTDs, at least in this model. A survey of 150 mouse mutants known in the literature showed that only 20% exhibit risk of either exencephaly and spina bifida or both, whereas 70% only develop exencephaly (Harris and Juriloff, 2007). Reduced expression of *Grhl3* can cause both spina bifida and exencephaly, and it is now apparent that *Lmnb1* can modify the risk of both conditions.

It is not yet know whether the 8E lamin B1 variant exacerbates a deleterious consequence of the diminished *Grhl3* expression in *curly tail* or increases the susceptibility to NTDs through an independent mechanism. The finding that nuclear morphology is partially normalised in $ct/ct^{TgGrhl3}$ cells, which over-express *Grhl3* but carry the 8E lamin B1 allele, perhaps argues that both lamin B1 and *Grhl3* can functionally affect nuclear structure and this is the basis of the genetic interaction. On the other hand, mild tail flexion defects and occasional exencephaly have been observed in wild-type embryos carrying the 8E lamin B1 variant ($+^{ct;8E}$), which suggests that on a permissive genetic background for NTDs the lamin B1 variant can cause NTDs even in the absence of a *Grhl3* mutation. This finding raises the possibility that lamin B1 polymorphisms could influence susceptibility to NTDs in other models.

Interestingly, the *Lmnb1* glutamic acid variant is present in the genetic background of *splotch* (Sp^{2H}) mutant mice in our laboratory. *Splotch* (Sp^{2H}) carry a mutation in the transcription factor *Pax3* (*paired box gene 3*), and homozygous embryos develop exencephaly (around 60% frequency) and almost fully penetrant spina bifida (Greene et al., 2009a). The primary cellular defect leading to NTDs in these embryos is in the neuroepithelium and neural crest cell migration is also defective (Greene et al., 2009a). As in *curly tail*, the frequency of NTDs in *splotch* mutants is also influenced by genetic background and environmental factors (Greene et al., 2009a). Homozygotes for another mutant allele of *Pax3*, the *Pax3-Cre* knock-in (Engleka et al., 2005), also display spina bifida in most cases but the frequency of exencephaly is only around 25% in our laboratory (N Greene, Personal Communication). Since both the Sp^{2H} and *Pax3-Cre* knock-in alleles are thought to be functionally null alleles, it is intriguing to speculate that the differences in frequency of exencephaly relates in part to an effect of the lamin B1 polymorphism. In future, it would be interesting to generate a *splotch* line carrying the lamin B1 9E variant, to test whether there is a decline in the penetrance of cranial NTDs.

6.2 Lamin B1 as a candidate gene to affect risk of human NTDs

Curly tail is probably the best characterised mouse model of spina bifida and similar to human NTDs, the risk is attributed to multifactorial inheritance and environmental factors (Van Straaten and Copp, 2001). The identification of lamin B1 as a modifier

gene raises the possibility that lamin B1 polymorphisms could influence risk of NTDs in humans. The glutamate repeat contains 8 residues in humans, perhaps casting doubt as to whether this repeat is likely to be deleterious for neural tube closure in humans. To follow up this study, it would be interesting to sequence human *LMNB1* in a cohort of spina bifida and exencephaly patients.

Duplications in *LMNB1* (over-expression) have been associated with the demyelinating disease adult-onset autosomal dominant leukodystrophy (ADLD; (Padiath et al., 2006; Meijer et al., 2008). In spite of the fact that ADLD has a phenotype similar to chronic progressive multiple sclerosis (MS), no duplications/deletions or point mutations were identified in a study of MS patients (Brussino et al., 2009). More recently, an Italian family with ADLD but without mutations in *LMNB1* has been reported, suggesting that ADLD is clinically and genetically heterogeneous (Brussino et al., 2010).

6.3 Possible relationship between lamin B1 and the effect of inositol status on risk of NTDs

Depletion of inositol in media used for whole embryo culture causes NTDs (Cockroft et al., 1992). Interestingly, embryos of the *CBA* and *curly tail* strains showed similar high incidence of cranial defects compared to the inbred *PO* (Pathology Oxford) strain. It was suggested that the greater sensitivity of the *ct* and *CBA* strains, compared to *PO*, was due to background genetic differences between the strains since *ct* and *CBA* share a similar background. In the current project it was shown that this shared genetic background includes the 8E lamin B1 variant, which affected susceptibility to cranial as well as spinal NTDs, and may therefore be implicated in predisposition to inositol deficiency-induced NTDs.

Spinal NTDs in *curly tail* embryos can be prevented by inositol supplementation at the time of posterior neuropore closure (Greene and Copp, 1997). This effect is exerted through protein kinase C (PKC), downstream of the inositol phospholipid cycle, which acts to phosphorylate as yet unknown target proteins and stimulates proliferation in the hindgut (Greene and Copp, 1997; Cogram et al., 2004). Interestingly, human lamin B1 protein is phosphorylated by protein kinase C-βII at serines 395 and 405 in the carboxyl-terminal domain, immediately adjacent to the central α-helical rod-domain

(Hocevar et al., 1993; Goss et al., 1994). In addition, in the mouse lamin B1 has been found to be a PKC-binding protein, where amino acids 200-217 of the calcium-dependent lipid binding (CaLB) domain of PKC-α seem to be essential for binding of lamin B1 at the carboxyl-terminus of the protein (Martelli et al., 2000; Tabellini et al., 2002). Another study have shown that the inositide-specific phospholipase Cβ1 (PLCβ1) also co-localises and physically interacts with lamin B1, and may play a role in G2/M progression of the cell cycle (Fiume et al., 2009).

As lamin B1 is a potential target for PKC it would be of interest to determine whether the tail domain of lamin B1 can interact with PKCßI and/or γ, the isoforms required for prevention of NTDs in *curly tail* (Cogram et al., 2004). To test for a functional role of lamin B1 phosphorylation in the protective mechanism of inositol it would be necessary to investigate the possibility of differential phosphorylation in inositol-treated and untreated samples. These two experiments might provide a clue to a possible correlation between inositol status and lamin B1 function in the rescue of spina bifida in *curly tail*.

6.4 *Grainyhead-like-3* and the pathogenesis of NTDs

In parallel with studies on the *curly tail* mouse, in which *Grhl3* is expressed at diminished levels, this project also investigated the effects of over-expressing *Grhl3* by making use of the $ct^{TgGrhl3}$ strain. The presence of severe spinal NTDs in 'double' transgenic embryos, demonstrated that both over-expression, as well as insufficient expression of *Grhl3* can cause NTDs. Together these data suggest that regulation of *Grhl3* expression is crucial for neural tube closure (summarised in **Figure 6.1**).

Key questions remain to be answered related to the role of *Grhl3* and the mechanism of neural tube closure. Primary neurulation of the spinal cord involves elevation of the neural plate, apposition of the neural folds and their subsequent fusion. Neural fold elevation involves cell shape changes, cell rearrangements and cell division within the neuroepithelium. In addition, forces extrinsic to the neuroepithelium can affect closure, as is the case in *curly tail* embryos where reduced proliferation in the hindgut leads indirectly to impaired closure (Greene and Copp, 2004). As *Grhl3* is a transcription factor the deleterious effect of altered expression levels is presumed to result from miss-regulation of target genes. A key step in understanding development of NTDs in *curly*

tail and *Grhl3*-transgenic embryos will be identification of the key downstream genes. The possible range of genes that could be involved is illustrated by the large number and diversity of mouse models for NTDs (Harris and Juriloff, 2007; Harris and Juriloff, 2010). The genes implicated include transcription factors, signalling proteins, cytoskeletal proteins, cell membrane proteins, nuclear receptors and tumor repressors.

The causative defect in *curly tail* embryos is localised in the hindgut, resulting in increased axial curvature which is apparent from about the 25 somite stage and more evident at somite stages 27-29 (Brook et al., 1991). The proliferation defect correlates with the expression of *Grhl3* in the hindgut at this stage. In contrast, measurements of the posterior neuropore in $ct^{TgGrhl3}/ct^{TgGrhl3}$ embryos suggest that the defects arise earlier in development than in *ct/ct*, at a stage when *Grhl3* is expressed in the surface ectoderm and neuroepithelium. The stage at which defects arise in $Grhl3^{-/-}$ embryos has not been accurately determined (Ting et al., 2003a; Rifat et al., 2010), but recent studies in our laboratory suggest that closure fails from as early as the 15 somite stage (Dr N Greene, Personal Communication).

In embryos with moderately up-regulated expression of *Grhl3* ($ct/ct^{TgGrhl3}$), expression was first detected in the surface ectoderm adjacent to the tips of the dorsal neural folds. This correlates with expression reported in wild-type embryos (N Greene, Personal Communication) and in embryos carrying a *Grhl3*-Cre knock-in allele with a lacZ reporter (Camerer et al., 2010b). Expression of *Grhl3* in $ct^{TgGrhl3}/ct^{TgGrhl3}$ embryos is observed in appropriate sites but at higher intensity, but it is also detected in the dorsal neural folds at E8.5. Therefore, it is possible that the cellular defect which causes spinal NTDs in these embryos could be localised in the surface ectoderm, neural folds or both. Expression of *Grhl3* also persists in the ventral neural folds of $ct^{TgGrhl3}/ct^{TgGrhl3}$ at E10.5, a later stage than observed in wild-type embryos. However, as spinal neural tube closure is already abnormal prior to this stage the ectopic expression in the ventral neural folds appears less likely to be the cause of NTDs.

In order to test further the tissue localisation of the causative defect in *Grhl3* over-expressing embryos it may be possible to make use of intercrosses between *Grhl3* over-expressing and conditional mutant mice. An initial experiment would be to test whether knock-out of endogenous *Grhl3* is sufficient to rescue the *Grhl3* over-expression

phenotype, and vice versa. If double homozygotes do not show NTDs it would suggest that the *Grhl3* expression level has been brought within a range that is compatible with neural tube closure. In this case it may then be possible to make use of conditional *Grhl3* mutant mice (Yu et al., 2006), together with mice expressing Cre recombinase in the neuroepithlium which would allow deletion of *Grhl3* selectively in this tissue. A breeding scheme would be performed to generate embryos in which endogenous *Grhl3* is deleted specifically in the neural folds but *Grhl3* is over-expressed from the BAC in homozygosity. If these embryos complete neural tube closure it would suggest that NTDs associated with *Grhl3* over-expression result from a defect in the neuroepithelium, that is rescued by reduction of *Grhl3* expression in this tissue (through deletion of the endogenous gene).

Ybot-Gonzalez et al. (2002) showed that DLHP formation requires signals from the surface ectoderm, and it could be hypothesised that *Grhl3* expression in the surface ectoderm is required for this signalling. It has been reported that dorsolateral hinge points (DLHP), which are normally formed in the neural folds from E9.5 (Ybot-Gonzalez et al., 2007a), are absent in the neural folds of $Grhl3^{-/-}$ embryos (Rifat et al., 2010). However, this phenotype was shown in sections at E10.5 and distant from the site where closure fails so it is possible that the reported lack of DLHPs is a secondary consequence of a very large open PNP. To investigate the possible contribution of abnormal DLHP formation in $Grhl3^{-/-}$ spinal NTDs, it will be necessary to analyse transverse sections through the caudal region of embryos from somite stage 14-15. The presence or absence of DLHP in $ct^{TgGrhl3}/ct^{TgGrhl3}$ embryos has not yet been assessed.

It is thought that the initial contact of the neural folds during closure may occur at the junction of neural folds and surface ectoderm. It is therefore possible that the loss or over-expression of *Grhl3* may have a cell autonomous effect leading to failure of the fusion process. Alternatively, over-expression of *Grhl3* in an ectopic location in the dorsal neural folds at E8.5 may alter cellular properties required for closure. As *Grhl3* is required for correct proliferation in the hindgut, it could be speculated that high levels of *Grhl3* could result in excessively high proliferation rates in the neural folds that compromise closure. Overall, differences in the stage at which defects arise and the possible affected tissues will need to be considered in analysing gene expression

abnormalities that may be causally related to NTDs in the *Grhl3* related models (**Table 6.1**).

Strain	**Predicted site of cellular defect**	**Possible mechanism**
ct/ct	Hindgut	Proliferation
$ct^{TgGrhl3}/ct^{TgGrhl3}$	Surface ectoderm? Neural folds?	Proliferation? Fusion? Signalling – DLHP?
$Grhl3^{-/-}$	Surface ectoderm? Neural folds (?)	

Table 6.1 Possible mechanisms underlying development of NTDs in *Grhl3* related mouse models. In *ct/ct* the spinal NTDs are due to a proliferation defect in the hindgut. The molecular and cellular defects leading to NTDs in *Grhl3* null or over-expressing mice remain to be determined. Abbreviation: DLHP, dorsolateral hinge points.

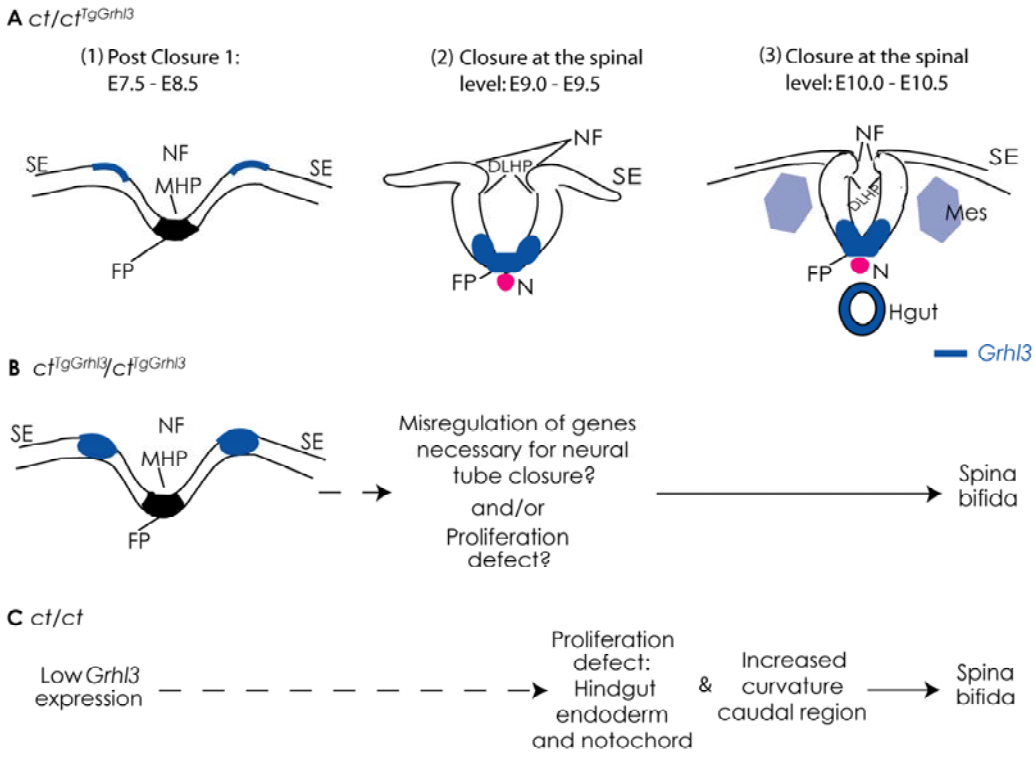

Figure 6.1 The relationship between *Grhl3* expression and development of NTDs. (**A**) *Grhl3* domains (blue) of expression during the events of neural tube closure in the *ct/ct*^{TgGrhl3} strain. (**1**) From E7.5 *Grhl3* is expressed dorsally in the surface ectoderm, at the tips of the neural folds (NF) after initial site of neural tube closure (Closure 1). (**2**) At the spinal level, E9.0-9.5, *Grhl3* is expressed in the ventral neural folds including the floor plate (FP). During this period, dorsolateral hinge points (DLHP) are formed, which facilitate apposition of the tips of the folds. (**3**) At E10.5, neural tube closure culminates with adhesion and fusion of the folds at the level of the posterior neuropore, when *Grhl3* is expressed in the hindgut endoderm and still expressed in the ventral neural folds (although this expression is not detected in wild-type or *ct/ct* embryos. (**B**) The *ct*^{TgGrhl3}/*ct*^{TgGrhl3} embryos exhibit the same domains of *Grhl3* expression as in *ct/ct*^{TgGrhl3}, but expression levels are elevated. In addition, expression is observed in the dorsal neural folds at E8.5. Spinal closure fails in these embryos from E9.5. (**C**) *Curly tail* embryos express low levels of *Grhl3*. At E10.0 a cellular defect in the hindgut (Hgut) and notochord (N) leads to ventral curvature, this mechanically apposes dorsal closure of the neural folds, resulting in spina bifida. Closure 1 occurs normally in the *ct*^{TgGrhl3}/*ct*^{TgGrhl3} and in *ct/ct* embryos. Abbreviations: Mes, mesoderm; MHP, median hinge point; SE, surface ectoderm.

6.5 *GRHL3* as a candidate gene for NTDs in humans

The human orthologue of *Grhl3* is localised on human chromosome 1p36, a region often somatically deleted in Merckel cell carcinoma (Leonard et al., 2000), basal cell carcinomas (Jin et al., 2001), and melanoma (Zhang et al., 1999). Whether *GRHL3* itself is involved in these conditions is yet to be determined.

As loss of *Grhl3* function causes NTDs in mice it is speculated that *GRHL3* represents a candidate gene for NTDs in humans, but to date no putative *GRHL3* mutations have been reported. However, studies in the mouse have shown that regulation of *Grhl3* expression level is critically important for neural tube closure, even when the coding sequence is intact. This raises the possibility that regulatory mutations, which affect expression levels of *GRHL3*, could also increase risk of NTDs in the human population. It would also be of interest to screen NTD cases for variation in *GRHL3* gene copy number that could affect the expression level during development.

References

Attardi,L.D., Von,S.D., and Tjian,R. (1993). Ectopic expression of wild-type or a dominant-negative mutant of transcription factor NTF-1 disrupts normal Drosophila development. Proc. Natl. Acad. Sci. U. S. A *90*, 10563-10567.

Auden,A., Caddy,J., Wilanowski,T., Ting,S.B., Cunningham,J.M., and Jane,S.M. (2006). Spatial and temporal expression of the Grainyhead-like transcription factor family during murine development. Gene Expr. Patterns. *6*, 964-970.

Ausma,J., van Eys,G.J., Broers,J.L., Thone,F., Flameng,W., Ramaekers,F.C., and Borgers,M. (1996). Nuclear lamin expression in chronic hibernating myocardium in man. J. Mol. Cell Cardiol. *28*, 1297-1305.

bdul-Aziz,N.M., Turmaine,M., Greene,N.D., and Copp,A.J. (2009). EphrinA-EphA receptor interactions in mouse spinal neurulation: implications for neural fold fusion. Int. J. Dev. Biol. *53*, 559-568.

Beaudin,A.E. and Stover,P.J. (2009). Insights into metabolic mechanisms underlying folate-responsive neural tube defects: a minireview. Birth Defects Res. A Clin. Mol. Teratol. *85*, 274-284.

Beaudin,A.E. and Stover,P.J. (2007). Folate-mediated one-carbon metabolism and neural tube defects: balancing genome synthesis and gene expression. Birth Defects Res. C. Embryo. Today *81*, 183-203.

Beier,D.R., Dushkin,H., and Telle,T. (1995). Haplotype analysis of intra-specific backcross curly-tail mice confirms the localization of *ct* to Chromosome 4. Mamm. Genome *6*, 269-272.

Berggren,K., Chernokalskaya,E., Steinberg,T.H., Kemper,C., Lopez,M.F., Diwu,Z., Haugland,R.P., and Patton,W.F. (2000). Background-free, high sensitivity staining of proteins in one- and two-dimensional sodium dodecyl sulfate-polyacrylamide gels using a luminescent ruthenium complex. Electrophoresis *21*, 2509-2521.

Bergo,M.O., Leung,G.K., Ambroziak,P., Otto,J.C., Casey,P.J., Gomes,A.Q., Seabra,M.C., and Young,S.G. (2001). Isoprenylcysteine carboxyl methyltransferase deficiency in mice. J Biol Chem. *276*, 5841-5845.

Bjellqvist,B., Ek,K., Righetti,P.G., Gianazza,E., Gorg,A., Westermeier,R., and Postel,W. (1982). Isoelectric focusing in immobilized pH gradients: principle, methodology and some applications. J. Biochem. Biophys. Methods *6*, 317-339.

Boyles,A.L., Hammock,P., and Speer,M.C. (2005). Candidate gene analysis in human neural tube defects. Am. J. Med. Genet. C. Semin. Med. Genet. *135*, 9-23.

Bray,S.J., Johnson,W.A., Hirsh,J., Heberlein,U., and Tjian,R. (1988). A cis-acting element and associated binding factor required for CNS expression of the Drosophila melanogaster dopa decarboxylase gene. EMBO J. *7*, 177-188.

Bray,S.J. and Kafatos,F.C. (1991a). Developmental function of Elf-1: an essential transcription factor during embryogenesis in Drosophila. Genes Dev. *5*, 1672-1683.

Bray,S.J. and Kafatos,F.C. (1991b). Developmental function of Elf-1: an essential transcription factor during embryogenesis in Drosophila. Genes Dev. *5*, 1672-1683.

Broers,J.L., Machiels,B.M., Kuijpers,H.J., Smedts,F., van den,K.R., Raymond,Y., and Ramaekers,F.C. (1997). A- and B-type lamins are differentially expressed in normal human tissues. Histochem. Cell Biol. *107*, 505-517.

Brook,F.A., Estibeiro,J.P., and Copp,A.J. (1994). Female predisposition to cranial neural tube defects is not because of a difference between the sexes in rate of embryonic growth or development during neurulation. J. Med. Genet. *31*, 383-387.

Brook,F.A., Shum,A.S.W., Van Straaten,H.W.M., and Copp,A.J. (1991). Curvature of the caudal region is responsible for failure of neural tube closure in the curly tail (ct) mouse embryo. Development *113*, 671-678.

Brussino,A., D'Alfonso,S., Cagnoli,C., Di,G.E., Barberis,M., Padovan,S., Vaula,G., Pinessi,L., Squadrone,S., Abete,M.C., Collimedaglia,L., Guerini,F.R., Migone,N., and Brusco,A. (2009). Mutations in the lamin B1 gene are not present in multiple sclerosis. Eur. J. Neurol. *16*, 544-546.

Brussino,A., Vaula,G., Cagnoli,C., Panza,E., Seri,M., Di,G.E., Scappaticci,S., Camanini,S., Daniele,D., Bradac,G.B., Pinessi,L., Cavalieri,S., Grosso,E., Migone,N., and Brusco,A. (2010). A family with autosomal dominant leukodystrophy linked to 5q23.2-q23.3 without lamin B1 mutations. Eur. J. Neurol. *17*, 541-549.

Burgoon,J.M., Selhub,J., Nadeau,M., and Sadler,T.W. (2002). Investigation of the effects of folate deficiency on embryonic development through the establishment of a folate deficient mouse model. Teratology. *65*, 219-227.

Burren,K.A., Savery,D., Massa,V., Kok,R.M., Scott,J.M., Blom,H.J., Copp,A.J., and Greene,N.D. (2008). Gene-environment interactions in the causation of neural tube defects: folate deficiency increases susceptibility conferred by loss of Pax3 function. Hum. Mol. Genet. *17*, 3675-3685.

Burren,K.A., Scott,J.M., Copp,A.J., and Greene,N.D. (2010). The genetic background of the curly tail strain confers susceptibility to folate-deficiency-induced exencephaly. Birth Defects Res. A Clin. Mol. Teratol. *88*, 76-83.

Caddy,J., Wilanowski,T., Darido,C., Dworkin,S., Ting,S.B., Zhao,Q., Rank,G., Auden,A., Srivastava,S., Papenfuss,T.A., Murdoch,J.N., Humbert,P.O., Parekh,V., Boulos,N., Weber,T., Zuo,J., Cunningham,J.M., and Jane,S.M. (2010). Epidermal wound repair is regulated by the planar cell polarity signaling pathway. Dev. Cell *19*, 138-147.

Camerer,E., Barker,A., Duong,D.N., Ganesan,R., Kataoka,H., Cornelissen,I., Darragh,M.R., Hussain,A., Zheng,Y.W., Srinivasan,Y., Brown,C., Xu,S.M., Regard,J.B., Lin,C.Y., Craik,C.S., Kirchhofer,D., and Coughlin,S.R. (2010b). Local protease signaling contributes to neural tube closure in the mouse embryo. Dev. Cell *18*, 25-38.

Camerer,E., Barker,A., Duong,D.N., Ganesan,R., Kataoka,H., Cornelissen,I., Darragh,M.R., Hussain,A., Zheng,Y.W., Srinivasan,Y., Brown,C., Xu,S.M.,

Regard,J.B., Lin,C.Y., Craik,C.S., Kirchhofer,D., and Coughlin,S.R. (2010a). Local protease signaling contributes to neural tube closure in the mouse embryo. Dev. Cell *18*, 25-38.

Capell,B.C. and Collins,F.S. (2006). Human laminopathies: nuclei gone genetically awry. Nat. Rev. Genet. *7*, 940-952.

Carezani-Gavin,M., Clarren,S.K., and Steege,T. (1992). Waardenburg syndrome associated with meningomyelocele. Am. J. Med. Genet. *42*, 135-136.

Carter,M., Chen,X., Slowinska,B., Minnerath,S., Glickstein,S., Shi,L., Campagne,F., Weinstein,H., and Ross,M.E. (2005). Crooked tail (Cd) model of human folate-responsive neural tube defects is mutated in Wnt coreceptor lipoprotein receptor-related protein 6. Proc. Natl. Acad. Sci. U. S. A *102*, 12843-12848.

Cavalli,P. and Copp,A.J. (2002). Inositol and folate-resistant neural tube defects. J. Med. Genet. *39*, e5.

Cavalli,P., Tedoldi,S., and Riboli,B. (2008). Inositol supplementation in pregnancies at risk of apparently folate-resistant NTDs. Birth Defects Res. A Clin. Mol. Teratol. *82*, 540-542.

Cenci,C. and Gould,A.P. (2005). Drosophila Grainyhead specifies late programmes of neural proliferation by regulating the mitotic activity and Hox-dependent apoptosis of neuroblasts. Development *132*, 3835-3845.

Chatkupt,S. and Johnson,W.G. (1993). Waardenburg syndrome and myelomeningocele in a family. J. Med. Genet. *30*, 83-84.

Chen,W.-H., Morriss-Kay,G.M., and Copp,A.J. (1994). Prevention of spinal neural tube defects in the curly tail mouse mutant by a specific effect of retinoic acid. Dev. Dyn. *199*, 93-102.

Chen,W.-H., Morriss-Kay,G.M., and Copp,A.J. (1995). Genesis and prevention of spinal neural tube defects in the *curly tail* mutant mouse: involvement of retinoic acid and its nuclear receptors RAR-beta and RAR-gamma. Development *121*, 681-691.

Cockroft,D.L., Brook,F.A., and Copp,A.J. (1992). Inositol deficiency increases the susceptibility to neural tube defects of genetically predisposed (curly tail) mouse embryos in vitro. Teratology. *45*, 223-232.

Cogram,P., Hynes,A., Dunlevy,L.P.E., Greene,N.D.E., and Copp,A.J. (2004). Specific isoforms of protein kinase C are essential for prevention of folate-resistant neural tube defects by inositol. Hum. Mol. Genet. *13*, 7-14.

Cogram,P., Tesh,S., Tesh,J., Wade,A., Allan,G., Greene,N.D.E., and Copp,A.J. (2002). D-*chiro*-inositol is more effective than *myo*-inositol in preventing folate-resistant mouse neural tube defects. Hum. Reprod. *17*, 2451-2458.

Copp,A.J. (1985a). Relationship between timing of posterior neuropore closure and development of spinal neural tube defects in mutant (curly tail) and normal mouse embryos in culture. J. Embryol. Exp. Morphol. *88*, 39-54.

Copp,A.J. (1985b). Relationship between timing of posterior neuropore closure and development of spinal neural tube defects in mutant (curly tail) and normal mouse embryos in culture. J. Embryol. Exp. Morphol. *88*, 39-54.

Copp,A.J. and Bernfield,M. (1994). Etiology and pathogenesis of human neural tube defects: Insights from mouse models. Curr. Opin. Pediatr. *6*, 624-631.

Copp,A.J., Brook,F.A., Estibeiro,J.P., Shum,A.S.W., and Cockroft,D.L. (1990). The embryonic development of mammalian neural tube defects. Prog. Neurobiol. *35*, 363-403.

Copp,A.J., Brook,F.A., and Roberts,H.J. (1988a). A cell-type-specific abnormality of cell proliferation in mutant (curly tail) mouse embryos developing spinal neural tube defects. Development *104*, 285-295.

Copp,A.J., Checiu,I., and Henson,J.N. (1994). Developmental basis of severe neural tube defects in the *loop-tail* (*Lp*) mutant mouse: Use of microsatellite DNA markers to identify embryonic genotype. Dev. Biol. *165*, 20-29.

Copp,A.J., Crolla,J.A., and Brook,F.A. (1988b). Prevention of spinal neural tube defects in the mouse embryo by growth retardation during neurulation. Development *104*, 297-303.

Copp,A.J. and Greene,N.D. (2010). Genetics and development of neural tube defects. J. Pathol. *220*, 217-230.

Copp,A.J., Greene,N.D.E., and Murdoch,J.N. (2003). The genetic basis of mammalian neurulation. Nat. Rev. Genet. *4*, 784-793.

Copp,A.J., Seller,M.J., and Polani,P.E. (1982). Neural tube development in mutant (curly tail) and normal mouse embryos: the timing of posterior neuropore closure in vivo and in vitro. J. Embryol. Exp. Morphol. *69*, 151-167.

Czeizel,A.E. (2009). Periconceptional folic acid and multivitamin supplementation for the prevention of neural tube defects and other congenital abnormalities. Birth Defects Res. A Clin. Mol. Teratol. *85*, 260-268.

Czeizel,A.E. and Dudás,I. (1992). Prevention of the first occurrence of neural-tube defects by periconceptional vitamin supplementation. N. Engl. J. Med. *327*, 1832-1835.

Dai,Q., Choy,E., Chiu,V., Romano,J., Slivka,S.R., Steitz,S.A., Michaelis,S., and Philips,M.R. (1998). Mammalian prenylcysteine carboxyl methyltransferase is in the endoplasmic reticulum. J. Biol. Chem. *273*, 15030-15034.

de Castro,S.C., Leung,K.Y., Savery,D., Burren,K., Rozen,R., Copp,A.J., and Greene,N.D. (2010). Neural tube defects induced by folate deficiency in mutant curly tail (Grhl3) embryos are associated with alteration in folate one-carbon metabolism but are unlikely to result from diminished methylation. Birth Defects Res. A Clin. Mol. Teratol. *88*, 612-618.

Deacon,R., Chanarin,I., Lumb,M., and Perry,J. (1985). Role of folate dependent transformylases in synthesis of purine in bone marrow of man and in bone marrow and liver of rats. J. Clin. Pathol. *38*, 1349-1352.

Detrait,E.R., George,T.M., Etchevers,H.C., Gilbert,J.R., Vekemans,M., and Speer,M.C. (2005). Human neural tube defects: developmental biology, epidemiology, and genetics. Neurotoxicol. Teratol. *27*, 515-524.

Dheen,S.T., Tay,S.S., Boran,J., Ting,L.W., Kumar,S.D., Fu,J., and Ling,E.A. (2009). Recent studies on neural tube defects in embryos of diabetic pregnancy: an overview. Curr. Med. Chem. *16*, 2345-2354.

Doudney,K., Ybot-Gonzalez,P., Paternotte,C., Stevenson,R.E., Greene,N.D., Moore,G.E., Copp,A.J., and Stanier,P. (2005). Analysis of the planar cell polarity gene Vangl2 and its co-expressed paralogue Vangl1 in neural tube defect patients. Am. J. Med. Genet. A *136A*, 90-92.

Dunlevy,L.P., Chitty,L.S., Burren,K.A., Doudney,K., Stojilkovic-Mikic,T., Stanier,P., Scott,R., Copp,A.J., and Greene,N.D. (2007). Abnormal folate metabolism in foetuses affected by neural tube defects. Brain *130*, 1043-1049.

Dunlevy,L.P.E., Burren,K.A., Chitty,L.S., Copp,A.J., and Greene,N.D.E. (2006a). Excess methionine suppresses the methylation cycle and inhibits neural tube closure in mouse embryos. FEBS Lett. *580*, 2803-2807.

Dunlevy, L. P. E., Burren, K. A., Mills, K., Chitty, L. S., Copp, A. J., and Greene, N. D. E. Integrity of the methylation cycle is essential for mammalian neural tube closure. Birth Defects Research (Part A) . 2006b.
Ref Type: In Press

Dynlacht,B.D., Attardi,L.D., Admon,A., Freeman,M., and Tjian,R. (1989). Functional analysis of NTF-1, a developmentally regulated Drosophila transcription factor that binds neuronal cis elements. Genes Dev. *3*, 1677-1688.

Echelard,Y., Epstein,D.J., St-Jacques,B., Shen,L., Mohler,J., McMahon,J.A., and McMahon,A.P. (1993). Sonic hedgehog, a member of a family of putative signaling molecules, is implicated in the regulation of CNS polarity. Cell *75*, 1417-1430.

Embury,S., Seller,M.J., Adinolfi,M., and Polani,P.E. (1979). Neural tube defects in curly-tail mice. I. Incidence and expression. Proc. R. Soc. Lond. B *206*, 85-94.

Engleka,K.A., Gitler,A.D., Zhang,M.Z., Zhou,D.D., High,F.A., and Epstein,J.A. (2005). Insertion of Cre into the *Pax3* locus creates a new allele of *Splotch* and identifies unexpected *Pax3* derivatives. Dev. Biol. *280*, 396-406.

Essien,F.B. (1992). Maternal methionine supplementation promotes the remediation of axial defects in *Axd* mouse neural tube mutants. Teratology. *45*, 205-212.

Estibeiro,J.P., Brook,F.A., and Copp,A.J. (1993). Interaction between splotch (*Sp*) and curly tail (*ct*) mouse mutants in the embryonic development of neural tube defects. Development *119*, 113-121.

Fiume,R., Ramazzotti,G., Teti,G., Chiarini,F., Faenza,I., Mazzotti,G., Billi,A.M., and Cocco,L. (2009). Involvement of nuclear PLCbeta1 in lamin B1 phosphorylation and G2/M cell cycle progression. FASEB J. *23*, 957-966.

Fleming,A. and Copp,A.J. (1998). Embryonic folate metabolism and mouse neural tube defects. Science *280*, 2107-2109.

Frye,M. and Watt,F.M. (2006). The RNA methyltransferase Misu (NSun2) mediates Myc-induced proliferation and is upregulated in tumors. Curr. Biol. *16*, 971-981.

Gerace,L. and Foisner,R. (1994). Integral membrane proteins and dynamic organization of the nuclear envelope. Trends Cell Biol. *4*, 127-131.

Glass,J.R. and Gerace,L. (1990). Lamins A and C bind and assemble at the surface of mitotic chromosomes. J. Cell Biol. *111*, 1047-1057.

Goldman,R.D., Gruenbaum,Y., Moir,R.D., Shumaker,D.K., and Spann,T.P. (2002). Nuclear lamins: building blocks of nuclear architecture. Genes Dev. *16*, 533-547.

Gont,L.K., Steinbeisser,H., Blumberg,B., and De Robertis,E.M. (1993). Tail formation as a continuation of gastrulation: The multiple cell populations of the *Xenopus* tailbud derive from the late blastopore lip. Development *119*, 991-1004.

Gorg,A., Boguth,G., Obermaier,C., and Weiss,W. (1998). Two-dimensional electrophoresis of proteins in an immobilized pH 4-12 gradient. Electrophoresis *19*, 1516-1519.

Gorg,A., Postel,W., and Johann,P. (1985). pH, urea and substrate gradients for the optimization of ultrathin polyacrylamide gel zymograms. J. Biochem. Biophys. Methods *10*, 341-350.

Goss,V.L., Hocevar,B.A., Thompson,L.J., Stratton,C.A., Burns,D.J., and Fields,A.P. (1994). Identification of nuclear beta II protein kinase C as a mitotic lamin kinase. J. Biol. Chem. *269*, 19074-19080.

Greene,N.D. and Copp,A.J. (2005). Mouse models of neural tube defects: investigating preventive mechanisms. Am. J. Med. Genet. C. Semin. Med. Genet. *135*, 31-41.

Greene,N.D. and Copp,A.J. (2009b). Development of the vertebrate central nervous system: formation of the neural tube. Prenatal Diag. *29*, 303-311.

Greene,N.D. and Copp,A.J. (2009a). Development of the vertebrate central nervous system: formation of the neural tube. Prenat. Diagn. *29*, 303-311.

Greene,N.D., Massa,V., and Copp,A.J. (2009a). Understanding the causes and prevention of neural tube defects: Insights from the splotch mouse model. Birth Defects Res. A Clin. Mol. Teratol. *85*, 322-330.

Greene,N.D., Stanier,P., and Copp,A.J. (2009b). Genetics of human neural tube defects. Hum. Mol. Genet. *18*, R113-R129.

Greene,N.D.E. and Copp,A.J. (1997). Inositol prevents folate-resistant neural tube defects in the mouse . Nature Med. *3*, 60-66.

Greene,N.D.E. and Copp,A.J. (2004). The embryonic basis of neurulation. In Neural Tube Defects. From Origin to Treatment; D.F.Wyszynski, ed. (Oxford: Oxford University Press).

Greene,N.D.E., Gerrelli,D., Van Straaten,H.W.M., and Copp,A.J. (1998). Abnormalities of floor plate, notochord and somite differentiation in the *loop-tail* (*Lp*) mouse: a model of severe neural tube defects. Mech. Dev. *73*, 59-72.

Greene,N.D.E., Leung,K.Y., Wait,R., Begum,S., Dunn,M.J., and Copp,A.J. (2002). Differential protein expression at the stage of neural tube closure in the mouse embryo. J. Biol. Chem. *277*, 41645-41651.

Gruenbaum,Y., Margalit,A., Goldman,R.D., Shumaker,D.K., and Wilson,K.L. (2005). The nuclear lamina comes of age. Nat. Rev. Mol. Cell Biol. *6*, 21-31.

Gustavsson,P., Copp,A.J., and Greene,N.D. (2008). Grainyhead genes and mammalian neural tube closure. Birth Defects Res. A Clin. Mol. Teratol. *82*, 728-735.

Gustavsson,P., Greene,N.D., Lad,D., Pauws,E., de Castro,S.C., Stanier,P., and Copp,A.J. (2007). Increased expression of Grainyhead-like-3 rescues spina bifida in a folate-resistant mouse model. Hum. Mol. Genet. *16*, 2640-2646.

Harborth,J., Elbashir,S.M., Bechert,K., Tuschl,T., and Weber,K. (2001). Identification of essential genes in cultured mammalian cells using small interfering RNAs. J. Cell Sci. *114*, 4557-4565.

Harris,M.J. (2001). Why are the genes that cause risk of human neural tube defects so hard to find? Teratology. *63*, 165-166.

Harris,M.J. (2009). Insights into prevention of human neural tube defects by folic acid arising from consideration of mouse mutants. Birth Defects Res. A Clin. Mol. Teratol. *85*, 331-339.

Harris,M.J. and Juriloff,D.M. (2007). Mouse mutants with neural tube closure defects and their role in understanding human neural tube defects. Birth Defects Res. A Clin. Mol. Teratol. *79*, 187-210.

Harris,M.J. and Juriloff,D.M. (2010). An update to the list of mouse mutants with neural tube closure defects and advances toward a complete genetic perspective of neural tube closure. Birth Defects Res. A Clin. Mol. Teratol. *88*, 653-669.

Hegele,R.A., Cao,H., Liu,D.M., Costain,G.A., Charlton-Menys,V., Rodger,N.W., and Durrington,P.N. (2006). Sequencing of the reannotated LMNB2 gene reveals novel mutations in patients with acquired partial lipodystrophy. Am. J. Hum. Genet. *79*, 383-389.

Heins,S. and Aebi,U. (1994). Making heads and tails of intermediate filament assembly, dynamics and networks. Curr. Opin. Cell Biol. *6*, 25-33.

Heiss,A., DuChesne,A., Denecke,B., Grotzinger,J., Yamamoto,K., Renne,T., and Jahnen-Dechent,W. (2003). Structural basis of calcification inhibition by alpha 2-HS glycoprotein/fetuin-A. Formation of colloidal calciprotein particles. J. Biol. Chem. *278*, 13333-13341.

Hetzer,M., Meyer,H.H., Walther,T.C., Bilbao-Cortes,D., Warren,G., and Mattaj,I.W. (2001). Distinct AAA-ATPase p97 complexes function in discrete steps of nuclear assembly. Nat. Cell Biol. *3*, 1086-1091.

Hirata,H., Tomita,K., Bessho,Y., and Kageyama,R. (2001). Hes1 and Hes3 regulate maintenance of the isthmic organizer and development of the mid/hindbrain. EMBO J. *20*, 4454-4466.

Hocevar,B.A., Burns,D.J., and Fields,A.P. (1993). Identification of protein kinase C (PKC) phosphorylation sites on human lamin B. Potential role of PKC in nuclear lamina structural dynamics. J. Biol. Chem. *268*, 7545-7552.

Holmberg,J., Clarke,D.L., and Frisén,J. (2000). Regulation of repulsion versus adhesion by different splice forms of an Eph receptor. Nature *408*, 203-206.

Huang,J.D., Dubnicoff,T., Liaw,G.J., Bai,Y., Valentine,S.A., Shirokawa,J.M., Lengyel,J.A., and Courey,A.J. (1995). Binding sites for transcription factor NTF-1/Elf-1 contribute to the ventral repression of decapentaplegic. Genes Dev. *9*, 3177-3189.

Hussain,S., Benavente,S.B., Nascimento,E., Dragoni,I., Kurowski,A., Gillich,A., Humphreys,P., and Frye,M. (2009). The nucleolar RNA methyltransferase Misu (NSun2) is required for mitotic spindle stability. J. Cell Biol. *186*, 27-40.

Hutchison,C.J. (2002b). Lamins: building blocks or regulators of gene expression? Nat. Rev. Mol. Cell Biol. *3*, 848-858.

Hutchison,C.J. (2002a). Lamins: building blocks or regulators of gene expression? Nat. Rev. Mol. Cell Biol. *3*, 848-858.

Hutchison,C.J., Bridger,J.M., Cox,L.S., and Kill,I.R. (1994). Weaving a pattern from disparate threads: lamin function in nuclear assembly and DNA replication. J. Cell Sci. *107 (Pt 12)*, 3259-3269.

Ishibashi,M., Ang,S.-L., Shiota,K., Nakanishi,S., Kageyama,R., and Guillemot,F. (1995). Targeted disruption of mammalian *hairy* and *Enhancer of split* homolog-1 (*HES-1*) leads to up-regulation of neural helix-loop-helix factors, premature neurogenesis, and severe neural tube defects. Genes Dev. *9*, 3136-3148.

Jin,Y., Martins,C., Salemark,L., Persson,B., Jin,C., Miranda,J., Fonseca,I., and Jonsson,N. (2001). Nonrandom karyotypic features in basal cell carcinomas of the skin. Cancer Genet. Cytogenet. *131*, 109-119.

Juriloff,D.M., Gunn,T.M., Harris,M.J., Mah,D.G., Wu,M.K., and Dewell,S.L. (2001). Multifactorial genetics of exencephaly in SELH/Bc mice. Teratology. *64*, 189-200.

Kibar,Z., Bosoi,C.M., Kooistra,M., Salem,S., Finnell,R.H., De,M.P., Merello,E., Bassuk,A.G., Capra,V., and Gros,P. (2009). Novel mutations in VANGL1 in neural tube defects. Hum. Mutat. *30*, E706-E715.

Kibar,Z., Salem,S., Bosoi,C.M., Pauwels,E., De,M.P., Merello,E., Bassuk,A.G., Capra,V., and Gros,P. (2010). Contribution of VANGL2 mutations to isolated neural tube defects. Clin. Genet.

Kibar,Z., Torban,E., McDearmid,J.R., Reynolds,A., Berghout,J., Mathieu,M., Kirillova,I., De,M.P., Merello,E., Hayes,J.M., Wallingford,J.B., Drapeau,P., Capra,V., and Gros,P. (2007). Mutations in VANGL1 associated with neural-tube defects. N. Engl. J. Med. *356*, 1432-1437.

Kim,E., Ambroziak,P., Otto,J.C., Taylor,B., Ashby,M., Shannon,K., Casey,P.J., and Young,S.G. (1999). Disruption of the mouse Rce1 gene results in defective Ras processing and mislocalization of Ras within cells. J. Biol. Chem. *274*, 8383-8390.

Kim,T.H., Goodman,J., Anderson,K.V., and Niswander,L. (2007). Phactr4 regulates neural tube and optic fissure closure by controlling PP1-, Rb-, and E2F1-regulated cell-cycle progression. Dev. Cell *13*, 87-102.

Kirke,P.N., Molloy,A.M., Daly,L.E., Burke,H., Weir,D.G., and Scott,J.M. (1993). Maternal plasma folate and vitamin B_{12} are independent risk factors for neural tube defects. Q. J. Med. *86*, 703-708.

Klose,J., Nock,C., Herrmann,M., Stuhler,K., Marcus,K., Bluggel,M., Krause,E., Schalkwyk,L.C., Rastan,S., Brown,S.D., Bussow,K., Himmelbauer,H., and Lehrach,H. (2002). Genetic analysis of the mouse brain proteome. Nat. Genet *30*, 385-393.

Kokubu,C., Heinzmann,U., Kokubu,T., Sakai,N., Kubota,T., Kawai,M., Wahl,M.B., Galceran,J., Grosschedl,R., Ozono,K., and Imai,K. (2004). Skeletal defects in *ringelschwanz* mutant mice reveal that Lrp6 is required for proper somitogenesis and osteogenesis. Development *131*, 5469-5480.

Kudryavtseva,E.I., Sugihara,T.M., Wang,N., Lasso,R.J., Gudnason,J.F., Lipkin,S.M., and Andersen,B. (2003). Identification and characterization of Grainyhead-like epithelial transactivator (GET-1), a novel mammalian Grainyhead-like factor. Dev. Dyn. *226*, 604-617.

Lee,S.K., Jurata,L.W., Nowak,R., Lettieri,K., Kenny,D.A., Pfaff,S.L., and Gill,G.N. (2005). The LIM domain-only protein LMO4 is required for neural tube closure. Mol. Cell Neurosci. *28*, 205-214.

Leonard,J.H., Cook,A.L., Nancarrow,D., Hayward,N., Van,G.M., Van,R.N., and Speleman,F. (2000). Deletion mapping on the short arm of chromosome 1 in Merkel cell carcinoma. Cancer Detect. Prev. *24*, 620-627.

Letts,V.A., Schork,N.J., Copp,A.J., Bernfield,M., and Frankel,W.N. (1995). A curly-tail modifier locus, mct1, on mouse chromosome 17. Genomics *29*, 719-724.

Lippincott-Schwartz,J., Snapp,E., and Kenworthy,A. (2001). Studying protein dynamics in living cells. Nat. Rev. Mol. Cell Biol. *2*, 444-456.

Loeken,M.R. (2005). Current perspectives on the causes of neural tube defects resulting from diabetic pregnancy. Am. J. Med. Genet. C. Semin. Med. Genet. *135*, 77-87.

Mace,K.A., Pearson,J.C., and McGinnis,W. (2005). An epidermal barrier wound repair pathway in *Drosophila* is mediated by *grainy head*. Science *308*, 381-385.

Maeno,H., Sugimoto,K., and Nakajima,N. (1995). Genomic structure of the mouse gene (Lmnb1) encoding nuclear lamin B1. Genomics *30*, 342-346.

Majerus,P.W., Wilson,D.B., Zhang,C., Nicholas,P.J., and Wilson,M.P. (2010). Expression of inositol 1,3,4-trisphosphate 5/6-kinase (ITPK1) and its role in neural tube defects. Adv. Enzyme Regul. *50*, 365-372.

Malhas,A., Lee,C.F., Sanders,R., Saunders,N.J., and Vaux,D.J. (2007). Defects in lamin B1 expression or processing affect interphase chromosome position and gene expression. J. Cell Biol. *176*, 593-603.

Malhas,A.N., Lee,C.F., and Vaux,D.J. (2009). Lamin B1 controls oxidative stress responses via Oct-1. J. Cell Biol. *184*, 45-55.

Manning,S.M., Jennings,R., and Madsen,J.R. (2000). Pathophysiology, prevention, and potential treatment of neural tube defects. Ment. Retard. Dev. Disabil. Res. Rev. *6*, 6-14.

Martelli,A.M., Tabellini,G., Bortul,R., Manzoli,L., Bareggi,R., Baldini,G., Grill,V., Zweyer,M., Narducci,P., and Cocco,L. (2000). Enhanced nuclear diacylglycerol kinase activity in response to a mitogenic stimulation of quiescent Swiss 3T3 cells with insulin-like growth factor I. Cancer Res. *60*, 815-821.

Martinez-Barbera,J.P., Rodriguez,T.A., Greene,N.D.E., Weninger,W.J., Simeone,A., Copp,A.J., Beddington,R., and Dunwoodie,S. (2002). Folic acid prevents exencephaly in *Cited2* deficient mice. Hum. Mol. Genet. *11*, 283-293.

Maske,C.P., Hollinshead,M.S., Higbee,N.C., Bergo,M.O., Young,S.G., and Vaux,D.J. (2003). A carboxyl-terminal interaction of lamin B1 is dependent on the CAAX endoprotease Rce1 and carboxymethylation. J. Cell Biol. *162*, 1223-1232.

Massa,V., Savery,D., Ybot-Gonzalez,P., Ferraro,E., Rongvaux,A., Cecconi,F., Flavell,R., Greene,N.D., and Copp,A.J. (2009). Apoptosis is not required for mammalian neural tube closure. Proc. Natl. Acad. Sci. U. S. A *106*, 8233-8238.

McKeon,F.D., Kirschner,M.W., and Caput,D. (1986). Homologies in both primary and secondary structure between nuclear envelope and intermediate filament proteins. Nature *319*, 463-468.

Meijer,I.A., Simoes-Lopes,A.A., Laurent,S., Katz,T., St-Onge,J., Verlaan,D.J., Dupre,N., Thibault,M., Mathurin,J., Bouchard,J.P., and Rouleau,G.A. (2008). A novel duplication confirms the involvement of 5q23.2 in autosomal dominant leukodystrophy. Arch. Neurol. *65*, 1496-1501.

Menegola,E., Broccia,M.L., and Giavini,E. (2001). Atlas of rat fetal skeleton double stained for bone and cartilage. Teratology. *64*, 125-133.

Mersereau,P., Kilker,K., Carter,H., Fassett,E., Williams,J., Flores,A., Prue,C., Williams,L., Mai,C., and Mulinare,J. (2004). Spina bifida and anencephaly before and after folic acid mandate - United States, 1995-1996 and 1999-2000. MMWR *53(17)*, 362-365.

Mikkat,S., Lorenz,P., Scharf,C., Yu,X., Glocker,M.O., and Ibrahim,S.M. (2010). MS characterization of qualitative protein polymorphisms in the spinal cords of inbred mouse strains. Proteomics. *10*, 1050-1062.

Moir,R.D., Montag-Lowy,M., and Goldman,R.D. (1994). Dynamic properties of nuclear lamins: lamin B is associated with sites of DNA replication. J. Cell Biol. *125*, 1201-1212.

Molloy,A.M., Brody,L.C., Mills,J.L., Scott,J.M., and Kirke,P.N. (2009). The search for genetic polymorphisms in the homocysteine/folate pathway that contribute to the etiology of human neural tube defects. Birth Defects Res. A Clin. Mol. Teratol. *85*, 285-294.

Moretti,M.E., Bar-Oz,B., Fried,S., and Koren,G. (2005). Maternal hyperthermia and the risk for neural tube defects in offspring: systematic review and meta-analysis. Epidemiology *16*, 216-219.

Muller,J.M., Deinhardt,K., Rosewell,I., Warren,G., and Shima,D.T. (2007). Targeted deletion of p97 (VCP/CDC48) in mouse results in early embryonic lethality. Biochem. Biophys. Res. Commun. *354*, 459-465.

Murdoch,J.N., Doudney,K., Paternotte,C., Copp,A.J., and Stanier,P. (2001). Severe neural tube defects in the *loop-tail* mouse result from mutation of *Lpp1*, a novel gene involved in floor plate specification. Hum. Mol. Genet. *10*, 2593-2601.

Neumann,P.E., Frankel,W.N., Letts,V.A., Coffin,J.M., Copp,A.J., and Bernfield,M. (1994). Multifactorial inheritance of neural tube defects: Localization of the major gene and recognition of modifiers in *ct* mutant mice. Nature Genet. *6*, 357-362.

Olivier,E., Soury,E., Ruminy,P., Husson,A., Parmentier,F., Daveau,M., and Salier,J.P. (2000). Fetuin-B, a second member of the fetuin family in mammals. Biochem. J. *350 Pt 2*, 589-597.

Otto,J.C., Kim,E., Young,S.G., and Casey,P.J. (1999). Cloning and characterization of a mammalian prenyl protein-specific protease. J. Biol. Chem. *274*, 8379-8382.

Padiath,Q.S., Saigoh,K., Schiffmann,R., Asahara,H., Yamada,T., Koeppen,A., Hogan,K., Ptacek,L.J., and Fu,Y.H. (2006). Lamin B1 duplications cause autosomal dominant leukodystrophy. Nat. Genet. *38*, 1114-1123.

Peeters,M.C.E., Schutte,B., Lenders,M.H.J.N., Hekking,J.W.M., Drukker,J., and Van Straaten,H.W.M. (1998). Role of differential cell proliferation in the tail bud in aberrant mouse neurulation. Dev. Dyn. *211*, 382-389.

Peeters,M.C.E., Shum,A.S.W., Hekking,J.W.M., Copp,A.J., and Van Straaten,H.W.M. (1996). Relationship between altered axial curvature and neural tube closure in normal and mutant (*curly tail*) mouse embryos. Anat. Embryol. *193*, 123-130.

Peters,L.M., Anderson,D.W., Griffith,A.J., Grundfast,K.M., San Agustin,T.B., Madeo,A.C., Friedman,T.B., and Morell,R.J. (2002). Mutation of a transcription factor, TFCP2L3, causes progressive autosomal dominant hearing loss, DFNA28. Hum. Mol. Genet. *11*, 2877-2885.

Pietromonaco,S.F., Simons,P.C., Altman,A., and Elias,L. (1998). Protein kinase C-theta phosphorylation of moesin in the actin-binding sequence. J. Biol. Chem. *273*, 7594-7603.

Pinson,K.I., Brennan,J., Monkley,S., Avery,B.J., and Skarnes,W.C. (2000). An LDL-receptor-related protein mediates Wnt signalling in mice. Nature *407*, 535-538.

Raggiaschi,R., Lorenzetto,C., Diodato,E., Caricasole,A., Gotta,S., and Terstappen,G.C. (2006). Detection of phosphorylation patterns in rat cortical neurons by combining phosphatase treatment and DIGE technology. Proteomics. *6*, 748-756.

Rampersaud,E., Bassuk,A.G., Enterline,D.S., George,T.M., Siegel,D.G., Melvin,E.C., Aben,J., Allen,J., Aylsworth,A., Brei,T., Bodurtha,J., Buran,C., Floyd,L.E., Hammock,P., Iskandar,B., Ito,J., Kessler,J.A., Lasarsky,N., Mack,P., Mackey,J., McLone,D., Meeropol,E., Mehltretter,L., Mitchell,L.E., Oakes,W.J., Nye,J.S., Powell,C., Sawin,K., Stevenson,R., Walker,M., West,S.G., Worley,G., Gilbert,J.R., and Speer,M.C. (2005). Whole genomewide linkage screen for neural tube defects reveals regions of interest on chromosomes 7 and 10. J. Med. Genet. *42*, 940-946.

Rifat,Y., Parekh,V., Wilanowski,T., Hislop,N.R., Auden,A., Ting,S.B., Cunningham,J.M., and Jane,S.M. (2010). Regional neural tube closure defined by the Grainy head-like transcription factors. Dev. Biol. *345*, 237-245.

Sakita-Suto,S., Kanda,A., Suzuki,F., Sato,S., Takata,T., and Tatsuka,M. (2007). Aurora-B regulates RNA methyltransferase NSUN2. Mol. Biol. Cell *18*, 1107-1117.

Scaffidi,P. and Misteli,T. (2005). Reversal of the cellular phenotype in the premature aging disease Hutchinson-Gilford progeria syndrome. Nat. Med. *11*, 440-445.

Schirmer,E.C., Guan,T., and Gerace,L. (2001). Involvement of the lamin rod domain in heterotypic lamin interactions important for nuclear organization. J. Cell Biol. *153*, 479-489.

Schorah,C. (2009). Dick Smithells, folic acid, and the prevention of neural tube defects. Birth Defects Res. A Clin. Mol. Teratol. *85*, 254-259.

Scott,J. and Weir,D. (1994). Folate/vitamin B12 inter-relationships. Essays Biochem. *28*, 63-72.

Seller,M.J. (1987). Neural tube defects and sex ratios. Am. J. Med. Genet. *26*, 699-707.

Seller,M.J., Embury,S., Polani,P.E., and Adinolfi,M. (1979). Neural tube defects in curly-tail mice. II. Effect of maternal administration of vitamin A. Proc. R. Soc. Lond. B *206*, 95-107.

Seller,M.J. and Perkins,K.J. (1986). Effect of mitomycin C on the neural tube defects of the curly-tail mouse. Teratology. *33*, 305-309.

Shum,A.S.W. and Copp,A.J. (1996). Regional differences in morphogenesis of the neuroepithelium suggest multiple mechanisms of spinal neurulation in the mouse. Anat. Embryol. *194*, 65-73.

Smitherman,M., Lee,K., Swanger,J., Kapur,R., and Clurman,B.E. (2000). Characterization and targeted disruption of murine Nup50, a p27(Kip1)-interacting component of the nuclear pore complex. Mol. Cell Biol. *20*, 5631-5642.

Stewart,C.L., Kozlov,S., Fong,L.G., and Young,S.G. (2007). Mouse models of the laminopathies. Exp. Cell Res. *313*, 2144-2156.

Stiefel,D. and Meuli,M. (2007). Scanning electron microscopy of fetal murine myelomeningocele reveals growth and development of the spinal cord in early gestation and neural tissue destruction around birth. J. Pediatr. Surg. *42*, 1561-1565.

Stuurman,N., Heins,S., and Aebi,U. (1998). Nuclear lamins: their structure, assembly, and interactions. J. Struct. Biol. *122*, 42-66.

Tabellini,G., Bortul,R., Aluigi,M., Billi,A.M., Bareggi,R., Grill,V., Narducci,P., and Martelli,A.M. (2002). Binding of elements of protein kinase C-alpha regulatory domain to lamin B1. Cell Signal. *14*, 819-827.

Tannu,N.S., Sanchez-Brambila,G., Kirby,P., and Andacht,T.M. (2006). Effect of staining reagent on peptide mass fingerprinting from in-gel trypsin digestions: a comparison of SyproRuby and DeepPurple. Electrophoresis *27*, 3136-3143.

Teixeira,P.F., Cerca,F., Santos,S.D., and Saraiva,M.J. (2006). Endoplasmic reticulum stress associated with extracellular aggregates. Evidence from transthyretin deposition in familial amyloid polyneuropathy. J. Biol. Chem. *281*, 21998-22003.

Ting,S.B., Caddy,J., Hislop,N., Wilanowski,T., Auden,A., Zhao,L.L., Ellis,S., Kaur,P., Uchida,Y., Holleran,W.M., Elias,P.M., Cunningham,J.M., and Jane,S.M. (2005). A homolog of Drosophila grainy head is essential for epidermal integrity in mice. Science *308*, 411-413.

Ting,S.B., Wilanowski,T., Auden,A., Hall,M., Voss,A.K., Thomas,T., Parekh,V., Cunningham,J.M., and Jane,S.M. (2003a). Inositol- and folate-resistant neural tube defects in mice lacking the epithelial-specific factor Grhl-3. Nature Med. *9*, 1513-1519.

Ting,S.B., Wilanowski,T., Cerruti,L., Zhao,L.L., Cunningham,J.M., and Jane,S.M. (2003b). The identification and characterization of human Sister-of-Mammalian Grainyhead (SOM) expands the grainyhead-like family of developmental transcription factors. Biochem. J. *370*, 953-962.

Torban,E., Patenaude,A.M., Leclerc,S., Rakowiecki,S., Gauthier,S., Andelfinger,G., Epstein,D.J., and Gros,P. (2008). Genetic interaction between members of the Vangl family causes neural tube defects in mice. Proc. Natl. Acad. Sci. U. S. A *105*, 3449-3454.

Tran,P., Hiou-Tim,F., Frosst,P., Lussier-Cacan,S., Bagley,P., Selhub,J., Bottiglieri,T., and Rozen,R. (2002). The curly-tail (ct) mouse, an animal model of neural tube defects,

displays altered homocysteine metabolism without folate responsiveness or a defect in Mthfr. Mol. Genet. Metab *76*, 297-304.

Tsukumo,Y., Tomida,A., Kitahara,O., Nakamura,Y., Asada,S., Mori,K., and Tsuruo,T. (2007). Nucleobindin 1 controls the unfolded protein response by inhibiting ATF6 activation. J. Biol. Chem. *282*, 29264-29272.

Van Straaten,H.W.M., Blom,H., Peeters,M.C.E., Rousseau,A.M.J., Cole,K.J., and Seller,M.J. (1995). Dietary methionine does not reduce penetrance in *curly tail* mice but causes a phenotype-specific decrease in embryonic growth. J. Nutr. *125*, 2733-2740.

Van Straaten,H.W.M. and Copp,A.J. (2001). Curly tail: a 50-year history of the mouse spina bifida model. Anat. Embryol. *203*, 225-237.

Vergnes,L., Péterfy,M., Bergo,M.O., Young,S.G., and Reue,K. (2004). Lamin B1 is required for mouse development and nuclear integrity. Proc. Natl. Acad. Sci. USA *101*, 10428-10433.

Wald,N., Sneddon,J., Densem,J., Frost,C., Stone,R., and MRC Vitamin Study Res Group (1991). Prevention of neural tube defects: Results of the Medical Research Council Vitamin Study. Lancet *338*, 131-137.

Wang,Y., Lian,L., Golden,J.A., Morrisey,E.E., and Abrams,C.S. (2007). PIP5KI gamma is required for cardiovascular and neuronal development. Proc. Natl. Acad. Sci. U. S. A *104*, 11748-11753.

Waugh,M.G., Minogue,S., Anderson,J.S., Balinger,A., Blumenkrantz,D., Calnan,D.P., Cramer,R., and Hsuan,J.J. (2003). Localization of a highly active pool of type II phosphatidylinositol 4-kinase in a p97/valosin-containing-protein-rich fraction of the endoplasmic reticulum. Biochem. J. *373*, 57-63.

Wilanowski,T., Caddy,J., Ting,S.B., Hislop,N.R., Cerruti,L., Auden,A., Zhao,L.L., Asquith,S., Ellis,S., Sinclair,R., Cunningham,J.M., and Jane,S.M. (2008). Perturbed desmosomal cadherin expression in grainy head-like 1-null mice. EMBO J. *27*, 886-897.

Wilanowski,T., Tuckfield,A., Cerruti,L., O'Connell,S., Saint,R., Parekh,V., Tao,J., Cunningham,J.M., and Jane,S.M. (2002). A highly conserved novel family of mammalian developmental transcription factors related to Drosophila grainyhead. Mech. Dev. *114*, 37-50.

Wilson,M.P., Hugge,C., Bielinska,M., Nicholas,P., Majerus,P.W., and Wilson,D.B. (2009). Neural tube defects in mice with reduced levels of inositol 1,3,4-trisphosphate 5/6-kinase. Proc. Natl. Acad. Sci. U. S. A *106*, 9831-9835.

Wilson,V. and Beddington,R.S.P. (1996). Cell fate and morphogenetic movement in the late mouse primitive streak. Mech. Dev. *55*, 79-89.

Worman,H.J. and Bonne,G. (2007). "Laminopathies": a wide spectrum of human diseases. Exp. Cell Res. *313*, 2121-2133.

Worman,H.J., Fong,L.G., Muchir,A., and Young,S.G. (2009). Laminopathies and the long strange trip from basic cell biology to therapy. J. Clin. Invest *119*, 1825-1836.

Yamagata,A., Kristensen,D.B., Takeda,Y., Miyamoto,Y., Okada,K., Inamatsu,M., and Yoshizato,K. (2002). Mapping of phosphorylated proteins on two-dimensional polyacrylamide gels using protein phosphatase. Proteomics. *2*, 1267-1276.

Ybot-Gonzalez,P., Cogram,P., Gerrelli,D., and Copp,A.J. (2002). Sonic hedgehog and the molecular regulation of neural tube closure. Development *129*, 2507-2517.

Ybot-Gonzalez,P. and Copp,A.J. (1999). Bending of the neural plate during mouse spinal neurulation is independent of actin microfilaments. Dev. Dyn. *215*, 273-283.

Ybot-Gonzalez,P., Gaston-Massuet,C., Girdler,G., Klingensmith,J., Arkell,R., Greene,N.D., and Copp,A.J. (2007a). Neural plate morphogenesis during mouse neurulation is regulated by antagonism of Bmp signalling. Development *134*, 3203-3211.

Ybot-Gonzalez,P., Savery,D., Gerrelli,D., Signore,M., Mitchell,C.E., Faux,C.H., Greene,N.D., and Copp,A.J. (2007b). Convergent extension, planar-cell-polarity signalling and initiation of mouse neural tube closure. Development *134*, 789-799.

Yon,J.M., Baek,I.J., Lee,S.R., Jin,Y., Kim,M.R., Nahm,S.S., Kim,J.S., Ahn,B., Lee,B.J., Yun,Y.W., and Nam,S.Y. (2008). The spatio-temporal expression pattern of cytoplasmic Cu/Zn superoxide dismutase (SOD1) mRNA during mouse embryogenesis. J. Mol. Histol. *39*, 95-103.

Young,S.G., Fong,L.G., and Michaelis,S. (2005). Prelamin A, Zmpste24, misshapen cell nuclei, and progeria--new evidence suggesting that protein farnesylation could be important for disease pathogenesis. J. Lipid Res. *46*, 2531-2558.

Yu,Z., Bhandari,A., Mannik,J., Pham,T., Xu,X., and Andersen,B. (2008). Grainyhead-like factor Get1/Grhl3 regulates formation of the epidermal leading edge during eyelid closure. Dev. Biol. *319*, 56-67.

Yu,Z., Lin,K.K., Bhandari,A., Spencer,J.A., Xu,X., Wang,N., Lu,Z., Gill,G.N., Roop,D.R., Wertz,P., and Andersen,B. (2006e). The Grainyhead-like epithelial transactivator Get-1/Grhl3 regulates epidermal terminal differentiation and interacts functionally with LMO4. Dev. Biol. *299*, 122-136.

Yu,Z., Lin,K.K., Bhandari,A., Spencer,J.A., Xu,X., Wang,N., Lu,Z., Gill,G.N., Roop,D.R., Wertz,P., and Andersen,B. (2006a). The Grainyhead-like epithelial transactivator Get-1/Grhl3 regulates epidermal terminal differentiation and interacts functionally with LMO4. Dev. Biol. *299*, 122-136.

Yu,Z., Lin,K.K., Bhandari,A., Spencer,J.A., Xu,X., Wang,N., Lu,Z., Gill,G.N., Roop,D.R., Wertz,P., and Andersen,B. (2006b). The Grainyhead-like epithelial transactivator Get-1/Grhl3 regulates epidermal terminal differentiation and interacts functionally with LMO4. Dev. Biol. *299*, 122-136.

Yu,Z., Lin,K.K., Bhandari,A., Spencer,J.A., Xu,X., Wang,N., Lu,Z., Gill,G.N., Roop,D.R., Wertz,P., and Andersen,B. (2006c). The Grainyhead-like epithelial

transactivator Get-1/Grhl3 regulates epidermal terminal differentiation and interacts functionally with LMO4. Dev. Biol. *299*, 122-136.

Yu,Z., Lin,K.K., Bhandari,A., Spencer,J.A., Xu,X., Wang,N., Lu,Z., Gill,G.N., Roop,D.R., Wertz,P., and Andersen,B. (2006d). The Grainyhead-like epithelial transactivator Get-1/Grhl3 regulates epidermal terminal differentiation and interacts functionally with LMO4. Dev. Biol. *299*, 122-136.

Yu,Z., Mannik,J., Soto,A., Lin,K.K., and Andersen,B. (2009). The epidermal differentiation-associated Grainyhead gene Get1/Grhl3 also regulates urothelial differentiation. EMBO J. *28*, 1890-1903.

Zhang,J., Glatfelter,A.A., Taetle,R., and Trent,J.M. (1999). Frequent alterations of evolutionarily conserved regions of chromosome 1 in human malignant melanoma. Cancer Genet. Cytogenet. *111*, 119-123.